Palaeoceanography of the Northeastern Pacific Ocean off Vancouver Island, Canada

by

Jennifer Lynn McKay

H.B.Sc. The University of Western Ontario, 1988
M.Sc., The University of Western Ontario, 1992

A thesis submitted in partial fulfillment of the
requirements for the degree of

Doctor of Philosophy

in

The Faculty of Graduate Studies
(Department of Earth and Ocean Sciences)

We accept this thesis as conforming to the required standards

THE UNIVERSITY OF BRITISH COLUMBIA

September 2003

In presenting this thesis in partial fulfilment of the requirements for an advanced degree at the University of British Columbia, I agree that the Library shall make it freely available for reference and study. I further agree that permission for extensive copying of this thesis for scholarly purposes may be granted by the head of my department or by his or her representatives. It is understood that copying or publication of this thesis for financial gain shall not be allowed without my written permission.

Department of _Earth and Ocean Sciences (Oceanography)_

The University of British Columbia
Vancouver, Canada

Date ___6/10/2003___

Abstract

Marine sediment cores from the continental margin off Western Canada (48° to 50°N, 125 to 128°W) yield evidence of dramatic changes in oceanographic conditions over the last 16 kyr. During the late Glacial the accumulation of marine organic matter was greatly reduced. This reflects low primary and export production because glacial-mode atmospheric circulation did not drive coastal upwelling. At the start of the Bølling warm period (~14.3 kyr B.P.), and coincident with the retreat of glaciers from the continental shelf, there was a substantial increase in the burial of organic matter. However, much of this material was "old" terrestrial organic detritus derived in part from the erosion of shelf sediments. It was not until the Allerød (~13.5 to 12.6 kyr B.P.) that the accumulation of marine organic matter increased substantially. Other paleoproductivity proxies (i.e., % biogenic Ba, % opal and alkenone abundances) also indicate very high marine productivity at this time. Since primary production in the region is controlled by the upwelling of nutrient-rich subsurface waters, this suggests upwelling was enhanced during the Allerød. A decrease in benthic-planktonic age differences (i.e., older planktonic foram ages) supports this interpretation. There was a brief return to glacial conditions (i.e., lower primary and export production) during the Younger Dryas, followed by a slight rise in organic carbon burial between ~11 and 10 kyr B.P.. In general, the accumulation of organic carbon was low throughout the Holocene despite high primary productivity. Low sedimentation rates and the resulting long oxidant exposure times as well as extensive biological recycling appear to be the primary causes of low organic carbon burial, although lower productivity relative to the Allerød cannot be ruled out.

Changes in the vertical settling flux of organic carbon to the sediment had a direct impact on sedimentary redox conditions at Site JT96-09 (920 m water depth). At present, near-surface sediments become suboxic within millimetres of the sediment-water interface and Re enrichment is observed below the depth of bioturbative mixing. However, anoxic conditions do not develop despite relatively low bottom water oxygen concentrations (0.3 ml/l) and relatively high organic carbon flux to the sea floor. The situation was much different during the deglacial.

During the Allerød, when the organic flux to the sediment peaked, Mo enrichment is observed (>2 µg/g) implying that near-surface sediments were anoxic at this time. The benthic foraminifera assemblage (i.e., the dominance of *Bolivina* spp.) likewise suggests that sediments were more oxygen-depleted. These results imply that the bottom waters at Station JT96-09 were more oxygen-depleted during the Allerød and since JT96-09 is located within the oxygen minimum zone (OMZ), it follows that the OMZ was more intense. The increase in marine organic carbon accumulation and the lack of evidence of decreased ventilation suggests that OMZ intensification was a response to increased primary production and carbon export. Deglacial intensification of the OMZ is documented along the entire length of the California Current System, but it appears to have been delayed by ~1500 years off Vancouver Island. It is probable that the presence of the Laurentide and Cordilleran ice sheets continued to influence atmospheric circulation, and in turn oceanic circulation, in the region until at least the Allerød.

It is possible to use redox-sensitive trace metals as palaeo-proxies in the deglacial sediments of Core JT96-09 because sedimentation rates were quite high (>100 cm/kyr). In contrast, in the slowly deposited Holocene sediments (5 cm/kyr) the trace metal record is corrupted due to the precipitation of trace metals decimetres below the sediment-water interface. This enrichment obscures the original palaeo-signal, which formed shortly after sediment deposition. Rapid fluctuations in the sedimentation rate can also complicate trace metal records. In the deglacial deposits of Core JT96-02 the formation of Mo and Re concentration spikes is the direct consequence of episodic deposition of turbidites that restricted oxygen influx into the sediment and thus allowed anoxic conditions to develop.

Intriguing results were obtained from the measurement of sedimentary Ag concentration in near-surface sediments. Unlike the other redox-sensitive trace metals, for example Cd which has a similar geochemical behaviour, the primary control on Ag concentration is not sedimentary redox conditions. Rather, it seems that Ag accumulates in, and is transferred to the sediment by, settling organic particles in much the same way that Ba is. Hence, measuring the Ag concentration of sediments may provide another means of assessing palaeoproductivity.

Table of Contents

List of Figures

List of Tables

Acknowledgements

Yes IT is finally done, but it would not have been possible without the help of many people.

First and foremost to my advisor Dr. Tom Pedersen. Thank you for taking the risk of accepting me as a PhD student. I'm sure you had your doubts about the sanity of that decision but I hope in the end that you think it proved sagacious. Thank you for your guidance, patience and understanding and your research money. Thank you for helping me to discover the world of palaeoceanography and the world in general.

To Dr. Steve Calvert. I'm at a loss for words. You are an incredible scientist in every sense. Your love for, and dedication to, science is truly inspiring. It has been an honour to get to know you and to learn from you.

To my thesis committee (Steve Calvert, Kristen Orians and Kurt Grimm). I am indebted to you for keeping me on track and for reviewing my thesis. I hope it was not too trying.

To Bente, Bert, Kathy and Maureen. Your help in the lab was tremendous and your friendship equally as important. Thank you for everything.

To the members of the geochemistry group. Thank you for the stimulating discussions and feedback on my work. A special thank to Stephanie Kienast without whom there would be no SST record on which so much of my work relies. Stephanie, it has been a pleasure to work with you and if I'm very fortunate I will have the opportunity to do so again in the future.

Endless thanks to my office mates in the NCE building for answering all of my biology, chemistry and physical oceanography questions, and for putting up with my hyper and stressed-out self. A special thanks to the Aussies. Your unique sense of humor never failed to cheer me up when things were going to heck in the lab. As a special note to Andrew, people watching is just not the same without you.

To the office staff of Earth and Ocean Sciences. I greatly appreciate all of your help throughout my stay at UBC. Special thanks to Alex and Carol for keeping me in touch when I ran off to Montreal.

Lastly to my friends and family. Thank you for your love and support over the seemingly endless years of schooling. I may not have said it often enough but I love you all very much. Now just a warning. The thesis may be done but the science continues. If you haven't guessed by now I actually like the endless hours in the lab, the stress when things don't work and the thrill when they do, the field work and of course the conferences (Hawaii...need I say more). For better or for worse, I'm in this for life.

Just one last thing. It is now OK to use the "T" word.

1. Palaeoceanography of the Northeastern Pacific Ocean off Vancouver Island, Canada

1.1 Introduction

With the recognition that the activities of mankind are impacting Earths climate (IPCC, 2001) there has been renewed interest in the study of natural climate change, its magnitude, the speed at which it occurs and the response of various earth systems, for example the biosphere and cryosphere, to such change. Some of the best records of climate variability over the past 500,000 years have been obtained from the Greenland and Antarctica ice sheets (e.g., Barnola et al., 1987; Dansgaard et al., 1993; Petit et al., 1999). Marine sediment cores are another source of information and their analysis provides a better global coverage, although obtaining high resolution data equivalent in quality to information obtained from ice cores is often hindered by bioturbation coupled with slow sedimentation that characterize the majority of sedimentary deposits on the sea floor.

Many initial palaeoceanographic studies focused on the Atlantic Ocean and in particular the North Atlantic, in part because this is a principal location of deepwater formation at present. In rather stark contrast, less work has been conducted in the Pacific Ocean and very little in the Subarctic Northeast Pacific. Only four palaeoceanographic studies exist for the Gulf of Alaska (Zahn et al., 1991; Sabin and Pisias, 1996; de Vernal and Pedersen, 1997; McDonald et al., 1999), and even fewer exist for the region off western Canada. Only two cores have been studied in any detail (TT39-PC17 and TT39-PC12; Sabin and Pisias, 1996) and these were collected from sites located hundreds of kilometres offshore. There have been no palaeoceanographic studies of the upwelling region off Vancouver Island, that is until very recently (Kienast and McKay, 2002).

The northeast Pacific Ocean is a region of primary interest for a number of reasons:

i) The North Pacific is the terminus of deep water circulation. As such, the deep waters in the region are a reservoir of substantial amounts of CO_2. Depending on various factors (e.g., primary productivity, upwelling, sea-surface temperature, wind mixing) the North Pacific could be a source or sink for atmospheric CO_2. Recent work has suggested that the North Pacific was a significant CO_2 sink from 1979 to 1992 (Wong et al., in review), although other studies suggest the exact opposite (e.g., Stephens et al., 1995). In the Pleistocene, periods of high diatom productivity caused reduced $[CO_2](aq)$ in mixed-layer (McDonald et al., 1999) and could potentially have driven the uptake of atmospheric CO_2.

ii) The North Pacific is a region of intermediate water formation and ventilation. Changes in the ventilation rate of intermediate waters could have influenced the intensity (i.e., degree of oxygen depletion) of the oxygen minimum zone (OMZ) throughout the North Pacific. This has important implications for the oceanic nitrogen cycle (i.e., nitrate availability) and in turn ocean productivity (Ganeshram et al., 1995).

iii) The California Current System (CCS), which extends from Vancouver Island, Canada to Baja, California, is one of four major eastern boundary current systems. Upwelling of nutrient-rich waters causes these regions to be important locations of organic matter production, export and burial. However, because upwelling is primarily wind-driven, it is highly susceptible to even minor changes in wind strength and atmospheric circulation patterns. It is thus reasonable to assume that the large scale changes in atmospheric circulation patterns that accompanied glaciations (COHMAP, 1988) would have had a significant impact on upwelling and thus ocean productivity. Such was the case off Oregon and northern California during the last glacial (Lyle et al., 1992; Dean et al., 1997; Ortiz et al., 1997; Mix et al., 1999). In turn, there is the potential that atmospheric CO_2 concentrations could have been affected.

iv) Changes in sea surface temperatures in the north Pacific, for example the 6°C increase observed off Vancouver Island during the last deglacial (Kienast and McKay, 2002), could impact the hydrological budget of North America and more generally that of the northern hemisphere (Peteet et al., 1997).

This thesis presents the first comprehensive palaeogeochemical investigation of the late Pleistocene to Holocene evolution of the northeast Pacific Ocean in the area west of Vancouver Island, Canada. As such, it addresses directly the existing dearth of information on the palaeoceanography of this important but understudied region.

1.2 The study area

Sediment cores were collected during a 1996 cruise of the Canadian Coast Guard research vessel the John Tully. Box- and multicores were collected at six stations (01, 02, 04, 05, 06 and 09; Fig. 1.1). Piston cores were also collected at stations 02, 05, 06 and 09 (Fig. 1.1). A second suite of piston cores from the same area were made available by Dr. George Spence of the University of Victoria. Two of these cores (Tul96-03 and Tul96-05; Fig. 1.1) were sampled for palaeoceanographic analysis. Core locations and a summary of the data available for each core are provided in Table 1.1.

Preliminary analyses revealed that only piston cores JT96-09pc and JT96-02pc were suitable for in depth palaeoceanographic analysis of the last deglaciation and Holocene. Piston Core JT96-05pc contained too many sandy turbidites while Piston Core JT96-06pc did not yield a recognizable glacial-interglacial oxygen-isotope stratigraphy that is critical for palaeoceanographic studies. Analysis of Piston Core Tul96-03 ceased when it became apparent from the $\delta^{18}O$ measurements made on benthic foraminifera that a significant portion of the core top, including all of the Holocene, had been lost during collection of the core. Piston Core Tul96-05 also contained a large time gap from ~10.9 to 27.9 calendar kyr B.P., and this limited its usefulness.
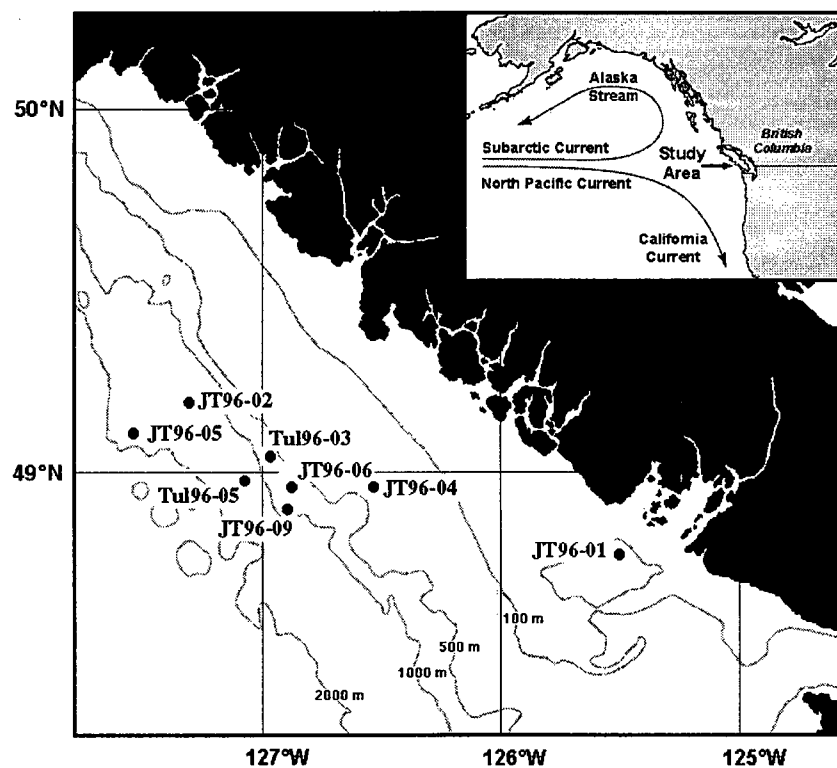
Fig. 1.1. The study area off the west coast of Vancouver Island, British Columbia, Canada (Inset) showing the locations where cores were collected. Further details can be found in Table 1.1.

Table 1.1. List of the cores collected, their geographic locations and water depths, as well as the various types of data provided in the appendices.

Station[1]	Location	Water Depth (m)	Sediment Core Type[2]	Stratigraphic Description	CTD data	Dissolved O_2 data	Magnetic Susceptibility	^{14}C data	^{210}Pb data	$d^{13}C$ and $d^{18}O$ for foraminifera	Geochemical Data
JT96-01	48° 45.945' N 125° 29.566' W	120	mc	Appendix 2	Appendix 3	Appendix 4	none	Appendix 6	Appendix 7	none	Appendix 9
JT96-04	49° 00.705' N 126° 49.818' W	407	mc	Appendix 2	Appendix 3	Appendix 4	none	none	none	none	Appendix 11
JT96-06	48° 58.727' N 126° 52.678' W	721	bc, mc, pc	Appendix 2 (bc only)	Appendix 3	Appendix 4	Appendix 5	none	none	Appendix 8	Appendix 13
JT96-09	48° 54.76' N 126° 53.44' W	920	mc, pc	Appendix 2	Appendix 3	Appendix 4	Appendix 5	Appendix 6	Appendix 7	Appendix 8	Appendix 14
JT96-02	49° 12.805' N 127° 18.567' W	1340	mc, pc	Appendix 2	Appendix 3	Appendix 4	Appendix 5	Appendix 6	Appendix 7	Appendix 8	Appendix 10
JT96-05	49° 07.910' N 127° 33.115' W	1750	bc, pc, tc	Appendix 2 (bc only)	none	Appendix 4	Appendix 5	Appendix 6	none	none	Appendix 12
Tul96-03	49° 03.33' N 126° 58.20' W	650	tc, pc	none	none	none	none	none	none	Appendix 8	Appendix 15
Tul96-05	49° 00.01' N 127° 03.27' W	1390	tc, pc	none	none	none	none	Appendix 6	none	Appendix 8	Appendix 16

[1] Data from the following cores were used in this thesis:

JT96-09pc (Chapters 2 and 3)

JT96-01mc, JT96-04mc, JT96-06bc, JT96-09mc, JT96-02mc and JT96-05bc (Chapter 4)

JT96-02pc (Chapter 5)

[2] mc - multicore, bc - box core, pc - piston core and tc - trigger core.

The study area is located at the northern end of the California Current System (CCS) where the eastward flowing Subarctic and North Pacific currents split into the northward flowing Alaska Current and southward flowing California Current (Fig. 1.1). It is situated in a transitional zone where even minor changes in atmospheric and oceanic circulation might influence sea surface temperature (SST), salinity, water column stratification, as well as primary productivity via changes in nutrient supply. Given the appropriate conditions, these changes may be recorded in the underlying sediments. However, palaeoceanographic studies in the region have been hindered by the occurrence of turbidites and the scarcity of foraminifera which makes the development of a robust chronostratigraphy difficult (Zahn et al., 1991). Furthermore, the character of sedimentation on the Vancouver Island Continental Margin has changed dramatically over time. During the last glacial piedmont-type glaciers extended on to the shelf as far as the shelf edge west of the Strait of Juan de Fuca and almost to the shelf edge west of Barkley Sound (Herzer and Bornhold, 1982). These glaciers reached their maximum extent between ~15 and 14 ^{14}C kyr and then began to rapidly retreat (Clague and James, 2002). Coincident with deglaciation, sedimentation rates on the slope (Station JT96-09) increased substantially (i.e., from ~47 cm/kyr up to 169 cm/kyr). Ice had retreated from the shelf by ~13 ^{14}C kyr (Blaise et al., 1990; Josenhans et al., 1995). This was a period of global sea level rise; however, as a result of isostatic rebound the land rose and relative sea level was ~150 m lower than at present between at ~10 ^{14}C kyr B.P. (Josenhans et al., 1995; Barrie and Conway, 1999). Modern sea level was not established until ~9.1 ^{14}C kyr (Josenhans et al., 1995). There was a substantial decrease in the sedimentation rate on the shelf as sea level rose due to trapping of sediments within the fjords of Vancouver Island and winnowing by waves and currents (Bornhold and Yorath, 1984). As a result, Holocene sediments on the inner and mid-shelf typically comprise sand and gravel lag deposits, while on the outer shelf Pleistocene clays are mantled by thin layers ($\leq$ 30 cm) of sandy sediments (Bornhold and Barrie, 1991; Bornhold and Yorath, 1984). Modern sedimentation rates on the upper slope are also low (<2 cm/kyr; Stations JT96-04 and JT96-06).

6

1.3 Objectives

A number of specific question are addressed in this thesis:

i) How has primary productivity, export productivity, and carbon burial on the Vancouver Island Continental Margin varied on glacial-interglacial and shorter timescales?

ii) Has nutrient availability and utilization varied over the last 16 kyr? If so, can these variations be related to changes in upwelling and/or climatic conditions?

iii) At present, the region is characterized by a moderately intense oxygen minimum zone (OMZ) (~ 0.3 ml/l O_2 at 920 m water depth). Has the intensity (i.e., degree of oxygen-depletion), thickness and/or depth of the OMZ varied over time. If so, have denitrification within the water column and organic carbon burial been affected? Are variations in OMZ intensity related to changes in intermediate water mass hydrography (i.e., ventilation) and/or changes in the settling flux of organic matter (i.e., primary productivity)?

iv) How does the palaeoceanography of the study area compare with other regions within the California Current System? What do the similarities and differences tell us about the response of the northeast Pacific to climate change?

1.4 Presentation of results

This thesis has been written in paper format. Each chapter, excluding the introduction and summary (i.e., Chapters 1 and 6, respectively), represents one paper that deals with specific palaeoceanographic questions.

Chapter 2 (McKay et al., in press) presents an investigation of the nature of organic matter accumulation on the continental slope (Piston Core JT96-09, 920 m water depth) off

Vancouver Island. Both concentration and mass accumulation rates of organic carbon in marine sediments are commonly used as palaeoproductivity proxies (e.g., Pedersen, 1983; Sarnthein et al., 1988). However, marine deposits often contain substantial quantities of terrestrial organic matter, particularly along the continental margin (e.g., Prahl et al., 1994). It is therefore necessary to quantify the fraction of marine organic matter if variations in primary and export production are to be inferred. Furthermore, the relative abundances of marine and terrestrial organic matter must be known if other data, for example the $\delta^{13}C$ of organic carbon ($\delta^{13}C_{org}$) and $\delta^{15}N$ of bulk sediments, are to be correctly interpreted. The identification and quantification of terrestrial organic matter are made in Chapter 2 using a variety of data (i.e., C_{org}/N ratios, C and N isotope data, n-alkane concentrations and radiocarbon ages of bulk organic matter). The total organic carbon data are then corrected for the terrigenous input to yield the accumulation rate of marine organic carbon for the past 16 kyr B.P.. These results are compared with other palaeoproductivity records based on the mass accumulation rates of biogenic barium and opal, as well as the abundance of C_{37} alkenones. It should be noted that the analysis of biomarkers (i.e., alkenones and n-alkanes) was conducted in co-operation with S. Kienast at the University of British Columbia.

Chapter 3 investigates whether the intensity (i.e., degree of oxygen-depletion) of the oxygen minimum zone (OMZ) off Vancouver Island has changed in the past 16 kyr B.P. and if so, why. Piston Core JT96-09, that comes from the most intense portion of the modern OMZ (920 m water depth), is studied. Along the southern portion of the California Current System the OMZ has fluctuated on glacial-interglacial and shorter timescales (Keigwin and Jones, 1990; Behl and Kennett, 1996; Dean et al., 1997; Ganeshram et al., 1995; Cannariato and Kennett, 1999; Zheng et al., 2000). Redox-sensitive trace metal and benthic foraminifera species data presented in this chapter suggest that the OMZ off Vancouver Island has also fluctuated. Two possible causes are discussed: i) a change in ventilation of intermediate waters, and/or ii) a change in primary productivity and the subsequent export and degradation of the organic matter. Radiocarbon dating of coeval benthic and planktonic foraminifera is

employed to assess whether fluctuations in OMZ intensity are the result of ventilation changes. This method assumes that the apparent age of surface waters, recorded by planktonic foraminifera, have not changed while the age of intermediate waters, which is recorded by benthic foraminifera, might have varied. The accumulation rate of marine organic carbon, determined in Chapter 2, is employed as a proxy for palaeoproductivity. The possibility that organic carbon accumulation is influenced by OMZ intensity is also discussed.

In Chapter 4 the accumulation of redox-sensitive trace metals (Re, U, Cd, Mo and Ag) in near-surface sediments deposited on the continental margin off Vancouver Island is investigated. Data for multicores and boxcores from six stations (01, 02, 04, 06, 05 and 09; Fig. 1.1) are presented. The sedimentary concentrations of such trace metals can be influenced by redox conditions within the sediment. Sedimentary redox conditions are in turn influenced by organic carbon flux to the sediment and oxygen concentrations in the overlying bottom water. Changes in the accumulation of redox-sensitive elements are thus commonly used to identify changes in palaeoproductivity and/or bottom water oxygenation over time (e.g., Crusius et al., 1999; Yarincik et al., 2000; Adelson et al., 2001; Pailler et al., 2002). However, a variety of other factors (e.g., sedimentation rate, metal source and post-depositional migration) can also influence metal concentrations. An understanding of the key processes that govern such accumulation is required if trace metal palaeo-records are to be correctly interpreted.

In Chapter 5 data for Piston Core JT96-02 (1340 m water depth) are presented. The deglacial clay in this core contains numerous centimetre-scale, organic- and sulphide-rich layers. A 16 cm interval containing three such layers was sampled at very high resolution (3 mm spacing) and a variety of geochemical measurements were made. Three issues are addressed: i) what was the nature of deglacial sedimentation on the Vancouver Island Continental Margin, ii) why did the sulphide-rich layers form, and iii) what factors controlled the accumulation of redox-sensitive trace metals in these layers. The final conclusion is that

9

an abrupt increase in sedimentation rate due to the episodic deposition of thin turbidites was ultimately responsible for the development of anoxic conditions and formation of the sulphide-layers. There was no apparent decrease in bottom water oxygen concentration or increase in organic carbon accumulation. Thus, this chapter highlights the dangers of using trace metals as palaeo-proxies for bottom water ventilation and organic carbon flux.

Each of chapters 2 through 5 has been submitted as a stand-alone paper, and four different journals have been targeted as venues for publication. This approach unavoidably leads to some overlap in the chapters, which is primarily limited to description of the study area and the hydrography of the region.

1.5 References

Adelson, J.M. Helz, G.R., Miller, C.V., 2001. Reconstructing the rise of recent coastal anoxia; molybdenum in Chesapeake Bay sediments. Geochimica et Cosmochimica Acta 65, 237-252.

Barnola, J.M., Raynaud, D., Korotkevich, Y.S., Lorius, C., 1987. Vostok ice core provides 160,000-year record of atmospheric CO_2. Nature 329, 408-414.

Barrie, J.V., Conway, K.W., 1999. Late Quaternary glaciation and postglacial stratigraphy of the Northern Pacific margin of Canada. Quaternary Research 51, 113-123.

Behl, R.J., Kennett, J.P., 1996. Brief interstadial events in the Santa Barbara Basin, NE Pacific, during the past 60 kyr. Nature 379, 243-246.

Blaise, B., Clague, J.J., Mathewes, R.W., 1990. Time of maximum Late Wisconsin glaciation, west coast of Canada. Quaternary Research 34, 282-295.

Bornhold, B.D., Barrie, J.V., 1991. Surficial sediments on the western Canadian continental shelf. Continental Shelf Research 11, 685-699.

Bornhold, B.D., Yorath, C.J., 1984. Surficial geology of the continental shelf, northwestern Vancouver Island. Marine Geology 57, 89-112.

Cannariato, K.G., Kennett, J.P., 1999. Climatically related millenial-scale fluctuations in strength of California margin oxygen-minimum zone during the past 60 k.y.. Geology 27, 975-978.

Clague, J.J., James, T.S., 2002. History and isostatic effects of the last ice sheet in southern British Columbia. Quaternary Science Reviews 21, 71-87.

COHMAP Members, 1988. Climatic changes of the last 18,000 years: Observations and model simulations. Science 241, 1043-1052.

Crusius, J., Pedersen, T.F., Calvert, S.E., Cowie, G.L., Oba, T., 1999. A 36 kyr geochemical record from the Sea of Japan of organic matter flux variations and changes in intermediate water oyxgen concentrations. Paleoceaography 14, 248-259.

Dansgaard, W., Johnsen, S.J., Clausen, H.B., Dahl-Jensen, D., Gundestrupt, N.S., Hammer, C.U., Hvidberg, C.S., Steffensen, J.P., Sveinbjornsdottier, A.E., Jouzel, J., Bond, G., 1993. Evidence for general instability of past climate from a 250-kyr ice-core record. Nature 364, 218-220.

Dean, W.E., Gardner, J.V., Piper, D.Z., 1997. Inorganic geochemical indicators of glacial interglacial changes in productivity and anoxia on the California continental margin. Geochemica et Cosmochimica Acta 61, 4507-4518.

de Vernal, A., Pedersen, T.F., 1997. Micropaleontology and palynology of core PAR87A-10: A 23,000 year record of paleoenvironmental changes in the Gulf of Alaska, northeast North Pacific. Paleoceanography 12, 821-829.

11

Ganeshram, R.S., Pedersen, T.F., Calvert, S.E., Murray, J.W., 1995. Large changes in oceanic nutrient inventories from glacial to interglacial periods. Nature 376, 755-758.

Herzer, R.H., Bornhold, B.D., 1982. Glaciation and post-glacial history of the continental shelf off southwestern Vancouver Island, British Columbia. Marine Geology 48, 285-319.

Josenhans, H.W., Fedje, D.W., Conway, K.W., Barrie, J.V., 1995. Post glacial sea levels on the Western Canadian continental shelf: evidence for rapid change, extensive subaerial exposure and early human habitation. Marine Geology 125, 73-94.

Keigwin, L.D., Jones, G.A. 1990. Deglacial climatic oscillations in the Gulf of California. Paleoceanography 5, 1009-1023.

Kienast, S.S., McKay, J.L., 2001. Sea surface temperature in the subarctic northeast Pacific reflect millennial-scale climate oscillations during the last 16 kyrs. Geophysical Research Letters 28, 1563-1566.

Lyle, M., Zahn, R., Prahl, F. Dymond, J., Colier, R. Pisias, N., Suess, E., 1992. Paleoproductivity and carbon burial across the California Current: The mulitracers transect, 42°N. Paleoceanography 7, 251-272.

McDonald, D., Pedersen, T.F, Crusius, J., 1999. Multiple late Quaternary episodes of exceptional diatom production in the Gulf of Alaska. Deep Sea Research II 46, 2993-3017.

McKay, J.L., Pedersen, T.F., Kienast, S.S., in press. Organic carbon accumulation over the last 16 kyr off Vancouver Island, Canada: Evidence for increased marine productivity during the deglacial. Quaternary Science Reviews.

Mix, A.C., Lund, D.C., Pisias, N.G., Boden, P., Bornmalm, L., Lyle, M., Pike, J., 1999. Rapid climate oscillation in the northeast Pacific during the last deglaciation reflect northern and southern hemisphere sources. In: Mechanisms of Global Climate Change at Millennial Time Scales, Geophysical Monograph 112, 127-148.

Ortiz, J., Mix, A., Hostetler, S., Kashgarian, M., 1997. The California Current of the last glacial maximum: Reconstruction at 42°N based on multiple proxies. Paleoceanography, v. 12, p. 191-205.

Pailler, D., Bard, E., Rostek, F., Zheng, Y., Mortlock, R., van Geen, A., 2002. Burial of redox sensitive metals and organic matter in the equatorial Indian Ocean linked to precession. Geochimica et Cosmochimica Acta 66, 849-865.

Pedersen, T.F., 1983. Increased productivity in the eastern equatorial Pacific during the last glacial maximum (19,000 to 14,000 yr B.P.). Geology 11, 16-19.

Peteet, D., Genio, A.D., Lo, K.K.W., 1997. Sensitivity of the northern hemisphere air temperatures and snow expansion to North Pacific sea surface temperature in the Goddard Institute for space studies general circulation model. Journal of Geophysical Research 102, 23781-23791.

Petit, J.R., Jouzel, J., Raynaud, D., Barkov, N.I., Barnola, J.-M., Basile, I., Benders, M., Chappellaz, J., Davis, M., Delaygue, G., Delmotte, M., Kotlyakov, V.M., Legrand, M., Lipenkov, V.Y., Lorius, C., Pepin, L., Ritz, C., Saltzman, E., Stievenard, M., 1999. Climate and atmospheric history of the past 420,000 years from the Vostok ice core, Antarctica. Nature 399, 429-413.

Prahl, F.G., Ertel, J.R., Goni, M.A., Sparrow, M.A., Eversmeyer, B., 1994. Terrestrial organic carbon contributions to sediments on the Washington margin. Geochimica et Cosmochimica Acta 58, 3035-3048.

Sabin, A.L., Pisias, N.G., 1996. Sea surface temperature changes in the northeastern Pacific Ocean during the past 20,000 years and their relationship to climate change in northwestern North America. Quaternary Research 46, 48-61.

Sarnthein, M., Winn, K., 1990. Reconstruction of low and mid latitude export productivity, 30,000 years B.P. to present: Implications for control of global carbon reservoirs. In: Climate-Ocean Interaction (ed. M.E. Schlesinger), Klewer Academic Publishers, p. 319-342.

Stephens, M.P., Samuels, G., Olson, D.B., Fine, R.A., Takahashi, T., 1995. Sea-air flux of CO_2 in the North Pacific using shipboard and satellite data. Journal of Geophysical Research 100, 13571-13583.

Wong, C.S., Chan, Y.-H., Feely, R.A., Goyet, C., Inoue, H., in review. North Pacific Ocean as a significant CO_2 sink during 1979-1992. Science.

Yarincik, K.M., Murray, R.W., Lyons, T.W., Petersen, L.C., Haug, G.H., 2000. Oxygenation history of bottom waters in the Cariaco Basin, Venezuela, over the past 578,000 years: Results from redox-sensitive metals (Mo, V, Mn, and Fe). Paleoceanography 15, 593-604.

Zahn, R., Pedersen, T.F., Bornhold, B.D., Mix, A.C., 1991. Water mass conversion in the glacial subarctic Pacific (54°N, 148°W): Physical constraints and the benthic-planktonic stable isotope record. Paleoceanography 6, 543-560.

Zheng, Y., van Geen, A., Anderson, R.F., Gardner, J.V., Dean, W.E., 2000. Intensification of the northeast Pacific oxygen minimum zone during the Bolling-Allerod warm period. Paleoceanography 15, 528-536.

2. Organic Carbon Accumulation over the Last 16 kyr off Vancouver Island, Canada: Evidence for Increased Marine Productivity during the Deglacial

2.1 Introduction

The history of palaeoproductivity, or more correctly export production, can be inferred using a variety of proxies such as the abundance and/or mass accumulation rate of organic carbon (e.g., Pedersen, 1983; Sarnthein et al., 1988), biogenic barite (e.g., Schmitz, 1987; Dymond et al., 1992) and opal (e.g., Lyle et al., 1992; Gardner et al., 1997) in marine sediments, as well as the concentrations of various marine biomarkers (e.g., Prahl et al., 1989; Jasper and Gagosian, 1993; Ohkouchi et al., 1997; Schubert et al., 1998; Werne et al., 2000). However, each proxy has its own particular set of problems and limitations. For example, proxies may be preferentially preserved when sedimentation rates are high.

Palaeoproductivity estimates based on the amount and/or accumulation rate of organic carbon are further complicated by the presence of terrestrial organic matter which can constitute a large fraction of nearshore, non-deltaic marine sediments (> 50%; Prahl et al., 1994). Even deep ocean sediments in some areas can have a significant terrestrial component (e.g., 20%) due to aeolian transport (Prahl et al., 1989; Ohkouchi et al., 1997) and ice-rafting (Villanueva et al., 1997a). It is therefore necessary to estimate the relative abundance of marine and terrestrial organic matter when using organic carbon as a palaeoproductivity proxy. This information is also required if bulk, rather than compound specific, $\delta^{13}C$ values of organic matter are to be used in the estimation of dissolved CO_2 concentrations (e.g., Rau et al., 1991; Rau, 1994), and if sedimentary $\delta^{15}N$ data are to be correctly interpreted.

Little is known about palaeoproductivity and marine organic matter accumulation on the Western Canadian Continental Margin, in part because it has been extremely difficult to collect cores that preserve a continuous record of hemipelagic sedimentation. In this paper,

we present the first estimates of marine and terrestrial organic matter accumulation on the continental slope west of Vancouver Island for the last 16 kyr. These results are part of a larger IMAGES-program study of productivity history for the Late Quaternary along the western margin of the Americas. The study area is located at the northern end of the California Current System (CSS) off Vancouver Island, British Columbia, Canada (48° 54' N, 126° 53' W; Fig. 2.1). This region sits within a transition zone where the eastward-flowing Subarctic and North Pacific currents split into the northward flowing Alaska Current and southward flowing California Current (Fig. 2.1; Thomson, 1981). At present, the area immediately west of Vancouver Island is characterized by high primary productivity driven by seasonal (spring - summer) wind-induced upwelling which is related to the northerly position (38°N) of the North Pacific High (Thomas et al., 1994; Hickey, 1998). The strength of this upwelling is determined by the strength of the northerly, alongshore wind that is in turn controlled by the atmospheric pressure gradient between the land and ocean (Bakun, 1990). In winter, when the North Pacific High shifts southward to ~28°N and the Aleutian Low influences the region there is a reversal of the wind direction and cessation of upwelling.

Palaeo-evidence suggests that during the last glacial maximum (LGM) the North Pacific High was weaker and displaced south of its present position (COHMAP, 1988; Thunell and Mortyn, 1995; Mortyn et al., 1996; Sabin and Pisias, 1996; Doose et al., 1997). As a result, upwelling was substantially reduced or non-existent along the central and northern portions of the CCS and in turn export productivity was lower (Dymond et al., 1992; Lyle et al., 1992; Sancetta et al., 1992; Ortiz et al., 1997; Dean and Gardner, 1998; Mix et al., 1999). However, in this paper we show that off Vancouver Island the mass accumulation rate of total organic carbon was higher during the late glacial in comparison to present. To explain the contrast with regions directly to the south a variety of geochemical data are used to characterize the type of organic matter and then the terrigenous input is then quantified using C- and N-isotopic data. The concentration and mass accumulation rate of

total organic carbon are corrected for the input of terrestrial organic matter to yield a palaeo-record of marine organic matter accumulation over the last 16 kyr. Finally, to circumvent concerns that variable preservation may have influenced the organic carbon record a variety of other palaeoproductivity proxies (i.e., biogenic barium, opal and C_{37} alkenone contents) are presented for comparison.

2.2 Materials and methods

Sediment cores were collected from the continental slope off the west coast of Vancouver Island, British Columbia, Canada during a 1996 Canadian Joint Global Ocean Flux Study (CJGOFS) cruise. Data are presented here for a 374 cm long piston core (JT96-09pc) and a corresponding 40 cm long multicore (JT96-09mc), both collected at the same site (48° 54' N, 126° 53' W; Fig. 2.1) from a water depth of 920 m. The multicore and upper 51 cm of the piston core are composed of a homogeneous, carbonate-poor, olive-green mud. In the piston core this mud is underlain by 85 cm of gray-green clay at the base of which is a 16 cm thick sandy turbidite. The remainder of the core (222 cm) is composed of a dense, gray clay. The sediment-water interface was intact in the multicore and a comparison of geochemical data from the multicore and piston core suggests that ~12 cm, not 20 cm as stated in Kienast and McKay (2001), were lost off the top of the latter during its collection. As a result, piston core depths have been corrected for this loss (+12 cm) and for the presence of the turbidite (-16 cm). Records from the two cores were then merged to yield a composite record for site JT96-09.

The age model for JT96-09 is based on nine accelerator mass spectrometry (AMS) radiocarbon dates for mixed assemblages of planktonic foraminifera (*N. pachyderma* right- and left-coiling and *G. bulloides*; Table 2.1). The radiocarbon age of bulk organic carbon in eight samples was also measured, following removal of carbonate material with dilute phosphoric acid and preheating to 150°C to drive off adsorbed water. All radiocarbon dating

16
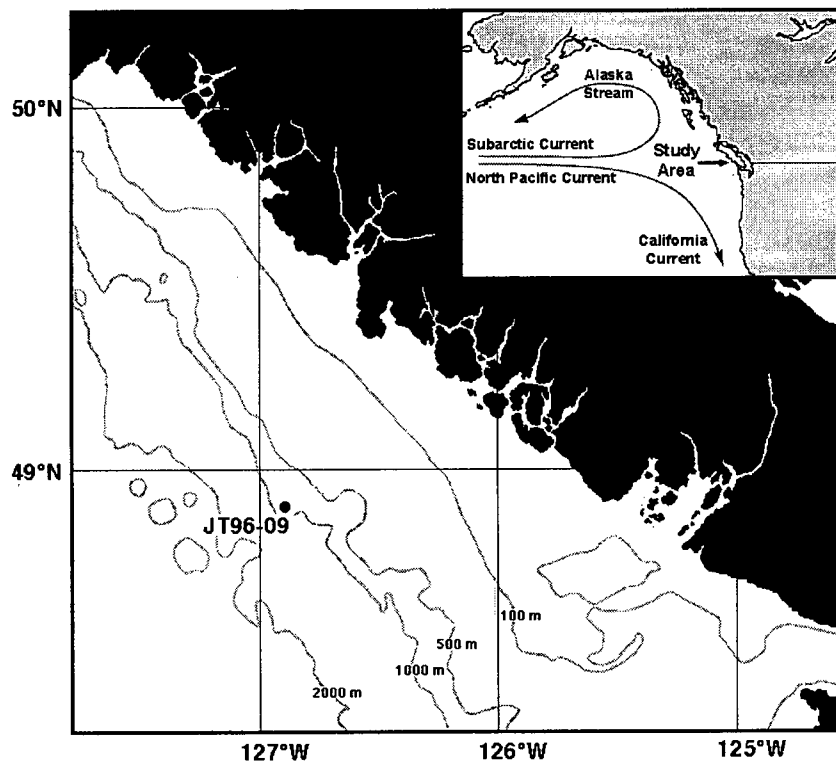
Fig. 2.1. The study area is located off the west coast of Vancouver Island, British Columbia, Canada (Inset). Sediment cores were collected from Station JT96-09 that is located on the continental slope at a water depth of 920 m.

was conducted at the Lawrence Livermore National Laboratory. Results for the planktonic foraminifera were converted from radiocarbon to calendar years using CALIB 4.3 (Stuiver et al., 1998) assuming a reservoir age of 800 years for radiocarbon ages younger than 12 kyr and 1100 years for those dates that are older (Kienast and McKay, 2001). It should be noted that the age model for the Holocene used here is slightly different than that in Kienast and McKay (2001) as a result of the new estimate of sediment loss during coring. Unless otherwise stated all dates presented in this paper are in calendar years B.P.

Alkenone-based palaeothermometry conducted on Core JT96-09 yielded evidence of rapid sea-surface temperature (SST) fluctuations of during the last deglacial (Fig. 2.2a; Kienast and McKay, 2001). The pattern of deglacial SST fluctuations is remarkably similar to temperature fluctuations in the GISP-2 ice core record suggesting that the Bølling-Allerød and Younger Dryas events are recorded in Core JT96-09 (Kienast and McKay, 2001). More importantly these events appear to be nearly synchronous with those in GISP-2 and this allows the palaeo-records from Core JT96-09 to be placed in a more global context. However, the match between the GISP-2 and JT96-09 records is not perfect (see Kienast and McKay, 2001). Offsets between the two records, in some instances in the order of hundreds of years, most probably reflect errors in the age model of Core JT96-09 resulting from: i) problems inherent to radiocarbon dating (e.g., ^{14}C plateaus); ii) a poorly known reservoir age; iii) bioturbation, although the effects of this are limited by the high sedimentation rates during the deglacial; and iv) large errors associated with the radiocarbon dating of small samples.

Sedimentation rates, that were calculated by assuming linearity between age picks, range from 5 cm/kyr during the Holocene to between 14 and 169 cm/kyr during the deglacial. The sedimentation rate in the late glacial is ~47 cm/kyr. Mass accumulation rates (MARs) were calculated as the product of linear sedimentation rate (cm/kyr) and sediment dry bulk density (g/cm^3). The latter was determined using chlorinity data and a pore water salinity of 35 to estimate porosity, and by assuming an average grain density of 2.5 g/cm^3.

Core JT96-09 was subsampled at 5 cm intervals for geochemical analysis, yielding a resolution of 1200 years for the Holocene and from <100 to 350 years for the period from 10 to 16 kyr B.P. Samples were prepared for geochemical analysis by freeze-drying followed by hand grinding with an agate pestle and mortar. Total carbon (TC) and total nitrogen (TN) were measured by high temperature combustion using a Carlo Erba 1500 CNS analyzer. Two marine sediment standards (PACS-1 and MESS-1; National Research Council of Canada) were analyzed with each batch of samples and yielded relative standard deviations (RSD, 1σ) of 3 % and 5 % for carbon and nitrogen, respectively. The amount of carbonate carbon (i.e., inorganic carbon, IC) was measured by coulometry. Results for a calcium carbonate standard yielded an RSD of ~1 % (i.e., 11.93 ± 0.13, n=141). The amount of organic carbon (OC) was calculated by difference (OC = TC - IC) and the aggregate RSD for these data is ~4 %.

Stable isotope data were obtained by continuous-flow mass spectrometry using a Fisons NA 1500 elemental analyzer attached to a VG Prism mass spectrometer. Samples for carbon isotopic analysis of organic matter ($\delta^{13}C_{org}$) were pretreated with 10% HCl to remove carbonate material and then dried at 50°C overnight. These samples were not washed with distilled water prior to drying. Nitrogen isotope results ($\delta^{15}N$) were obtained for untreated bulk sediment samples. Data are reported in the standard δ-notation relative to VPDB for carbon and atmospheric N_2 for nitrogen. The isotopic results for an in-house sediment standard are ± 0.1‰ for carbon and ± 0.2‰ for nitrogen. Repeat analyses of samples are generally better than this.

Total Ba and Al concentrations were measured by X-ray fluorescence (XRF) according to the method of Calvert (1990). The concentration of biogenic barium was calculated using Equation 2.1, following the method of Dymond et al. (1992):

$$\text{Bio-barium} = \text{Total Ba} - (\text{Al} \times \text{Ba/Al}_{\text{lith}}) \tag{2.1}$$

A Ba/Al lithogenic ratio (Ba/Al$_{lith}$) of 0.0027 was employed. This value is significantly lower than the average Ba/Al$_{lith}$ ratio of crustal rocks (0.0075; Dymond et al., 1992); however, the latter can vary greatly depending on the composition of the sediment source (e.g., 0.005 to 0.010; Taylor and McLennan, 1985). The geology of Vancouver Island is complex and includes a mixture of metamorphic, igneous and sedimentary rock types (Yorath and Nasmith, 1995); thus it is not possible to chose a Ba/Al$_{lith}$ ratio representative of any particular rock type. Rather, the Ba/Al$_{lith}$ ratio used here (i.e., 0.0027) was determined from an exponential regression of the Ba/Al ratios of surface sediments versus water depth (Chapter 4). This method assumes that the fraction of biogenic Ba increases seaward and that close to land (i.e., ~0 m water depth) all of the Ba is terrigenous in origin. The low Ba/Al$_{lith}$ estimated using this regression method was confirmed by chemically extracting the bio-barium using a 2M solution of NH_4Cl and then measuring the barium content of the residue (i.e., the lithogenic Ba) by XRF (Chapter 4). While the average Ba/Al$_{lith}$ ratio is slightly higher (0.0033) using this method, possibly due to incomplete dissolution of the bio-barium, the results show that there is no change in the ratio over the last 16 kyr B.P.

Biogenic silica (i.e., opal) content was determined by alkaline dissolution following the procedure of Mortlock and Froelich (1989). The concentration of Si was measured by spectrophotometry and then converted to wt.% opal by multiplying by 2.4 (this assumes 10% water in opal; Mortlock and Froelich, 1989). The RSD (1σ) for two in-house standards (SNB and JV5) and repeat samples was ≤4 %. However, the precision of the method is much poorer at opal concentrations <10 % (R. Ganeshram, pers. comm.), possibly due to the dissolution of volcanic glass and clay minerals.

Organic geochemical analysis was carried out using the solvent extraction method of Villanueva et al. (1997b). The organic fraction was extracted from 3 to 10 mg of freeze-dried sediment using dichloromethane (CH_2Cl) followed by saponification with a mixture of 6 % KOH in methanol. The organic fraction was then extracted with n-hexane and run through a silica column. The fraction containing the n-alkanes and C$_{37}$ alkenones was eluted

from the column with a mixture of dichloromethane and n-hexane. Analyses were made by manual-injection on an HP 5880 gas chromatograph. The n-alkanes and C_{37} alkenones were identified using an internal standard (i.e., mixture of C_{19}, C_{36} and C_{40}), and the identification of C_{37} alkenones was confirmed by GC-MS. The concentrations of C_{29} n-alkanes and C_{37} alkenones were calculated by assuming that their concentrations were proportional to the chromatogram peak area and that the response factor was the same as for the internal standard. Only the di- and tri-unsaturated C_{37} alkenones were quantified, as the amount of tetra-unsaturated C_{37} alkenone was generally below the detection limit of 10 ng.

2.3 Results

2.3.1 Radiocarbon data for bulk organic carbon

The age of bulk organic matter ranges from 9920 to 24500 ^{14}C years (Table 2.1). If most of the organic carbon in a sample is of marine origin and formed contemporaneously with planktonic foraminifera shells, the difference between the organic carbon and shell ages should be small. The greater the input of old organic carbon, the larger this difference will be. For the two youngest samples the radiocarbon age difference is less than 2000 ^{14}C years, but for all other samples it is substantially higher (3435 to 12370 ^{14}C kyrs; Table 2.1). These results suggest that between 12.3 and 16.0 kyr B.P. there was a large amount of old organic matter being deposited off Vancouver Island. Assuming that all of the old organic carbon is of infinite radiocarbon age we estimate that between 22 and 51 % of the total organic carbon present in late glacial and early deglacial sediments is reworked material. These are however minimum estimates because a portion of the old organic carbon may not be of infinite age.

2.3.2 Organic carbon content

Table 2.1. Radiocarbon data and estimates of the input of organic matter of infinite radiocarbon age for Composite Core JT96-09.

Sample[1]	Calendar Age (kyrs B.P.)	Radiocarbon Age (yrs)				Radiocarbon Age Difference[4]	% Old Organic Matter[5]	% Terrigenous Organic Matter[6]
		Measured Age of Planktonic Forams	Measured Age of Benthic Forams	Estimated Age of Planktonic Forams	Measured Age of Bulk Organic Matter			
38-40 mc	8.23	-	9830 ± 110	9030[3]	9920	890	9	14
35-36	10.03[2]	9760 ± 60	-	-	-	-	-	-
36-37	10.10	-	-	9760	11380	1620	14	17
65-66	12.24[2]	11210 ± 120	-	-	-	-	-	-
66-67	12.29	-	-	11210	14790	3580	24	35
75-76	12.73[2]	11500 ± 110	-	-	-	-	-	-
90-91	12.84[2]	11600 ± 80	-	-	-	-	-	-
96-97	13.04	-	-	12225	15660	3435	22	24
100-101	13.17[2]	12460 ± 120	-	-	-	-	-	-
130-131	13.43[2]	12640 ± 90	-	-	-	-	-	-
165-166	13.55	-	13210 ± 150					
166-167	13.55	-	-	12110[3]	24480	12370	51	54
265-266	14.14[2]	13410 ± 80	-	-				
266-267	14.15	-	-	13410	24500	11090	45	55
290-291	14.30[2]	13520 ± 70	-	-	-	-	-	-
350-351	15.57[2]	14140 ± 70	-	-	-	-	-	-
351-352	15.59	-	-	14150	21440	7290	34	57
370-371	16.01	-	-	14525	20320	5795	29	59

[1] Samples taken from the multicore are labelled with mc.

[2] Calendar ages used in the creation of an age model for Composite Core JT96-09. These data were first published in Kienast and McKay (2001).

[3] Planktonic ages for samples 38-40mc and 166-167 were estimated by subtracting the reservoir age from the benthic foraminifera age. For samples younger than 12000 ^{14}C years a reservoir correction of 800 years was applied while for older ages a correction of 1100 years was used. All other planktonic ages were estimated using the measured planktonic age of the overlying sample.

[4] The radiocarbon age difference is the difference between the estimated age of planktonic forams and the age of bulk organic carbon.

[5] Old organic matter refers to organic matter of infinite radiocarbon age. It is calculated using the following formula:
% Old carbon = (Radiocarbon age difference / Radiocarbon age of bulk organic carbon)*100

[6] % Terrigenous Organic matter is calculated using Equation 2.2 (i.e., $\delta^{13}C_{org}$ data). See the text for a further discussion.

Organic carbon (OC) values range from 0.07 to 3.07% (Table 2.2). Sediments deposited between ~11 kyr B.P. and the present have the highest OC content while late glacial and deglacial sediments are characterized by concentrations <1 % (Fig. 2.2b). Due to the large variations in sedimentation rate it was necessary to calculate the mass accumulation rate (MAR) of organic carbon. MAR values are relatively low (0.09 to 0.21 $g/cm^2/kyr$) prior to 14.3 kyr B.P. and after 12.7 kyr B.P., and substantially higher (>0.5 $g/cm^2/kyr$) from 14.3 to 12.7 kyr (Fig. 2.2b). High organic carbon accumulation occurred during a period of high sea-surface temperature off Vancouver Island that has been correlated to the Bølling-Allerød (Fig. 2.2a; Kienast and McKay, 2001). The data also suggest a slight increase in the MAR of total organic carbon at the Pleistocene-Holocene boundary (10.8 to 9.2 kyr B.P.), also a time of warmer sea-surface temperatures (Kienast and McKay, 2001). Interestingly, MAR values during the late glacial are generally higher than MAR values in the Holocene.

2.3.3 Organic carbon/nitrogen ratios

Organic carbon to total nitrogen weight ratios (OC/TN) range from 7.0 to 11.2 (Table 2.2) with an average value of 9.4. The highest ratios (>10) are observed in deglacial sediments (i.e., 14.6 to 11.6 kyr B.P.; Fig. 2.3). In general, the relatively low OC/TN values suggest the dominance of marine organic carbon; however, as will be discussed later these data are misleading.

2.3.4 Carbon- and nitrogen-isotope data

The carbon isotopic composition of organic matter ($\delta^{13}C_{org}$) in Core JT96-09 varies by 4 ‰ (-25.2 to -21.1 ‰; Table 2.2) while the nitrogen isotopic composition of the bulk sediment ($\delta^{15}N$) varies by almost 6 ‰ (+2.9 to +8.9 ‰; Table 2.2). As seen in Figure 2.2c, both $\delta^{13}C_{org}$ and $\delta^{15}N$ values are low during the late glacial to early deglacial, particularly

Fig. 2.2. Geochemical data for Core JT96-09. a) Alkenone-derived sea-surface (SST) temperature data from Kienast and McKay (2001). SST data are provided in Table 2.1. The precision for SST measurements is ±1.5 °C. Arrows indicate the position of radiocarbon dates used in the creation of the age model. b) Total organic carbon concentration (OC, open squares) and mass accumulation rate of organic carbon (MAR, solid squares). The precision of organic carbon measurements is 4 %. Note, multicore samples are labeled with the letters mc. c) Carbon-isotopic data for organic matter ($\delta^{13}C_{org}$, solid circles) and nitrogen-isotopic data for the bulk sediment ($\delta^{15}N$, open circles). The errors are ±0.1 ‰ and ±0.2 ‰ (C- and N-isotopic results, respectively). d) Biogenic barium concentration (crosses) and mass accumulation rate of biogenic barium (MAR, squares). The error associated with the estimation of biogenic barium concentrations is relatively large (RSD = 30%). e) Opal concentration (open triangles) and mass accumulation rate of opal (MAR, solid triangles). Opal concentration data have a RSD of 4 %. f) Concentration profile of the terrestrial biomarker C_{29} *n*-alkane normalized to total organic carbon (C_{29}/OC, solid diamonds) and concentration profile of the marine biomarker C_{37} alkenone normalized to total organic carbon (C_{37}/OC, open diamonds).

The linear sedimentation rate during the Bølling (~14.3 to 13.5 kyr B.P.) is 169 cm/kyr, during the Allerød (~13.5 to 12.7 kyr B.P.) it ranges from 20 to 143 cm/kyr, and by the Holocene it has decreased to 5 cm/kyr.

2.2a)

Sea Surface Temperature (°C)

Younger Dryas

Allerod

Bolling

Calendar Age (kyrs)

2.2b)

Organic Carbon (OC; wt.%)

MAR   OC

mc

MAR Organic Carbon (g/cm^2/kyr)

2.2c)

δ^{13}Corg (permil vs PDB)

δ^{13}Corg

δ^{15}N

δ^{15}N (permil vs air)

2.2d)

Bio-barium (ppm)

MAR   Bio-Ba

Calendar Age (kyrs)

MAR bio-barium (g/cm^2/kyr)

2.2e)

Opal (wt. %)

MAR   Opal

MAR Opal (g/cm^2/kyr)

2.2f)

C$_{29}$ n-alkane/organic carbon (C$_{29}$/OC; ug/g)

C$_{29}$/OC   C$_{37}$/OC

alkenone/organic carbon (C$_{37}$/OC; ug/g)

25
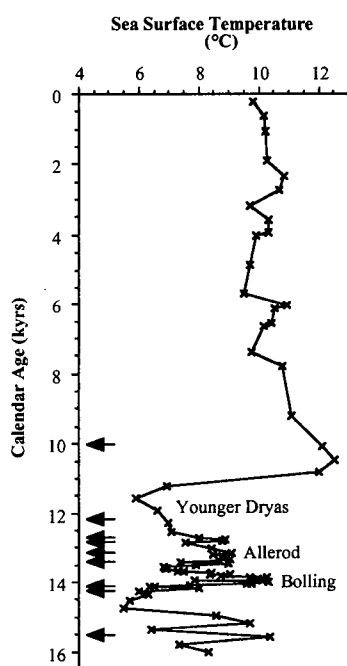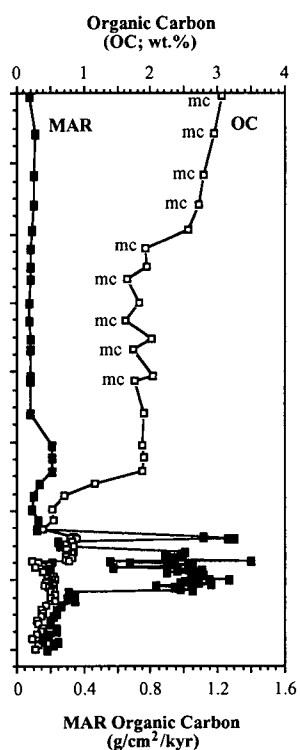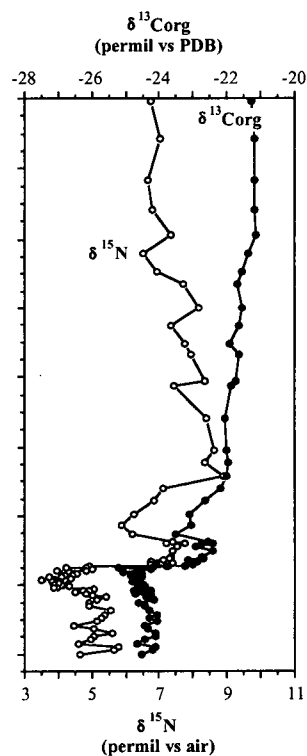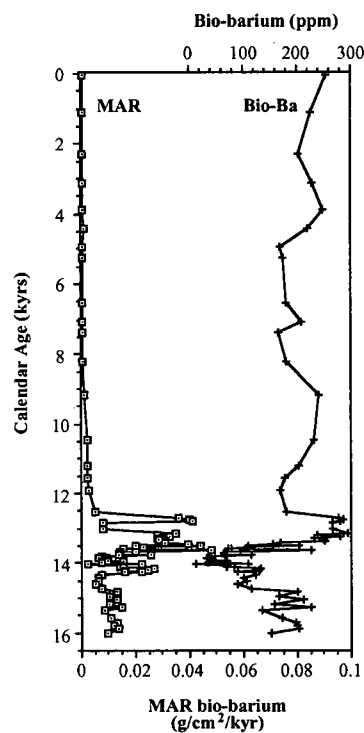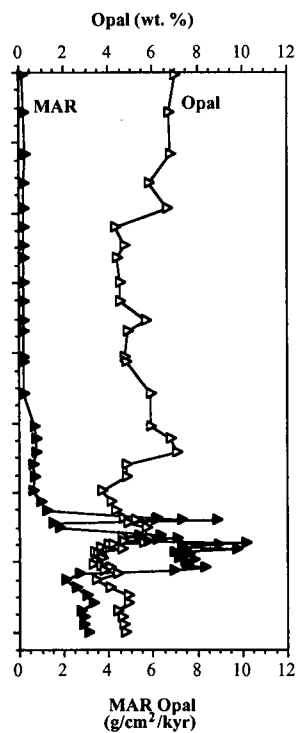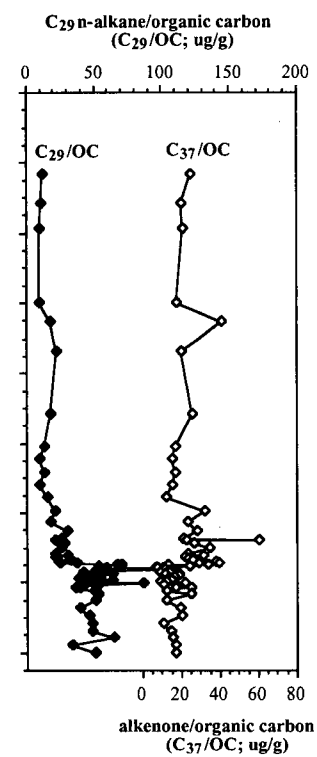
Table 2.2. Geochemical data for Composite Core JT96-09.

Sample [1]	Corrected Depth (cm)	Calendar Age (kyrs B.P.)	SST [2] (°C)	$\delta^{15}N$ (permil)	$\delta^{13}Corg$ (permil)	TN [3] (wt. %)	TC [3] (wt. %)	IC [3] (wt. %)	OC [3] (wt. %)	OC/TN [4]	Total Al (%)	Total Zr (ppm)	Total Ba (ppm)	Bio-barium (ppm)	Opal (wt. %)	C_{20} n-alkanes ng/g dry sed.	Alkenones ng/g dry sed.
0-1 mc	0.5	0.11		6.74	-21.28	0.35	3.20	0.13	3.07	8.7	13.61	146	624	257	7.0		
0-2 mc	1.0	0.21	9.83													290.3	1110.3
1-2 mc	1.5	0.32				0.36	3.16	0.11	3.05	8.4							
2-3 mc	2.5	0.53				0.37	3.17	0.10	3.07	8.3							
2-4 mc	3.0	0.63	10.19													309.7	636.9
3-4 mc	3.5	0.74				0.36	3.07	0.08	2.99	8.4							
4-5 mc	4.5	0.95				0.36	3.09	0.06	3.03	8.4							
4-6 mc	5.0	1.06	10.23														
5-6 mc	5.5	1.16		7.03	-21.19	0.35	3.03	0.07	2.96	8.5	14.74	139	624	226	6.7		
6-8 mc	7.0	1.48				0.35	3.01	0.04	2.97	8.5							
8-10 mc	9.0	1.90	10.27			0.35	3.01	0.04	2.97	8.5						357.8	979.9
10-12 mc	11.0	2.32	10.83	6.66	-21.19	0.31	2.80	0.02	2.78	8.9	15.38	151	617	202	6.8	318.6	682.5
12-14 mc	13.0	2.74	10.67			0.33	2.84	0.04	2.80	8.6						203.6	465.9
14-16 mc	15.0	3.17	9.72	6.81	-21.17	0.31	2.75	0.04	2.71	8.7	14.92	153	633	230	5.8	265.1	548.9
16-18 mc	17.0	3.59	10.34			0.32	2.79	0.04	2.75	8.6						214.1	357.9
6-7	18.5	3.91	10.34	7.33	-21.13	0.30	2.67	0.10	2.57	8.5	14.94	160	652	249	6.6	237.7	534.7
18-20 mc	19.0	4.01	9.92			0.23	2.11	0.04	2.07	8.9						249.4	294.1
20-22 mc	21.0	4.43		6.50	-21.39	0.20	1.96	0.05	1.91	9.4	14.01	155	598	220	4.3		
22-24 mc	23.0	4.86	9.69			0.19	1.79	0.09	1.70	9.1						276.4	561.3
11-12	23.5	4.96		6.95	-21.55	0.21	2.02	0.09	1.94	9.2	15.10	160	576	168	4.7		
24-26 mc	25.0	5.28		7.71	-21.67	0.18	1.79	0.14	1.65	9.3	15.64	156	596	174	4.4		
26-28 mc	27.0	5.70	9.50			0.18	1.83	0.22	1.61	9.0						319.9	367.1
16-17	28.5	6.02	10.96	8.17	-21.56	0.20	2.08	0.26	1.82	9.1					4.5	169.2	326.5
28-30 mc	29.0	6.12	10.53			0.18	1.90	0.25	1.64	9.0						214.9	406.3
30-32 mc	31.0	6.54	10.45	7.35	-21.64	0.18	1.91	0.28	1.63	9.2	15.81	155	608	181	4.5	280.9	660.8
19-20	31.5	6.65	10.16													412.3	1025.4
32-34 mc	33.0	6.97				0.19	1.99	0.29	1.70	9.1							
21-22	33.5	7.07		7.77	-21.92	0.21	2.29	0.28	2.01	9.4	15.67	148	631	208	5.7		
34-36 mc	35.0	7.39	9.77	7.93	-21.63	0.18	2.01	0.28	1.72	9.4	15.72	147	591	167	4.9	383.4	349.9
36-38 mc	37.0	7.81	10.81			0.20	2.08	0.29	1.79	9.1						265.6	492.0
26-27	38.5	8.13		8.33	-21.75	0.22	2.26	0.22	2.04	9.2	15.90				4.7		
38-40 mc	39.0	8.23		7.45	-21.85	0.19	2.07	0.32	1.76	9.2	16.16	151	618	182	4.8		
31-32	43.5	9.18	11.11	8.38	-22.04	0.20	2.23	0.33	1.90	9.3	14.83	138	640	240	5.9	322.8	483.0
36-37	48.5	10.10	11.94	8.61	-22.02	0.20	2.46	0.59	1.87	9.1	15.18				5.9	228.2	314.0
39-40	51.5	10.32	10.20													349.4	625.2
41-42	53.5	10.47	12.38	8.34	-21.96	0.20	2.55	0.65	1.90	9.6	15.20	135	642	232	6.8	164.5	287.6
44-45	56.5	10.69	10.85													456.3	570.6
46-47	58.5	10.84	12.01	8.89	-21.99	0.19	2.41	0.53	1.87	9.7	14.87				7.1	229.3	317.5
48-49	60.5	10.99	9.79													352.3	667.4
48.5-50	61.2	11.04	10.38													215.5	382.9
51-52	63.5	11.21	6.93	7.10	-22.19	0.12	1.47	0.30	1.17	9.4	15.41	136	618	202	4.8	111.1	182.5
53-54	65.5	11.35	6.46													325.7	421.8
56-57	68.5	11.57	5.93	6.86	-22.67	0.07	0.93	0.22	0.71	10.0	15.64	134	600	178	4.8	108.1	84.3
58-59	70.5	11.72	5.96													180.5	381.5
61-62	73.5	11.94	6.63	6.23	-23.11	0.06	0.80	0.27	0.53	8.7	15.90	140	599	170	3.7	108.7	169.5
66-67	78.5	12.29	6.99	5.89	-23.08	0.05	0.77	0.23	0.55	11.2	14.51				4.1	96.0	126.2
71-72	83.5	12.54	7.07	6.21	-23.53	0.04	0.73	0.33	0.39	10.8	13.92	212	555	179	4.3	116.3	109.8
76-77	88.5	12.74	8.00	7.41	-22.54	0.09	1.20	0.35	0.85	9.8	16.39	127	718	275	4.7	209.7	178.7
81-82	93.5	12.78	8.89	7.75	-22.75	0.10	1.38	0.48	0.90	9.3	15.93	120	715	285	5.2	169.2	477.6
86-87	98.5	12.81	8.80	7.20	-22.42	0.09	1.21	0.32	0.89	9.6	16.27	120	720	281	6.1	180.1	196.9
91-92	103.5	12.87	7.54	7.52	-22.91	0.09	1.30	0.48	0.82	9.1	16.97	118	724	266	4.8	228.0	215.3
96-97	108.5	13.04	8.41	7.38	-22.44	0.09	1.28	0.45	0.84	9.8	16.23	121	704	266	5.7	209.0	288.1
101-102	113.5	13.18	9.10	7.36	-22.75	0.10	1.34	0.49	0.85	8.9	16.37	122	736	294		170.8	200.5
106-107	118.5	13.22	8.50	7.28	-22.69	0.08	1.24	0.41	0.83	9.9	16.30	121	677	237	5.3	247.8	262.0
111-112	123.5	13.27	8.81	7.10	-23.16	0.08	1.18	0.42	0.76	9.1	14.67	121	676	280	4.6	158.9	164.4
116-117	128.5	13.31	8.95	6.77	-22.87	0.08	1.15	0.41	0.74	9.7	16.48	123	676	231	5.8	165.4	172.3
121-122	133.5	13.36	9.06	7.37	-23.01	0.09	1.16	0.34	0.82	9.0	16.03	124	683	250	5.3	261.1	212.7
126-127	138.5	13.40	8.67	6.75	-23.01	0.08	1.10	0.36	0.74	9.5	16.42	125	696	253	4.7	173.2	276.3
131-132	143.5	13.44	7.42	7.23	-23.26	0.09	1.12	0.36	0.77	9.8	16.28	128	608	168	5.6	183.4	304.5
136-137	148.5	13.47	8.98	4.92	-23.75	0.02	0.45	0.23	0.22	9.1	14.19	172	539	156		79.7	64.2
141-142	153.5	13.47		7.02	-23.39	0.04	0.76	0.31	0.45	10.2	15.49	226	598	180		206.2	273.8
146-147	158.5	13.47		2.93	-23.32	0.01	0.17	0.11	0.07	6.8	13.26	165	486	128		16.6	6.5
151-152	163.5	13.47		4.79	-24.24	0.05	0.77	0.21	0.56	11.0	14.57	131	512	119		752.3	71.3
156-157	152.5	13.49	7.93	4.84	-24.22	0.05	0.74	0.23	0.52	10.1	17.03	131	569	109	4.0	343.2	174.5
161-162	157.5	13.52		4.22	-25.20	0.04	0.73	0.41	0.32	8.3	15.94	173	635	205	4.2	224.0	42.3
166-167	162.5	13.55	6.82	5.00	-24.26	0.05	0.78	0.28	0.50	9.7	16.57	138	556	109		265.8	119.3
171-172	167.5	13.58	6.91	4.81	-24.64	0.05	0.71	0.20	0.51	9.7	16.68	124	526	76	3.6	297.2	52.2
176-177	172.5	13.61	6.86	3.98	-24.62	0.05	0.67	0.19	0.49	10.2	16.61	127	522	74		466.3	34.5
181-182	177.5	13.64		4.33	-25.05	0.04	0.75	0.48	0.27	6.9	16.55	167	673	226	4.6	285.6	31.1
186-187	182.5	13.67	7.30	4.57	-24.51	0.05	0.70	0.21	0.48	10.5	16.74	126	547	95		240.7	62.7
191-192	187.5	13.70	7.52	4.44	-24.86	0.05	0.65	0.18	0.46	9.1	16.70	125	520	69	3.4	192.7	40.2
196-197	192.5	13.73	8.41	4.21	-24.79	0.05	0.67	0.15	0.51	11.0	16.68	119	513	63		273.3	71.6
201-202	197.5	13.76	8.37	4.11	-24.68	0.05	0.67	0.16	0.51	9.8	16.70	121	516	65	3.5	282.4	58.1
206-207	202.5	13.79	9.06	3.72	-24.52	0.04	0.64	0.24	0.40	10.2	16.53	137	561	115		251.1	74.4
211-212	207.5	13.82	8.73	4.38	-24.69	0.05	0.68	0.18	0.50	9.5	16.93	126	494	37	3.6	218.0	93.6
216-217	212.5	13.85	10.29	3.50	-24.71	0.05	0.66	0.15	0.51	10.9	16.86	120	496	41		249.5	80.2
221-222	217.5	13.88	9.70	4.06	-24.62	0.06	0.71	0.16	0.55	9.9	16.93	125	490	33	3.7	206.8	78.8
226-227	222.5	13.91	9.99	3.81	-24.60	0.05	0.66	0.15	0.50	10.7	16.92	119	500	43		270.7	63.6
231-232	227.5	13.94	10.12	4.03	-24.68	0.05	0.63	0.17	0.46	9.5	16.44	133	486	42	3.4	286.9	67.3
236-237	232.5	13.97	7.87	3.85	-24.47	0.05	0.73	0.16	0.57	11.1	16.82	119	523	69		258.2	69.6
241-242	237.5	14.00	10.34	4.29	-24.62	0.05	0.68	0.14	0.53	10.1	15.92	124	464	34	3.4	242.1	44.9
246-247	242.5	14.03	9.75	4.31	-24.42	0.05	0.74	0.25	0.49	10.2	16.85	131	565	110		420.2	106.1

26

Table 2.2. (continued)

Sample[1]	Corrected Depth (cm)	Calendar Age (kyrs B.P.)	SST[2] (°C)	$\delta^{15}N$ (permil)	$\delta^{13}Corg$ (permil)	TN[3] (wt. %)	TC[3] (wt. %)	IC[3] (wt. %)	OC[3] (wt. %)	OC/TN[4]	Total Al (%)	Total Zr (ppm)	Total Ba (ppm)	Bio-barium (ppm)	Opal (wt. %)	C_{20} n -alkanes ng/g	Alkenones ng/g
251-252	247.5	14.06	9.59	3.96	-24.59	0.05	0.59	0.16	0.44	9.7	16.83	135	466	12	3.3	231.2	45.9
256-257	252.5	14.09	7.71	3.85	-24.49	0.05	0.69	0.17	0.52	10.4	16.89	122	524	68		221.1	86.6
261-262	257.5	14.12	6.38	5.08	-24.49	0.05	0.75	0.20	0.55	10.3	16.55	136	515	68	3.6	205.4	96.7
266-267	262.5	14.15	6.51	4.72	-24.27	0.05	0.76	0.20	0.56	10.5	16.93	127	539	82		218.0	139.2
271-272	267.5	14.18	8.03	4.91	-24.74	0.05	0.74	0.33	0.41	· 8.9	16.34	156	572	131	4.1	146.0	70.0
276-277	272.5	14.21		4.50	-24.41	0.05	0.78	0.29	0.49	10.0	16.39	142	572	129			
281-282	277.5	14.25	5.99	4.85	-24.71	0.06	0.81	0.27	0.53	9.5	16.21	139	525	87	3.8	258.0	64.5
286-287	282.5	14.28		5.03	-24.24	0.05	0.92	0.37	0.55	10.3	16.20	138	556	119			
291-292	287.5	14.33	6.34	5.44	-24.37	0.06	0.91	0.40	0.51	9.2	16.27	150	561	122	4.4	271.2	124.7
296-297	292.5	14.43		5.14	-24.15	0.06	0.96	0.39	0.57	10.2	16.38	133	544	102			
301-302	297.5	14.54	5.70	4.93	-24.60	0.05	0.88	0.37	0.50	9.2	16.37	144	547	105	3.5	249.5	60.0
306-307	302.5	14.60	.	4.91	-24.43	0.05	0.84	0.27	0.57	10.3	16.58	128	536	88			
311-312	307.5	14.75	5.48	5.58	-24.28	0.05	0.93	0.50	0.43	8.8	15.12	172	523	115	4.1	166.5	82.2
316-317	312.5	14.85		5.38	-24.07	0.04	0.83	0.46	0.36	8.8	15.54	185	618	198			
321-322	317.5	14.96	8.58	5.31	-24.30	0.04	0.80	0.41	0.39	9.0	15.85	184	595	167	4.9	180.1	79.4
326-327	322.5	15.06		5.16	-24.23	0.04	0.78	0.42	0.36	9.1	16.04	178	644	211			
331-332	327.5	15.17	9.69	4.45	-24.42	0.04	0.75	0.46	0.29	7.7	15.05	203	562	156	4.8	138.0	30.1
336-337	332.5	15.27		5.08	-24.36	0.04	0.75	0.45	0.31	8.7	15.53	187	646	227			
341-342	337.5	15.38	6.42	5.59	-24.09	0.04	0.82	0.44	0.38	8.6	16.25	186	573	134	4.4	184.4	53.8
346-347	342.5	15.48		5.07	-24.09	0.04	0.89	0.52	0.37	9.4	15.41						
351-352	347.5	15.56	10.39	4.98	-24.41	0.04	0.74	0.45	0.29	7.7	15.32	202	587	173	4.6	184.9	43.2
356-357	352.5	15.69		4.58	-24.64	0.03	0.65	0.41	0.24	8.7	14.99	209	602	197			
361-362	357.5	15.80	7.35	5.81	-24.10	0.05	0.80	0.39	0.40	8.7	14.07	185	581	201	4.7	134.7	68.4
366-367	362.5	15.90		5.65	-24.22	0.04	0.74	0.42	0.32	9.0	15.68	190	628	205			
371-372	367.5	16.01	8.30	4.66	-24.52	0.03	0.67	0.41	0.27	7.7	14.84	195	551	150	4.7	136.5	44.5

[1] Sample taken from the multicore are labelled with mc.

[2] Sea-surface temperature (SST) record is from Kienast and McKay (2001).

[3] TN = total nitrogen; TC = total carbon; IC = inorganic carbon; OC = organic carbon.

[4] OC/TN are weight, not atomic, ratios.
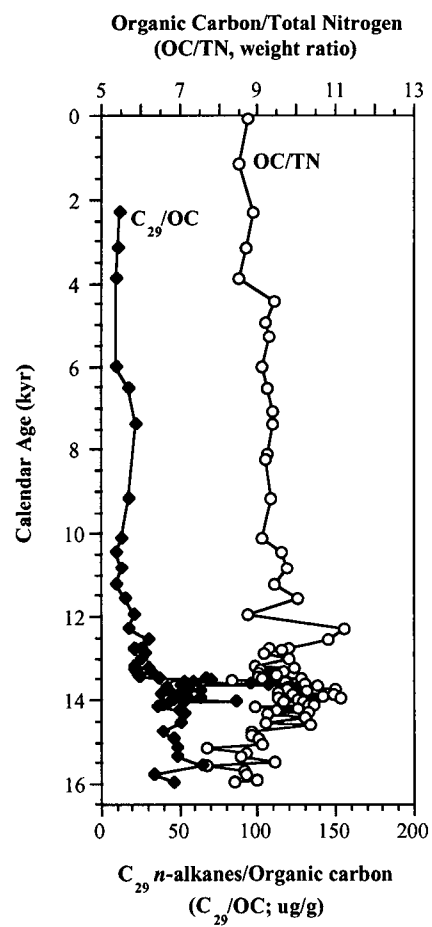
Fig. 2.3. Downcore profiles of the organic carbon/total nitrogen ratio (OC/TN) and C_{29} n-alkane/organic carbon ratio (C_{29}/OC).

between 14.3 and 13.5 kyr B.P. (i.e., the Bølling). Isotopic values abruptly increase at 13.5 kyr B.P. (i.e., the beginning of Allerød), remain high throughout the Allerød, decrease in the Younger Dryas (~12.7 to 11.0 kyr B.P.) and rise again at the close of the Younger Dryas (Figs. 2.2a and 2.2c). The $\delta^{15}N$ values peak at ~10.8 kyr B.P. and then slowly decrease throughout the Holocene while $\delta^{13}C_{org}$ values increase slightly through the Holocene. $\delta^{13}C_{org}$ and $\delta^{15}N$ exhibit a very strong positive correlation in late Pleistocene sediments, but are negatively correlated in Holocene deposits (Fig. 2.4).

2.3.5 Biogenic barium and opal data

The concentration of biogenic barium (i.e., bio-barium) ranges from 11 to 294 ppm (Table 2.2). Values are lowest (generally <100 ppm) between 14.3 and 13.5 kyr B.P., when sedimentation rate is highest, and are highest (>200 ppm) between 13.5 and 12.7 kyr B.P. (Fig. 2.2d). Interestingly, Holocene and late deglacial sediments have a similar bio-barium content (Fig. 2.2d). The highest bio-barium mass accumulation rates (> 0.02 $g/cm^2/kyr$) occur between 14.3 and 12.5 kyr B.P. (Fig. 2.2d) contemporaneously with a time of high SST that is believed to be the Bølling-Allerød.

Opal content ranges from 3.3 to 7.1 wt.% (Table 2.2). Concentrations are highest at ~13.0 kyr B.P., between 11.0 and 10.0 kyr B.P., and in late Holocene sediments (Fig. 2.2e). Opal mass accumulation rates, which range from 0.16 to 10.17 $g/cm^2/kyr$ are relatively low during the late glacial, high between 14.3 and 13.5 kyr B.P. and very low during the Holocene (Fig. 2.2e).

2.3.6 Biomarker data

Long chain n-alkanes (C_{25} to C_{31}) with an odd-carbon number predominance are present in all samples analyzed and the distribution is similar to that observed in Columbia
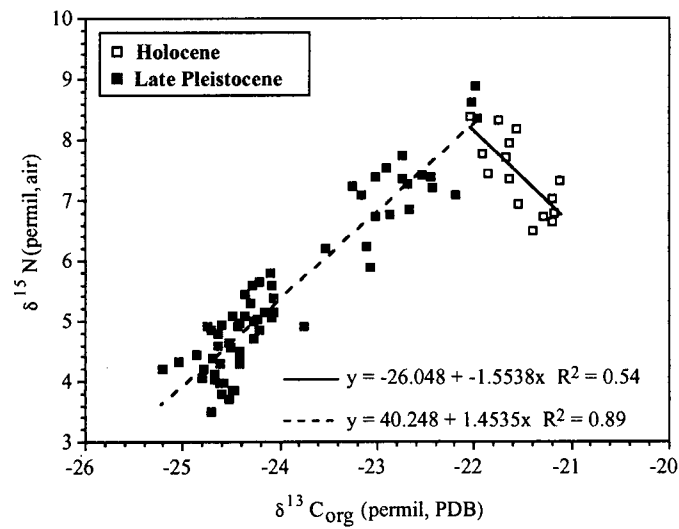
Fig. 2.4. N-isotopic composition of the bulk sediment ($\delta^{15}N$) versus the C-isotopic composition of organic matter ($\delta^{13}C_{org}$). Note the positive correlation between $\delta^{15}N$ and $\delta^{13}C_{org}$ for Late Pleistocene samples and the negative correlation for Holocene samples. Two clusters of Late Pleistocene samples are observed. Those samples characterized by $\delta^{15}N$ values of < -24‰ and $\delta^{13}C_{org}$ values of < +6‰ are older than 13.5 kyr B.P.

River sediments with a peak at C_{29} (Prahl et al., 1994). The concentrations of C_{29} n-alkane in Core JT96-09 range from 17 to 46 ng/g dry sediment (Table 2.2). To circumvent the problem of varying amounts of dilution by inorganic material, a reflection of the highly variable sedimentation rate over the last 16 kyr, the concentration of C_{29} n-alkanes has been normalized to the organic carbon concentration. The C_{29}/OC ratios, which range from 9 to 132 μg/gC, are high during late glacial and early deglacial, particularly between 14.3 and 13.5 kyr B.P. (i.e., the Bølling; Fig. 2.2f). At 13.5 kyr B.P. C_{29}/OC ratios abruptly drop, then decrease more slowly until ~11 kyr B.P. and remain relatively low after this time (Fig. 2.2f). High C_{29}/OC ratios correlate very well with low $\delta^{13}C$ and $\delta^{15}N$ values (Figs. 2.5a and b).

The concentration of C_{37} alkenones ranges from 7 to 1110 ng/g dry sediment (Table 2.2) and the C_{37}/OC ratio ranges from 7 to 61 μg/gC. C_{37}/OC ratios are low in the glacial and early deglacial, when C_{29} n-alkane content is high, and then increase abruptly at 13.5 kyr B.P. and remain high until ~11.9 kyr (i.e., the Allerød and early part of the Younger Dryas; Fig. 2.2f). C_{37}/OC ratios decrease from 11.6 to 10.1 kyr B.P. and only rise slightly in the Holocene (Fig. 2.2f). In general, Holocene C_{37}/OC ratios are only slightly higher than glacial values.

2.4 Discussion

2.4.1 Organic carbon

The mass accumulation rate of total organic carbon off Vancouver Island was highest during the last deglacial. While this is primarily a reflection of the very high sedimentation rates at this time, there is also an increase in the absolute concentration of organic carbon during the latter half this period (i.e., the Allerød; Fig. 2.2b). The data also suggest that the accumulation of organic carbon was higher during the late glacial (16.0 to 14.3 kyr B.P.) than during the Holocene. These results are contrary to what is expected based on climate

2.5a)

$$y = -313.32 + -14.897x \quad R^2 = 0.67$$

C$_{29}$ / Organic carbon (μg/g)

δ^{13}C$_{org}$ (permil, PDB)

2.5b)

$$y = 102.12 + -11.079x \quad R^2 = 0.63$$

C$_{29}$ / Organic carbon (μg/g)

δ^{15}N (permil, air)
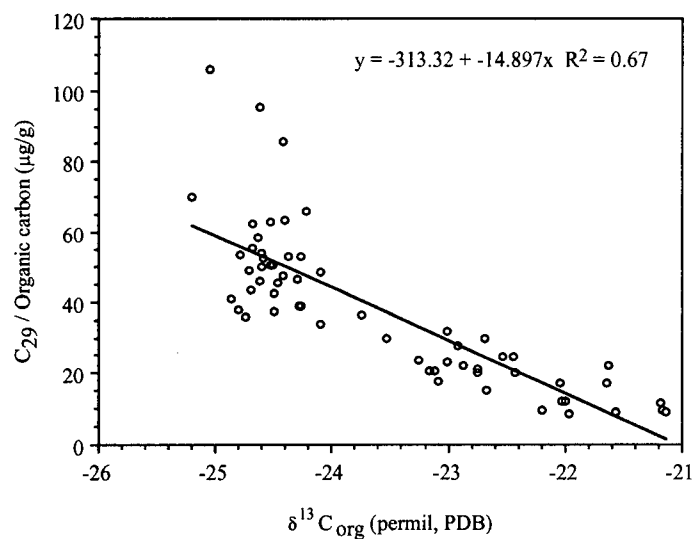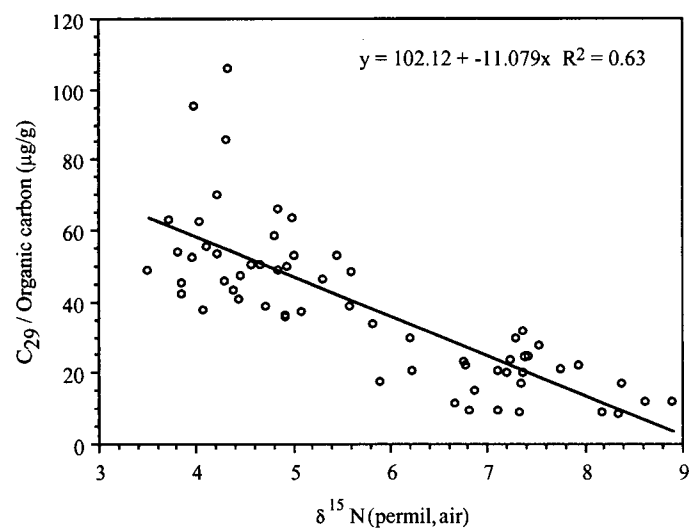
Fig. 2.5. C$_{29}$ *n*-alkane normalized to organic carbon (C$_{29}$/OC) versus a) the C-isotopic composition of organic matter (δ^{13}C$_{org}$) and b) the N-isotopic composition (δ^{15}N) of the bulk sediment.

modeling and palaeoproductivity data from other regions within the California Current System. Climate modeling suggest that during the last glacial the Aleutian Low pressure system dominated the Northeast Pacific region (COHMAP, 1988). The situation should have been similar to present-day winter conditions when winds are from the south and thus do not drive upwelling. As a result of this seasonal switch in atmospheric forcing, modern productivity off Vancouver Island is indeed lower in winters (Thomas et al., 1994). The same situation should have held true for the last glacial, and this suggestion is supported by geochemical and palaeontological studies that indicate that coastal upwelling and marine productivity were significantly reduced as far south as central California during the last glacial maximum (Dymond et al., 1992; Lyle et al., 1992; Sancetta et al., 1992; Ortiz et al., 1997; Dean and Gardner, 1998; Mix et al., 1999).

Radiocarbon data indicate that a significant percentage (22 to 51 %; Table 2.1) of the organic matter deposited during the late glacial and early deglacial is, in radiocarbon terms, of infinite age. Therefore, bulk organic carbon data cannot be used to infer changes in palaeoproductivity. Instead, it is necessary to determine and correct for the amount of old organic matter in each sample. To do this we first determine whether the old organic matter is of marine and/or terrestrial origin.

The ratio of organic carbon to total nitrogen (OC/TN) is commonly used to determine whether the dominant source of organic matter in sediments is terrestrial or marine. Low OC/TN ratios (<10) are often cited as evidence that marine organic matter dominates while higher ratios (>20) indicate the presence of abundant terrestrial organic matter. If our interpretation was based solely on OC/TN ratios, which range from 6.9 to 11.2, we would conclude that much of the organic matter in Core JT96-09 is marine, except for a slight relative increase in the terrestrial content during the deglacial (Fig. 2.3). However, this interpretation conflicts with n-alkane results. N-alkanes are organic compounds that occur in epicuticular waxes of higher terrestrial plants (Eglinton and Hamilton, 1967) and they are commonly used as a terrestrial biomarker. When the C_{29} n-alkane concentration is

normalized to organic carbon, to correct for problems of variable dilution by inorganic materials, it can be seen that a relatively larger fraction of the total organic carbon deposited prior to ~13.5 kyr B.P. is terrestrial (Fig. 2.3). It is rather surprising that high C_{29}/OC ratios are not accompanied by OC/TN ratios substantially greater than 11. Contamination by inorganic and microbial nitrogen can lead to anomalously low OC/TN ratios in organic-poor sediments (Meyers, 1997). However, in Core JT96-09 the concentration of inorganic N is quite low (~ 0.0025 %) and does not significantly influence OC/TN values. The unusually low OC/TN numbers are also not the result of post-depositional alteration of organic matter since this tends to attack the N-rich compounds, thus increasing OC/TN values. However, not all types of terrigenous organic matter are characterized by high OC/TN ratios. Fine-grained terrigenous organic detritus has OC/TN ratios similar to those of marine organic material (7 to 15; Hedges and Oades, 1997). It is quite possible, given the fine-grained nature of the sediments in Core JT96-09, that this accounts for the relatively low OC/TN values observed. We conclude that OC/TN ratios are of little use in this instance and are even rather misleading.

A strong positive correlation between $\delta^{13}C_{org}$ and $\delta^{15}N$ values occurs in the late glacial and deglacial sediments (Fig. 2.4). While many factors can influence both carbon and nitrogen isotope values, their positive correlation here suggests that mixing of terrestrial and marine organic matter may provide the primary control on the isotopic composition of these deposits. This interpretation is supported by the strong correlation between C_{29}/OC ratios and both $\delta^{13}C_{org}$ and $\delta^{15}N$ (Figs. 2.5a and b). The fraction of terrestrial organic matter can be estimated using Equation 2.2 (Jasper and Gagosian, 1993; Minoura et al., 1997; Fernandes and Sicre, 2000).

$$\text{Terrigenous fraction} = (\delta^{13}C_{smpl} - \delta^{13}C_{mar}) / (\delta^{13}C_{terr} - \delta^{13}C_{mar}) \qquad (2.2)$$

where $\delta^{13}C_{smpl}$, $\delta^{13}C_{mar}$ and $\delta^{13}C_{terr}$ are the isotopic compositions of the sample, the marine endmember and the terrestrial endmember, respectively. Application of this equation requires that we know, or can reasonably estimate, $\delta^{13}C_{mar}$ and $\delta^{13}C_{terr}$.

The $\delta^{13}C$ composition of marine organic matter ranges from -35 to -16 ‰ (Goericke and Fry, 1994). Much of this variability can be explained by changes in the concentration of CO_2 dissolved in seawater, because the $\delta^{13}C$ of marine organic matter varies inversely with CO_2 concentration (e.g., a 3-4 µmolar increase in CO_2 roughly equates to a 1-2 ‰ decrease in $\delta^{13}C$; Popp et al., 1989; Rau et al., 1989; Rau et al., 1991). However, other factors including phytoplankton growth rate (Fry and Wainright, 1991; Law et al, 1995; Rau et al., 1997), cell geometry (Popp et al., 1998; Popp et al., 1999), and cell membrane permeability (Francois et al., 1994) also influence $\delta^{13}C$. At present, the $\delta^{13}C$ of settling particulate organic matter off Vancouver Island ranges from -23.0 to -20.6 ‰, with an annual flux-weighted average of -21.9 ‰ (Wu et al., 1999a). Surface sediments deposited on the continental slope are characterized by similar values (-21.5 to -21.2 ‰; Chapter 4) suggesting the isotopic composition of organic matter is not altered as it settles through the water column. Furthermore, there is no change in the $\delta^{13}C_{org}$ composition in the upper 20 cm of slope deposits (Chapter 4) so post-depositional diagenesis is of little concern, even in the slowly accumulating Holocene deposits. These data suggest that a $\delta^{13}C_{mar}$ value of -21 ‰ is most applicable in Equation 2.2. Our choice of -21 ‰ is confirmed using the linear regression equation obtained when $\delta^{13}C$ values are plotted versus C_{29}/OC (Fig. 2.5a).

The $\delta^{13}C$ of terrestrial organic matter ($\delta^{13}C_{terr}$) can be highly variable due to different carbon uptake pathways. Terrestrial C3 plants (e.g., trees, shrubs and cool-climate grasses), that passively transport carbon dioxide into their cells, have relatively low $\delta^{13}C$ values (-23 ‰ to -34 ‰; Faure, 1986). In comparison, C4 plants (e.g., tropical grasses, sedges and salt marsh plants) that employ a carbon dioxide concentrating mechanism have relatively high $\delta^{13}C$ values (-19 to -6 ‰; Faure, 1986). The $\delta^{13}C$ value for terrestrial organic matter transported to the Pacific by the Fraser River in southwestern British Columbia is -27 ‰

(Wu, 1997). This value is similar to estimates of $\delta^{13}C_{terr}$ for Columbia River sediments (-25.7 ‰; Prahl et al., 1994) and terrestrial organic matter found in northeast Pacific sediments (-26 ‰; Peters et al., 1978). A $\delta^{13}C_{terr}$ value of -27 ‰ is also consistent with the modern vegetation, which is dominated by C3 plants (i.e., coniferous forests). Pollen data from the Queen Charlotte Islands suggest that prior to the Holocene, grasses and sedges were relatively more important contributors to the terrestrial vegetative cover in the region (Mathewes et al., 1993). Nevertheless, regression of the carbon and nitrogen isotopic data for the late Pleistocene yields a $\delta^{13}C_{terr}$ value of -27 ‰, assuming a $\delta^{15}N_{terr}$ endmember value of 1‰, and argues for a dominantly C3 plant source over the last 16 kyr. A $\delta^{13}C_{terr}$ value of -27 ‰ is therefore used in Equation 2.2.

The resulting calculations show that the terrigenous fraction accounts for 50 to 70 % of the total organic sedimentary organic matter pool during the late glacial and early deglacial (i.e., prior to 13.5 kyr B.P.; Fig. 2.6). The terrigenous fraction is approximately half this proportion (20 to 40 %) between 13.4 and 11.2 kyr B.P., and then progressively decreases to only a few percent in the latter part of the Holocene (Fig. 2.6). We have assumed that the endmember values assigned to both $\delta^{13}C_{mar}$ and $\delta^{13}C_{terr}$ have remained constant for the last 16 kyr. However, during the last glacial a lower atmospheric CO_2 concentration and thus lower concentration of dissolved CO_2 in the surface ocean might have led to a higher $\delta^{13}C_{mar}$ value (Jasper and Hayes, 1990; Rau et al., 1991). Substituting a value of -19 ‰ in Equation 2.2 increases the estimate of terrigenous organic matter content by 10 to 20% (late glacial and Holocene, respectively), but the temporal variations remain unchanged. An increase in the $\delta^{13}C_{terr}$ value, due to a higher C4 plant input during the glacial, would have a similar effect.

In general, the terrigenous fraction estimates determined using $\delta^{13}C$ data are similar to those obtained from the radiocarbon dating of bulk organic matter, assuming an infinite age for the old organic carbon, and suggest that most of the old organic carbon is terrestrial in origin. However, in the late glacial sediments (i.e., older than 15.6 kyr B.P.) the estimates of

Terrigenous Fraction
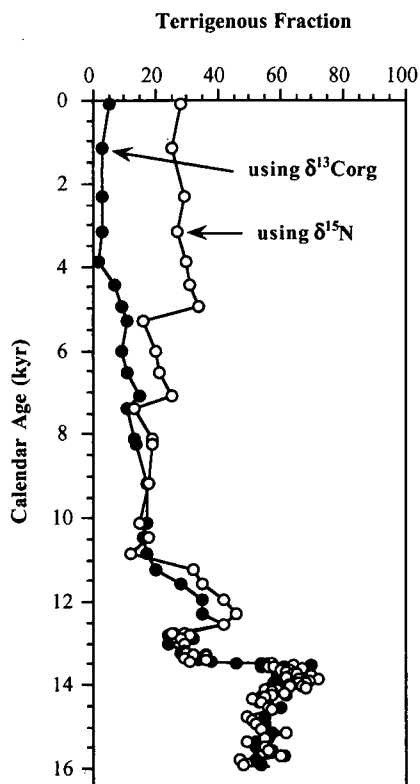
Fig. 2.6. The percentage of terrigenous organic carbon (i.e., the terrigenous fraction) in Core JT96-09 estimated using both the $\delta^{13}C_{org}$ and $\delta^{15}N$ data. The following endmember isotopic compositions were employed: $\delta^{13}C_{terr}$ = -27 ‰, $\delta^{13}C_{mar}$ = -21 ‰, $\delta^{15}N_{terr}$ = +1 ‰ and $\delta^{15}N_{mar}$ = +9 ‰. If the endmember isotopic compositions are assumed to have an error of ± 1 ‰ then the final terrigenous fraction estimates could vary by as much as 20 % but the trends remain unchanged. The values estimated using both the C and N isotope data compare very well for the Late Pleistocene and Early Holocene but diverge significantly for the Mid- to Late Holocene. The values determined using the $\delta^{15}N$ data are though to be too high in the Holocene because the $\delta^{15}N$ composition of marine organic matter has not remained constant over time. See the text for further discussion.

37

% terrestrial organic matter are noticeably higher than the estimates of % old organic carbon (Table 2.1). This discrepancy suggests that some fraction of the terrigenous organic matter may not be of infinite age and/or that our estimates of terrigenous input determined using Equation 2.2 are high. Lowering the estimated terrigenous input would require decreasing one (or both) of the $\delta^{13}C$ endmember values. During the glacial, lower atmospheric CO_2 concentrations and a switch from C3 to C4 plants would increase, not decrease, $\delta^{13}C_{terr}$ values and thus cannot explain the discrepancy in % old organic carbon and % terrigenous estimates. However, if the local concentration of CO_2 dissolved in seawater was higher during the last glacial as a result of colder sea-surface temperatures and/or lower productivity then it is quite possible that $\delta^{13}C_{mar}$ values were lower. A final explanation for the discrepancy could lie in a switch from a diatom-dominated ecosystem to one based on nanoplankton, similar to what occurs from summer to winter off Vancouver Island at present (Wu et al., 1999a and 1999b). Such a switch, for which micropalaeontological evidence is required, would have resulted in a more negative $\delta^{13}C_{mar}$ value.

The estimates of terrigenous input for Holocene sediments off Vancouver Island ($\leq$ 20 %) are lower than expected for a continental margin setting. The organic matter in shelf sediments off Washington State, for example, is more than 50 % terrestrial organic matter while slope sediments contain 20 to 30 % terrigenous material (Prahl et al., 1994). The source of this allochthonous detritus in this region is the Columbia River (Prahl et al., 1994). In contrast, the low terrigenous fraction in Holocene sediments off Vancouver Island can be explained by the high trapping efficiency of river-borne detritus within the fjords that are ubiquitous along the British Columbia coast. Such trapping in conjunction with high wave and current energies also explains the very low sedimentation rate characteristic of the present-day shelf and upper slope west of Vancouver Island (Bornhold and Yorath, 1984). Holocene sedimentation rates are generally <2 cm/kyr, except in local depressions on the shelf where sediment focusing results in much higher values (e.g., 40 cm/kyr; Chapter 4).

Concentration profiles for the terrestrial and marine organic carbon fractions, calculated using the $\delta^{13}C_{org}$ data, are shown in Figure 2.7. The validity of the marine carbon estimates is supported by a strong positive correlation with the measured concentrations of alkenones (Fig. 2.8a). A positive, though weaker, correlation is also observed between the terrigenous organic carbon estimates and the concentration of the terrigenous biomarker C_{29} n-alkane (Fig. 2.8b). To try to circumvent the problems associated with varying degrees of dilution, and to get a better understanding of the flux of carbon to the sediment, mass accumulation rates (MARs) have also been calculated (Fig. 2.7). During the late glacial (16.0 to 14.3 kyr B.P.) the MAR of terrestrial organic matter was relatively high, while that for marine organic matter was low. The accumulation of both fractions increased at ~14.3 kyr B.P., coincident with a substantial increase in sedimentation rate (i.e., from ~ 47 up to 169 cm/kyr). During the initial stage of the deglacial between 14.3 and 13.5 kyr B.P. (i.e., the Bølling) terrestrial organic matter dominated the bulk organic fraction. This situation reversed at 13.5 kyr and marine organic matter accumulation was dominant between 13.5 and 12.7 kyr B.P. (i.e., the Allerød). The MAR of both fractions decreased at the end of the Allerød and remained low throughout the Younger Dryas. Marine organic carbon accumulation subsequently increased slightly between 11.2 and 10.0 kyr B.P., while terrestrial organic carbon accumulation continued to decrease.

By ~15.5 kyr B.P. deglaciation of the shelf off Vancouver Island had commenced (i.e., 15 to 14 ^{14}C kyr; Barrie and Conway, 1999; Clague and James, 2002). At this time the linear sedimentation rate at Site JT96-09 was quite high (e.g.,169 cm/kyr during the Bølling), in response to the influx of glacial rock flour generated by the rapid retreat of glaciers. At the beginning of the Allerød, deglaciation of the shelf was essentially complete and the sedimentation rate began to decrease. The relatively low sedimentation rates which characterize Site JT96-09 at present (~5 cm/kyr) were established in the Early Holocene as the shelf was flooded.

2.7a)   **2.7b)**

Terrigenous Organic Carbon   **Marine Organic Carbon**
           (wt.%)   **(wt.%)**
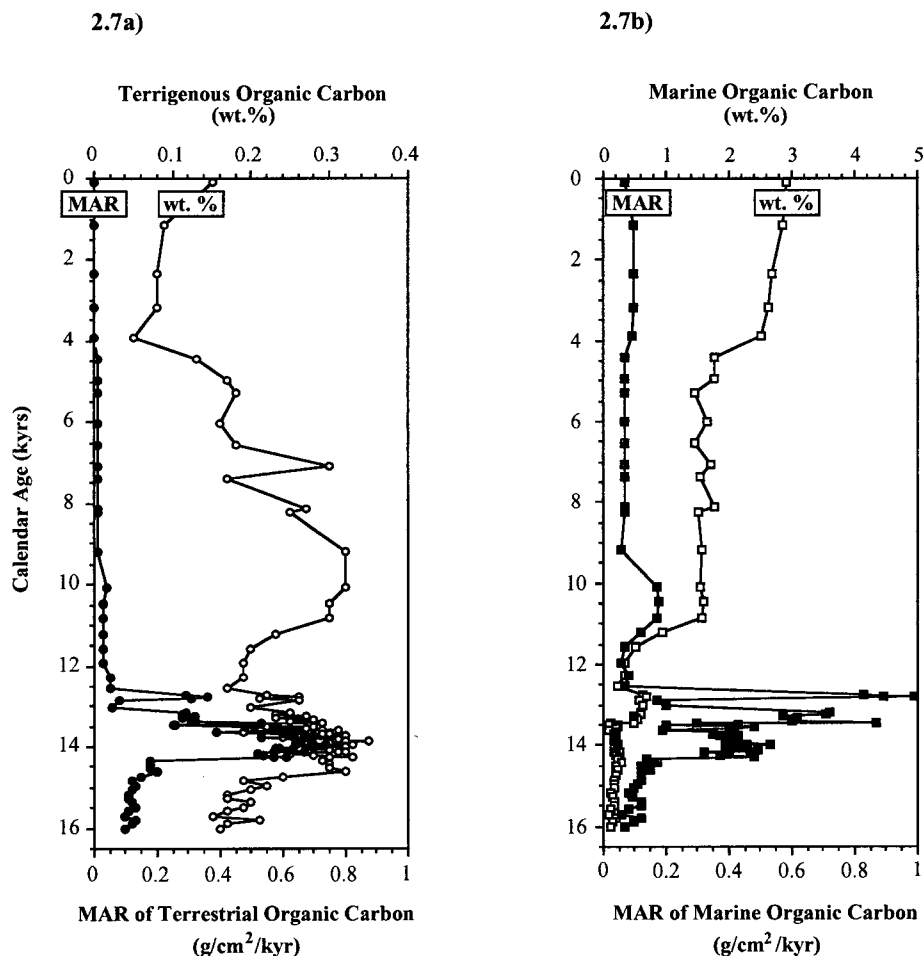
Fig. 2.7. a) Terrestrial organic matter concentration (open circles) and mass accumulation rate (MAR, solid circles) over the past 16 kyr B.P. b) Marine organic matter concentration (open squares) and mass accumulation rate (MAR, solid squares) over the past 16 kyr B.P. The concentrations of terrestrial and marine organic matter were obtained by first estimating the terrigenous fraction using the $\delta^{13}C_{org}$ data (see results in Fig. 2.6) and correcting the total organic carbon data accordingly. The estimated concentrations of terrestrial and marine organic matter have an estimated error of ~20 %.

2.8a)

$y = 50.119 + 218.23x$ $R^2 = 0.79$

Alkenone concentration
(ng/g sediment)

Marine Organic Carbon
(wt.%)

2.8b)

$y = 122.99 + 393.08x$ $R^2 = 0.12$

C_{29} n-alkane
(ng/g sediment)

Terrigenous Organic Carbon
(wt.%)
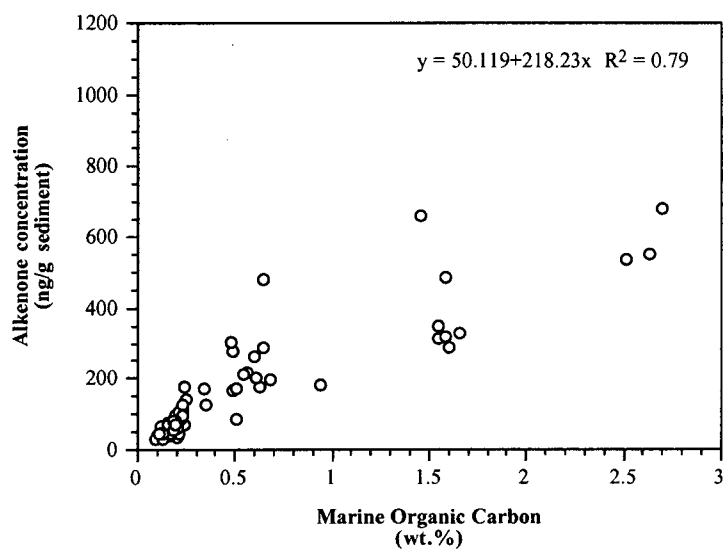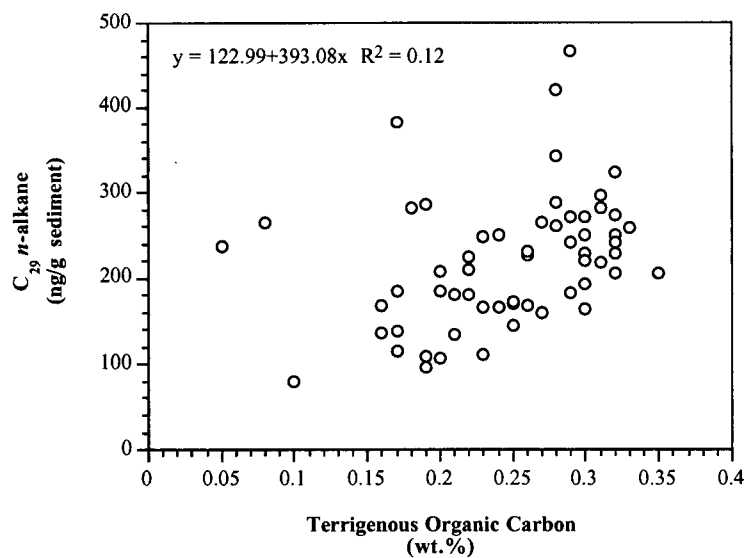
Fig. 2.8. The measured concentration of alkenones, a marine biomarker, versus the estimated marine organic carbon concentration. b) The measured concentration of C_{29} n-alkanes, a terrestrial biomarker, versus the estimated terrestrial organic carbon concentration.

There is no evidence that the downslope slumping and/or transport of material was responsible for the high deposition rates throughout the Bølling-Allerød. Such phenomena tend to increase the grain-size and heavy-mineral content of the material laterally transported and deposited on the mid- and upper continental margins (Ganeshram et al., 1999). Coarser-grained sediments are associated with higher Zr/Al ratios as a reflection of the increased zircon content. Thus, had downslope transport been responsible for the very high sedimentation rates during the deglacial, the deposits would be characterized by relatively high Zr/Al ratios. Instead, Zr/Al ratios in the deglacial interval are relatively low (Fig. 2.9), suggesting that these sediments are generally finer-grained than underlying glacial and overlying Holocene strata. The only exception to this general observation is the thin sandy turbidite deposited at the start of the Allerød (Fig. 2.9).

The dramatic changes in sedimentation rates over the past 16 kyr make it difficult to interpret changes in palaeoproductivity directly from MARs. For example, the increase in marine organic carbon MAR in the Bølling could simply be due to the large jump in sedimentation rate, given that there is no corresponding increase in the concentration of marine organic carbon. Despite such constraints, it is not possible to rule-out an increase in palaeoproductivity during the Bølling. During the Allerød both the MAR and concentration of marine organic carbon increase. There is no evidence that this is due to enhanced organic matter preservation due to the higher sedimentation rate and/or lower bottom water oxygen concentration at the time (Chapter 3). We therefore infer that export production (i.e., palaeoproductivity) was higher during the Allerød.

Increased export production during the deglacial (i.e., the Bølling/Allerød) has been documented for other regions of the CSS to the south of Vancouver Island (Lyle et al., 1992; Gardner et al., 1997; Dean and Gardner, 1998; Mix et al., 1999), and has been attributed to the initiation of upwelling as atmospheric circulation returned to its interglacial state. Sabin and Pisias (1992) used a radiolarian-based transfer function to infer that upwelling began at ~15 kyr B.P. and suggested that by 13.0 kyr B.P. present-day upwelling conditions had been
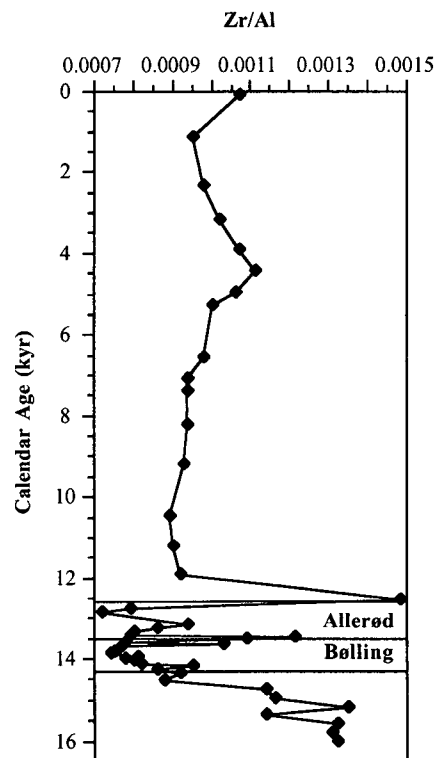
Fig. 2.9. The downcore Zr/Al profile for Core JT96-09.
The precision (as RSD) of these ratios is ~16 %
(i.e., ±0.0001 to 0.0002).

attained. Evidence of a return to seasonal upwelling off Vancouver Island during the deglacial and stronger upwelling than at present during the Allerød is provided by radiocarbon dating. During the Allerød the reservoir age of surface waters, recorded in an uplifted deposit found in the Fraser River lowlands, increased from 800 to 1100 years (Kovanen and Easterbrook, 2002) suggesting enhanced upwelling of old, ^{14}C-depleted water from depth. Furthermore, the age difference between contemporaneous benthic and planktonic foraminifera decreased during the Allerød (Chapter 4). The simplest explanation for this decrease is the upwelling of old, nutrient-rich water that would have stimulated primary production.

The relatively low marine organic carbon accumulation rates observed for the Holocene are unexpected given that the west coast of Vancouver Island is characterized by high primary productivity at present (~250 gC/m^2/yr on the lower slope to 400 gC/m^2/yr on the shelf; Antoine et al., 1996). In large part, the decrease in mass accumulation rates reflects the substantial decrease in sedimentation rate, but preservational influences may also have played a role. Numerous studies have shown that organic carbon is better preserved when sedimentation rate is high, possibly because exposure time to various oxidants is limited (Hedges and Keil, 1995; Gélinas et al., 2001). It is also possible that the large supply of fine-grained aluminosilicate particles, associated with a higher sedimentation rate, offers more mineral surface area on which organic compounds can be adsorbed (Keil et al., 1994; Mayer, 1994). Once adsorbed this organic material maybe protected from degradation. In contrast, when the sedimentation rate is low there is continued exposure to oxidants via bioturbation and diffusive influx, and less mineral surface area on which organics may be adsorbed. In summary, the very low sedimentation rate (i.e., poor preservation) and apparently lower primary productivity relative to the deglacial lead to a lower rate of organic matter accumulation throughout the Holocene.

2.4.2 Biogenic barium and opal accumulation

Barium is often enriched in sediments beneath highly productive surface waters (Goldberg and Arrhenius, 1958; Dehairs et al., 1980; Dehairs et al., 1992), presumably because authigenic barite formation is linked to the supply of organic particles. The exact mechanism responsible for the precipitation of barite is still not fully understood, but it appears to be related to the formation of the mineral within decaying organic particles, such as fecal pellets (Dehairs et al., 1980; Bishop, 1988; Bernstein et al.1992; Ganeshram et al., in press). Based on the observed spatial correlation with export production, the barium content of sediments is commonly used as a palaeoproductivity indicator (e.g., Schmitz, 1987; Dymond et al., 1992; Gingele and Dahmke, 1994; Shimmield et al., 1994; Francois et al., 1995; Ganeshram, 1996; Nurnberg et al., 1997; Thompson and Schmitz, 1997).

In Core JT96-09, both the concentration and MAR of bio-barium are high throughout the Allerød. These increases are contemporaneous with the increase in marine organic carbon accumulation, which supports the interpretation that export production was high during this interval. However, the mass accumulation rate of bio-barium is also relatively high during the Bølling. Most if not all, of this apparent increase is a reflection of the dramatically higher sedimentation rate at this time (169 cm/kyr) and the influence this has on the calculation of mass accumulation rates. Likewise, the higher MARs during the late glacial, relative to the Holocene, can be explained by differences in sedimentation rates (47 cm/kyr versus 5 cm/kyr for the late glacial and Holocene, respectively) and do not imply that export production was higher during the glacial. Only when both concentrations and accumulation rates increase contemporaneously, such as during the Allerød, is it possible to infer higher export production.

The primary source of biogenic silica (i.e., opal) in these sediments is diatoms. As with organic carbon and bio-barite, opal preservation efficiency increases as sediment accumulation rate increases (Ragueneau et al., 2000) because rapid sedimentation more

quickly isolates porewaters from diffusive contact with Si-undersaturated bottom waters. Given this strong preservational artifact, there is some question as to whether opal content is a reliable indicator of surface productivity (Archer et al., 1993). Nevertheless, various studies have shown that if used cautiously the opal content of sediments can reflect export production history (Lyle et al., 1992; Francois et al., 1997; Ganeshram et al., 2000).

In Core JT96-09 the slowly accumulating Holocene sediments (5 cm/kyr) have a higher opal content than the more rapidly deposited glacial and deglacial sediments (48 to 169 cm/kyr). This trend is opposite to what is expected if sedimentation rate was the only control on opal concentration. Export of opal from surface waters to the sediment must also have influenced sedimentary concentrations. As already discussed, MAR data for Core JT96-09 may be somewhat misleading, given the large variability in sedimentation rates. However, in the Allerød both the concentration and MAR of opal increase, coincident with the increase in organic carbon and bio-barium concentrations and MARs. Thus, opal data further support the interpretation that marine productivity and subsequent export flux to the sediment was probably relatively high during the Allerød.

2.4.3 Alkenones

C_{37} alkenones are produced by certain prymnesiophyte algae (family Gephyrocapsaceae) and thus can be used as a biomarker for these phytoplankton (Marlowe et al., 1990). The coccolithophorid *Emiliania huxleyi* is the most important alkenone producer in the northeast Pacific (Okada and Honjo, 1973; Prahl and Wakeham, 1987; Marlowe et al., 1990), although a minor contribution by other prymesiophytes cannot be discounted. Relative alkenone abundance (i.e., C_{37}/OC) in Core JT96-09 reaches a maximum between 13.5 and 11.9 kyr B.P., at approximately the same time that other palaeoproductivity proxies peak (Fig. 2.2). However, the relative abundance remains high when the accumulation rates of the other proxies decrease at ~12.5 kyr B.P. (i.e., the start of Younger Dryas). In part, this

can be attributed to differences in the factors that control the productivity of coccolithophorids compared to those that control diatoms. When nutrient concentrations are high, such as during upwelling events, diatoms are favoured whereas coccolithophorids can thrive when waters become nutrient-depleted (Werne et al., 2000 and references therein). The low accumulation rates of marine organic carbon, bio-barium and opal during the Younger Dryas suggest that nutrient supply and thus diatom-based productivity was diminished at this time. However, given the ecological contrasts between diatoms and coccolithophorids this would not have had the same impact on alkenone production.

2.4.4 Nitrogen-isotope record

During nitrate uptake, marine phytoplankton preferentially incorporate ^{14}N into organic matter, but as nitrate becomes scarce there is less discrimination against ^{15}N (Montoya et al., 1994 and references therein). Thus, the nitrogen isotopic composition of organic matter is commonly used as a proxy for nitrate utilization, with relatively high $\delta^{15}N$ values reflecting high nitrate utilization relative to the supply (Altabet et al., 1991; Altabet and Francois, 1994a and b; Farrell et al., 1995). However, other factors such as nitrogen fixation, diagenesis, water column denitrification, the presence of inorganic nitrogen, changes in trophic cycling, and the presence of terrestrial organic matter also may influence the $\delta^{15}N$ composition of sediments (Montoya, 1994).

Nitrogen-fixation involves little isotopic fractionation and thus produces organic matter with low $\delta^{15}N$ values (~ 0‰; Montoya et al., 1994; Carpenter et al., 1997). However, this process is currently believed to be important only under oligotropic conditions and in tropical to subtropical waters where the cyanobacterium *Trichodesmium* occurs (Carpenter et al., 1997; Capone et al., 1997). This process can therefore be ruled-out as the cause of low $\delta^{15}N$ values in late glacial and deglacial sediments.

The influence that diagenesis has on the $\delta^{15}N$ composition of organic settling through the water column is dependant on water depth. In the deep ocean a diagenetic offset of as much as +4 to +7 ‰ may occur between sinking particles collected from deep waters and surface sediments (Saino and Hattori, 1987; Altabet and Francois, 1994b, Altabet, 1996). But when the water depth is relatively shallow and settling is rapid there is little change in the $\delta^{15}N$ (Altabet et al., 1999; Pride et al., 1999). Such is likely the case for Core JT96-09 that was collected from 920 m water depth. The influence that sedimentary diagenesis has on the $\delta^{15}N$ composition of organic matter is more ambiguous. Some studies have documented a decrease in $\delta^{15}N$ of a few permil due the degradation (i.e., loss) of ^{15}N-enriched organic compounds (De Lange et al., 1994; Prahl et al., 1997). In contrast, other studies observe an increase in $\delta^{15}N$ (Sigman et al., 1999; Freudenthal et al., 2001) or no change at all (Ganeshram et al., 2000). In near-surface sediments collected from the continental margin off Vancouver Island there is no change in bulk sediment $\delta^{15}N$ values to a depth of 20 cm below the sediment-water interface (Chapter 4). These data suggest that, despite very slow Holocene sedimentation rates, degradation of organic matter in this environment has little effect on the $\delta^{15}N$ composition of organic matter.

Low sedimentary $\delta^{15}N$ values can be the result of adsorption of inorganic nitrogen onto illitic clay minerals (Freudenthal et al., 2001). The presence of inorganic (or excess) nitrogen would be recorded by a positive intercept on the nitrogen-axis of a C-N plot. No such positive N-intercept is observed for samples from Core JT96-09 when total organic carbon and total nitrogen are plotted, but when the concentration of marine organic carbon is plotted versus nitrogen a N-intercept of 0.0025 wt. % is obtained. This suggests that some inorganic N is present, but the concentration is so low as to have a negligible effect on $\delta^{15}N$ values.

We have shown above that the input of terrigenous organic matter is largely responsible for the low $\delta^{13}C_{org}$ values of late glacial and early deglacial sediments off Vancouver Island, and it is reasonable to assume that a similar effect should be seen in the

$\delta^{15}N$ data. Terrestrial organic matter is typified by low $\delta^{15}N$ values, reflecting the uptake and fixation of atmospheric N_2 by land plants. Indeed, there is a clear decrease in $\delta^{15}N$ values during the Bølling when terrestrial input was highest and an increase in $\delta^{15}N$ values during the Allerød when terrestrial input decreased (Fig. 2.2c). If terrestrial organic matter input was the only factor controlling the N-isotopic composition it should be possible to estimate the terrigenous proportion using $\delta^{15}N$ data in the same way that $\delta^{13}C_{org}$ data were used, and the results should be similar. This calculation requires reasonable estimates for the $\delta^{15}N$ composition of terrigenous and marine organic matter ($\delta^{15}N_{terr}$ and $\delta^{15}N_{mar}$, respectively). The $\delta^{15}N_{terr}$ can be calculated using the regression equation of late Pleistocene carbon- and nitrogen-isotopic data (Equation 2.3; see Fig. 2.4).

$$\delta^{15}N_{terr} = 40.25 + 1.45(\delta^{13}C_{terr}) \quad (r = 0.94) \qquad (2.3)$$

Assuming a terrestrial endmember $\delta^{13}C_{terr}$ value of -27‰ (Wu, 1997) yields a $\delta^{15}N_{terr}$ value of +1.1‰. A slightly higher $\delta^{15}N_{terr}$ value of +2.6‰ is obtained if a $\delta^{13}C_{terr}$ value of -26‰ is instead used. These $\delta^{15}N_{terr}$ estimates are similar to measured values for organic matter from various California rivers and lakes (0.3 to 6.9 ‰, avg. 4 ‰; Peters et al., 1978). Estimating the nitrogen isotopic composition of the marine end-member ($\delta^{15}N_{mar}$) is more complicated because $\delta^{15}N_{mar}$ values can vary spatially and seasonally within an upwelling system. Surface sediments from the continental shelf off Vancouver Island have relatively low $\delta^{15}N$ values (+4.8‰) while slope sediments are characterized by higher $\delta^{15}N$ values (+6.3 to +6.8‰; Chapter 4). This difference is the result of upwelling of water onto the shelf followed by the preferential uptake of ^{14}N-enriched nitrate by phytoplankton that leaves the residual nitrate ^{15}N-enriched. As waters are advected away from the site of upwelling (i.e., offshore) they become progressively more ^{15}N-enriched due to continued biological activity. The organic matter produced from this nitrate and which is eventually deposited on the slope is thus ^{15}N-enriched relative to that deposited on the shelf (Chapter 4). Data from sediment

traps moored on the upper slope off Vancouver Island indicate that the $\delta^{15}N$ of settling particulate organic matter (SPOM) is relatively heavy, ranging from +7.7 ‰ during bloom events in summer and fall up to +9.0 ‰ in winter, with an average annual flux-weighted value of +8.1 ‰ (Wu, et al., 1999a). However, surface sediments from the slope have lower values (+6.3 to +6.8 ‰) than this SPOM possibly due to the input of minor terrestrial organic matter and/or the downslope transport of ^{14}N-enriched organic matter from the shelf. Our best estimate of $\delta^{15}N_{mar}$ is obtained using Equation 2.3 and a marine $\delta^{13}C_{org}$ value of -21 ‰. This calculation yields a $\delta^{15}N_{mar}$ value of +9.8 ‰ which is significantly higher than the $\delta^{15}N$ composition of trap and surface sediments. The regression derived from a plot of C_{29}/OC and $\delta^{15}N$ data yields a similar value (+9.5 ‰; Fig. 2.5b).

The $\delta^{15}N_{mar}$ values obtained from the linear regression of the data are more similar to the $\delta^{15}N$ values of settling particulate organic matter in winter (~ 9 ‰) rather than the annual flux-weighted value of Wu et al., (1999a). Thus, the present-day winter ecosystem (i.e., nanoplankton-dominated community) may be a better model for the late glacial ecosystem. Although speculative, this is consistent with the inference that upwelling was greatly diminished or non-existent off Vancouver Island during the last glacial and thus the nitrate supply was reduced. Under such conditions a nanoplankton-dominated ecosystem, which is based on the use of regenerated forms of nitrogen (i.e., urea), would have been favoured. However, it is also possible that the isotopic composition of the source nitrate (i.e., the nitrate that is supplied to the euphotic zone) was different. This possibility is discussed below.

Substituting the $\delta^{15}N$ values of terrestrial and marine organic matter (+1 and +9 ‰, respectively) for their $\delta^{13}C$ counterparts in Equation 2.2 yields terrigenous values of 40 to 70 % for the late glacial and early deglacial, <10 to 40 % for the late deglacial, and 8 to 31 % for the Holocene (Fig. 2.6). These estimates compare moderately well with $\delta^{13}C$-based estimates for the late glacial, deglacial and early Holocene, but are up to 25 % higher for the mid- to late Holocene. (Fig. 2.6) Deriving mid to late Holocene values that are comparable to estimates based on $\delta^{13}C$ values requires using either a lower $\delta^{15}N_{terr}$ value (< +1 ‰) or a

lower $\delta^{15}N_{mar}$ value (+7 ‰). It is unlikely that $\delta^{15}N_{terr}$ values would have varied or been less than 1 ‰. It is more likely that $\delta^{15}N_{mar}$ changed over time. Variations in $\delta^{15}N_{mar}$ could have resulted from a change in the ecosystem (e.g., diatom-dominated, shorter foodwebs result in lower $\delta^{15}N_{mar}$ values; Montoya et al., 1994; Wu et al., 1999a and b). It is also possible that the isotopic composition of the source nitrate changed. At present, the $\delta^{15}N$ of source nitrate off Vancouver Island ranges from approximately +5 to +6‰ (Wu et al., 1997; Kienast et al., 2002). Waters with nitrate $\delta^{15}N$ values substantially higher than +5 ‰ (i.e., up to +19 ‰) are found in regions characterized by water column denitrification (Cline and Kaplan, 1975; Brandes et al., 1998; Altabet et al., 1999). While denitrification is not occurring off Vancouver Island at present it may have occurred in the past when the oxygen minimum zone (OMZ) was more intense (i.e., more oxygen depleted). Episodes of OMZ intensification during the Allerød and at the Pleistocene-Holocene boundary are characterized by relatively high sedimentary $\delta^{15}N$ values (Chapter 3). While high sedimentary $\delta^{15}N$ values suggest that denitrification influenced the N-isotopic composition of organic matter off Vancouver Island, they do not provide conclusive evidence that denitrification was occurring in this specific region. It is also possible that ^{15}N-enriched nitrate was imported from the Equatorial East Pacific by the California Undercurrent (Liu and Kaplan, 1989; Altabet et al., 1999; Kienast et al., 2002). If this is the case, then the $\delta^{15}N$ composition of nitrate off Vancouver Island would have been influenced by secular changes in denitrification in the Equatorial East Pacific (Ganeshram et al., 1995; Pride et al., 1999) and by the strength of California Undercurrent (Kienast et al., 2002). Ongoing work based on new cores collected from the region will hopefully resolve this question.

2.5 Summary

At the end of the last glacial (~14.3 kyr B.P.) the nature of organic matter accumulation on the continental margin off Western Canada changed dramatically. Prior to

14.3 kyr B.P. the accumulation of terrestrial organic matter was high while the accumulation of marine organic matter was relatively low. This was a reflection of low primary production, and resulting low export production, because glacial-mode atmospheric circulation did not drive upwelling in the region. At the start of the deglacial (i.e., the Bølling) the accumulation of marine organic matter increased, suggesting a return to modern atmospheric and oceanic circulation. However, most if not all of this apparent increase is due to the very high sedimentation rate (169 cm/kyr), although higher marine export production cannot be totally discounted. Marine organic matter deposited during the early deglacial was diluted by abundant terrestrial organic matter, generated as glaciers retreated from the continental shelf. This situation continued until the start of the Allerød when the input of terrestrial organic matter decreased and the accumulation of marine organic matter doubled. The combination of higher marine organic carbon concentrations and mass accumulation rates suggests that marine productivity did increase at this time. There was a brief return to glacial-like conditions during the Younger Dryas and a corresponding decrease in marine organic matter accumulation. Palaeo-proxy data suggest the accumulation of marine organic matter during the Holocene was, and still is, lower than during the late Pleistocene. This may be a reflection of low organic matter preservation due to the relatively low sedimentation rates (i.e., relatively long oxygen exposure times; see Chapter 3) and intense biological utilization.

2.6 References

Altabet, M.A., 1996. Nitrogen and carbon isotopic tracers of the source and transformation of particles in the deep-sea. In: Ittekkot, V., Schafer, P., Honjo, S., Depetris, P.J. (Eds.), Particle Flux in the Ocean. John Wiley and Sons, London, pp. 155-184.

Altabet, M.A., Francois, R., 1994a. Sedimentary nitrogen isotopic ratio as a recorder for surface ocean nitrate utilization. Global Biogeochemical Cycles 8, 103-116.

Altabet, M.A., Francois, R., 1994b. The use of nitrogen isotopic ratios for reconstruction of past
changes in surface ocean nutrient utilization. In: Zahn, R., Pedersen, T.F., Kaminski, M.A., Labeyrie, L. (Eds.), Carbon Cycling in the Glacial Ocean: Constraints on the Ocean's Role in Global Change. NATO ASI Series, Vol. 117. Springer-Verlag, Berlin, pp. 281-306.

Altabet, M.A., Deuser, W.G., Honjo, S., Stienen, C., 1991. Seasonal and depth-related changes
in the source of sinking particles in the North Atlantic. Nature 354, 136-138.

Altabet, M.A., Pilskaln, C., Thunell, R., Pride, C., Sigman, D., Chavez, F., Francois, R., 1999. The nitrogen isotope biogeochemistry of sinking particles from the margin of the Eastern North Pacific. Deep Sea Research (I) 46, 655-679.

Antoine, D., Andre, J.M., Morel, A., 1996. Oceanic primary production. 2. Estimation at global scale from satellite (coastal zone colour scanner) chlorophyll. Global Biogeochemical Cycles 10, 57-69.

Archer, D., Lyle, M., Rodgers, K., Froelich, P., 1993. What controls opal preservation in tropical deep-sea sediment? Paleoceanography 8, 7-21.

Bakun, A., 1990. Global climate change and intensification of coastal ocean upwelling. Science 247, 198-201.

Bard, E., Hamelin, B., Arnold, M., Montaggioni, L., Cabioch, G., Faure, G., Rougerie, F., 1996. Deglacial sea-level record from Tahiti corals and the timing of global meltwater discharge. Nature 382, 241-244.

Barry, J.V., Conway, K.W., 1999. Late Quaternary glaciation and postglacial stratigraphy of the Northern Pacific Margin of Canada. Quaternary Research 51, 113-123.

Bernstein, R.E., Byrne, R.H., Betzer, P.R., Greco, A.M., 1992. Morphologies and transformations of celestite in seawater: The role of acantharians in strontium and barium geochemistry. Geochimica et Cosmochimica Acta 56, 3273-3279.

Bishop, J.K.B., 1988. The barite-opal-organic carbon association in oceanic particulate matter. Nature 332, 341-343.

Bornhold, B.D., Yorath, C.J., 1984. Surficial geology of the continental shelf, northwestern Vancouver Island. Marine Geology 57, 89-112.

Brandes, J.A., Devol, A.H., Yoshinari, T., Jayakumar, D.A., Naqvi S.W.A., 1998. Isotopic composition of nitrate in the central Arabian Sea and eastern tropical North Pacific: A tracer for mixing and nitrogen cycles. Limnology and Oceanography 43, 1680-1689.

Calvert, S.E., 1990. Geochemistry and origin of the Holocene sapropel in the Black Sea. In: Ittekkot, V., Kempe, S., Michaelis, W., Spitzy, A. (Eds.), Facets of Modern Biogeochemistry. Springer-Verlag, Berlin, pp. 326-352.

Capone, D.G., Zehr, J.P., Paerl, H.W., Bergman, B., Carpenter, E.J., 1997. *Trichodesmium*, a globally significant marine cyanobacterium. Science 276, 1221-1229.

Carpenter, E.J., Harvey, H.R., Fry, B., Capone, D.G., 1997. Biogeochemical tracers of the marine cyanobacterium *Trichodesmium*. Deep Sea Research (I) 44, 27-38.

Clague, J.J., James, T.S., 2002. History and isostatic effects of the last ice sheet in southern British Columbia. Quaternary Science Reviews 21, 71-87,

Cline, J.D., Kaplan, I.R., 1975. Isotopic fractionation of dissolved nitrate during denitrification in the Eastern Tropical North Pacific Ocean. Marine Chemistry 3, 271-299.

COHMAP Members, 1988. Climatic changes of the last 18,000 years: Observations and model simulations. Science 241, 1043-1052.

De Lange, G.J., Os, B.V., Pruysers, P.A., Middelburg, J.J., Castradori, D., Van Santvoort, P., Muller, P.J., Eggenkamp, H., Prahl, F.G., 1994. Possible early diagenetic alteration of palaeo proxies. In: Zahn, R., Pedersen, T.F., Kaminski, M.A., Labeyrie, L. (Eds.), Carbon Cycling

in the Glacial Ocean: Constraints on the Ocean's Role in Global Change. NATO ASI Series, Vol. 117. Springer-Verlag, Berlin, pp. 225-257.

Dean, W.E., Gardner, J.V., 1998. Pleistocene to Holocene contrasts in organic matter production and preservation on the California continental margin. Geological Society of America Bulletin 110, 888-899.

Dehairs, F., Chesselet, R., Jedwab, J., 1980. Discrete suspended particles of barite and the barium cycle in the open ocean. Earth and Planetary Science Letters 49, 528-550.

Dehairs, F., W. Baeyens, W., Goeyens, L., 1992. Accumulation of suspended barite at mesopelagic depths and export production in the Southern Ocean. Science 258, 1332-1335.

Doose, H., Prahl, F.G., Lyle, M.W., 1997. Biomarker temperature estimates for modern and last glacial surface waters of the California Current system between 33° and 42°N. Paleoceanography 12, 615-622.

Dymond, J., Suess, E., Lyle, M., 1992. Barium in deep-sea sediment: A geochemical proxy for paleoproductivity. Paleoceanography 7, 163-181.

Eglinton, G., Hamilton, R.H., 1967. Leaf epicuticular waxes. Science 156, 1322-1335.

Falkner, K.K., Klinkhammer, G.P., Bowers, T.S., Todd, J.F., Lewis, B.L., Landing, W.M., Edmond, J.M., 1993. The behavior of barium in anoxic marine waters. Geochimica et Cosmochimica Acta 57, 537-554.

Farrell, J.W., Pedersen, T.F., Calvert, S.E., Nielsen, B., 1995. Glacial-interglacial changes in nutrient utilization in the equatorial Pacific Ocean. Nature 377, 514-517.

Faure, G., 1986. Principles of Isotope Geology, 2nd edition. John Wiley & Sons Inc., New York, 589pp.

Fernandes, M.B., Sicre, M.-A., 2000. The importance of terrestrial organic carbon inputs on Kara Sea shelves as revealed by n-alkanes, OC and $\delta^{13}C$ values. Organic Geochemistry 31, 363-374.

Francois, R., Altabet, M.A., Goericke, R., 1994. Changes in the $\delta^{13}C$ of surface water particulate organic matter across the subtropical convergence in the S.W. Indian Ocean. In:

Zahn, R., Pedersen, T.F., Kaminski, M.A., Labeyrie, L. (Eds.), Carbon Cycling in the Glacial Ocean: Constraints on the Ocean's Role in Global Change. NATO ASI Series, Vol. 117. Springer-Verlag, Berlin, pp. 307-321.

Francois, R., Altabet, M.A., Yu, E.-F., Sigman, D.M., Bacon, M.P., Frank, M., Bohrmann, G., Bareille, G., Labeyrie, L.D., 1997. Contribution of Southern Ocean surface-water stratification to low atmospheric CO_2 concentrations during the last glacial period. Nature 389, 929-935.

Francois, R., Honjo, S., Manganini, S.J., Ravizza, G.E., 1995. Biogenic barium fluxes to the deep sea: Implications for paleoproductivity reconstruction. Global Biogeochemical Cycles 9, 289-303.

Freudenthal, T., Wagner, T., Wenzhofer, F., Zabel, M., Wefer, G., 2001. Early diagenesis of organic matter from sediments of the eastern subtropical Atlantic: Evidence from stable nitrogen and carbon isotopes. Geochimica et Cosmochimica Acta 65, 1795-1808.

Fry, B., Wainright, S.C., 1991. Diatom sources of ^{13}C-rich carbon in marine food webs. Marine Ecology Progress Series 76, 149-157.

Ganeshram, R.S., 1996. On the glacial-interglacial variability of upwelling, carbon burial and denitrification on the northwestern Mexican continental margin. Ph.D. dissertation thesis, University of British Columbia.

Ganeshram, R.S., Pedersen, T.F., Calvert, S.E., Murray, J.W., 1995. Large changes in oceanic nutrient inventories from glacial to interglacial periods. Nature 376, 755-758.

Ganeshram, R.S., Calvert, S.E., Pedersen, T.F., Cowie, G.A., 1999. Factors controlling the burial of organic carbon in laminated and bioturbated sediments off NW Mexico. Implications for hydrocarbon preservation. Geochimica et Cosmochimica Acta 63, 1723-1734.

Ganeshram, R.S., Pedersen, T.F., Calvert, S.E., McNeill, G.W., Fontugne, M.R., 2000. Glacial-interglacial variability in denitrification in the world's ocean: Causes and consequences. Paleoceanography 15, 361-376.

Ganeshram, R.S., Francois, R., Commeau, J., Brown-Leger, S.L., 2003. An experimental investigation of barite formation in seawater. Geochimica et Cosmochimica Acta 67, 2599-2605.

Gardner, J.V., Dean, W.E., Dartnell, P., 1997. Biogenic sedimentation beneath the California Current system for the past 30 kyr and its paleoceanographic significance. Paleoceanography 12, 207-225.

Gélinas, Y., Baldock, J.A., Hedges, J.I., 2001. Organic carbon composition of marine sediments: Effect of oxygen exposure on oil generation potential. Science 294, 145-148.

Gingele, F., Dahmke, A., 1994. Discrete barite particles and barium as tracers of paleoproductivity in South Atlantic sediments. Paleoceanography 9, 151-168.

Goericke, R., Fry, B., 1994. Variations of marine plankton $\delta^{13}C$ with latitude, temperature, and dissolved CO_2 in the world ocean. Global Biogeochemical Cycles 8, 85-90.

Goldberg, E.D., Arrhenius, G., 1958. Chemistry of Pacific pelagic sediments. Geochimica et Cosmochimica Acta 13, 153-212.

Hedges, J.I., Keil, R.G., 1995. Sedimentary organic matter preservation: An assessment and speculative synthesis. Marine Chemistry 49, 81-115.

Hedges, J.I., Oades, J.M., 1997. Comparative organic geochemistry of soils and marine sediments. Organic Geochemistry 27, 319-361.

Hickey, B.M., 1998. Coastal oceanography of western North America from the tip of Baja California to Vancouver Island. In: Robinson, A.R., Brink, K.H. (Eds.), The sea. John Wiley & Sons Inc., pp. 345-391.

Jasper, F.P., Gagosian, R.B., 1993. The relationship between sedimentary organic carbon isotopic composition and organic biomarker compound concentration. Geochimica et Cosmochimica Acta 57, 167-186.

Jasper, J.P., Hayes, J.M., 1990. A carbon isotope record of CO_2 levels during the late Quaternary. Nature 347, 462-464.

Keil, R.G., Tsamakis, E., Fuh, C.B., Giddings, J.C., Hedges, J.I., 1994. Mineralogical and textural controls on the organic composition of coastal marine sediments: Hydrodynamic separation using SPLITT-fractionation. Geochimica et Cosmochimica Acta 58, 879-893.

Kienast, S.S, McKay, J.L., 2001. Sea surface temperatures in the subarctic Northeast Pacific reflect millennial-scale climate oscillations during the last 16 kyrs. Geophysical Research Letters 28, 1563-1566.

Kienast, S.S., Calvert, S.E., Pedersen, T.F., 2002. Nitrogen isotope and productivity variations along the northeast Pacific margin over the last 120 kyr: Surface and subsurface palaeoceanography. Paleoceanography 17, doi: 10.1029/2001PA000650.

Kovanen, D.J., Easterbrook, D.J., 2002. Paleodeviations of radiocarbon marine reservoir values for the northeast Pacific. Geology 30, 243-246.

Law, E.A., Popp, B.N., Bidigare, R.R., Kennicutt, M.C., Macko, S.A., 1995. Dependence of phytoplankton carbon isotopic composition on growth rate and $[CO_2]_{aq}$: Theoretical considerations and experimental results. Geochimica et Cosmochimica Acta 59, 1131-1138.

Liu, K.-K., Kaplan, I.R., 1989. The eastern tropical Pacific as a source of ^{15}N-enriched nitrate in seawater off southern California. Limnology and Oceanography 35, 820-830.

Lyle, M., Zahn, R., Prahl, F., Dymond, J., Colier, R., Pisias, N., Suess, E., 1992. Paleoproductivity and carbon burial across the California Current: The mulitracers transect, 42°N. Paleoceanography 7, 251-272.

Mayer, L.M., 1994. Surface area control of organic carbon accumulation in continental shelf sediments. Geochimica et Cosmochimica Acta 58, 1271-1284.

Marlowe, I.T., Brassell, S.C., Eglinton, G., Green, J.C., 1990. Long-chain alkenones and alkyl alkenoates and the fossil coccolith record of marine sediments. Chemical Geology 88, 349-375.

Mathewes, R.W., Heusser, L.E., Patterson, R.T., 1993. Evidence for a Younger Dryas-like cooling event on the British Columbia coast. Geology 21, 101-104.

McManus, J., Berelson, W.M., Klinkhamer, G.P., Kilgore, T.E., Hammon, D.E., 1994. Remobilization of barium in continental margin sediments. Geochimica et Cosmochimica Acta 58, 4899-4907.

McManus, J., Berelson, W.M., Klinkhammer, G.P., Johnson, K.S., Coale, K.H., Anderson, R.F., Kumar, N., Burdige, D.J., Hammond, D.E., Brumsack, H.J., McCorkle, D.C., Rushdi, A., 1998. Geochemistry of barium in marine sediments: Implications for its use as a paleoproxy. Geochimica et Cosmochimica Acta 62, 3453-3473.

Meyers, P.A., 1997. Organic geochemical proxies of paleoceanographic, paleolimnologic, and paleoclimatic processes. Organic Geochemistry 27, 213-250.

Minoura, K., Hoshino, K., Nakamura, T., Wada, E., 1997. Late Pleistocene-Holocene paleoproductivity circulation in the Japan Sea: Sea-level control on $\delta^{13}C$ and $\delta^{15}N$ records of sediment organic material. Palaeogeography, Palaeoclimatology, Palaeoecology 135, 41-50.

Mix, A.C., Lund, D.C., Pisias, N.G., Bodén, P., Bornmalm, L., Lyle, M., Pike, J., 1999. Rapid climate oscillations in the northeast Pacific during the last deglaciation reflect northern and southern hemisphere sources. In: Clark, P.U., Webb, R.S., Keigwin, L.D. (Eds.), Mechanisms of Global Climate Change at Millennian Time Scales, Geophysical Monograph 112. American Geophysical Union, Washington, D.C., pp. 127-148.

Montoya, J.P., 1994. Nitrogen isotope fractionation in the modern ocean: Implications for the sedimentary record. In: Zahn, R., Pedersen, T.F., Kaminski, M.A., Labeyrie, L. (Eds.), Carbon Cycling in the Glacial Ocean: Constraints on the Ocean's Role in Global Change. NATO ASI Series, Vol. 117. Springer-Verlag, Berlin, pp. 259-279.

Mortlock, R.A., Froelich, P.N., 1989. A simple method for the rapid determination of biogenic opal in pelagic marine sediments. Deep Sea Research 36, 1415-1426.

Mortyn, P.G., Thunell, R.C., Anderson, D.M., Stott, L.D., Le, J., 1996. Sea surface temperature changes in the Southern California Borderlands during the last glacial-interglacial cycle. Paleoceanography 11, 415-430.

Nurnberg, C.C., Bohrmann, G., Schluter, M., 1997. Barium accumulation in the Atlantic sector of the Southern Ocean: Results from 190,000-year records. Paleoceanography 12, 594-603.

Ohkouchi, N., Kawamura, K., Taira, A., 1997. Molecular paleoclimatology: Reconstruction of climate variabilities in the late Quaternary. Organic Geochemistry 27, 173-183.

Okada, H., Honjo, S., 1973. The distribution of oceanic coccolithophorids in the Pacific. Deep Sea Research 20, 355-374.

Ortiz, J., Mix, A., Hostetler, S., Kashgarian, M., 1997. The California Current of the last glacial maximum: Reconstruction at 42°N based on multiple proxies. Paleoceanography 12, 191-205.

Pedersen, T.F., 1983. Increased productivity in the eastern equatorial Pacific during the last glacial maximum (19,000 to 14,000 yr B.P.). Geology 11, 16-19.

Peters, K.E., Sweeney, R.E., Kaplan, I.R., 1978. Correlation of carbon and nitrogen stable isotope ratios in sedimentary organic matter. Limnology and Oceanography 23, 598-604.

Popp, B.N., Takigiku, R., Hayes, J.M., Louda, J.W., Baker, E.W., 1989. The post-Paleozoic chronology and mechanism of ^{13}C depletion in primary marine organic matter. American Journal of Science 289, 436-454.

Popp, B.N., Laws, E.A., Bidigare, R.R., Dore, J.E., Hanson, K.L., Wakeham, S.G., 1998. Effect of phytoplankton cell geometry on carbon isotopic fractionation. Geochimica et Cosmochimica Acta 62, 69-77.

Popp, B.N., Trull, T., Kenig, F., Wakeham, S.G., Rust, T.M., Tilbrook, B., Griffiths, F.B., Wright, S.W., Marchant, H.J., Bidigare, R.R., Laws, E.A., 1999. Controls on the carbon isotopic composition of Southern Ocean phytoplankton. Global Biogeochemical Cycles 11, 827-843.

Prahl, F.G., Wakeham, S.G., 1987. Calibration of unsaturation patterns in long-chain ketone compositions for palaeotemperature assessment. Nature 330, 367-369.

Prahl, F.G., Muehlhausen, L.A., Lyle, M., 1989. An organic geochemical assessment of oceanographic conditions at MANOP Site C over the past 26,000 years. Paleoceanography 4, 495-510.

Prahl, F.G., Ertel, J.R., Goni, M.A., Sparrow, M.A., Eversmeyer, B., 1994. Terrestrial organic carbon contributions to sediments on the Washington margin. Geochimica et Cosmochimica Acta 58, 3035-3048.

Prahl, F.G., De Lange, G.J., Scholten, S., Cowie, G.L., 1997. A case of post-depositional aerobic degradation of terrestrial organic matter in turbidite deposits from the Madeira Abyssal Plain. Organic Geochemistry 27, 141-152.

Pride, C., Thunell, T., Sigman, D., Keigwin, L., Altabet, M., Tappa, E., 1999. Nitrogen isotopic variations in the Gulf of California since the last deglaciation: Response to global climate change. Paleoceanography 14, 397-409.

Ragueneau, O., Tréguer, P., Leynaert, A., Anderson, R.F., Brzezinski, M.A., DeMaster, D.J., Dugdale, R.C., Dymond, J., Fischer, G., Francois, R., Heinze, C., Maier-Reimer, E., Martin-Jézéquel, V., Nelson, D.M., Quéguiner, B., 2000. A review of the Si cycle in the modern ocean: Recent progress and missing gaps in the application of biogenic opal as a paleoproductivity proxy. Global Planetary Change 26, 317-365.

Rau, G.H., 1994. Variations in sedimentary organic $\delta^{13}C$ as a proxy for past changes in ocean and atmospheric $[CO_2]$. In: Zahn, R., Pedersen, T.F., Kaminski, M.A., Labeyrie, L. (Eds.), Carbon Cycling in the Glacial Ocean: Constraints on the Ocean's Role in Global Change. NATO ASI Series, Vol. 117. Springer-Verlag, Berlin, pp. 307-322.

Rau, G.H., Takahashi, T., Des Marais, D.J., 1989. Latitudinal variations in plankton $\delta^{13}C$: implications for CO_2 and productivity in past oceans. Nature, 341, 516-518.

Rau, G.H., Froelich, P.N., Takahashi, T., Des Marais, D.J., 1991. Does sedimentary organic $\delta^{13}C$ record variations in Quaternary ocean $[CO_2(aq)]$? Paleoceanography 6, 335-347.

Rau, G.H., Riebesell, U., Wolf-Gladrow, D., 1997. CO_2aq-dependent photosynthesis ^{13}C fractionation in the ocean: A model versus measurements. Global Biogeochemical Cycles 11, 267-278.

Sabin, A.L., Pisias, N.G., 1996. Sea surface temperature changes in the northeastern Pacific Ocean during the past 20,000 years and their relationship to climate change in northwestern North America. Quaternary Research 46, 48-61.

Saino, T., Hattori, A., 1987. Geographical variations of the water column distribution of suspended particulate organic nitrogen and its ^{15}N natural abundance in the Pacific and its marginal seas. Deep Sea Research 34, 807-827.

Sancetta, C., Lyle, M., Heusser, L., Zahn, R., Bradbury, J., 1992. Late-glacial to Holocene changes in winds and upwelling, and seasonal production of the northern California Current system. Quaternary Research 38, 359-370.

Sarnthein, M., Winn, K., Duplessy, J.-C., Fontugne, M.R., 1988. Global variations of surface ocean productivity in low and mid latitudes: Influence on CO_2 reservoirs of the deep ocean and atmosphere during the last 21,000 years. Paleoceanography 3, 361-399.

Schmitz, B., 1987. Barium, equatorial high productivity, and the northward wandering of the Indian continent. Paleoceanography 2, 63-77.

Schubert, C.J., Villanueva, J., Calvert, S.E., Cowie, G.L., von Rad, U., Schulz, H., Berner, U. and Erlenkeuser, H., 1998. Stable phytoplankton community structure in the Arabian Sea over the past 200,000 years. Nature 394, 563-566.

Shimmield, G., Derrick, S., Mackensen, A., Grobe, H., Pudsey, C., 1994. The history of barium, biogenic silica and organic carbon accumulation in the Weddell Sea and Antarctic Ocean over the last 150,000 years. In: Zahn, R., Pedersen, T.F., Kaminski, M.A., Labeyrie, L. (Eds.), Carbon Cycling in the Glacial Ocean: Constraints on the Ocean's Role in Global Change. NATO ASI Series, Vol. 117. Springer-Verlag, Berlin, pp. 555-574.

Sigman, D.M., Altabet, M.A., Francois, R., McCorkle, D.C., Gaillard, J.-F., 1999. The isotopic composition of diatom-bound nitrogen in Southern Ocean sediments. Paleoceanography, 118-134.

Stuiver, M., Reimer, P.J., Bard, E., Beck, J.W., Burr, G.S., Hughen, K.A., Dromer, B., McCormac, G., Van der Plicht, J., Spurk, M., 1998. INTCAL98 radiocarbon age calibration, 24,000-0 cal BP. Radiocarbon 40, 1041-1083.

Taylor, R.S., McLennan, S.M., 1985. The Continental Crust: Its Composition and Evolution. Blackwell Scientific, Boston, 312pp.

Thompson, E.I., Schmitz, B., 1997. Barium and the late Paleocene $\delta^{13}C$ maximum: Evidence of increased marine surface productivity. Paleoceanography 12, 239-254.

Thomas, A.C., Huang, F., Strub, P.T., James, C., 1994. Comparison of the seasonal and interannual variability of phytoplankton pigment concentrations in the Peru and California Current systems. Journal of Geophysical Research 99, 7355-7370.

Thomson, R.E., 1981. Oceanography of the British Columbia Coast. Canadian Special Publication of Fisheries and Aquatic Sciences 56, 291pp.

Thunell, R.C, Mortyn, P.G., 1995. Glacial climate instability in the Northeast Pacific Ocean. Nature 376, 504-506.

Toggweiler, J.R., 1999. Variations of atmospheric CO_2 by ventilation of the ocean's deepest water. Paleoceanography 14, 571-588.

Villanueva, J., Grimalt, J.O., Cortijo, E., Vidal, L., Labeyrie, L., 1997a. A biomarker approach to the organic matter deposited in the North Atlantic during the last climatic cycle. Geochimica et Cosmochimica Acta 61, 4633-4646.

Villanueva, J., Pelejero, C., Grimalt, J.O., 1997b. Clean-up procedures for the unbiased estimation of C37-C39 alkenones sea surface temperatures and terrigenous *n*-alkane inputs in paleoceanography. Journal of Chromatography A757, 145-151.

von Breymann, M.T., Emeis, K.-C., Suess, E., 1992. Water depth and diagenetic constraints on the use of barium as a palaeoproductivity indicator. In: Summerhayes, C.P., Prell, W.L., Emeis, K.-C. (Eds.), Upwelling Systems: Evolution Since the Early Miocene. Geological Society Special Publication 64, pp. 273-284.

Werne, J.P., Hollander, D.J., Lyons, T.W., Peterson, L.C., 2000. Climate-induced variations in productivity and planktonic ecosystem structure from the Younger Dryas to Holocene in the Cariaco Basin, Venezuela. Paleoceanography 15, 19-29.

Wu, J., 1997. The carbon and nitrogen isotope compositions of particulate organic matter in the subarctic northeast Pacific Ocean. PhD. Thesis, University of British Columbia, 252p.

Wu, J., Calvert, S.E., Wong, C.S., 1997. Nitrogen isotope variations in the subarctic northeast Pacific: relationships to nitrate utilization and trophic structure. Deep Sea Research 44, 287-314.

Wu, J., Calvert, S.E., Wong, C.S., 1999a. Carbon and nitrogen isotope ratios in sedimenting particulate organic matter at an upwelling site off Vancouver Island. Estuarine, Coastal and Shelf Science 48, 193-203.

Wu, J., Calvert, S.E., Wong, C.S., Whitney, F.A., 1999b. Carbon and nitrogen isotopic composition of sedimenting particulate material at Station Papa in the subarctic northeast Pacific. Deep Sea Research (II) 46, 2793-2832.

Yorath, C.J., Nasmith, H.W., 1995. The Geology of Southern Vancouver Island. Orca Book Publishers, Victoria, Canada, 172pp.

3. Intensification of the Oxygen Minimum Zone in the Northeast Pacific during the Last Deglaciation: Ventilation or Export Production?

3.1 Introduction

Extensive evidence indicates that the intensity (i.e., degree of oxygen depletion) of the oxygen minimum zone (OMZ) along the eastern margin of the North Pacific Ocean has fluctuated significantly over time. Laminated sediments have been observed in cores collected from the Gulf of California (Keigwin and Jones, 1990), partially isolated basins within the California Borderlands region (e.g., Santa Barbara Basin - Behl and Kennett, 1996; and Santa Monica Basin - Stott et al., 2000b) and from the open continental margin off California (Gardner and Hemphill-Haley, 1986; Anderson et al., 1987; Dean et al., 1994; van Geen et al., 1996) and northwestern Mexico (Ganeshram, 1996). The light and dark layers that constitute a single lamination are seasonal layers preserved when bottom water containing <0.1 ml/l oxygen inhibits bioturbation (e.g., Thunell et al., 1995; Pilskaln and Pike, 2001). The laminated deposits are interbedded with partly- to well-homogenized sediments that were bioturbated when the bottom water was more oxygenated. In addition to preserving laminations, a low dissolved oxygen concentration in the bottom water also directly influences the species of benthic foraminifera that occur in the underlying sediments (Kaiho, 1994). In cores collected from the California margin for example, a foraminiferal assemblage tolerant of very low oxygen conditions alternates with an assemblage that requires better oxygenation (Cannariato et al., 1999; Cannariato and Kennett, 1999), and in the Santa Barbara Basin the appearance of a foraminiferal assemblage tolerant of low oxygen conditions is synchronous with the change to laminated sediments (Cannariato et al., 1999). The concentrations of redox-sensitive trace metals (e.g., Mo) in sediments have also varied on glacial to interglacial and shorter time scales (Nammeroff, 1996; Dean et al., 1997; Zheng et al., 2000; Ivanochko, 2001) further indicating that bottom water oxygen levels have

fluctuated. Collectively, the accumulated evidence suggests that the OMZ along the eastern margin of the North Pacific was less intense (i.e., relatively oxygen-rich) during colder intervals such as the Younger Dryas, MIS 2, and stadials within MIS 3 and 4, and more intense (i.e., relatively oxygen-depleted) during warm periods (Keigwin and Jones, 1990; Kennett and Ingram, 1995; Behl and Kennett, 1996). Not only has the intensity of the OMZ fluctuated, but its boundaries may have shifted vertically causing the OMZ to expand and contract over time (van Geen et al., 1996; Cannariato and Kennett; 1999; Stott et al., 2000b).

The intensity of the OMZ is a function of two primary variables: i) ocean circulation, hence-forth referred to as ventilation; and ii) oxygen consumption (Wyrtki, 1962). Ventilation refers to any advective process that transfers surface conditions, in this instance high oxygen concentrations, to subsurface waters (Van Scoy and Druffel, 1993). It may occur via the cropping out of a particular isopycnal at the ocean surface (and then its' subduction), by the formation of a denser water mass during, for example, winter cooling and sea ice formation, and/or by vertical mixing (Talley, 1991). Oxygen consumption refers to the utilization of oxygen during degradation of organic matter, both as it settles through the water column and after deposition on the sea floor. The higher the rate of export of labile organic matter from surface waters, the greater the oxygen depletion of the underlying intermediate waters. There is considerable debate over which of these mechanisms, ventilation or productivity, or some combination of the two was responsible for changes in intensity of the OMZ along the eastern margin of the North Pacific.

At present, ventilation of the OMZ in the northeast Pacific Ocean reflects a balance between the relatively oxygen-rich North Pacific Intermediate Water (NPIW) and the oxygen-poor Subtropical Subsurface Water (SSW). NPIW is identified by a salinity minimum at a density of 26.7 to 26.9 σ_θ (Reid, 1965). This water mass occurs throughout the North Pacific Subtropical Gyre and extends as far north as the Gulf of Alaska (Talley, 1993). NPIW forms in the region of the Sea of Okhotsk where Western Subarctic Water, which is carried south by the Oyashio Current, mixes with cold and relatively fresh Sea of

Okhotsk Water (Talley, 1991; Freeland et al., 1998; Wong et al. 1998). The resulting water is then modified by mixing with Kuroshio Water in the region just to the east of the Sea of Okhotsk and NPIW is produced (Talley, 1993; Kono, 1996). There is also evidence of ventilation of NPIW within the Alaskan gyre due to winter mixing and occasional cropping out at the surface of the 26.8 σ_θ density surface (Van Scoy et al., 1991a and b; You et al., 2000).

A number of studies have suggested that enhanced formation of NPIW can explain the weakening of the OMZ during cold climatic periods (Duplessy et al., 1988; Keigwin and Jones, 1990; Kennett and Ingram, 1995; van Geen et al., 1996; Behl and Kennett, 1996; Keigwin, 1998; Zheng et al., 2000). Indeed, coupled ocean-atmosphere climate models predict enhanced NPIW formation during the Younger Dryas (Mikolajewicz et al., 1997) and the Last Glacial Maximum (Ganopolski et al., 1998). Better ventilation of NPIW during the last glacial has been inferred from relatively high $\delta^{13}C$ values of benthic foraminifera which suggest the presence of a younger, relatively nutrient-poor water mass in the northwest Pacific at intermediate water depths (Duplessy et al., 1988; Keigwin et al., 1998). Radiocarbon data for coeval benthic and planktonic foraminifera (i.e., benthic-planktonic age differences) for a core from northwestern Pacific also suggest increased ventilation during the last glacial, as well as decreased ventilation (i.e., older intermediate water) during the deglacial (Duplessy et al., 1989). On the eastern side of the Pacific, radiocarbon data from the Santa Barbara Basin indicate increased ventilation during the Last Glacial Maximum and Younger Dryas (Ingram and Kennett, 1995; Kennett and Ingram, 1995). Radiocarbon data from cores collected on the open California margin are more ambiguous, indicating decreased ventilation between 11 and 9 kyr B.P. at a water depth of 800 m at 35°N (van Geen et al., 1996). However, ^{14}C measurements made on ODP Hole 1019 collected from the continental slope (980 m) off northern California (41°N) suggest increased, not decreased, ventilation during the early Holocene and Bølling-Allerød at the same time as intensification of the OMZ occurred (Mix et al., 1999).

Most previous studies that have focused on the history of the OMZ in the eastern Pacific have dwelt on changes in NPIW formation and have ignored possible changes in the supply and/or oxygen content of Subtropical Subsurface Water (SSW; Wyrtki, 1967). This water mass is characterized by relatively high temperature, high salinity, high nutrient content and a low oxygen concentration (Lynn and Simpson, 1987). Oxygen depletion of SSW is the result of high productivity in the Equatorial East Pacific and subsequent degradation of the exported organic matter (Wyrtki, 1967). This oxygen-depleted water is then transported northward along the west coast of North America as far north as Vancouver Island, Canada by the California Undercurrent (Reed and Halpern, 1976; Mackas et al., 1987). However, mixing with adjacent water masses modifies the physical and chemical properties of SSW as it moves northward (e.g., decreasing temperature - Halpern et al., 1978; decreasing $\delta^{15}N$ values - Kienast et al., 2002). Off Vancouver Island the highest percentage of SSW is observed at a depth of 100 to 300 m where the California Undercurrent (CUC) is strongest (Reed and Halpern, 1976). Weaker flow below 300 m allows increased mixing of SSW with other water masses; however, SSW is still recognizable as deep as 1300 m (Reed and Halpern, 1976). Because the percentage of SSW in intermediate waters is controlled by the strength of the CUC it is probable that changes in CUC strength would influence the oxygen concentration of intermediate waters.

During the Last Glacial Maximum, the Aleutian Low was situated more to the east, over the Northeast Pacific (COHMAP, 1988) and the Subarctic Gyre expanded southward (Doose et al., 1997). As a result, the CUC would not have extended as far north as Vancouver Island and thus the supply of imported oxygen-poor SSW should have been cut off. In regions that remained within the California Current System it is also possible that the supply of oxygen-poor waters was reduced during the glacial, but for different reasons. Evidence from the continental slope off Mazatlan, Mexico indicates that the OMZ was relatively oxygen-rich during the Last Glacial Maximum (Ganeshram et al., 1995). Thus, SSW carried northward by the CUC would have contained more oxygen than at present.

Also, the strength of the California Current appears to have been significantly reduced north of ~35°N (Doose et al., 1997) and presumably so was the strength of the CUC. Weakening of the CUC would have allowed increased mixing between SSW and more oxygen-rich water masses such as Pacific Subarctic Water and NPIW. Thus increased ventilation may have occurred even if the strength of NPIW formation had remained constant.

From what is known at present, it is still unclear whether changes in ventilation are responsible for variations in the intensity of the OMZ along the northeastern margin of the Pacific Ocean. Furthermore, all previous research has focused on the OMZ off southern Oregon, California and Mexico but nothing is known about the history of the OMZ north of 42°N. This study was initiated to fill this gap in our knowledge. The study area is located off the west coast of Vancouver Island, Canada (48°54'N, 126°53'W; Fig. 3.1) and sits at the northern end of the California Current System where the eastward-flowing Subarctic Current and North Pacific Current split into the northward flowing Alaska Current and southern flowing California Current (Thomson, 1981). In this region high primary productivity is driven by seasonal (spring-summer), wind-driven upwelling which is related to the northerly position (38°N) of the North Pacific High (Huyer, 1983). In winter, the North Pacific High shifts southward to 28°N and is replaced by the expanded Aleutian Low. This leads to a reversal of the wind direction, cessation of upwelling off Vancouver Island, and stronger winter storms crossing into North America.

Over the last 16 calendar kyr B.P. primary productivity and organic carbon flux to the sediment has varied substantially in this region (Chapter 2). Variability in organic carbon production may have influenced the intensity of the OMZ locally. However, the study area is also proximal to regions of NPIW formation and ventilation. Therefore, if variations in the intensity of the OMZ were related to changes in ventilation of intermediate waters by NPIW, we would expect to see evidence of this off Vancouver Island. The primary objectives of this study are thus to investigate changes in the intensity of the OMZ, focusing on the period
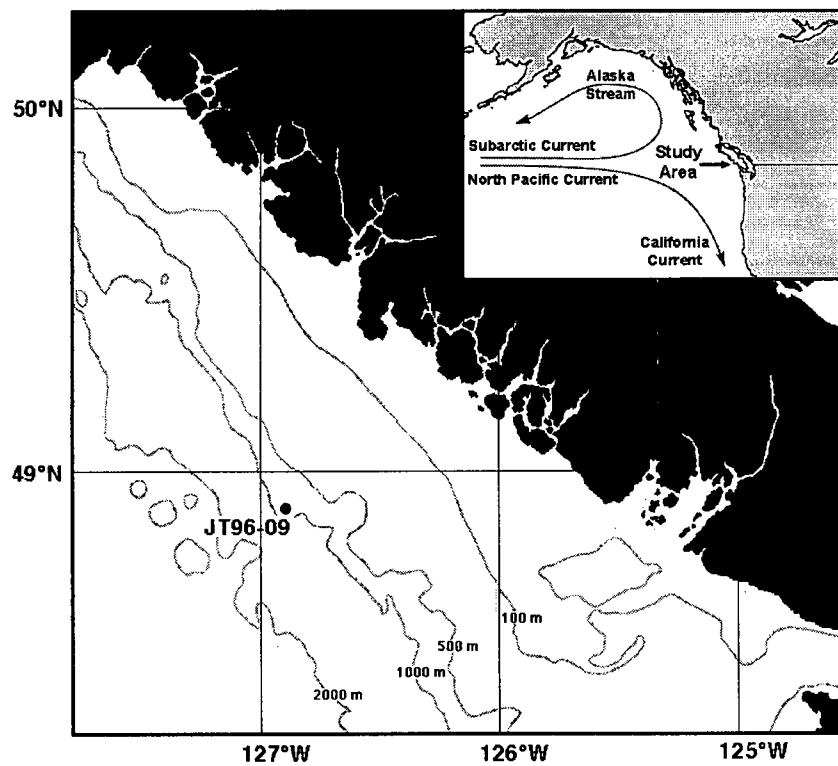
Fig. 3.1. The study area is located off the west coast of Vancouver Island, British Columbia, Canada (Inset). Sediment cores were collected from Station JT96-09 that is located on the continental slope at a water depth of 920 m.

between 16 and 10 calendar kyr B.P., and to determine whether such changes are the result of fluctuations in ventilation and/or export productivity.

Analyses were conducted on Piston Core JT96-09, raised from a water depth of 920 m, within the core of the present-day OMZ. Changes in the intensity of the OMZ are inferred from trace metal data and benthic-forminifera species information. Radiocarbon dating of benthic and planktonic foraminiferal pairs is used to determine if variability in the intensity of the OMZ is the result of changes in ventilation, while variations in palaeoproductivity are estimated using a variety of proxies (e.g., organic carbon, biogenic barium, opal and alkenone concentrations and/or mass accumulation rates). These data are discussed in detail in Chapter 2.

3.2 Materials and methods

Sediment cores were collected from the continental slope (920 m water depth) west of Vancouver Island, British Columbia, Canada during a 1996 Canadian Joint Global Ocean Flux Study cruise. Data are presented here for a 374 cm long Piston Core (JT96-09pc) and a corresponding 40 cm long multicore (JT96-09mc), both collected at the same site (48°54'N, 126°53'W; Fig. 3.1). The multicore and upper 51 cm of the piston core are composed of a homogeneous, organic carbon-rich (1 to 3 wt.%) and carbonate-poor (<1 wt.%), olive green mud. In the piston core this mud is underlain by 85 cm of grayish green clay and at the base of this clay is a 16 cm thick sandy turbidite. The remainder of the core (222 cm) is a dense, cohesive gray clay. It is important to note that no laminated sediments were observed.

The sediment-water interface was captured in the multicore and a comparison of geochemical data from the multi- and piston cores suggests that ~12 cm of sediment, not 20 cm as originally stated in Kienast and McKay (2001), were lost off the top of the piston core during its collection. Piston core depths have been corrected for this loss (+12 cm) and for

the presence of the turbidite (-16 cm), and the records for both cores have been merged to yield a composite record for site JT96-09.

The age model for JT96-09 is based on nine accelerator mass spectrometry (AMS) radiocarbon dates measured at the Lawrence Livermore National Laboratory on a mixed assemblage of planktonic foraminifera (*N. pachyderma* right- and left-coiling and *G. bulloides*). Results were converted from radiocarbon to calendar ages using CALIB 4.3 (Stuiver et al., 1998) assuming a reservoir age of 800 years for radiocarbon ages younger than 12.5 ^{14}C kyr and a reservoir age of 1100 years was applied to older ages. Details of the age model are discussed in Kienast and McKay (2001); however, as a result of the new estimate of sediment loss during coring, the age model for the Holocene differs slightly from that previously published. Sedimentation rates, which were calculated by assuming linearity between calendar-age dates, range from 5 cm/kyr during the Holocene up to 169 cm/kyr during the deglacial (Fig. 3.2). Therefore, although Core JT96-09 does not extend back to the Last Glacial Maximum it does yield a high resolution record of the last deglaciation.

Alkenone palaeothermometry measurements previously conducted on Core JT96-09 yielded evidence of rapid sea-surface temperature (SST) fluctuations during the deglacial (Kienast and McKay, 2001). The pattern of deglacial SST fluctuations is remarkably similar to temperature fluctuations in the GISP-2 ice core record suggesting that the Bølling-Allerød and Younger Dryas events are recorded in Core JT96-09. More importantly these events appear to be nearly synchronous with those in GISP-2, although the match is not perfect (see Kienast and McKay, 2001). Offsets between the two records, in some instances in the order of hundreds of years, most probably reflect errors in the age model of Core JT96-09 resulting from: i) problems inherent to radiocarbon dating (e.g., ^{14}C plateaus); ii) a poorly known reservoir age (e.g., using a reservoir age of 800 yrs rather than 1100 yrs for samples older than 12.0 ^{14}C years increases most ages by ~300 yrs); iii) bioturbation, although the effects of this are limited by the high sedimentation rates during the deglacial; and iv) large errors associated with the radiocarbon dating of small samples.

Possible changes in intermediate water ventilation are determined by calculating the age difference between benthic and planktonic foraminifera separated from the same sample. This method assumes that the effects of bioturbation can be ignored, a reasonable assumption given the high sedimentation rates that prevailed during the deglacial (>>10 cm/kyr). However, the age difference may be biased by another influence. Uvigerina and Bolivina spp. are infaunal organisms and probably grew at depth alongside the shells of previously deposited planktonic foraminifera. This would increase the benthic-planktonic age difference, but given the high sedimentation rates, the quantitative impact of such an effect should be trivial. No attempt has been made to correct for it. A further complication may arise from the degradation of "old" (i.e., ^{14}C-depleted) organic matter and ensuing addition of "old" CO_2 to the porewaters that could theoretically increase the apparent age of deeper-dwelling infaunal species. This possibility is discussed in more detail below.

No foraminifera occur in the upper 30 cm of the composite core (~0 to 5 kyr B.P.), while in sediments deposited between 5 and 10 kyr B.P. foram shells are present but extensive dissolution is observed (i.e., fragments are abundant). The paucity of shells in the Holocene deposits can be attributed to the highly corrosive nature of North Pacific waters (Zahn et al., 1991; Karlin et al., 1992) and the adverse effect that degradation of organic matter has on carbonate preservation (De Lange et al., 1994; Jahnke et al., 1997). In contrast, foraminifera are abundant and well preserved in sediments older than 10 kyr B.P. apparently reflecting less-corrosive conditions in the past. No single species of benthic or planktonic foraminifera is found throughout the entire core and therefore, it was necessary to use a variety of taxa for ^{14}C dating. Radiocarbon data were obtained for 10 benthic-planktonic foraminiferal pairs spanning the period between 10.0 and 15.6 kyr B.P. Planktonic samples comprise a mixture of *N. pachyderma* (right and left coiling) and *G. bulloides*. Most benthic samples consist of either *Uvigerina* spp. or *Bolivina argentea*. In two instances it was necessary to use a mixture of *Bolivina* spp. (*B. argentea* and *B. spissa*) to obtain enough material; however, these results were not used for reasons that will be discussed below.

Sample size ranged from <1 to 4.8 mg carbonate (usually 1.3 to 4.8 mg). Prior to radiocarbon dating, samples were sonicated in methanol and briefly etched with 0.0001N HCl.

When conducting stable isotope studies of benthic foraminifera, the preference is to use epifaunal species such as *Cibicidoides* which obtain their carbon from the overlying water (McCorkle et al., 1990). In Core JT96-09 no such species are present and thus a combination of *Uvigerina* spp. (3-15 individuals) and *Bolivina argentea* (>10 individuals) were used. As noted earlier, these are shallow-dwelling infaunal taxa (McCorkle et al., 1990; Stott 2000a). The isotopic composition of *Bolivina pacifica*, a deeper dwelling infaunal species (Stott et al., 2000a), was also measured. Prior to analysis foraminifera were sonicated in methanol and roasted under vacuum for 30 minutes at 430°C. The samples were then reacted in a common orthophosphoric acid bath at 90°C and analyzed using a PRISM series 1, triple ion collector mass spectrometer. Data are reported in the standard δ-notation relative to Vienna Peedee belemnite (VPDB). The reproducibility of three in-house laboratory standards (Mexical, UQ6 and a foraminiferal standard), which were calibrated using the international standard NBS-19, was ± 0.15 ‰ for $\delta^{18}O$.

Trace metal concentrations (i.e., Re, Ag, Cd, Mo and U) were measured by isotope-dilution inductively-coupled plasma mass spectrometery. Sample preparation involved adding known amounts of isotopically-enriched spike solutions to ~20 mg of powdered sediment. Samples were then microwave digested in a mixture of concentrated HNO_3, HCl and HF. The digests were evaporated on a hotplate overnight and then re-digested in 5N HCl. Aliquots were taken for Mo and U analysis. The remaining sample was run through an anion exchange column (Dowex 1-X8 resin) to remove Zr and Nb which form compounds (ZrO, ZrOH and NbO) that interfere with the analysis of Ag, and Mo that forms MoO^- which interferes with Cd analysis. Further details of the sample preparation can be found in Ivanochko (2001). To check precision a University of British Columbia sediment standard (SNB) was analyzed with each batch of samples. The resulting RSD (1σ) for Re, U, Mo, Cd

and Ag analyses were 11 %, 9 %, 7 %, 10 % and 8 %, respectively. Accuracy was assessed by measuring the concentrations of these metals in the NRC sediment standard MESS-1 and was 8 % or better for Re, Mo and U, and ~14 % for Cd.

3.3 Results

Radiocarbon data are summarized in Table 3.1. Benthic-planktonic age differences range from 610 to 1550 years. The errors for these data (i.e., the square root of $a^2 + b^2$; where a and b are the individual errors) range from ± 92 to 305 years. Errors greater than 200 years are the result of using very small samples (<1 mg carbonate). For sample 1 (Table 3.1 and Fig. 3.2), the benthic-planktonic age difference was calculated using two separate benthic species (i.e., *Uvigerina* spp. and *Bolivina argentea*) and the results are identical within the error (950 ± 92 and 890 ± 114 years, respectively). Therefore, changes in benthic-planktonic age differences observed in Core JT96-09 are most probably not the result of using two different benthic foraminifera taxa. However, this conclusion is only valid because *Bolivina argentea* and *Uvigerina* spp. are shallow infaunal species that obtain most of their carbon from the overlying bottom water. The same assumption does not hold true when a mixture of *Bolivina* spp. is used because different species live at different depths in the sediment. Deeper-dwelling species very probably obtain a larger amount of their carbon from the degradation of organic matter. In the deglacial sediments of Piston Core JT96-09 bulk organic matter is 2000 to 3000 years older than planktonic foraminifera in the same sample (Chapter 2). Therefore, it is probable that deeper-dwelling infaunal species are anomalously depleted in ^{14}C. As a result, radiocarbon data for samples that contain mixed *Bolivina* spp. (e.g., samples 3 and 5; Table 3.1 and Fig. 3.2), which include deeper dwelling species, are likely biased toward older ages and benthic-planktonic age differences will be larger. These data are therefore considered unreliable and are not discussed further.
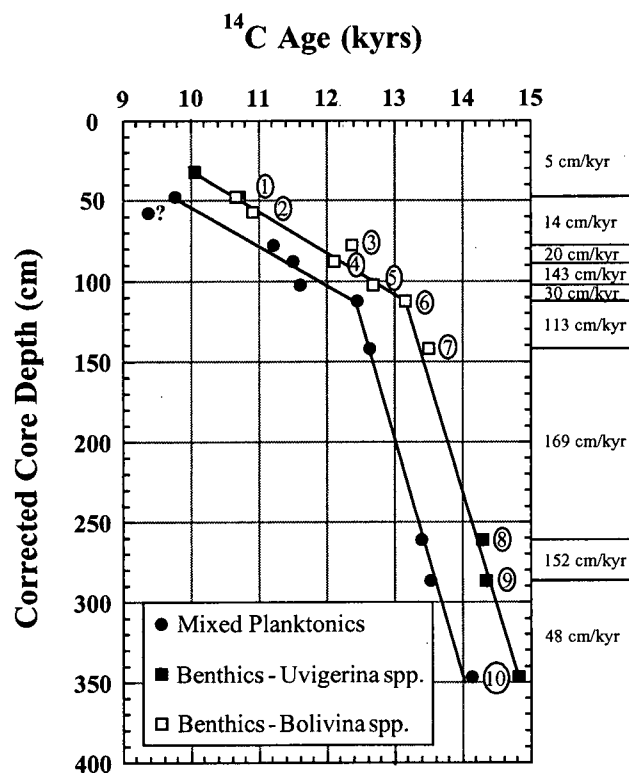
Fig. 3.2. Plot of ^{14}C ages of planktonic and benthic foraminifera versus sample depth in Core JT96-09. Sedimentation rates, which are indicated along the right axis, were calculated using ^{14}C ages of planktonic foraminifera and assuming a linear sedimentation rate between age picks. Circled numbers correspond to sample numbers in Table 3.1.

Table 3.1. Radiocarbon ages of planktonic and benthic foraminifera in Composite Core JT96-09.

Sample	Depth Range (cm)	Corrected Depth (cm)	Calendar Age (kyr B.P.)	^{14}C Age Mixed Planktonics	^{14}C Age Benthics Uvigerina spp.	Bolivina spp.	Benthic-Planktonic Age Difference (yrs)
1	35-36	47.5	10.03 [1]	9760 ± 70	10710 ± 60	10650 ± 90	950 ± 92, 890 ± 114
2	45-46	57.5	10.76 [1]	9360 ± 240		10910 ± 70	1550 ± 250
3	65-66	77.5	12.24 [1]	11210 ± 120		12380 ± 280 [3]	1170 ± 305
4	75-76	87.5	12.73 [1]	11500 ± 110		12110 ± 80	610 ± 136
5	90-91	102.5	12.84 [1]	11600 ± 80		12700 ± 70 [3]	1100 ± 106
6	100-101	112.5	13.17 [2]	12460 ± 120		13170 ± 100	710 ± 156
7	130-131	142.5	13.43 [2]	12640 ± 90		13500 ± 80	860 ± 120
8	265-266	261.5	14.14 [2]	13410 ± 80	14290 ± 110		880 ± 136
9	290-291	286.5	14.30 [2]	13520 ± 70	14350 ± 120		830 ± 139
10	350-351	346.5	15.57 [2]	14140 ± 70	14830 ± 280		680 ± 289

[1] Calculated using a reservoir age of 800 years.

[2] Calculated using a reservoir age of 1100 years.

[3] A mixture of *Bolivina spp.* were used to make these measurements. All other *Bolivina* samples are monospecific.

The single late glacial sample yields a benthic-planktonic age difference of 680 ± 289 years. Benthic-planktonic age differences for the deglacial range from 830 to 880 years ± 139 to 136 years for the period between 14.3 and 13.4 kyr B.P. and then decrease to 610 ± 136 and 710 ± 156 years between 13.2 and 12.7 kyr B.P. Due to a paucity of foraminifera no data are available for the period from 12.7 to 10.8 kyr B.P. The highest benthic-planktonic age difference (1550 ± 250 years; sample 2 in Table 3.1) occurs at the end of the Pleistocene (10.76 cal. kyr B.P.); however, this large value appears to be partly the result of an anomalously young planktonic age (Fig. 3.2). At the Pleistocene-Holocene boundary the benthic-planktonic age difference ranges from 890 ± 114 to 950 ± 92 years. Given the scale of the error estimates, and excluding sample 2, we cannot conclusively state that real differences exist between samples. However, some intriguing changes in benthic-planktonic age differences over time are suggested by the data.

Alkenone palaeothermometry of Core JT96-09 has identified a number of rapid SST fluctuations that appear to be coeval with the Bølling-Allerød and Younger Dryas (Kienast and McKay, 2001). When the benthic-planktonic age difference data are placed into this time frame it is observed that values may be slightly higher during the Bølling and at the start of the Allerød and relatively low throughout the Allerød (Fig. 3.3). Due to the lack of foraminifera no data are available for the Younger Dryas. Just prior to the Holocene the benthic-planktonic age difference reaches its highest value (1550 ± 250 years) and then decreases at the Pleistocene-Holocene boundary (Fig. 3.3).

Trace metal data for composite Core JT96-09 are presented in Figure 3.4. Rhenium concentrations range from <1 to 65 ng/g, U from 1.1 to 5.8 μg/g, Cd from <0.1 to 1.4 μg/g, Mo from 0.3 to 3.7 μg/g and Ag from 71 to 395 ng/g. To correct for possible fluctuations in metal content due to changes in dilution by biogenic components (i.e., carbonate and organic matter) over time metal concentrations have been normalized to Al. Concentrations and metal/Al ratios are low during the glacial and early deglacial (16.0 to 13.5 kyr B.P.). At 13.5 kyr B.P. (i.e., the start of the Allerød) these ratios increase substantially and remain high until
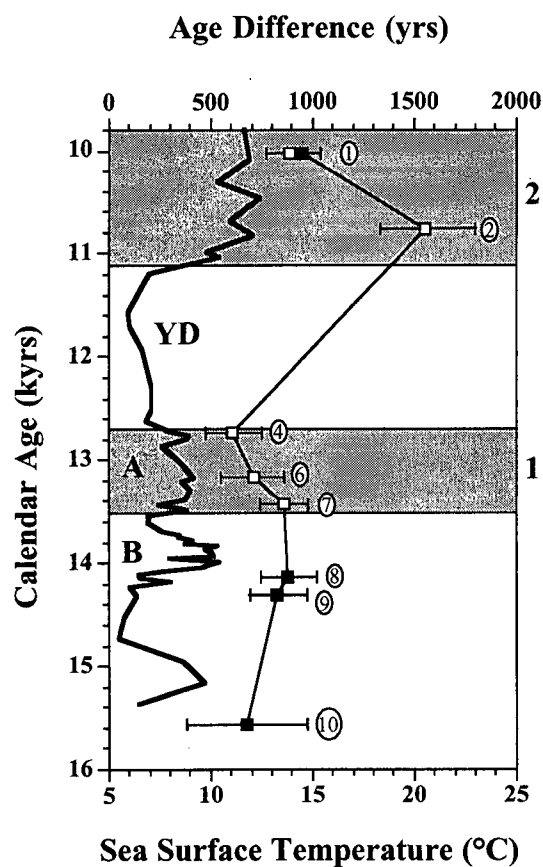
Fig. 3.3. Benthic-planktonic age differences are plotted against calendar age. The two periods of OMZ intensification are indicated by the shading (i.e., zones 1 and 2). The sea-surface temperature record of Kienast and McKay (2001) is also shown and the Bølling (B), Allerød (A) and Younger Dryas (YD) events are labeled. Circled numbers correspond to sample numbers in Fig. 3.2 and Table 3.1.
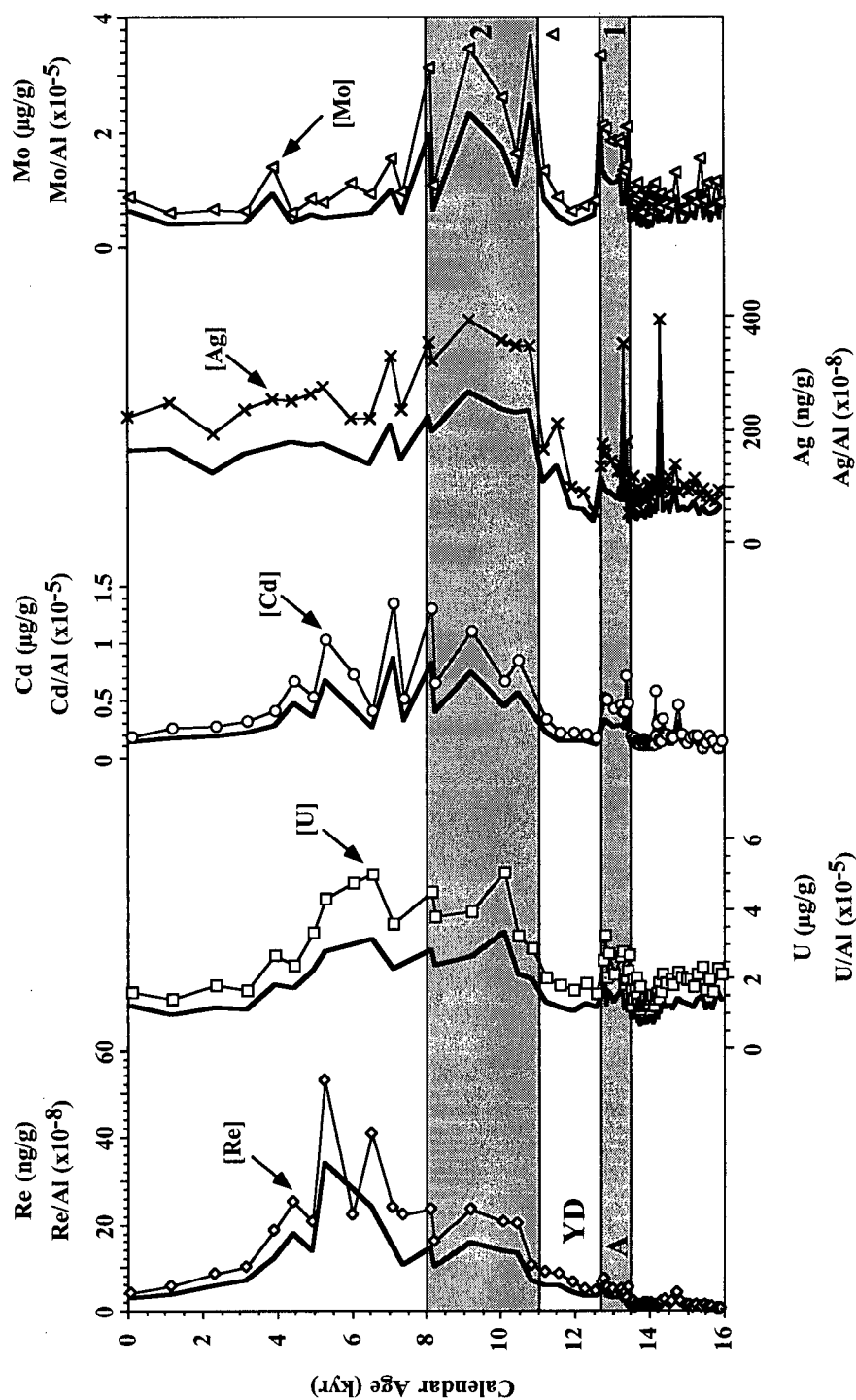
Fig. 3.4. Redox-sensitive trace metal concentrations (symbols) and metal/Al ratios (thick lines) in Core JT96-09. Two periods of high trace metal accumulation are indicated by the shading (zones 1 and 2). Zone 1 corresponds to the Allerød (A), the period of relatively low trace metal accumulation between zones 1 and 2 is the Younger Dryas (YD) and Zone 2 extends across the Pleistocene/Holocene boundary at 10 kyr B.P. Note, the precision (as RSD) of all trace metal concentration data is generally ≤10 % and the detection limits are as follows: <1 ppb for Re, 0.01 ppm for U, 0.1 ppm for Cd, 57 ppb for Ag and 0.5 ppm for Mo.

the Younger Dryas at ~12.7 kyr B.P. Metal/Al ratios are low throughout the Younger Dryas, and then rise again at 11.0 kyr. The is some evidence that in the early part of the Younger Dryas the low trace metal content might reflect dilution by coarser-grained materials as the Zr/Al ratio is Early to mid Holocene sediments host the highest trace metal enrichments and have correspondingly high metal/Al ratios. The Ag/Al ratio remains high in the late Holocene; however the Re/Al, U/Al, Cd/Al and Mo/Al ratios decrease to near glacial values.

No foraminiferal counts were conducted on Core JT96-09 because of the limited number of foraminifera present. However, while picking specimens for stable isotopic analysis and radiocarbon dating it became apparent that certain species of benthic foraminifera occur in specific zones of the core. Two zones are characterized by abundant *Bolivina* spp., (i.e., *B. argentea, B. spissa and B. pacifica*), but no *Uvigerina* spp. (zones 1 and 2; Fig. 3.5a). In comparison, Holocene sediments contain a mixture of *Uvigerina* spp. and *Bolivina* spp. (only *B. argentea*), and sediments older than 13.5 kyr B.P. contain *Uvigerina* spp. and few, if any, *Bolivina* spp.

The $\delta^{18}O$ results are shown in Figure 3.5a. The large decrease in $\delta^{18}O$ values of benthic foraminifera at ~13.5 kyr B.P. (Fig. 3.5a) most probably represents the mixing in to the ocean of Meltwater Pulse 1A (Fairbanks, 1989). The decrease in benthic $\delta^{18}O$ is contemporaneous with an increase in sea-surface temperature (SST) that is inferred to be the Allerød. This timing is similar to that observed in other marine records (e.g., Tahiti corals; Bard, 1996), suggesting that the age model for Core JT96-09 is reasonable and that sea-surface temperature fluctuations in this core are coeval with temperature fluctuations in the GISP-2 ice core, as suggested by Kienast and McKay (2001).

3.4 Discussion

3.4.1 Evidence of OMZ intensification
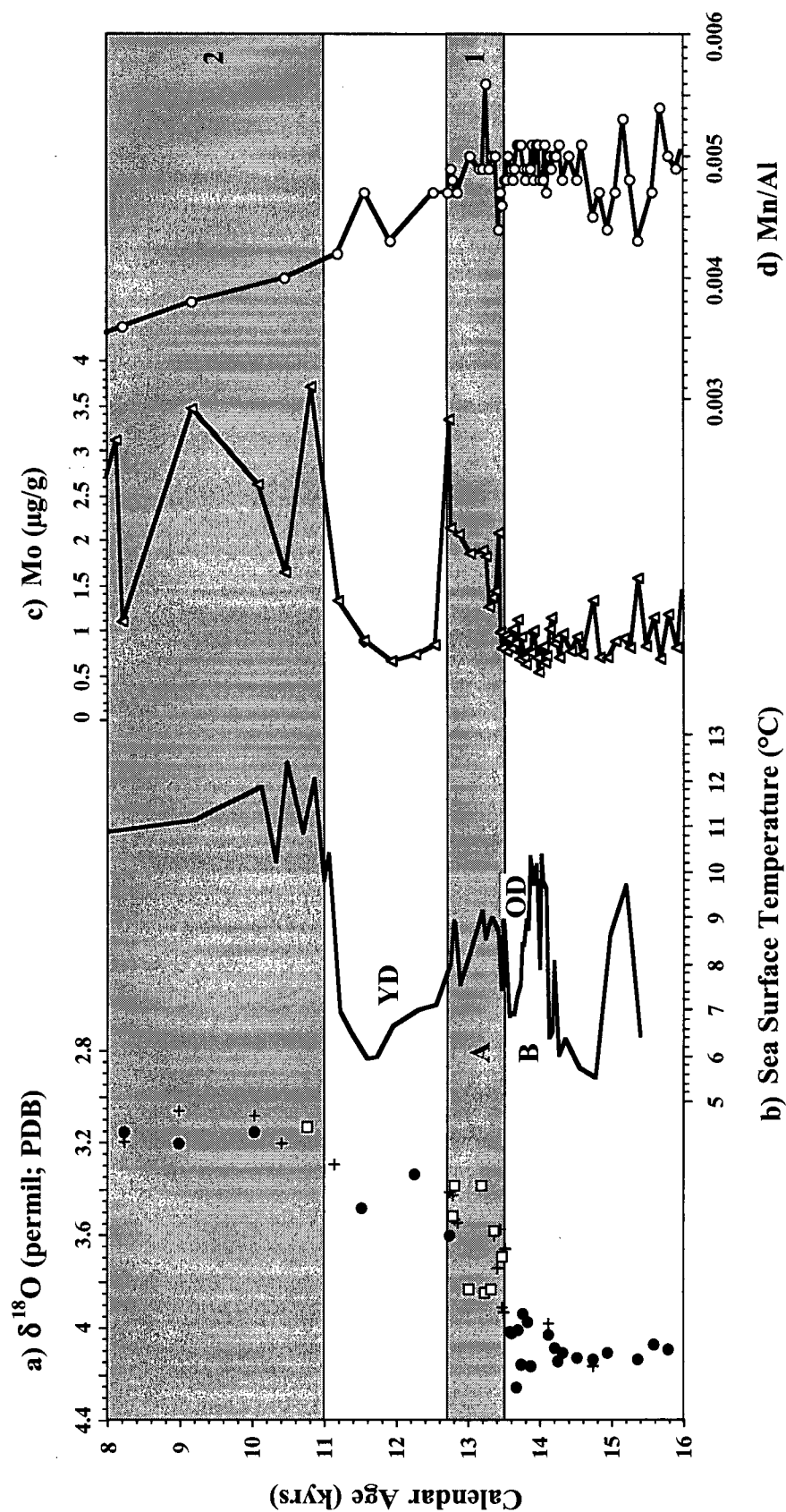
Fig. 3.5. Various paleo-records for Core JT96-09 (8 to 16 kyr B.P.). Two periods of OMZ intensification are identified (zones 1 and 2). a) Oxygen isotope data for benthic foraminifera (Uvigerina spp. - solid circles; Bolivina argentea - crosses; Bolivina spissa - open circles). The error on these data is ±0.15 ‰. b) Sea-surface temperature record derived from alkenone paleothermometry (Kienast and McKay, 2001). The error on SST data is ±1.5 °C. The Bølling (B), Older Dryas (OD), Allerød (A) and Younger Dryas (YD) events are identified. c) Molybdenum concentration data (RSD = 7 %). d) Mn/Al ratios (RSD = 16 %).

The OMZ, defined as that portion of the water column where oxygen is ≤ 0.5 ml/l, extends from approximately 750 to 1300 m water depth off the west coast of Vancouver Island (see data in Appendix A5). During the 1996 research cruise the lowest oxygen concentration (0.3 ml/l) was measured at a water depth of 920 m (i.e., the site where Core JT96-09 was collected). Unlike cores from the California and Mexican continental margins, no laminated sediments have been preserved in Core JT96-09 over the past 16 kyr B.P. However, this does not necessarily imply that fully oxygenated conditions existed over this period because laminated sediments are only preserved when bottom water oxygen levels drop below 0.1 ml/l (Behl and Kennett, 1996). Significant variations in bottom water oxygen concentrations (i.e., OMZ intensity) over the past 16 kyr are inferred from changes in the accumulation of redox-sensitive trace metals and by changes in the assemblage of benthic foraminifera.

The reduction and subsequent precipitation of Re and U begins once porewater O_2 is depleted and this leads to their enrichment in suboxic and anoxic sediments (Ravizza et al, 1991; Colodner et al., 1993; Crusius et al., 1996). Silver and Cd have a single redox state, but form insoluble sulphides when trace amounts of H_2S are available (Koid et al., 1986; Rosenthal et al., 1995). This leads to minor Ag and Cd accumulation in suboxic sediments and large accumulations in anoxic sediments. In comparison, Mo enrichment is only observed in anoxic sediments (Francois et al., 1988; Emerson and Huested, 1991; Crusius et al., 1996; Ivanochko, 2001; Morford et al., 2001). Molybdenum accumulation is related to the conversion of MoO_4^{2-} to MoS_4^{2-} (i.e., thiomolybdate) which is readily adsorbed onto Fe-bearing particles such as Fe-sulphides (Helz et al., 1996). The formation of thiomolybdate only occurs when the porewater H_2S concentration exceeds ~11 μm (Erickson and Helz, 2000) and thus Mo enrichment is restricted to fully anoxic sediments. At present, sediments deposited within the OMZ off Vancouver Island become suboxic within millimetres of the sediment-water interface (Chapter 4). However, near-surface sediments never become fully anoxic and thus Mo enrichment does not occur in the upper 50 cm (i.e., <1 μg/g Mo; Fig.

3.4). This observation is consistent with measured bottom water oxygen concentrations (> 0.3 ml/l) because, in general, Mo accumulation only occurs when oxygen levels drop below ~0.2 ml/l (Zheng et al., 2000). In comparison, two periods of Mo enrichment are observed in older sediments (zones 1 and 2; Fig. 3.4) and these are accompanied by Re, U, Cd and Ag enrichments.

The first episode of marked trace metal enrichment is observed in the deglacial clay deposited during the Allerød (Zone 1; Fig. 3.4). There is no evidence that this enrichment is result of metal remobilization due to oxygen influx (i.e., burndown) and subsequent reprecipitation in underlying reduced sediments because the distribution of all redox-sensitive metals is similar. Burndown commonly re-distributes elements at different depths due to their different chemical behaviours (Colodner et al., 1992; Thomson et al., 1993; Thomson et al., 1995; Crusius and Thomson, 2000). Therefore, metal enrichment in Zone 1 must reflect the development of anoxic conditions within the sediment. Such conditions may have developed as a result of: i) increased sedimentation rate and corresponding decrease in oxygen influx; ii) decreased ventilation of the bottom water; and/or iii) increased carbon flux to the sediment. Increased sedimentation is ruled out as the cause of trace metal enrichment because the sedimentation rate was substantially higher (>150 cm/kyr; Fig. 3.2) during deposition of the trace metal-poor sediments in the Bølling, between 14.3 and 13.5 kyr B.P. (290 and ~130 cm sub-bottom depth, respectively). Whether oxygen depletion in near-surface sediments was the result of decreased ventilation of bottom waters and/or increased organic carbon flux to the sediment, which also would have caused water column oxygen content to decline, is discussed in Sections 3.4.2 and 3.4.3. In either case, trace metal data imply that the OMZ was more intense during the Allerød.

The second interval of trace metal enrichment occurs in sediments deposited between 11 and 8 kyr B.P. (Zone 2; Fig. 3.4). Several factors, acting collectively, appear to have produced the observed enrichments. The increase in Re at ~4 kyr B.P. (i.e., 20 cm below the sediment-water interface) reflects the approximate depth where Re reduction and

accumulation are occurring at present (Chapter 4). Relatively low sedimentation in the Holocene (~5 cm/kyr) coupled with sufficient oxidant demand has allowed significant authigenic metal enrichment to occur well below the sediment-water interface. Thus, trace metal enrichments do not necessarily indicate stronger reducing conditions at, or shortly after, sediment deposition. Although this observation constrains detailed interpretation of OMZ history during the Holocene, these data clearly indicated that near-surface sediments at Station JT96-09 have been continuously reducing since the Younger Dryas, and imply low bottom water oxygen concentrations throughout the Holocene. This conclusion is consistent with deductions made to the south along the eastern margin of the North Pacific (Anderson et al., 1987; Ganeshram et al., 1995; Behl and Kennett, 1996; Cannariato and Kennett, 1999), all of which imply that a relatively intense OMZ has been a permanent fixture during the Holocene.

Molybdenum enrichment in the Allerød is contemporaneous with a shift from a *Uvigerina*-dominated benthic foraminifera assemblage to one composed almost entirely of *Bolivina* spp. (Fig. 3.5a). A similar species shift occurs between ~10 and 11 kyr B.P. which is also a period of enhanced Mo accumulation. Bottom water oxygen concentration has a direct influence on the species of benthic foraminifera that occur in sediments (Kaiho, 1994). *Bolivina*-dominated assemblages are typical of the most intense portions of the OMZ in the eastern Pacific and thrive at dissolved oxygen levels of < 0.3 ml/l (Mullins et al., 1985; Sen Gupta and Machain-Castillo, 1993). In contrast, *Uvigerina* spp. prefer a more oxygenated environment. This relationship has been documented at many locations along the northeastern Pacific margin (e.g., Mullins et al., 1985; Quinterno and Gardner, 1987) and it appears to hold true in the past (Behl and Kennett, 1996; Cannariato et al., 1999; Cannariato and Kennett, 1999). The presence of *Uvigerina* spp. also may be related to a high organic carbon supply to the sediment (Quinterno and Gardner, 1987), but this association is not observed if bottom water oxygen is low (Kaiho, 1994). We conclude that the occurrence of a benthic foraminifera assemblage composed almost exclusively of *Bolivina* spp. in sediments

characterized by Mo enrichment provides further evidence that bottom water oxygen levels were very low (< 0.3 ml/l).

The combination of trace element and benthic foraminifera data suggest that intensification of the OMZ in the region off Vancouver Island occurred during the deglacial between 13.5 and 12.7 kyr B.P. (i.e., Allerød) and possibly again between 11.0 and 8.0 kyr B.P. In general, intensification occurred contemporaneously with times of high SST and brackets the Younger Dryas (Fig. 3.5). In this respect the timing of OMZ intensification off Vancouver Island is similar to the timing off California and Mexico, with one notable difference. Intensification of the OMZ in the southern CCS apparently occurs at the beginning of the Bølling (Cannariato and Kennett, 1999; Mix et al., 1999; Zheng et al, 2000, Ivanochko, 2001) while off Vancouver Island it is delayed until the Allerød, a lag of ~1.5 kyr.

3.4.2 Ventilation changes?

The age of intermediate water at a depth of 920 m is recorded by benthic foraminifera while the age of surface waters is recorded by planktonic foraminifera. The difference in the ages of benthic and planktonic foraminifera obtained from the same sample therefore establishes the age difference between the intermediate and surface waters. If the intensification of the OMZ inferred from trace element and faunal data discussed above was the result of decreased ventilation, the benthic-planktonic (B-P) age difference should be greater, reflecting the reduced influence of relatively young NPIW and the increased influence of older, oxygen-depleted SSW.

Lack of foraminifera in surface sediments precludes direct determination of the modern B-P age difference. However, using $\Delta^{14}C$ water column data of Östlund and Stuiver (1980) for the North Pacific off the coast of California we estimate that benthic foraminifera from a depth of 900 m off Vancouver Island should be ~1780 years old, or perhaps slightly

younger given that our study area lies closer to regions of NPIW ventilation. The present age of planktonic foraminifera growing within surface waters (i.e., reservoir age of surface water) is ~800 years (Robinson and Thompson, 1981; Southon et al., 1990). Thus, the modern B-P age difference should be ~1000 years. Similar values are found in late glacial and early deglacial sediments studied here (Fig. 3.3). These results do not indicate increased ventilation of the OMZ during the late glacial as suggested for other locations by Duplessy et al. (1989) and Ingram and Kennett (1995). During the Allerød (i.e., the first period of OMZ intensification) the B-P age difference appears to decrease slightly from 860 ± 120 to 610 ± 136 years (Fig. 3.3). This decrease, which we note is not statistically robust, implies better ventilation of the OMZ, but it is inconsistent with geochemical and foraminiferal data that indicate OMZ intensification. Thus, if the reduced age difference observed during the Allerød is real, it must have resulted from some other factor.

Rapid, short-term fluctuations in the atmospheric ^{14}C concentration ($\Delta^{14}C_{atm}$) can influence the reservoir age of surface waters, and thus B-P age differences. Radiocarbon calibration data for the Allerød (Hughen et al., 2000; Kitagawa and van der Plicht, 2000) show no evidence for a rapid and sustained decline in $\Delta^{14}C_{atm}$ that could explain the slightly lower B-P age difference seen in the Allerød in Core JT96-09. The reservoir age will also be influenced by factors which affect exchange between the atmosphere and ocean (e.g., wind mixing), as well as by changes in oceanic circulation (Bard, 1988). The present-day reservoir age for the Northeast Pacific is approximately 800 years (Robinson and Thomson; 1981; Southon et al., 1990) and this has not changed significantly since the Younger Dryas (Southon et al., 1990). Kovanen and Easterbrook (2002) recently documented a reservoir age of 1100 years during the Allerød. These authors speculated that melting of Cordilleran ice might have supplied relative old CO_2 to surface waters, thereby increasing their apparent age. If this were the case regional B-P age differences should have decreased when the rapid retreat of the Cordilleran ice sheet commenced at ~15.5 kyr B.P. (i.e., 15.0 and 14.0 ^{14}C kyr; Clague and James, 2002). Thus, substantial meltwater influx must have occurred in the

region prior to the Allerød (13.5 to 12.7 cal. kyr B.P.) and it could therefore not have contributed to an increase in surface-water reservoir age at that time. A more likely possibility is that upwelling brought ^{14}C -depleted subsurface waters to the surface during the Allerød, thus increasing planktonic ages. Upwelling was greatly reduced along the northern and central portions of the California Current System during the Last Glacial Maximum (Sabin and Pisias, 1996) because the Aleutian Low dominated, producing southerly winds and inducing downwelling. Atmospheric circulation in the Northeast Pacific returned to its interglacial mode and upwelling was re-established by ~13.0 calendar kyr (Sabin and Pisias, 1996). Thus, the apparent lower B-P age difference observed for the Allerød in Core JT96-09 could have resulted from the upwelling of relatively old water. If this hypothesis is correct primary production should have been enhanced. We present evidence in support of this scenario in the following section.

3.4.3 Changes in productivity?

During interglacial periods in the sub-tropical northeast Pacific off northwest Mexico, increased export production led to a decrease in oxygen within the OMZ (Ganeshram et al., 1995). Similar observations have been made off central California (Gardner et al, 1997; Dean and Gardner, 1998) and northern California and Oregon (Lyle et al., 1992; Mix et al., 1999; Kienast et al., 2002). It is not unreasonable, therefore, to suggest that changes in primary and export production at the end of the last glacial affected the intensity of the OMZ along the entire northeastern margin of the Pacific Ocean. But did such changes extend as far north as Vancouver Island?

Modern primary production off the west coast of Vancouver Island is influenced by large scale atmospheric circulation. In late spring and summer the North Pacific High drives northerly winds, offshore Ekman transport and upwelling of nutrient-rich water (Huyer, 1983). The strength of these winds and thus upwelling intensity is affected by the strength of

the pressure gradient between the North Pacific High and the continental thermal low, such that the larger the gradient the more intense the upwelling (Bakun, 1990). In winter when the North Pacific High shifts southward from ~38°N to ~28°N and is replaced by the Aleutian Low, winds switch direction and upwelling ceases north of ~40°N (Huyer, 1983). Climate modeling and palaeo-evidence suggest that during the Last Glacial Maximum the North Pacific High was positioned further south in summer (COHMAP, 1988; Thunell and Mortyn, 1995; Mortyn et al., 1996; Sabin and Pisias, 1996; Doose et al., 1997), a situation analogous to modern winters. As a result, upwelling along the central and northern portions of the California Current System was greatly diminished and primary productivity was reduced during the Last Glacial Maximum (Dymond et al., 1992; Lyle et al., 1992; Sancetta et al., 1992; Ortiz et al., 1997; Dean and Gardner, 1998; Mix et al., 1999). Off Vancouver Island the burial of marine organic matter was also relatively low during the late glacial, but it began to increase at the start of the Bølling (~14.3 kyr B.P.; Fig. 3.6). The most dramatic increase in marine organic carbon burial (i.e., an apparent six-fold increase relative to late glacial) occurred during the Allerød (~13.5 to 12.6 kyr B.P.) and was coincident with the first period of OMZ intensification (Fig. 3.6). A minor increase in organic carbon accumulation is also evident during the second period of OMZ intensification.

It could be argued that rather than causing intensification of the OMZ, increased organic carbon burial was the result of better preservation due to lower oxygen concentrations in the bottom water (e.g., Dean et al., 1994; Zheng et al., 2000). In the geological record, laminated sediments commonly have high organic carbon contents and this led to the hypothesis that organic matter preservation is enhanced in anoxic environments (Emerson, 1985), the presumption being that anaerobic bacteria are less efficient at degrading complex organic molecules. However, the sediments in Core JT96-09 are bioturbated, even during periods of inferred OMZ intensification, and thus bottom waters never became anoxic. Therefore, simple enhanced preservation of organic matter resulting from anoxic bottom waters cannot explain increased organic carbon burial during the

Marine Organic Carbon
(wt.%)
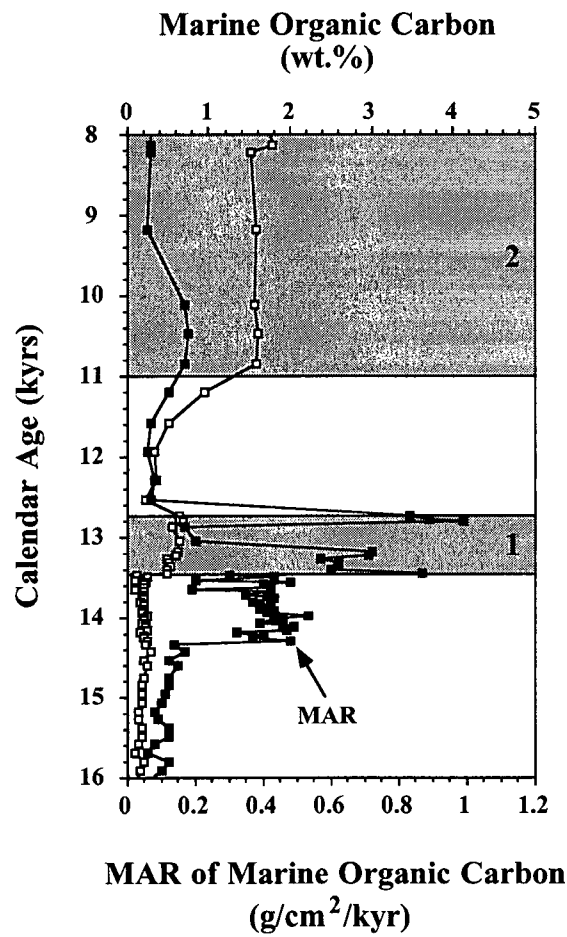
Fig. 3.6. Marine organic carbon concentration (open squares) and mass accumulation rate (MAR, solid squares) at Station JT96-09 from 8 to 16 kyr B.P. Data are from McKay et al. (submitted).

90

Allerød. It has been suggested recently that high sedimentation rate and low oxygen work in combination to enhance organic matter preservation by controlling the length of time that organic compounds are exposed to oxygen (Hedges and Keil, 1995; Gelinas et al., 2001). We have estimated oxygen exposure times (OETs) for the Holocene, Allerød, Bølling and the Late Glacial at site JT96-09 (Table 3.2). If the oxygen penetration depth remained constant then OETs for the Allerød and Bølling are similar (i.e., 1.7 and 1.3 years, respectively). If the oxygen penetration depth decreased in the Allerød, as the trace metal data imply, but remained the same for the Bølling, computed OETs remain similar (i.e., <1 and 1.3 years). Establishment of a substantial difference in Allerød and Bølling OETs would have required a deeper penetration depth in the Bølling. There is however no evidence to suggest that oxygen penetrated more deeply during the Bølling than during the Holocene. Sedimentary Mn/Al ratios, for example, are low during both periods (0.0035 and 0.0045, respectively) indicating that the near-surface sediments have been continuously suboxic. Furthermore, the higher sedimentation rate during the Bølling would have hindered oxygen penetration. We cannot rule out the possibility that a combination of high sedimentation rate and reduced supply of oxidants from the bottom water played a role in enhancing organic matter accumulation during the Allerød. However, the large increase in the mass accumulation of marine organic matter during the Allerød relative to the Bølling, given that OETs were probably similar, suggests that high export productivity was the dominant factor. Finally, changes in OET should not have affected the burial of barium or opal, yet these palaeo-proxies also imply relatively high export production during the Allerød (Chapter 2). Thus, these observations lead us to conclude that high organic carbon accumulation during the Allerød was primarily the result of increased export production and that the increased settling flux of organic matter caused intensification of the OMZ. Increased production was probably caused by the initiation of upwelling off Vancouver Island as atmospheric and oceanic circulation switched from a glacial to interglacial mode. Upwelling of relatively old

Table 3.2. Oxygen exposure times for sediments in Composite Core JT96-09.

Time Period	Sedimentation Rate (cm/kyr)	Oxygen Penetration [1] Depth (cm)	OET [1,3] (years)
Holocene	5	0.2 (-) [2]	40 (-)
Allerod	116	0.2 (0.1)	1.7 (< 1)
Bolling	150	0.2 (1.0)	1.3 (7)
Late Glacial	48	0.2 (1.0)	4.2 (20)

[1] A second set of oxygen penetration depths and resulting OET values are given in brackets.

[2] The oxygen penetration depth of 0.2 cm is based on the thickness of the brown "fluff" layer observed in Multicore JT96-09mc. The switch from brown to greenish sediments is commonly assumed to be the oxic-suboxic boundary.

[3] Oxygen exposure Time (OET) = Oxygen penetration depth divided by sedimentation rate (Hedges and Keil, 1995).

waters also may explain why benthic-planktonic age difference decreased slightly during the Allerød.

If intensification of the OMZ along the eastern margin of the North Pacific Ocean was the result of increased marine export production at the end of the last glacial there should be evidence from other locations. In general, the last deglacial (13 to 8 kyr B.P.) was a period enhanced marine productivity throughout the North Pacific (e.g., the Northwest Pacific off Kamchatka - Keigwin et al., 1992; the Gulf of Alaska - de Vernal and Pedersen, 1996), as well as within the California Current System off Oregon (Lyle et al., 1992) and California (Gardner et al., 1997; Dean and Gardner, 1998; Mix et al., 1999). However, in the Santa Barbara Basin (California Borderlands region) there is no conclusive evidence that productivity increased during periods of OMZ intensification (Behl and Kennett, 1996), except during the Holocene (Ivanochko, 2001). At present, offshore Ekman transport is lower in the California Borderlands region in comparison to areas just north and south. This difference reflects the more offshore position of the California Current and the unfavorable orientation of the coastline relative to winds (Huyer, 1983). As a result, local upwelling in this region is almost absent in summer when upwelling is strongest along the northern and central portion of the CCS, but local upwelling does occur in winter and early spring (Hickey, 1998). The differences in offshore Ekman transport and upwelling are reflected in phytoplankton pigment concentrations which show that primary productivity within the Southern California Bight and off Baja is generally lower than primary productivity in the northern CCS (Thomas et al., 1994). This may explain why palaeoproductivity records in Santa Barbara Basin do not correlate to similar records for northern California and elsewhere within the CSS.

3.5 Summary

Trace metal and benthic foraminifera species data indicate that the OMZ in the northeastern Pacific off Vancouver Island, Canada was more intense (i.e., more oxygen-depleted) between 13.5 to 12.7 calendar kyr B.P. (i.e., the Allerød) and again between 11 and 8 kyr B.P.. The timing of OMZ intensification is similar to that off California and Mexico, suggesting it was a regional phenomenon. Radiocarbon dating of benthic-planktonic foraminiferal pairs indicate that by ~16 kyr B.P. ventilation of the intermediate water mass (920 m water depth) off Vancouver Island was similar to that at present. Furthermore, there is no evidence that ventilation decreased during periods of OMZ intensification. There is however, evidence that export production increased during times of OMZ intensification. During the Allerød organic carbon accumulation increased 6-fold relative to glacial values. The concentrations and accumulation rates of other palaeo-productivity proxies (e.g., bio-barium, opal and alkenone concentrations; Chapter 2) also increased during the Allerød, and to a lesser extend at the Pleistocene-Holocene boundary. These benthic-planktonic age data together with the geochemical indices suggest that increased export production, most probably the direct result of increased primary production in surface waters, was the principal cause of OMZ intensification. Primary productivity was probably stimulated by the re-initiation of upwelling as atmospheric and oceanic circulation switched from a glacial to an interglacial mode.

3.6 References

Anderson, R.Y., Hemphill-Haley, E., Gardner, J.V., 1987. Persistent late Pleistocene-Holocene seasonal upwelling and varves off the coast of California. Quaternary Research 28, 307-313.

Bard, E., 1988. Correction of accelerator mass spectrometry ^{14}C ages measured in planktonic foraminifera: Paleoceanographic implications. Paleoceanography 3, 635-645.

Bard, E., Hamelin, B., Arnold, M., Montaggioni, L., Cabioch, G., Faure, G., Rougerie, F., 1996. Deglacial sea-level record from Tahiti corals and the timing of global meltwater discharge. Nature 382, 241-244.

Bakun, A., 1990. Global climate change and intensification of coastal ocean upwelling. Science 247, 198-201.

Behl, R.J., Kennett, J.P., 1996. Brief interstadial events in the Santa Barbara Basin, NE Pacific, during the past 60 kyr. Nature 379, 243-246.

Cannariato, K.G., Kennett, J.P., Behl, R.J., 1999. Biotic response to Late Quaternary rapid climate switches in Santa Barbara Basin: Ecological and evolutionary implications. Geology 27, 63-66.

Cannariato, K.G., Kennett, J.P., 1999. Climatically related millennial-scale fluctuations in strength of California margin oxygen-minimum zone during the past 60 k.y.. Geology 27, 975-978.

Clague, J.J., James, T.S., 2002. Historoy and isostatic effects of the last ice sheet in southern British Columbia. Quaternary Science Reviews 21, 71-87.

COHMAP Members, 1988. Climatic changes of the last 18,000 years: Observations and model simulations. Science 241, 1043-1052.

Colodner, D., Sachs, J., Ravizza, G., Turekian, K., Edmond, J., Boyle, E., 1993. The geochemical cycle of rhenium: A reconnaissance. Earth and Planetary Science Letters 117, 205-221.

Colodner, D,C., Boyle, E.A., Edmond, J.M., Thomson, J., 1992. Post-depositional mobility of platinum, iridium and rhenium in marine sediments. Nature 358, 402-404.

Crusius, J., Calvert, S.E., Pedersen, T.F., Sage, D., 1996. Rhenium and molybdenum enrichments in sediments as indicators of oxic, suboxic and sulphidic conditions of deposition. Earth and Planetary Science Letters 145, 65-78.

Crusius, J., Thomson, J., 2000. Comparative behavior of authigenic Re, U, and Mo during reoxidation and subsequent long-term burial in marine sediments. Geochimica et Cosmochimica Acta 64, 2233-2242.

De Lange, G.J., Van Os, B., Pruysers, P.A., Middelburg, J.J., Castradori, D., Van Santvoort, P., Muller, P.J., Eggenkamp, H., Prahl, F.G., 1994. Possible early diagenetic alteration of palaeo proxies. In: Zahn, R., Pedersen, T.F., Kaminski, M.A., Labeyrie, L. (Eds.), Carbon

Cycling in the Glacial Ocean: Constraints on the Ocean's Role in Global Change, NATO ASI Series, Vol. 117, Springer-Verlag, Berlin, pp. 225-257.

Dean, W.E., Gardner, J.V., Anderson, R.Y., 1994. Geochemical evidence for enhanced preservation of organic matter in the oxygen minimum zone of the continental margin of northern California during the late Pleistocene. Paleoceanography 9, 47-61.

Dean, W.E., Gardner, J.V., 1998. Pleistocene to Holocene contrasts in organic matter production and preservation on the California continental margin. Geological Society of America Bulletin 110, 888-899.

Dean, W.E., Gardner, J.V., Piper, D.Z., 1997. Inorganic geochemical indicators of glacial-interglacial changes in productivity and anoxia on the California continental margin. Geochimica et Cosmochimica Acta 61, 4507-4518.

Doose, H., Prahl, F.G., Lyle, M.W., 1997. Biomarker temperature estimates for modern and last glacial surface waters of the California Current system between 33° and 42°N. Paleoceanography 12, 615-622.

Duplessy, J.-C., Shackleton, N.J., Fairbanks, R.G., Labeyrie, L., Oppo, D., Kallel, N., 1988. Deepwater source variations during the last climate cycle and their impact on the global deepwater circulation. Paleoceanography 3, 343-360.

Duplessy, J.-C., Arnold, M., Bard, E., Juillet-Leclerc, J., Kallel, N., Labeyrie, L., 1989. AMS ^{14}C study of transient events and of the ventilation rate of the Pacific Intermediate Water during the last deglaciation. Radiocarbon 31, 493-502.

Dymond, J., Suess, E., Lyle, M., 1992. Barium in deep-sea sediment: A geochemical proxy for paleoproductivity. Paleoceanography 7, 163-181.

Emerson, S.R., 1985. Organic carbon preservation in marine sediments. In: The carbon cycle and atmospheric CO_2: Natural variations Archean to Present. Geophysical Monograph Series, v. 32, American Geophysical Union, Washington, D.C., pp. 78-87.

Emerson, S.R., Huested, S.S., 1991. Ocean anoxia and the concentration of molybdenum and vanadium in seawater. Marine Chemistry 34, 177-196.

Erickson, B.E., Helz, G.R., 2000. Molybdenum(VI) speciation in sulfidic waters: Stability and lability of thiomolybdates. Geochimica et Cosmochimica Acta 64, 1149-1158.

Fairbanks, R.G., 1989. A 17,000-year glacio-eustatic sea level record: Influence of glacial melting rates on the Younger Dryas event and deep-ocean circulation. Nature 342, 637-642.

Francois, R., 1988. A study of the regulation of the concentrations of some trace metals (Rb, Sr, Zn, Pb, Cu, V, Cr, Ni, Mn and Mo) in Saanich Inlet Sediments, British Columbia, Canada. Marine Geology 83, 285-308.

Freeland, H.J., Bychkov, A.S., Whitney, F., Taylor, C., Wong, C.S., Yurasov, G.I., 1998. WOCE section P1W in the Sea of Okhotsk 1. Oceanographic data description. Journal of Geophysical Research 103, 15613-15623.

Ganeshram, R.S., 1996. On the glacial-interglacial variability of upwelling, carbon burial and denitrification on the northwestern Mexican continental margin. Ph.D. Thesis, University of British Columbia, 233p.

Ganeshram, R.S., Pedersen, T.F., Calvert, S.E., Murray, J.W., 1995. Large changes in oceanic nutrient inventories from glacial to interglacial periods. Nature 376, 755-758.

Ganopolski, A., Rahmstorf, S., Petoukhov, V., Claussen, M., 1998. Simulation of modern and glacial climates with a coupled global model of intermediate complexity. Nature 391, 351-356.

Gardner, J.V., Hemphill-Haley, E., 1986. Evidence for a stronger oxygen-minimum zone off central California during late Pleistocene to early Holocene. Geology 14, 691-694.

Gardner, J.V., Dean, W.E., Dartnell, P., 1997. Biogenic sedimentation beneath the California Current System for the past 30 kyr and its paleoceanographic significance. Paleoceanography 12, 207-225.

Gélinas, Y., Baldock, J.A., Hedges, J.I., 2001. Organic carbon composition of marine sediments: Effect of oxygen exposure on oil generation potential. Science 294, 145-148.

Halpern, D., Smith, R.L., Reed, R.K., 1978. On the California Undercurrent over the continental slope off Oregon. Journal of Geophysical Research 83, 1366-1372.

Hedges, J.I., Keil, R.G., 1995. Sedimentary organic matter preservation: An assessment and speculative synthesis. Marine Chemistry 49, 81-115.

Helz, G.R., Miller, C.V., Charnock, J.M., Mosselmans, J.F.W., Pattrick, R.A.D., Garner, C.D., Vaughan, D.J., 1996. Mechanisms of molybdenum removal from the sea and its concentration in black shales: EXAFS evidence. Geochimica et Cosmochimica Acta 60, 3631-3642.

Hughen, K.W., Southon, J.R., Lehman, S.J., Overpeck, J.T., 2000. Synchronous radiocarbon and climate shifts during the last deglaciation. Science 290, 1951-1954.

Huyer, A., 1983. Coastal upwelling in the California Current System. Progress in Oceanography 12, 259-284.

Ingram, B.L., Kennett, J.P., 1995. Radiocarbon chronology and planktonic-benthic foraminifera ^{14}C age differences in Santa Barbara Basin sediments, Hole 893A. In: Kennett, J.P., Baldauf, J.G., Lyle, M. (Eds.), Proceedings of the Ocean Drilling Program, Scientific Results, Vol. 146 (Pt. 2), pp. 19-27.

Ivanochko, T., 2001. Productivity influences on oxygenation of the Santa Barbara Basin, California, during the Late Quaternary. M.Sc. Thesis, University of British Columbia.

Jahnke, R.A., Craven, D.B., McCorkle, D.C., Reimers, C.E., 1997. $CaCO_3$ dissolution in California continental margin sediments: The influence of organic matter remineralizaiton. Geochimica et Cosmochimica Acta 61, 3587-3604.

Kaiho, K., 1994. Benthic foraminifera dissolved-oxygen index and dissolved-oxygen levels in the modern ocean. Geology 22, 719-722.

Karlin, R., Lyle, M., Zahn, R., 1992. Carbonate variations in the northeast Pacific during the late Quaternary. Paleoceanography 7, 43-61.

Keigwin, L.D., 1998. Glacial-age hydrography of the far northwest Pacific Ocean. Paleoceanography 13, 323-339.

Keigwin, L.D., Jones, G.A., 1990. Deglacial climatic oscillations in the Gulf of California. Paleoceanography 5, 1009-1023.

Keigwin, L.D., Jones, G.A., Froelich, P.N., 1992. A 15,000 year paleoenvironmental record from Meiji Seamount, far northwestern Pacific. Earth and Planetary Science Letters 111, 425-440.

Kennett, J.P., Ingram, B.L., 1995. A 20,000-year record of ocean circulation and climate change from the Santa Barbara basin. Nature 377, 510-514.

Kienast, S.S., Calvert, S.E., Pedersen, T.F., 2002. Nitrogen isotope and productivity variations along the North East Pacific margin over the last 120 kyr: Surface and subsurface palaeoceanography. Paleoceanography 17, doi: 10.1029/2001PA000650.

Kienast, S.S., McKay, J.L., 2001. Sea surface temperatures in the subarctic Northeast Pacific reflect millennial-scale climate oscillations during the last 16 kyrs. Geophysical Research Letters 28, 1563-1566.

Kitagawa, H., van der Plicht, J., 2000. Atmospheric radiocarbon calibration beyond 11900 cal BP from Lake Suigetsu laminated sediments. Radiocarbon 42, 369-380.

Koide, M., Hodge, V.F., Yang, J.S., Stallard, M., Goldberg, E.G., Calhoun, J., Bertine, K.K., 1986. Some comparative marine chemistries of rhenium, gold, silver and molybdenum. Applied Geochemistry 1, 705-714.

Kono, T., 1996. Modification processes of the intermediate subarctic water in the western North Pacific and its relation to formation of the North Pacific Intermediate Water. Bulletin Hokkaido National Fisheries Resources Institute 60, 145-223.

Kovanen, D.J., Easterbrook, D.J., 2002. Paleodeviations of radiocarbon marine reservoir values for the northeast Pacific. Geology 30, 243-246.

Lyle, M., Zahn, R., Prahl, F. Dymond, J., Colier, R. Pisias, N., Suess, E., 1992. Paleoproductivity and carbon burial across the California Current: The mulitracers transect, 42°N. Paleoceanography 7, 251-272.

Lynn, R.J., Simpson, J.J., 1987. The California Current System: The seasonal variability of its physical characteristics. Journal of Geophysical Research 92, 12,947-12,966.

Mackas, D.L., Denman, K.L., Bennett, A.F., 1987. Least squares multiple tracer analysis of water mass composition. Journal of Geophysical Research 92, 2907-2918.

McCorkle, D.C., Keigwin, L.D., Corliss, B.H., Emerson, S.R., 1990. The influence of microhabitats on the carbon isotopic composition of deep-sea benthic foraminifera. Paleoceanography 5, 161-185.

Mikolajewicz, U., Crowley, T.J., Schiller, A., Voss, R., 1997. Modelling teleconnections between the North Atlantic and North Pacific during the Younger Dryas. Nature 387, 384-387.

Mix, A.C., Lund, D.C., Pisias, N.G., Bodén, P., Bornmalm, L., Lyle, M., Pike, J., 1999. Rapid climate oscillations in the Northeast Pacific during the last deglaciation reflect northern and southern hemisphere sources. In: Clark, P.U., Webb, R.S., Keigwin, L.D. (Eds.), Mechanisms of Global Climate Change at Millennial Time Scales. Geophysical Monograph 112, American Geophysical Union, Washington, D.C., pp. 127-148.

Morford, J.L., Russell, A.D., Emerson, S., 2001. Trace metal evidence for changes in the redox environment associated with the transition from terrigenous clay to diatomaceous sediment, Saanich Inlet, BC. Marine Geology 174, 355-369.

Mortyn, P.G., Thunell, R.C., Anderson, D.M., Stott, L.D., Le, J., 1996. Sea surface temperature changes in the Southern California Borderlands during the last glacial-interglacial cycle. Paleoceanography 11, 415-430.

Mullins, H.T., Thompson, J.B., McDougall, K., Vercoutere, T.L., 1985. Oxygen-minimum zone edge effects: Evidence from the central California coastal upwelling system. Geology 13, 481-494.

Nameroff, T.J., 1996. Suboxic trace metal geochemistry and paleo-record in continental margin sediments of the Eastern Tropical North Pacific. Ph.D. Thesis, University of Washington.

Ortiz, J., Mix, A., Hostetler, S., Kashgarian, M., 1997. The California Current of the last glacial maximum: Reconstruction at 42°N based on multiple proxies. Paleoceanography 12, 191-205.

Östlund, H.G., Stuiver, M., 1980. GEOSECS Pacific radiocarbon. Radiocarbon 22, 25-53.

Pilskaln, C.H., Pike, J., 2001. Formation of Holocene sedimentary laminae in the Black Sea and the role of the benthic flocculent layer. Paleoceanography 16, 1-19.

Quinterno, P.J., Gardner, J.V., 1987. Benthic foraminifers on the continental shelf and upper slope, Russian River area, northern California. Journal of Foraminiferal Research 17, 132-152.

Ravizza, G., Turekian, K.K., Hay, B.J., 1991. The geochemistry of rhenium and osmium in recent sediments from the Black Sea. Geochimica et Cosmochimica Acta 55, 3741-3752.

Reed, R.K., Halpern, D., 1976. Observations of the California Undercurrent off Washington and Vancouver Island. Limnology and Oceanography 21, 389-398.

Reid, J.L., Jr., 1965. Intermediate waters of the Pacific Ocean. Johns Hopkins Oceanography Study, No. 2, 85pp.

Robinson, S.W., Thompson, G., 1981. Radiocarbon corrections for marine shell dates with applications to southern Pacific Northwest Coast prehistory. Syesis 14, 45-57.

Rosenthal, Y., Lam, P., Boyle, E.A., Thomson, J., 1995. Authigenic cadmium enrichments in suboxic sediments: precipitation and postdepositional mobility. Earth and Planetary Science Letters 132, 99-111.

Sabin, A.L., Pisias, N.G., 1996. Sea surface temperature changes in the northeastern Pacific Ocean during the past 20,000 years and their relationship to climate change in northwestern North America. Quaternary Research 46, 48-61.

Sancetta, C., Lyle, M., Heusser, L., Zahn, R., Bradbury, J., 1992. Late-glacial to Holocene changes in winds and upwelling, and seasonal production of the northern California Current system. Quaternary Research 38, 359-370.

Sen Gupta, B.K., Machain-Castillo, M.L., 1993. Benthic foraminifera in oxygen-poor habitats. Marine Micropalentology 20, 183-201.

Southon, J.R., Nelson, D.E., Vogel, J.S., 1990. A record of past ocean-atmosphere radiocarbon differences from the norhteast Pacific. Paleoceanography 5, 197-206.

Stott, L.D., Berelson, W., Douglas, R., Gorsline, D., 2000a. Increased dissolved oxygen in Pacific intermediate waters due to lower rates of carbon oxidation in sediments. Nature 407, 367-370.

Stott, L.D., Neumann, M., Hammond, D., 2000b. Intermediate water ventilation on the northeastern Pacific margin during the late Pleistocene inferred from benthic foraminiferal $\delta^{13}C$. Paleoceanography 15, 161-169.

Stuiver, M., Reimer, P.J., Bard, E., Beck, J.W., Burr, G.S., Hughen, K.A., Dromer, B., McCormac, G., Van der Plicht, J., Spurk, M., 1998. INTCAL98 radiocarbon age calibration, 24,000-0 cal BP. Radiocarbon 40, 1041-1083.

Talley, L.D., 1991. An Okhotsk Sea water anomaly: Implications for ventilation in the North Pacific. Deep Sea Research 38, S171-S190.

Talley, L.D., 1993. Distribution and formation of North Pacific Intermediate Water. Journal of Physical Oceanography 23, 517-537.

Thomson, J., Higgs, N.C., Croudace, I.W., Colley, S., Hydes, D.J., 1993. Redox zonation of elements as an oxic-post-oxic boundary in deep-sea sediments. Geochimica et Cosmochimica Acta 57, 579-595.

Thomson, J., Higgs, N.C., Wilson, T.R.S., Croudace, I.W., de Lange, G.J., van Santvoort, P.J.M., 1995. Redistribution and geochemical behaviour of redox-sensitive elements around S1, the most recent eastern Mediterranean sapropel. Geochimica et Cosmochimica Acta 59, 3487-3501.

Thomson, R.E., 1981. Oceanography of the British Columbia Coast. Canadian Special Publication of Fisheries and Aquatic Sciences 56, 291p.

Thunell, R.C., Mortyn, P.G., 1995. Glacial climate instability in the Northeast Pacific Ocean. Nature 376, 504-506.

Thunell, R.C., Tappa, E., Anderson, D.M., 1995. Sediment fluxes and varve formation in Santa Barbara Basin, offshore California. Geology 23, 1083-1086.

van Geen, A., Fairbanks, R.G., Dartnell, P., McGann, M., Gardner, J.V., Kashgarian, M., 1996. Ventilation changes in the northeast Pacific during the last deglaciation. Paleoceanography 11, 519-528.

Van Scoy, K.A., Fine, R.A., Ostlund, H.G., 1991a. Two decades of mixing tritium into the North Pacific Ocean. Deep Sea Research 38, S191-S219.

Van Scoy, K.A., Olson, D.B., Fine, R.A., 1991b. Ventilation of North Pacific intermediate waters: The role of the Alaska Gyre. Journal of Geophysical Research 96, 16801-16810.

Van Scoy, K.A., Druffel, E.R.M., 1993. Ventilation and transport of thermocline and intermediate watrs in the Northeast Pacific during recent El Ninos. Journal of Geophysical Research 98, 18083-18088.

Wong, C.S., Matear, R.J., Freeland, H.J., Whitney, F.A., Bychkov, A.S., 1998. WOCE line P1W in the Sea of Okhotsk 2. CFCs and the formation rate of intermediate water. Journal of Geophysical Research 103, 15,625-15642.

Wyrtki, K., 1962. The oxygen minima in relation to ocean circulation. Deep Sea Research 9, 11-23.

Wyrtki, K., 1967. Circulation and water masses in the eastern equatorial Pacific Ocean. International Journal of Oceanology and Limnology 1, 117-147.

You, Y., Suginohara, N., Fukasawa, M., Yasuda, I., Kaneko, I., Yoritaka, H., Kawamiya, M., 2000. Roles of the Okhotsk Sea and Gulf of Alaska in forming the North Pacific Intermediate Water. Journal of Geophysical Research 105, 3253-3280.

Zahn, R., Pedersen, T.F., Bornhold, B.D., Mix, A.C., 1991. Water mass conversion in the glacial Subarctic Pacific (54°N, 148°W): Physical constraints and the benthic-planktonic stable isotope record. Paleoceanography 6, 543-560.

Zheng, Y., van Geen, A., Anderson, R.F., Gardner, J.V., Dean, W.E., 2000. Intensification of the northeast Pacific oxygen minimum zone during the Bölling-Alleröd warm period. Paleoceanography 15, 528-536.

4. Accumulation of Redox-sensitive Trace Metals in Continental Margin Sediments off Western Canada

4.1 Introduction

The concentrations of certain metals in sediments are directly or indirectly controlled by redox conditions through either a change in redox state (e.g., Mn, Re and U) and/or speciation (e.g., Mo) which results in their accumulation or loss. Other redox-sensitive metals (e.g., Cd and Ag) have a single redox state but readily react with the reduced forms of other elements such as sulphur. The observation that certain metals are enriched under specific redox conditions, such as Mo in anoxic sediments, has led to their use as palaeoenvironmental proxies (e.g., Piper and Isaacs, 1995; Rosenthal et al., 1995a; Yang et al., 1995; Crusius et al., 1999; Yarincik et al., 2000; Gobeil et al., 2001; Adelson et al., 2001, Pailler et al., 2002). Changes in the intensity of the oxygen minimum zone on the northeastern margin of the Pacific, for example, have been inferred from variations in the sedimentary concentrations of redox-sensitive trace metals (Dean et al., 1997; Zheng, et al., 2000a; Ivanochko, 2001).

Trace metals are supplied to sediments via the settling fluxes of lithogenic and biogenic detritus, both of which may fluctuate over time due to changes in sediment provenance and grain-size, and surface water productivity. However, it is the authigenic flux (i.e., the diffusion of metals into the sediment from the overlying water column) that is of most interest because it is controlled by redox conditions in the sediment and overlying bottom water. The degree to which redox-sensitive trace elements accumulate is largely determined by their porewater concentration gradients. These drive diffusion and are influenced by the depth of the redox boundaries. In general, when the suboxic redox boundary (i.e., where oxygen content falls to zero) and anoxic redox boundary (i.e., where sulphate reduction commences) are shallow, diffusion gradients are steeper and the flux from the overlying water column into the sediment is enhanced. Such conditions commonly occur

where organic matter flux to the seafloor is high and/or oxygen concentration in the bottom water is low. However, as will be shown in this paper, it is also possible to build-up high metal concentrations even if the suboxic and anoxic redox boundaries are quite deep, as long as they remain relatively stationary for a long period of time. This occurs when sedimentation rate is relatively low, but oxidant demand is high (e.g., Pedersen et al., 1989). A high sedimentation rate can also lead to enhanced trace metal accumulation, but only for those metals that are very rapidly fixed within the sediment (e.g., Mo; Chapter 5).

Application of redox-sensitive trace metals as palaeo-proxies requires an understanding of their geochemistry in a wide variety of modern environments. Anoxic environments such as the Black Sea, Cariaco Basin and Saanich Inlet have been well studied (e.g., Francois, 1988; Calvert et al., 1990; Dean et al., 1999; Yarincik et al., 2000; Morford et al., 2001). However, detailed studies of continental margin environments are relatively limited (e.g., Crusius et al., 1996; Dean et al., 1997; Morford and Emerson, 1999; Nameroff et al., 2002). It is therefore a primary goal of this study to provide further insight on the sedimentary geochemistry of redox-sensitive trace metals (i.e., Re, U, Cd and Mo) in modern continental margin settings.

The geochemical behaviour of naturally occurring (i.e., non-anthropogenic) Ag in marine sediments is also discussed in this paper. It has been hypothesized that the concentration of sedimentary Ag might be useful as a proxy for the settling flux of diatoms since Ag is incorporated into, and delivered to the sediment with, opal (Friedl et al., 1997). We show here, however, that Ag accumulation in sediments is influenced by more than just the delivery of opal to the seafloor.

The study area is located at the northern end of the California Current System (CCS) off Vancouver Island, British Columbia, Canada (48° 54' N, 126° 53' W; Fig. 4.1). This region sits within a transition zone where the eastward-flowing Subarctic and North Pacific currents split into the northward flowing Alaska Current and southward flowing California Current (Thomson, 1981). With the exception of a local and relatively nearshore muddy

facies, much of the shelf along the western margin of Vancouver Island is covered by relict deposits (Bornhold and Yorath, 1984). This reflects three factors: i) intense turbulence and scouring associated with winter storm waves, ii) the lack of a large, proximal source of riverine detritus, and iii) efficient particle trapping by the fjords that are common along the western margin of Vancouver Island. The last two factors also limit sedimentation rates on the adjacent slope. The area immediately west of Vancouver Island is typified by high primary productivity (up to 400 $gC/m^2/yr$; Antoine et al., 1996) related to seasonal (spring - summer) wind-induced upwelling of nutrients (Hickey, 1998). The region is also characterized by a relatively intense oxygen minimum zone (OMZ) which is most pronounced between 750 and 1300 m with O_2 concentrations ranging from 0.3 to 0.5 ml/l. During periods of upwelling this oxygen-poor water is transported onto the shelf (Mackas et al., 1987). High primary productivity and resulting high organic carbon flux to the sediment in combination with low bottom water oxygen concentrations should normally establish strong reducing conditions within the sediment and foster high trace metal concentrations. However, we have found the near-surface sediments on the continental margin off Vancouver Island to be relatively metal-poor. The question is, why?

4.2 Methods

Boxcores (bc) and multicores (mc) were collected from six sites on the continental margin off the west coast of Vancouver Island (Fig. 4.1) along a transect that extended from the shelf down the slope to a depth of 1750 m. Cores 01mc, 04mc and 06bc were collected from above the OMZ (<750 m), 09mc from within the OMZ, and 02mc and 05bc from below the OMZ (>1300 m). The exact locations and water depths from which the cores were taken are provided in Table 4.1.

These cores were sampled every 1 to 2 cm, except in the lower portions of 01mc and 06bc which were sampled every 5 cm and 2 cm, respectively. Samples were freeze-dried and
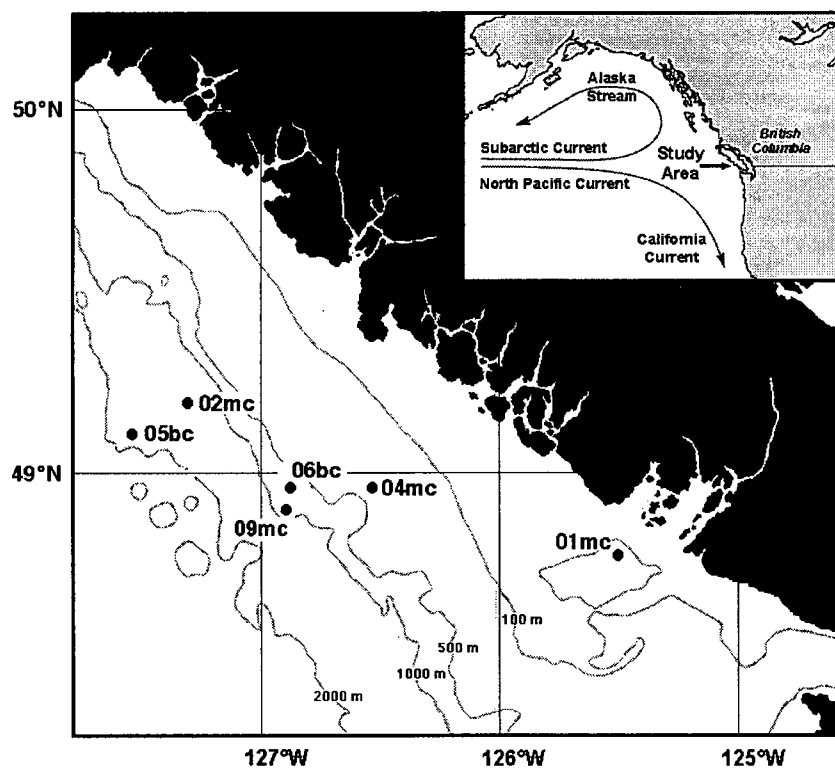
Fig. 4.1. The study area off the west coast of Vancouver Island, British Columbia, Canada (Inset) showing the locations where multicores (mc) and box cores (bc) were collected. Exact water depths and core descriptions are provided in Table 4.1.

Table 4.1. General data for sampling locations and core descriptions.

Core	Latitude	Longitude	Water Depth (m)	Bottom Water O_2 (ml/l)	Core Description
01mc	48° 45.95' N	125° 29.57' W	120	2.4	38 cm olive green mud
04mc	49° 00.71' N	126° 49.82' W	407	1.0	9 cm olive green muddy sand underlain by 10 cm gray clay
06bc	48° 58.73' N	126° 52.68' W	720	0.4	18 cm olive green sandy mud underlain by 17 cm gray clay
09mc	48° 54.76' N	126° 53.44' W	920	0.3	40 cm olive green mud
02mc	49° 12.81' N	127° 18.57' W	1340	0.4 [1]	18 cm olive green mud
05bc	49° 07.91' N	127° 33.12' W	1750	1.2	48 cm olive green mud

[1] dissolved O_2 concentration was measured at 1240 m.

in most instances hand ground, except for sandy sediments which were pulverized in a Tema WC disc mill.

A sedimentation rate for each core was estimated by assigning an age of 0 years to the core top and obtaining an age estimate from near the core base; linear sedimentation was assumed between the two assigned ages. Where possible ^{14}C dating was performed by accelerator mass spectrometry (AMS) on a mixed assemblage of planktonic foraminifera (i.e., Cores 09mc and 05bc). However, this was not always feasible given the scarcity of carbonate microfossils in these deposits. In Core 01mc no foraminifera were available so bulk organic carbon was dated by AMS. Such materials typically yield older than expected ages due to the presence of "old" organic matter. To validate the use of bulk organic carbon ages, ^{14}C measurements of coexisting benthic foraminifera and organic carbon were obtained for one sample taken from 09mc. For Cores 06bc and 04mc no radiocarbon measurements were made and sedimentation rates were calculated by assuming that the contact between the Holocene green mud and deglacial gray clay, which is observed in both cores, is the same age as the mud-clay contact observed in a nearby piston core. The sedimentation rate for Core 02mc was also estimated by dating sediments in a nearby core.

The depth of bioturbation was estimated using excess ^{210}Pb data. The method of Eakin and Morrison (1978), which determines the ^{210}Pb concentration by measuring the content of its ^{210}Po grand-daughter via alpha counting, was employed.

Total carbon (C_{tot}), nitrogen (N_{tot}) and sulphur (S_{tot}) were measured using a Carlo-Erba NA-1500 elemental analyzer. Precision and accuracy were determined for two National Research Council of Canada (NRC) standards (PACS-1 and MESS-1). The relative standard deviation (RSD, 1σ) was 3%, 5% and 6% for C, N and S, respectively and the accuracy was within 7% of the values recommended for all three elements. Carbonate carbon (C_{carb}) was determined by coulometry. Repeat analyses (n=141) of a $CaCO_3$ standard yielded a mean value of 11.93% and a RSD of 1%. The percent organic carbon (C_{org}) was calculated by difference ($C_{org} = C_{tot} - C_{carb}$) and has an aggregate error (as RSD) of ~4%.

Biogenic silica was measured using the Na_2CO_3 dissolution method of Mortlock and Froelich (1989). The RSD determined for two in-house standards SBS and JV5, which contain approximately 28% and 11% opal respectively, was 4%. However, the precision of the method is much poorer at opal concentrations <10% (R. Ganeshram, pers. comm.), possibly due to the dissolution of volcanic glass and clay minerals.

Major and minor element contents were determined by X-ray fluorescence spectrometry (XRF) following Calvert (1990) and have RSDs of 5% and 15%, respectively. Total Ba (Ba_{tot}) and Al data were used to calculate the percent biogenic barium (Ba_{bio}) via the Dymond et al. (1992) equation:

$$Ba_{bio} = Ba_{tot} - (Al \times Ba/Al_{lith}) \qquad (4.1)$$

An average Ba/Al lithogenic ratio (Ba/Al_{lith}) of 0.0027 was employed. This value is significantly lower than the average Ba/Al_{lith} ratio of crustal rocks (0.0075; Dymond et al., 1992); however, this ratio can vary greatly depending on the composition of the sediment source (e.g., 0.005 to 0.010; Taylor and McLennan, 1985). The geology of Vancouver Island is complex and includes a mixture of metamorphic, igneous and sedimentary rock types (Yorath and Nasmith, 1995); thus it is not possible to chose a Ba/Al_{lith} ratio representative of any particular rock type. Rather, the Ba/Al_{lith} ratio used here (i.e., 0.0027) was determined from an exponential regression of the Ba/Al ratios of surface sediments versus water depth following the method Klump et al. (2000). This method assumes that the fraction of biogenic Ba increases seaward and that close to land (i.e., ~0 m water depth) all of the Ba is terrigenous in origin. The low Ba/Al_{lith} estimated using this regression method was confirmed by chemically extracting the bio-barium from six samples using a 2M solution of NH_4Cl (Schenau et al., 2001) and measuring the barium content of the residue (i.e., the lithogenic Ba) by XRF. This chemical dissolution method yields a slightly higher average Ba/Al_{lith} ratio of 0.0033 (range 0.0026 to 0.0038; Table 4.2).

Table 4.2. Results of Biogenic Barium Dissolution Tests.

Core / Sample	Age (Cal. kyr)	Total Ba [1] (ppm)	Ba$_{lith}$ [2] (ppm)	Total Al (ppm)	Ba/Al$_{lith}$	Ba$_{bio}$ [3] (ppm)	Ba$_{bio}$ [4] (ppm)
JT96-01mc 0-1 cm	0.01	411	527	140000	0.0038	bdl	61
JT96-09mc 5-6 cm	1.16	624	529	147000	0.0036	96	226
JT96-09pc 241-242 cm	14.00	464	497	159200	0.0031	bdl	34
JT96-09pc 341-342 cm	15.38	573	622	162500	0.0038	bdl	135
JT96-02mc 5-6 cm	0.23	759	505	167000	0.0030	255	341
JT96-05bc 5-6 cm	1.20	1057	402	152000	0.0026	655	677
Average Ba/Al$_{lith}$ ratio					0.0033		

[1] Total Ba concentration in untreated samples.

[2] Lithogenic Ba measured in samples that were treated with NH_4Cl to remove biogenic Ba.

[3] Biogenic Ba calculated by difference (Batot - Balith).

[4] Biogenic Ba calculated using Equation 4.1 and a Ba/Al$_{lith}$ ratio of 0.0027.

Stable isotope data were obtained by continuous-flow mass spectrometry using a Fisons NA-1500 elemental analyzer in line with a VG Prism mass spectrometer. Samples for carbon isotopic analysis of organic matter ($\delta^{13}C_{org}$) were pretreated with 10% HCl to remove carbonate and then dried at 50°C overnight. These samples were not washed with distilled water prior to drying. Nitrogen isotope results ($\delta^{15}N$) were obtained for untreated bulk sediment samples. Data are reported in the standard δ-notation relative to VPDB for carbon and atmospheric N_2 for nitrogen. The reproducibility for an in-house isotopic standard was ± 0.1‰ for carbon and ± 0.2‰ for nitrogen.

Trace metal concentrations (i.e., Re, Ag, Cd, Mo and U) were measured by isotope-dilution inductively-coupled plasma mass spectrometry. Sample preparation involved adding known amounts of isotopically-enriched spike solutions to ~20 mg of powdered sediment. Samples were then microwave digested in a mixture of concentrated HNO_3, HCl and HF. The digests were evaporated on a hotplate overnight and then re-digested in 5N HCl. An aliquot was taken for Mo and U analysis. The remaining sample was run through an anion exchange column (Dowex 1-X8 resin) to remove Zr and Nb, as these form compounds (ZrO, ZrOH and NbO) that interfere with the analysis of Ag, and Mo as it forms MoO^- that interferes with Cd analysis. A detailed description of the sample preparation and analysis can be found Ivanochko (2001). To check precision, a University of British Columbia sediment standard (SNB) was analyzed with each batch of samples. The resulting RSD (1σ) for Re, U, Mo, Cd and Ag analyses were 11%, 9%, 7%, 10% and 8%, respectively. Accuracy, assessed by measuring the concentrations of these metals in the NRC sediment standard MESS-1, was 8% or better for Re, Mo and U, and ~14% for Cd. The accuracy for Ag could not be evaluated as there is no accepted Ag value for MESS-1 at present. Trace metal data are present as concentrations rather than metal/Al ratios because the concentration data yield a finer resolution and because the sediments are relatively homogeneous; thus downcore metal/Al and concentration profiles do not differ significantly. Also, no attempt

has been made to calculate the authigenic fraction because the lithogenic concentrations of these metals are poorly constrained.

4.3 Results

Core descriptions are provided in Table 4.1. The olive green muds, sandy muds and muddy sands observed in these near-surface sediment cores are typical of Holocene deposits off Vancouver Island (Bornhold and Barrie, 1991). The gray clay found at the base of Cores 04mc and 06bc is most probably Pleistocene in age and of glaciomarine origin (Bornhold and Yorath, 1984; Bornhold and Barrie, 1991).

Radiocarbon data and estimated sedimentation rates are given in Table 4.3. Holocene sedimentation rate for slope Cores 09mc and 05bc is ~5 cm/kyr. The radiocarbon date obtained for bulk organic carbon from a depth of 39 cm in 09mc (9920 ± 40 ^{14}C yrs) is essentially identical to the age determined by AMS dating of benthic foraminifera (9830 ± 110 ^{14}C yrs). This result suggests that bulk organic matter can be used for dating these near-surface sediments. However, the use of bulk organic carbon dates is only valid for Holocene sediments that contain little terrestrial organic matter and not for the Late Pleistocene sediments that contain up to 70 % old terrestrial organic matter (Chapter 2). For the inner-shelf Core 01mc radiocarbon dating bulk organic carbon yields an age of 923 calendar yrs and suggests a sedimentation rate of ~40 cm/kyr. No radiocarbon data are available for Multicore 02mc; however, ^{14}C data for nearby Piston core Tul96-05pc (see Table A6 in the Appendix) suggest that at a water depth of ~1300 m the Holocene sedimentation rate is ~23 cm/kyr. This is admittedly only a rough estimate as sedimentation rates could vary substantially between the two locations. No radiocarbon dates were obtained for Cores 04mc or 06bc, but the contact between the olive green mud and gray clay which is observed in both cores has been dated as ~11 calendar kyr B.P. in Piston Core JT96-09 (Chapter 2). Using

Table 4.3. Radiocarbon data and estimated sedimentation rates.

Core	Water Depth (m)	Material Dated	Sample Depth (cm)	^{14}C Age (yrs)	Calendar Age [3] (yrs)	Sedimentation Rate (cm/kyr)
01mc	120	bulk organic matter	36.5	1780 ± 30	923	39.5
04mc	407	-	-	-	-	0.8 [4]
06bc	720	-	-	-	-	1.6 [4]
09mc	920	planktonic forams [1]	47.5	9760 ± 70	10026	4.7
		benthic forams	39.0	9830 ± 110		
		bulk organic matter	39.0	9920 ± 40		
02mc	1340	planktonic forams [2]	234.5	9800 ± 90	10127	23.2
05bc	1750	planktonic forams	47.0	9960 ± 50	10290	4.6

[1] planktonic forams were obtained from piston core JT96-09 that was collected from the same location.

[2] determined using radiocarbon data obtained from nearby piston core Tul96-05.

[3] ^{14}C data were converted to calendar years using Calib 4.3 (Stuiver et al., 1998) and assuming a reservoir age of 800 yrs.

[4] estimated assuming that the contact between the Holocene muds and gray clay is at 11.0 calendar kyrs.

this date and assuming that the core top is 0 years yields sedimentation rates of 0.8 and 1.6 cm/kyr for Cores 04mc and 06bc, respectively.

Total ^{210}Pb concentrations in surface sediments range from 24.5 dpm/g in Core 01mc to 58.8 dpm/g in Core 02mc. Supported ^{210}Pb produced in situ by the decay of ^{226}Ra ranges from 1.8 to 2.8 dpm/g, similar to that in sediments from the Washington continental margin to the south (Carpenter et al., 1981). Unsupported or excess ^{210}Pb (i.e., ^{210}Pb scavenged from the water column) occurs to depths as deep as 10 cm in 02mc, 19 cm in 09mc, and 30 cm in 01mc (Fig. 4.2). Such depths of penetration are well below those expected given the estimated sedimentation rates (5 to 40 cm/kyr) and short half-life of ^{210}Pb (22.3 yrs) implying that these sediments are deeply bioturbated. By mixing younger and more radiocarbon-rich sediment downwards, such bioturbation will decrease the "true age" of subsurface deposits, resulting in overestimates of the "true" rates of sedimentation. No corrections for this effect have been applied to the sedimentation rates listed in Table 4.3.

Organic carbon, carbonate and opal concentrations in these near-surface cores are provided in Table 4.4 and their downcore profiles are shown in Figure 4.3. Organic carbon (C_{org}) contents are highest in the surface sediments of 02mc and 09mc (3.4 and 3.1 wt.%, respectively) and decrease with depth (Fig. 4.3a). Lower values (1.6 to 2.1 wt.%) are seen in 01mc, 05bc and 06bc and, with the exception of 06bc, decrease only slightly with depth (Fig. 4.3a). The abrupt decrease in C_{org} seen at ~20 cm depth in 06bc occurs at the contact between the Holocene mud and Pleistocene gray clay. The lowest C_{org} content (0.5 to 0.6 wt.%) is found in the sandy sediments of 04mc. The mass accumulation rate of C_{org}, calculated as the product of the linear sedimentation rate, the dry bulk density and the organic carbon concentration, is lowest in 09mc and 05bc (< 0.1 g/cm^2/kyr) and up to an order of magnitude higher in 01mc and 02mc (0.6 to 0.3 g/cm^2/kyr, respectively). The CaCO$_3$ content in all cores is low, ranging from <1.2 wt.% in surface sediments to 3 % in the lower portions of 09mc, 05bc and 06bc (Fig. 4.3b). Opal concentration ranges from < 3 to 11 wt.% in surface sediments and exhibits little change downcore (Fig. 4.3c).
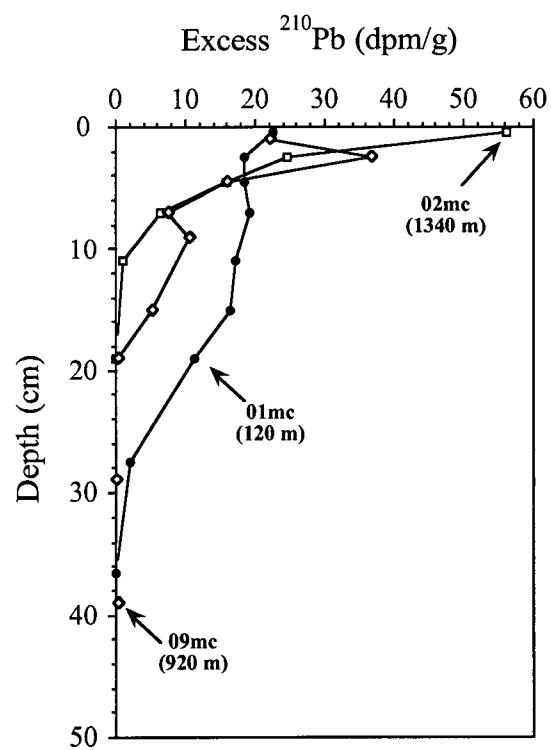
Fig. 4.2. Concentration of "excess" [210]Pb in near-surface sediment cores
01mc, 02bc and 09mc.
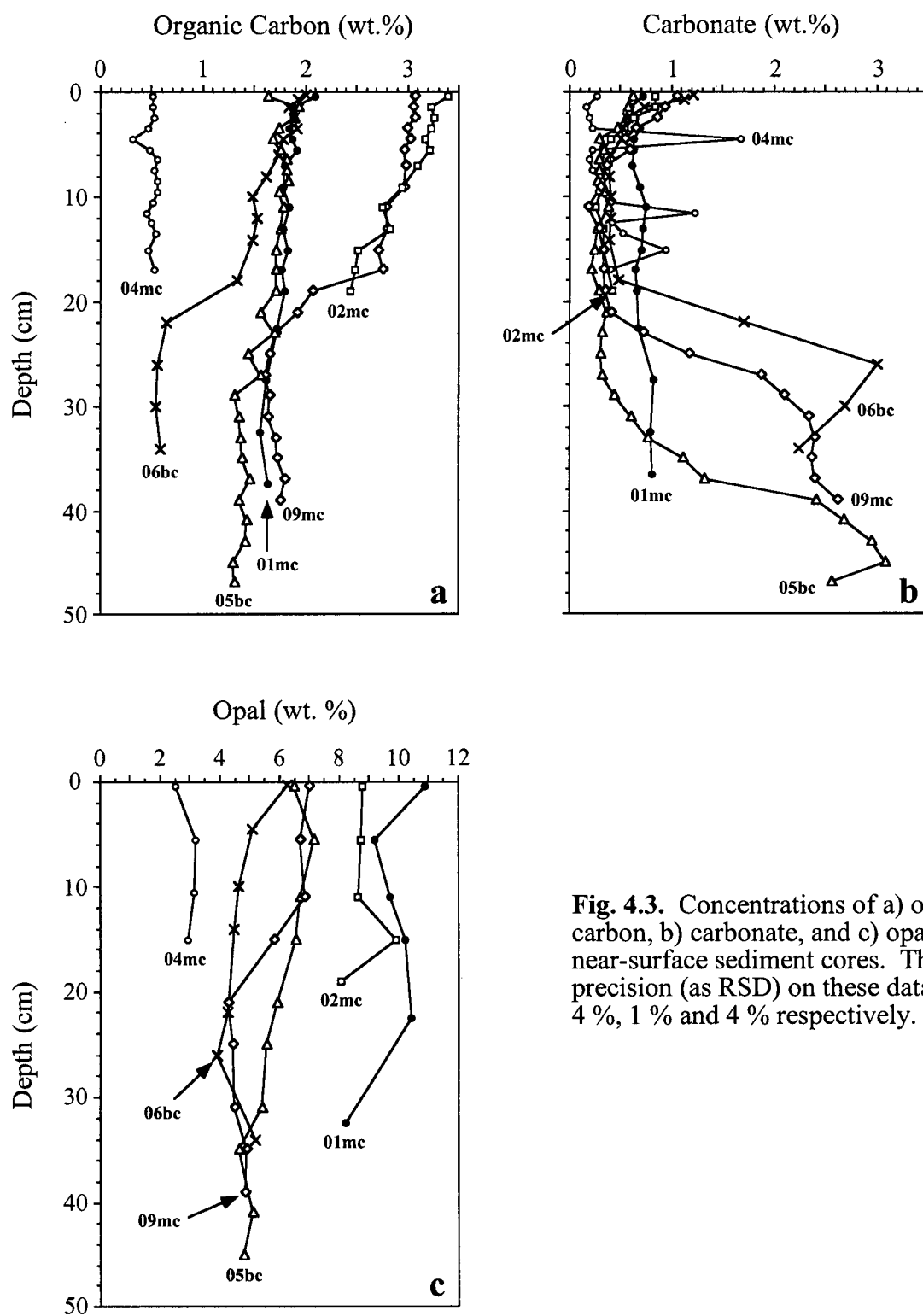
Fig. 4.3. Concentrations of a) organic carbon, b) carbonate, and c) opal in near-surface sediment cores. The precision (as RSD) on these data are 4 %, 1 % and 4 % respectively.

The carbon isotopic composition of organic matter ($\delta^{13}C_{org}$) in surface sediments ranges from -21.8 ‰ in 01mc to -20.5 ‰ in 04mc (Table 4.4), and changes little downcore except in 04mc and 06bc (Fig. 4.4a). The Pleistocene gray clay in the lower portion of these cores is characterized by relatively low $\delta^{13}C_{org}$ values (-23.7 to -23.3 ‰; Table 4.4).

The nitrogen isotopic composition of bulk surface sediments ($\delta^{15}N$) ranges from +4.8 ‰ in shelf Core 01mc to +6.8 ‰ in 06bc (Table 4.4), and is invariant in the upper 20 cm of all of the cores (Fig. 4.4b). Below this depth there is a minor increase in $\delta^{15}N$ in 05bc and 09mc (up to +7.9 ‰), and a decrease in 06bc (down to +5.8 ‰) at the boundary between the Holocene mud and underlying Pleistocene gray clay.

Manganese concentrations ranges from 293 to 791 µg/g (Table 4.5). In surface sediments Mn/Al ratios range from 0.0026 to 0.0050, substantially less than the ratio of average shale (0.0106; Turekian and Wedepohl, 1961), and decrease with depth in the upper 2 to 5 cm of all cores (Fig. 4.5a). The Pleistocene gray clay observed in the lower portion of Cores 04mc and 06bc exhibits relatively high Mn/Al ratios, similar to surface sediments in Cores 02mc and 05bc.

Iodine concentrations in surface sediments range from 104 to 968 µg/g. The I/C_{org} ratios of surface sediments range from 120 x 10^{-4} in 01mc to 500 x 10^{-4} in 05bc (Table 4.4), and decreases gradually with depth in all cores (Fig. 4.5b).

Total Ba content ranges from 291 µg/g in 04mc to 1057 µg/g in 05bc (Table 4.5). The ratio of Ba_{tot}/Al ranges from 0.0025 to 0.0070 and tends to increase with increasing water depth (Fig. 4.5c). The exception is Core 04mc that has relatively low Ba_{tot}/Al ratios, most probably reflecting the sandy nature of these sediments. Biogenic Ba concentrations, calculated using Equation 4.1 and assuming a Ba/Al_{lith} ratio of 0.0027, range from ~ 9 µg/g in 04mc to 661 µg/g in 05bc (Table 4.4) and increases with water depth.

Rhenium concentrations range from 2 to 65 ng/g (Table 4.5). Concentrations are relatively low (2 to 4 ng/g) in the upper 10 cm of all cores (Fig. 4.6a). There is no change in Re concentration with depth in Cores 01mc, 04mc and 06bc, but values rise to 65 ng/g in the
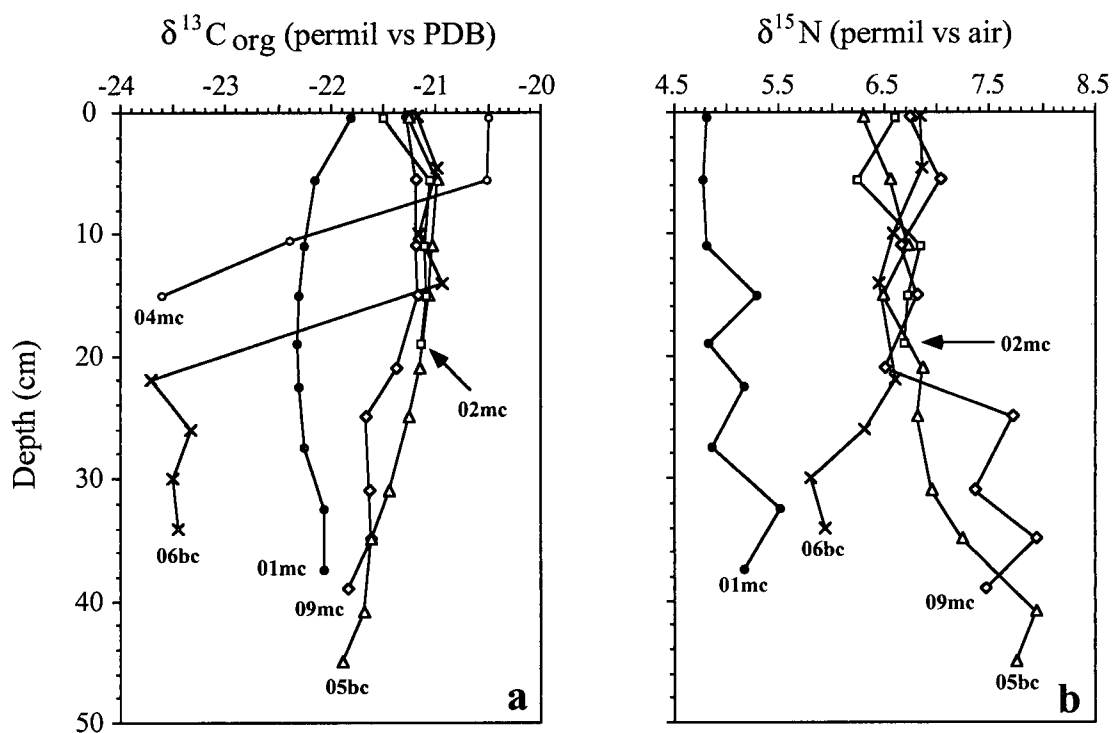
Fig. 4.4. a) The C-isotopic composition of organic matter ($\delta^{13}C_{org}$) and b) the N-isotopic composition of the bulk sediment ($\delta^{15}N$) in near-surface sediment cores. The errors on these data are ±0.1 ‰ and ±0.2 ‰ for C- and N-isotopic ratios respectively.
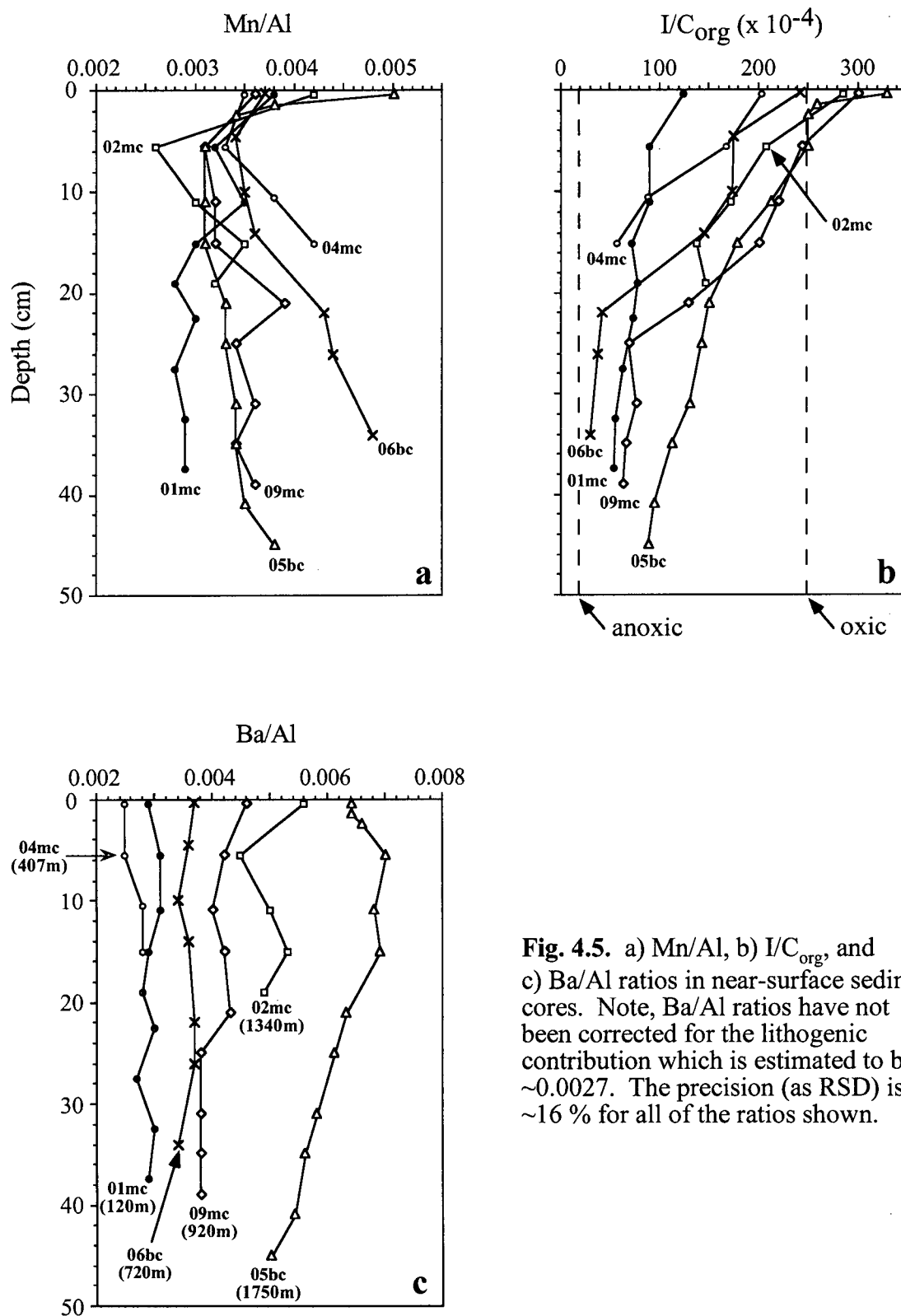
Fig. 4.5. a) Mn/Al, b) I/C$_{org}$, and c) Ba/Al ratios in near-surface sediment cores. Note, Ba/Al ratios have not been corrected for the lithogenic contribution which is estimated to be ~0.0027. The precision (as RSD) is ~16 % for all of the ratios shown.

lower portion of 09mc which was collected from the OMZ (Fig. 4.6a). Cores 02mc and 05bc, both of which were collected from below the OMZ, also exhibit Re enrichment at depth (Fig. 4.6a).

Uranium content ranges from <2 to 5.8 μg/g (Table 4.5). Concentrations are low (< 2 μg/g) in the upper 10 to 15 cm of all cores, and are slightly enriched at depth except in 04mc (Fig. 4.6b). The enrichment is greatest in OMZ Core 09mc (up to 5.8 μg/g). Comparison of the Re and U profiles (Figs. 4.6a and b, respectively) suggest that the enrichment of U occurs slightly deeper than that of Re.

Cadmium concentrations are generally low throughout these cores (< 1.0 μg/g; Table 4.5). Surface sediments contain <0.1 to 0.2 μg/g Cd and there is only a slight increase with depth in Cores 02mc, 05bc and 09mc (0.4 to 1.0 μg/g; Fig. 4.7a). These are the same cores that exhibit Re enrichments at depth. The highest Cd concentration occurs in OMZ Core 09mc.

Molybdenum contents range from 0.4 to 1.5 μg/g (Table 4.5). Surface sediments contain from 0.4 to 0.9 μg/g Mo (Fig. 4.7b). The concentration increases slightly with depth, particularly in shelf Core 01mc, but there is no evidence of substantial enrichments above the typical lithogenic background value (Fig. 4.7b).

Silver concentrations range from <100 to 357 ng/g in surface sediments (Table 4.5). Concentrations vary little downcore in 01mc, 04mc, 06bc and 09mc, but increase by over 200 ng/g in Cores 02mc and 05bc (up to 584 μg/g; Fig. 4.7c). In surface sediments there is a trend of increasing Ag content with increasing water depth, except in the sandy sediments of Cores 04mc and 06bc.

4.4 Discussion

4.4.1 C and N isotope data
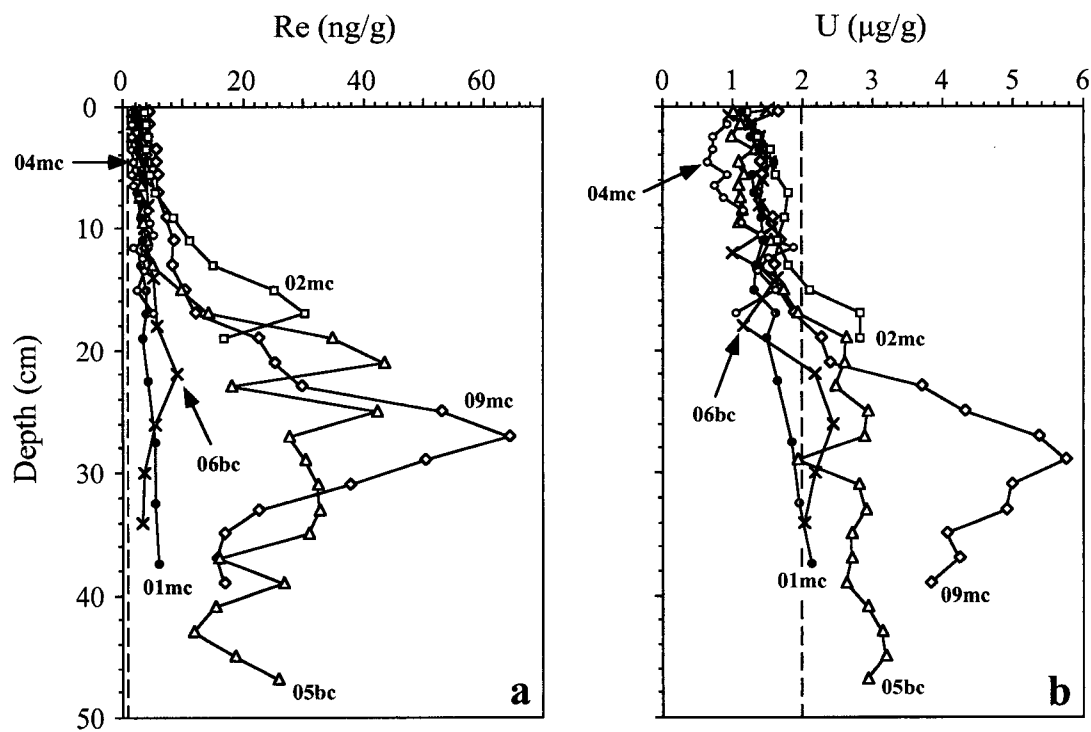
Fig. 4.6. a) Re and b) U concentrations in the near-surface sediment cores. Typical lithogenic concentrations are shown by the dashed lines. The precison (as RSD) of Re and U measurements is 11 % and 9 % respectively

Cd (μg/g)

Mo (μg/g)

Ag (ng/g)
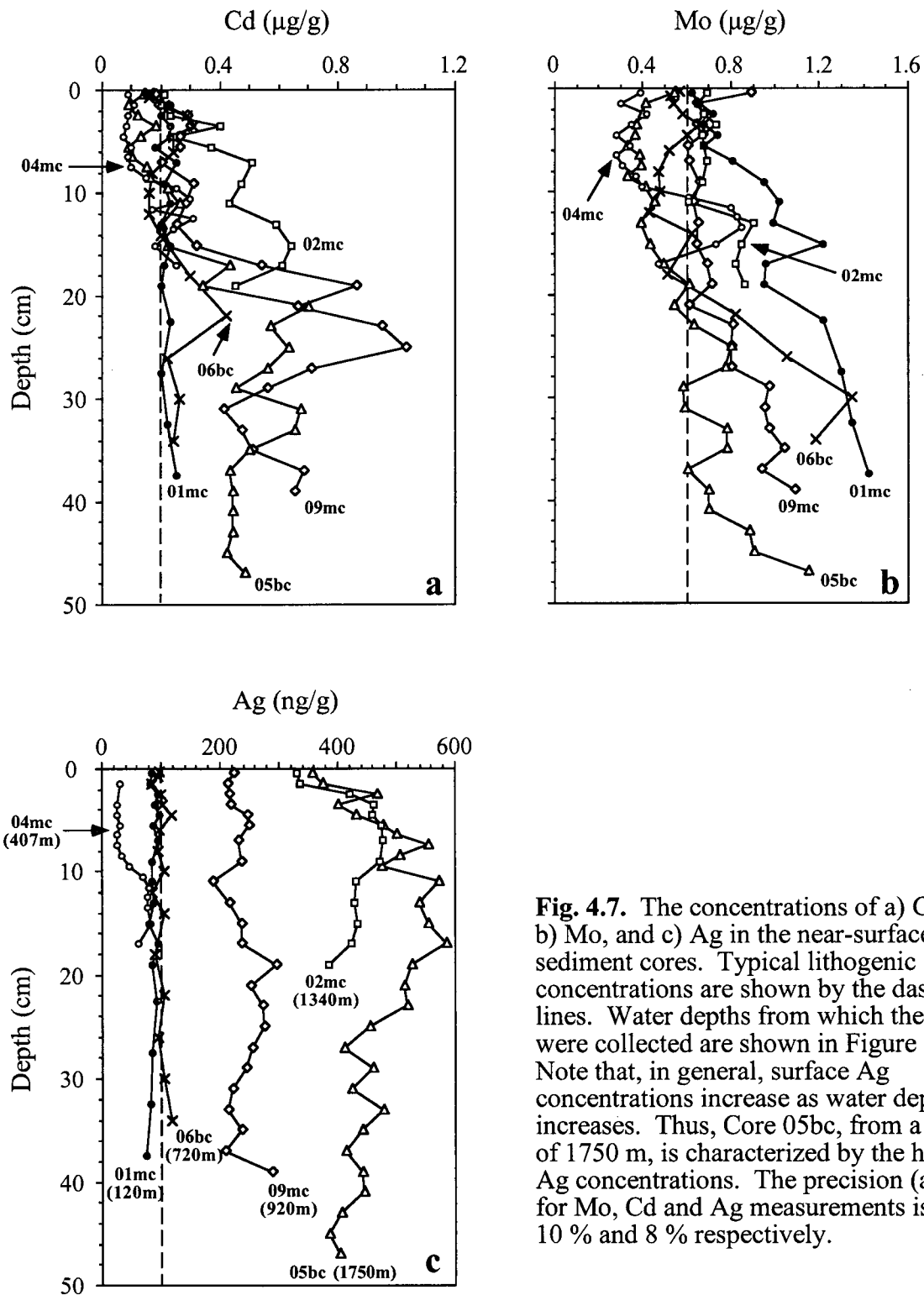
Fig. 4.7. The concentrations of a) Cd, b) Mo, and c) Ag in the near-surface sediment cores. Typical lithogenic concentrations are shown by the dashed lines. Water depths from which the cores were collected are shown in Figure 7c. Note that, in general, surface Ag concentrations increase as water depth increases. Thus, Core 05bc, from a depth of 1750 m, is characterized by the highest Ag concentrations. The precision (as RSD) for Mo, Cd and Ag measurements is 7 %, 10 % and 8 % respectively.

121

Table 4.4. General geochemical data for Vancouver Island Margin multicores (mc) and box cores (bc).

Core 01mc	Depth (cm)	Age (Cal. kyrs)	$\delta^{15}N$ (‰ vs air)	$\delta^{13}C_{org}$ (‰ vs VPDB)	C_{tot} (wt.%)	N_{tot} (wt.%)	S_{tot} (wt.%)	C_{carb} (wt.%)	C_{org} (wt.%)	C_{org}/N	Opal (wt.%)	Ba_{bio}[1] (µg/g)	I/C_{org} (x 10^{-4})
0-1	0.5	0.01	4.8	-21.8	2.2	0.2	0.3	0.7	2.1	8.6	10.9	61	124
1-2	1.5	0.04			2.0	0.2	0.2	0.6	1.9	8.7			
2-3	2.5	0.06			2.0	0.2	0.2	0.6	1.9	8.7			
3-4	3.5	0.09			1.9	0.2	0.3	0.7	1.8	8.6			
4-5	4.5	0.11			1.9	0.2	0.3	0.6	1.9	8.7			
5-6	5.5	0.14	4.8	-22.2	2.0	0.2	0.3	0.6	1.9	9.0	9.2	80	89
6-8	7.0	0.18			1.9	0.2	0.3	0.6	1.8	8.7			
8-10	9.0	0.23			1.9	0.2	0.3	0.7	1.8	8.7			
10-12	11.0	0.28	4.8	-22.3	1.9	0.2	0.3	0.7	1.8	8.9	9.7	85	89
12-14	13.0	0.33			1.9	0.2	0.3	0.7	1.8	8.8			
14-16	15.0	0.38	5.3	-22.3	1.9	0.2	0.3	0.7	1.8	9.0	10.2	65	72
16-18	17.0	0.43			1.8	0.2	0.3	0.6	1.8	9.1			
18-20	19.0	0.48	4.8	-22.3	1.9	0.2	0.3	0.7	1.8	9.2		40	78
20-25	22.5	0.57	5.2	-22.3	1.8	0.2	0.4	0.7	1.7	9.2	10.4	73	73
25-30	27.5	0.70	4.9	-22.3	1.7	0.2	0.5	0.8	1.6	9.3		29	62
30-35	32.5	0.82	5.5	-22.1	1.6	0.2	0.5	0.8	1.5	9.2	8.2	72	56
35-38	36.5	0.92	5.2	-22.1	1.7	0.2	0.6	0.8	1.6	10.0		61	54

Core 04mc	Depth (cm)	Age (Cal. kyrs)	$\delta^{15}N$ (‰ vs air)	$\delta^{13}C_{org}$ (‰ vs VPDB)	C_{tot} (wt.%)	N_{tot} (wt.%)	S_{tot} (wt.%)	C_{carb} (wt.%)	C_{org} (wt.%)	C_{org}/N	Opal (wt.%)	Ba_{bio}[1] (µg/g)	I/C_{org} (x 10^{-4})
0-1	0.5			-20.5	0.5	0.1	<0.1	0.3	0.5	8.2	2.5	9	203
1-2	1.5				0.5	0.1	<0.1	0.2	0.5	8.4			
2-3	2.5				0.5	0.1	<0.1	0.2	0.5	7.6			
3-4	3.5				0.5	0.1	<0.1	0.2	0.5	7.6			
4-5	4.5				0.5	0.1	<0.1	0.2	0.5	7.9			
5-6	5.5			-20.5	0.5	0.1	<0.1	0.2	0.5	7.9	3.2	9	168
6-7	6.5				0.6	0.1	<0.1	0.2	0.5	8.2			
7-8	7.5				0.6	0.1	<0.1	0.2	0.5	7.7			
8-9	8.5				0.6	0.1	<0.1	0.3	0.6	8.0			
9-10	9.5				0.6	0.1	0.1	0.3	0.6	8.5			
10-11	10.5			-22.4	0.6	0.1	0.2	0.4	0.5	8.8	3.2	59	88
11-12	11.5				0.6	<0.1	0.4	1.2	0.5	10.2			
12-13	12.5				0.5	0.1	0.3	0.4	0.5	9.5			
13-14	13.5				0.6	0.1	0.3	0.5	0.5	9.3			
14-16	15.0			-23.6	0.6	<0.1	0.3	0.9	0.5	9.5	2.9		57
16-18	17.0				0.6	0.1	0.1	0.4	0.5	8.9			

Core 06bc	Depth (cm)	Age (Cal. kyrs)	$\delta^{15}N$ (‰ vs air)	$\delta^{13}C_{org}$ (‰ vs VPDB)	C_{tot} (wt.%)	N_{tot} (wt.%)	S_{tot} (wt.%)	C_{carb} (wt.%)	C_{org} (wt.%)	C_{org}/N	Opal (wt.%)	Ba_{bio}[1] (µg/g)	I/C_{org} (x 10^{-4})
0-0.5	0.3		6.8	-21.2	2.1	0.2	0.2	1.2	2.0	8.3	6.3	164	242
0.5-1	0.8				2.1	0.2	0.1	1.1	1.9	8.2			
1-2	1.5				1.9	0.2	0.1	0.7	1.8	8.4			
2-3	2.5				2.0	0.2	0.1	0.6	1.9	8.3			
3-4	3.5				2.0	0.2	0.1	0.5	1.9	8.3			
4-5	4.5		6.9	-21.0	1.8	0.2	0.1	0.5	1.8	8.4	5.1	150	176
5-7	6.0				1.8	0.2	0.1	0.4	1.7	8.4			
7-9	8.0				1.7	0.2	0.1	0.4	1.6	8.4			
9-11	10.0		6.6	-21.2	1.5	0.2	0.1	0.4	1.5	8.5	4.6	125	173
11-13	12.0				1.6	0.2	0.1	0.4	1.5	8.4			
13-15	14.0		6.5	-20.9	1.5	0.2	0.1	0.4	1.5	8.5	4.5	146	146
17-19	18.0				1.4	0.2	0.1	0.5	1.3	8.6			
21-23	22.0		6.6	-23.7	0.8	0.1	0.3	1.7	0.6	9.5	4.3	205	42
25-27	26.0		6.3	-23.3	0.9	0.1	0.3	3.0	0.6	10.6	3.9	192	37
29-31	30.0		5.8	-23.5	0.9	0.1	0.3	2.7	0.5	9.8			
33-35	34.0		5.9	-23.5	0.8	0.1	0.4	2.2	0.6	9.7	5.2	142	30

Table 4.4 (continued)

Core 09mc	Depth (cm)	Age (Cal. kyrs)	$\delta^{15}N$ (‰ vs air)	$\delta^{13}C_{org}$ (‰ vs VPDB)	C_{tot} (wt.%)	N_{tot} (wt.%)	S_{tot} (wt.%)	C_{carb} (wt.%)	C_{org} (wt.%)	C_{org}/N	Opal (wt.%)	Ba_{bio}[1] (µg/g)	I/C_{org} (x 10^{-4})
0-1	0.5	0.09	6.7	-21.3	3.2	0.4	0.4	1.0	3.1	8.7	7.0	284	301
1-2	1.5	0.27			3.2	0.4	0.4	0.9	3.0	8.4			
2-3	2.5	0.45			3.2	0.4	0.3	0.8	3.1	8.3			
3-4	3.5	0.63			3.1	0.4	0.3	0.6	3.0	8.4			
4-5	4.5	0.81			3.1	0.4	0.3	0.5	3.0	8.4			
5-6	5.5	0.99	7.0	-21.2	3.0	0.3	0.2	0.6	3.0	8.5	6.7	256	244
6-8	7.0	1.26			3.0	0.3	0.2	0.4	3.0	8.5			
8-10	9.0	1.63			3.0	0.3	0.2	0.3	3.0	8.5			
10-12	11.0	1.99	6.7	-21.2	2.8	0.3	0.3	0.2	2.8	8.9	6.8	233	220
12-14	13.0	2.35			2.8	0.3	0.2	0.3	2.8	8.6			
14-16	15.0	2.71	6.8	-21.2	2.7	0.3	0.2	0.3	2.7	8.7	5.8	260	200
16-18	17.0	3.07			2.8	0.3	0.2	0.3	2.7	8.6			
18-20	19.0	3.43			2.1	0.2	0.2	0.3	2.1	8.9			
20-22	21.0	3.79	6.5	-21.4	2.0	0.2	0.2	0.4	1.9	9.4	4.3	247	129
22-24	23.0	4.15			1.8	0.2	0.1	0.7	1.7	9.1			
24-26	25.0	4.52	7.7	-21.7	1.8	0.2	0.2	1.2	1.6	9.3	4.4	205	69
26-28	27.0	4.88			1.8	0.2	0.2	1.9	1.6	9.0			
28-30	29.0	5.24			1.9	0.2	0.2	2.1	1.6	9.0			
30-32	31.0	5.60	7.4	-21.6	1.9	0.2	0.2	2.3	1.6	9.2	4.5	213	70
32-34	33.0	5.96			2.0	0.2	0.2	2.4	1.7	9.1			
34-36	35.0	6.32	7.9	-21.6	2.0	0.2	0.2	2.4	1.7	9.4	4.9	198	65
36-38	37.0	6.68			2.1	0.2	0.2	2.4	1.8	9.1			
38-40	39.0	7.05	7.5	-21.9	2.1	0.2	0.3	2.6	1.8	9.2	4.8	214	63

Core 02mc	Depth (cm)	Age (Cal. kyrs)	$\delta^{15}N$ (‰ vs air)	$\delta^{13}C_{org}$ (‰ vs VPDB)	C_{tot} (wt.%)	N_{tot} (wt.%)	S_{tot} (wt.%)	C_{carb} (wt.%)	C_{org} (wt.%)	C_{org}/N	Opal (wt.%)	Ba_{bio}[1] (µg/g)	I/C_{org} (x 10^{-4})
0-1	0.5	0.02	6.6	-21.5	3.5	0.4	0.4	0.8	3.4	8.5	8.8	378	285
1-2	1.5	0.06			3.3	0.4	0.4	0.8	3.2	8.4			
2-3	2.5	0.10			3.3	0.4	0.3	0.6	3.3	8.4			
3-4	3.5	0.14			3.3	0.4	0.3	0.5	3.2	8.3			
4-5	4.5	0.18			3.2	0.4	0.3	0.4	3.2	8.2			
5-6	5.5	0.23	6.2	-21.1	3.3	0.4	0.3	0.3	3.2	8.5	8.7	341	208
6-8	7.0	0.29			3.1	0.4	0.3	0.3	3.1	8.5			
8-10	9.0	0.37			3.0	0.4	0.3	0.3	3.0	8.4			
10-12	11.0	0.45	6.8	-21.1	2.8	0.3	0.2	0.2	2.8	8.8	8.6	368	172
12-14	13.0	0.53			2.9	0.3	0.3	0.3	2.8	8.6			
14-16	15.0	0.62	6.7	-21.1	2.6	0.3	0.3	0.3	2.5	8.8	9.9	371	138
16-18	17.0	0.70			2.5	0.3	0.3	0.4	2.5	8.7			
18-20	19.0	0.78	6.7	-21.1	2.5	0.3	0.3	0.4	2.4	8.8	8.1	345	147

Core 05bc	Depth (cm)	Age (Cal. kyrs)	$\delta^{15}N$ (‰ vs air)	$\delta^{13}C_{org}$ (‰ vs VPDB)	C_{tot} (wt.%)	N_{tot} (wt.%)	S_{tot} (wt.%)	C_{carb} (wt.%)	C_{org} (wt.%)	C_{org}/N	Opal (wt.%)	Ba_{bio}[1] (µg/g)	I/C_{org} (x 10^{-4})
0-1	0.5	0.11	6.3	-21.3	1.7	0.2	0.2	0.6	1.6	8.3	6.5	560	329
1-2	1.5	0.33			2.0	0.2	0.2	0.6	1.9	8.2		556	259
2-3	2.5	0.55			1.9	0.2	0.2	0.5	1.9	8.2		559	250
3-4	3.5	0.77			1.8	0.2	0.2	0.5	1.7	8.2			
4-5	4.5	0.99			1.7	0.2	0.2	0.3	1.7	8.3			
5-6	5.5	1.20	6.6	-21.0	1.8	0.2	0.2	0.3	1.8	8.4	7.1	677	250
6-7	6.5	1.42			1.9	0.2	0.2	0.3	1.8	8.3			
7-8	7.5	1.64			1.8	0.2	0.2	0.3	1.8	8.3			
8-9	8.5	1.86			1.9	0.2	0.2	0.3	1.8	8.3			
9-10	9.5	2.08			1.8	0.2	0.2	0.3	1.7	8.4			
10-12	11.0	2.41	6.7	-21.1	1.8	0.2	0.2	0.4	1.8	8.4	6.7	664	213
12-14	13.0	2.85			1.8	0.2	0.2	0.3	1.7	8.4			
14-16	15.0	3.28	6.5	-21.1	1.7	0.2	0.2	0.2	1.7	8.4	6.5	665	178

Table 4.4 (continued)

Core 05bc	Depth (cm)	Age (Cal. kyrs)	$\delta^{15}N$ (‰ vs air)	$\delta^{13}C_{org}$ (‰ vs VPDB)	C_{tot} (wt.%)	N_{tot} (wt.%)	S_{tot} (wt.%)	C_{carb} (wt.%)	C_{org} (wt.%)	C_{org}/N	Opal (wt.%)	Ba_{bio}[1] (µg/g)	I/C_{org} (x 10^{-4})
16-18	17.0	3.72			1.7	0.2	0.1	0.2	1.7	8.6			
18-20	19.0	4.16			1.7	0.2	0.1	0.3	1.7	8.5			
20-22	21.0	4.60	6.9	-21.2	1.6	0.2	0.1	0.4	1.6	8.7	5.9	584	150
22-24	23.0	5.04			1.7	0.2	0.1	0.3	1.7	8.5			
24-26	25.0	5.47	6.8	-21.3	1.5	0.2	0.1	0.3	1.4	8.7	5.5	552	142
26-28	27.0	5.91			1.6	0.2	0.1	0.3	1.6	8.7			
28-30	29.0	6.35			1.3	0.1	0.1	0.4	1.3	8.8			
30-32	31.0	6.79	7.0	-21.5	1.4	0.2	0.1	0.6	1.3	8.8	5.4	513	130
32-34	33.0	7.22			1.5	0.2	0.1	0.8	1.4	8.9			
34-36	35.0	7.66	7.2	-21.6	1.5	0.2	0.1	1.1	1.4	8.7	4.6	496	112
36-38	37.0	8.10			1.6	0.2	0.1	1.3	1.4	8.9			
38-40	39.0	8.54			1.6	0.2	0.1	2.4	1.4	8.9			
40-42	41.0	8.98	7.9	-21.7	1.7	0.2	0.1	2.7	1.4	8.8	5.1	456	94
42-44	43.0	9.41			1.8	0.2	0.1	2.9	1.4	8.9			
44-46	45.0	9.85	7.8	-21.9	1.7	0.1	0.2	3.1	1.3	9.0	4.8	385	88
46-48	47.0	10.29			1.6	0.1	0.2	2.6	1.3	9.6			

[1] Biogenic barium (Ba_{bio}) values were determined using the Dymond et al. (1992) equation $Ba_{bio} = Ba_{tot} - (Al \times Ba/Al_{lith})$.

Table 4.5. Major, minor and trace element data for Vancouver Island Margin multicores (mc) and box cores (bc).

Core 01mc	Al (wt.%)	Mn (µg/g)	Ba$_{tot}$ (µg/g)	Zr (µg/g)	Ag (ng/g)	Cd (µg/g)	Re (ng/g)	Mo (µg/g)	U (µg/g)
0-1	14.0	532	411	158	84	0.2	2	0.6	1.1
1-2					81	0.2	3	0.7	1.3
2-3					94	0.2	3	0.7	1.3
3-4					89	0.2	3	0.7	1.4
4-5					97	0.2	4	0.7	1.6
5-6	14.0	449	430	169	87	0.2	3	0.7	1.3
6-8					94	0.3	2	0.8	1.3
8-10					86	0.2	3	1.0	1.4
10-12	13.0	454	410	166	85	0.2	3	1.0	1.4
12-14					87	0.2	3	1.0	1.3
14-16	14.9	454	438	164	79	0.2	4	1.2	1.3
16-18					96	0.2	4	1.0	1.6
18-20	15.0	418	415	168	86	0.2	3	1.0	1.5
20-25	14.8	438	442	167	92	0.2	4	1.2	1.6
25-30	15.2	430	408	174	85	0.2	5	1.3	1.8
30-35	15.2	444	452	169	82	0.2	5	1.4	2.0
35-38	15.2	442	440	173	75	0.3	6	1.4	2.1

Core 04mc	Al (wt.%)	Mn (µg/g)	Ba$_{tot}$ (µg/g)	Zr (µg/g)	Ag (ng/g)	Cd (µg/g)	Re (ng/g)	Mo (µg/g)	U (µg/g)
0-1	11.7	404	291	129	-	0.1	2	0.4	-
1-2					32	0.1	1	0.3	0.9
2-3					-	0.1	2	0.4	0.7
3-4					27	0.1	1	0.4	0.7
4-5					27	0.1	2	0.3	0.7
5-6	11.9	397	293	146	32	0.1	2	0.3	0.9
6-7					27	0.1	2	0.3	0.8
7-8					26	0.1	3	0.3	0.9
8-9					33	0.2	4	0.4	1.2
9-10					47	0.3	5	0.4	1.1
10-11	14.3	550	397	144	70	0.3	5	0.6	1.4
11-12					79	0.2	2	0.8	1.9
12-13					77	0.3	3	0.8	1.5
13-14					76	0.2	4	0.9	1.4
14-16	15.9	672	451	144	81	0.2	3	0.7	1.6
16-18					62	0.3	5	0.5	1.0

Core 06bc	Al (wt.%)	Mn (µg/g)	Ba$_{tot}$ (µg/g)	Zr (µg/g)	Ag (ng/g)	Cd (µg/g)	Re (ng/g)	Mo (µg/g)	U (µg/g)
0-0.5	13.3	495	498	157	97	0.2	4	0.6	1.5
0.5-1					94	0.2	3	0.5	1.0
1-2					84	0.2	3	0.5	1.3
2-3					100	0.3	4	0.6	1.4
3-4					103	0.3	4	0.7	1.4
4-5	13.8	473	495	168	117	0.2	4	0.6	1.5
5-7					98	0.2	4	0.5	1.5
7-9					94	0.2	4	0.5	1.4
9-11	13.6	472	465	176	106	0.2	4	0.5	1.6
11-13					85	0.2	4	0.4	1.0
13-15	13.6	496	487	169	106	0.2	5	0.6	1.6
17-19					91	0.3	6	0.5	1.2
21-23	16.7	718	622	131	106	0.4	9	0.8	2.2
25-27	16.0	710	591	135	96	0.2	5	1.1	2.4
29-31					106	0.3	4	1.4	2.2
33-35	16.5	791	555	129	119	0.2	3	1.2	2.0

Table 4.5 (continued)

Core 09mc	Al (wt.%)	Mn (μg/g)	Ba$_{tot}$ (μg/g)	Zr (μg/g)	Ag (ng/g)	Cd (μg/g)	Re (ng/g)	Mo (μg/g)	U (μg/g)
0-1	13.6	492	624	146	223	0.2	4	0.9	1.6
1-2					213	0.2	4	0.6	1.2
2-3					215	0.3	4	0.7	1.4
3-4					219	0.3	5	0.6	1.4
4-5					247	0.3	5	0.7	1.4
5-6	14.7	456	624	139	248	0.3	6	0.6	1.4
6-8					231	0.2	6	0.6	1.3
8-10					235	0.3	7	0.7	1.6
10-12	15.4	492	617	151	187	0.3	8	0.6	1.7
12-14					215	0.3	8	0.7	1.6
14-16	14.9	475	633	153	236	0.3	10	0.6	1.7
16-18					236	0.5	12	0.7	1.9
18-20					295	0.9	22	0.7	2.3
20-22	14.0	542	598	155	251	0.7	25	0.6	2.4
22-24					271	1.0	30	0.8	3.7
24-26	15.6	534	596	156	275	1.0	53	0.8	4.3
26-28					254	0.7	65	0.8	5.4
28-30					245	0.6	50	1.0	5.8
30-32	15.8	570	608	155	221	0.4	41	1.0	5.0
32-34					212	0.5	22	1.0	4.9
34-36	15.7	533	591	147	236	0.5	17	1.0	4.4
36-38					207	0.7	15	0.9	4.2
38-40	16.2	574	618	151	3	0.7	17	1.1	3.8

Core 02mc	Al (wt.%)	Mn (μg/g)	Ba$_{tot}$ (μg/g)	Zr (μg/g)	Ag (ng/g)	Cd (μg/g)	Re (ng/g)	Mo (μg/g)	U (μg/g)
0-1	12.4	521	687	135	330	0.2	4	0.7	1.2
1-2					335	0.2	4	0.7	1.3
2-3					420	0.2	4	0.7	1.4
3-4					462	0.3	4	0.7	1.5
4-5					458	0.2	4	0.7	1.5
5-6	16.7	430	759	145	475	0.4	5	0.7	1.6
6-8					476	0.5	5	0.7	1.8
8-10					473	0.5	9	0.7	1.7
10-12	14.7	446	736	146	430	0.4	11	0.6	1.6
12-14					428	0.6	15	0.9	1.8
14-16	13.0	451	697	154	434	0.6	25	0.9	2.1
16-18					422	0.6	30	0.8	2.8
18-20	14.4	455	705	156	388	0.5	17	0.9	2.8

Core 05bc	Al (wt.%)	Mn (μg/g)	Ba$_{tot}$ (μg/g)	Zr (μg/g)	Ag (ng/g)	Cd (μg/g)	Re (ng/g)	Mo (μg/g)	U (μg/g)
0-1	14.4	723	920	132	357	0.1	1	0.5	1.0
1-2	14.2	543	911	129	375	0.1	2	0.4	1.1
2-3	13.7	473	902	124	466	0.1	2	0.4	1.0
3-4					400	0.2	3	0.4	1.3
4-5					431	0.1	2	0.4	1.1
5-6	15.2	475	1057	135	478	0.1	3	0.3	1.2
6-7					501	0.1	3	0.4	1.1
7-8					553	0.2	3	0.4	1.1
8-9					506	0.2	3	0.3	1.1
9-10					474	0.2	3	0.4	1.1
10-12	15.3	472	1046	136	573	0.3	4	0.5	1.5
12-14					538	0.2	5	0.4	1.4
14-16	15.2	478	1045	143	555	0.2	10	0.4	1.7

126

Table 4.5 (continued)

Core 05bc	Al (wt.%)	Mn (µg/g)	Ba$_{tot}$ (µg/g)	Zr (µg/g)	Ag (ng/g)	Cd (µg/g)	Re (ng/g)	Mo (µg/g)	U (µg/g)
16-18					584	0.4	14	0.5	1.9
18-20					527	0.3	35	0.6	2.6
20-22	15.5	503	970	145	513	0.7	43	0.5	2.6
22-24					519	0.6	18	0.6	2.5
24-26	15.3	503	935	144	453	0.6	42	0.8	2.9
26-28					410	0.6	27	0.8	2.9
28-30					459	0.5	30	0.6	1.9
30-32	15.7	525	904	142	423	0.7	32	0.6	2.8
32-34					477	0.7	33	0.8	2.9
34-36	15.9	539	892	147	441	0.5	31	0.8	2.7
36-38					413	0.4	16	0.6	2.7
38-40					442	0.4	27	0.7	2.6
40-42	15.7	552	848	140	445	0.4	15	0.7	2.9
42-44					405	0.4	12	0.9	3.1
44-46	15.5	586	774	135	385	0.4	19	0.9	3.2
46-48					402	0.5	26	1.2	2.9

Previous work has shown that much of the variation in $\delta^{13}C_{org}$ values of sediments from the continental margin off Vancouver Island is due to changes in the relative proportions of terrestrial and marine organic matter (Chapter 2). It is possible to estimate the fraction of terrestrial organic carbon present in near-surface sediments using the following equation:

$$\text{Terrigenous fraction} = (\delta^{13}C_{smpl} - \delta^{13}C_{mar})/(\delta^{13}C_{terr} - \delta^{13}C_{mar}) \qquad (4.2)$$

where $\delta^{13}C_{smpl}$, $\delta^{13}C_{mar}$ and $\delta^{13}C_{terr}$ are the isotopic compositions of the sample, the marine end member and the terrestrial end member, respectively. Assuming a $\delta^{13}C_{mar}$ value of -21 ‰ and a $\delta^{13}C_{terr}$ value of -27 ‰, as suggested in Chapter 2, it is estimated that Holocene sediments contain on average 8 % terrestrial organic matter with the highest concentration (22 %) being observed in shelf core 01mc. In comparison, the Pleistocene gray clay, which is present in the lower portion of Cores 04mc and 06bc, contains significantly more terrestrial organic matter (> 39 %). This result is consistent with a range of other data (i.e., n-alkane concentrations, ^{14}C data, $\delta^{13}C_{org}$ and $\delta^{15}N$ values) from the Pleistocene deposits in Piston Core JT96-09 (Chapter 2).

The relatively low $\delta^{15}N$ values measured for Pleistocene sediments in 06bc most probably reflect the presence of abundant terrestrial organic matter (>40 %). However, the significantly lower $\delta^{15}N$ values observed in 01mc, which contains <22 % terrestrial organic matter must have another explanation. Station 01 is located on the shelf and is thus directly influenced by newly upwelled, nitrate-rich water. When nitrate is abundant phytoplankton preferentially utilize ^{14}N-enriched nitrate, producing isotopically light organic matter and leaving isotopically heavier residual nitrate (Montoya, 1994 and references therein). As waters are advected away from the site of upwelling they become further ^{15}N-enriched due to continued biological activity and removal of ^{14}N in sinking organic detritus. Phytoplankton growing at sites increasingly more remote from the source of upwelled nutrients therefore

exhibit higher $\delta^{15}N$ signatures and the organic matter which eventually reaches the sediment is similarly enriched (e.g., Farrell et al., 1995; Martinez et al., 2000). This process most probably explains the low $\delta^{15}N$ values of shelf sediments (i.e., Core 01mc) and the higher $\delta^{15}N$ values exhibited by continental slope sediments off Vancouver Island. However, data from sediment traps moored on the upper slope off Vancouver Island indicate that $\delta^{15}N$ values of settling particulate organic matter (SPOM) ranges from +7.7 ‰ during bloom events in summer and fall up to +9.0 ‰ in winter, with an average annual flux-weighted value of +8.1 ‰ (Wu, et al., 1999). Surface sediments from the slope have lower values (+6.3 to +6.8 ‰) than this SPOM, possibly due to the input of minor terrestrial organic matter and/or the downslope transport of ^{14}N-enriched organic matter from the shelf.

4.4.2 Iodine and manganese

The Mn/Al ratios of all surface sediments are substantially lower than the average shale value (0.0106; Turekian and Wedepohl, 1961), even in 05bc which exhibits the thickest oxic surface layer. Low Mn concentrations indicate that within the upper 1 cm these sediments become sufficiently reducing to cause Mn(IV), present in oxyhydroxides, to be reduced to soluble Mn(II). Unfortunately, the sampling resolution does not permit the exact depth where Mn reduction begins to be determined.

It is well known that iodine species are adsorbed by marine organic matter at the sediment-water interface (Price and Calvert, 1977). Such adsorption occurs only under oxic conditions, where iodate (IO_3^-) is the principal dissolved species of iodine. Under suboxic conditions, where IO_3^- is reduced to I^-, no adsorption occurs, as I^- is not taken up by organic detritus. Therefore, sediments that accumulate in suboxic and anoxic settings are characterized by low I/C_{org} values (typically <20 x 10^4) while sediments in well oxygenated environments typically yield I/C_{org} values of >200 x 10^{-4} (Price and Calvert, 1977; Francois, 1987). Surface sediments in all cores from the Vancouver Island Margin, with the exception

of 01mc, are characterized by I/C_{org} ratios that exceed 200 x 10^{-4} (Fig. 4.5b). These data suggest that in general surface sediments in the area are sufficiently oxygenated to allow adsorption of iodine species onto organic matter. Iodine is then lost relative to carbon during the degradation of organic matter (Price and Calvert, 1973 and 1977; Francois, 1987) resulting in a commonly-observed decrease in I/C_{org} ratios with depth. However, in shelf Core 01mc I/C_{org} ratios are consistently low, even in surface sediments. Carbon-isotope data indicate that 01mc contains only slightly more terrestrial organic matter than the other cores. Therefore, the low I/C_{org} values of surface sediments in 01mc cannot be attributed to an abundance of terrigenous organic matter, which does not adsorb dissolved iodine species (Malcolm and Price, 1984). Rather, the low I/C_{org} ratios imply that, despite the presence of well-oxygenated bottom waters (> 2 ml/l O_2), surface sediments at station 01 are more reducing in comparison to the other stations. This may related to the relatively high organic carbon mass accumulation rate (~0.6 g/cm^2/kyr) at this site.

The combination of high I/C_{org} and low Mn/Al ratios in most cores indicates that the near-surface redox environment is perched within the suboxic zone, between Mn and I reduction. This is consistent with the lack of Re enrichment in the upper 10 to 15 cm (see Section 4.3). Reducing conditions appear to be more intense in Core 01mc; hence both Mn/Al and I/C_{org} ratios are low in the surface sediments.

4.4.3 Rhenium

Rhenium concentrations are low in oxic marine sediments ($\leq$ 0.5 ng/g; Boyko et al., 1986; Koide et al., 1986) but may be as much as 300 times higher in suboxic and anoxic deposits (Koide et al., 1986; Ravizza et al., 1991; Colodner et al., 1993; Crusius et al., 1996; Morford and Emerson, 1999). Enrichments of this magnitude are the result of Re diffusion from the overlying water into the sediment followed by its reduction from Re(VII) to Re(IV) under suboxic conditions and precipitation, possibly as ReO_2 (e.g., Crusius et al., 1996). In

general, significant enrichment occurs when porewater oxygen is consumed within 1 cm of the sediment-water interface (Morford and Emerson, 1999), and when sedimentation rates are low enough to allow Re to build-up in the deposits through ongoing diffusion and precipitation.

The concentration of Re in surface sediments from the Vancouver continental margin is only slightly elevated (1.6 to 4.2 ng/g) when compared to the typical concentrations in oxic sediments (≤ 0.5 ng/g). Thus, despite the development of suboxic conditions with 1 cm of the sediment-water interface, as indicated by the low Mn/Al ratios, there is no evidence of a large Re enrichment in the upper 10 to 15 cm of any of these cores. This implies that sedimentary redox conditions are not sufficiently reducing to cause Re reduction and precipitation at depths shallower than about 10 cm, which is consistent with I/C_{org} data. With the exception of Core 01mc, I/C_{org} ratios are relatively high, indicating that iodate persists in the uppermost porewater. According to Thomson et al. (1993) Re reduction should occur subsequent to I reduction. Thus, Re reduction and accumulation would not be anticipated in these near-surface sediments. However, below ~15 cm in cores 09mc, 02mc and 05bc Re is clearly enriched (Fig. 4.6). We hypothesize that this reflects ongoing Re diffusion to depths on the order of 20 cm and subsequent reduction and precipitation. Unfortunately, no porewater data are available to permit a direct assessment of this hypothesis. Instead, a simple steady-state linear-diffusion model is applied to determine whether or not the enrichments could reflect ongoing authigenesis. We use Fick's First Law,

$$J = (\Phi/F)D_b(dc/dz) \tag{4.3}$$

to compute the downward diffusion flux (J).

Simple calculations imply that Re diffusion and sub-surface precipitation is a dominant control on sedimentary Re profiles. The bulk in situ diffusivity (D_b) of the perrhenate ion is estimated to be similar to that of other oxyanions (i.e. ~ 6 x 10^{-6} cm^2 sec^{-1}; Li

and Gregory, 1974). The porosity (Φ) is assigned a value of 0.8, while the formation factor (F) is taken to be 1.3 (Manheim, 1970), a value typical of silty clays. The concentration gradient (dc/dz) is assumed to be linear and is computed as the quotient of the difference in concentration between bottom water (7.8 ng kg^{-1}; Anbar et al., 1992) and a precipitation point 20 cm below the sediment-water interface where the porewater Re content is assumed to be zero. This yields an estimated flux of 45 ng $cm^{-2}kyr^{-1}$. The mass accumulation rate (MAR) of the sediments in Core 09mc, computed as the product of the linear sedimentation rate (~5 cm/kyr) and the dry bulk density [(1- Φ) times the grain density of 2.5 g cm^{-3}], is 2.5 g $cm^{-2}kyr^{-1}$. The ratio of J/MAR represents the steady-state concentration of Re that could be added to the sediments via downward diffusion to a fixation depth of 20 cm, and in this example that equals ~18 ng/g. This is of the same order of magnitude as the observed Re concentration at 20 cm depth in 09mc (i.e., 22 ng/g). Application of the same calculation to Core 02mc which has a higher sedimentation rate (~23 cm/kyr) and a shallower precipitation point (10 cm) yields a steady-state Re enrichment of 9 ng/g which is also close to what is observed in the core. These admittedly crude and assumption-dependent results suggest that downward diffusion and sub-surface precipitation is indeed a credible mechanism for enriching Re in these deposits. However, the degree of enrichment is very sensitive to sedimentation rate. When redox boundaries are relatively deep, as they are in the Vancouver margin cores, large enrichments are only possible when sedimentation rates are low.

4.4.4. Uranium

In oxygenated seawater U(VI) occurs as the uranyl-carbonate complex $UO_2(CO_3)_3^{-4}$ (Langmuir, 1978). Under suboxic conditions U(VI) is reduced to U(IV) at approximately the same redox potential as Fe reduction (Langmuir, 1978; Cochran et al., 1986; Zheng, et al., 2002) or at a slightly lower potential (Klinkhammer and Palmer, 1991). Diffusion of uranium into sediments followed by its reduction and precipitation as UO_2 under suboxic and

anoxic conditions can lead to U enrichments in excess of 5 µg/g where sedimentation rates are relatively low (Thomson et al., 1990; Klinkhammer and Palmer, 1991; Legeleux et al., 1994; Crusius et al., 1996; Nath et al., 1997).

Uranium, like Re, is not significantly enriched in the upper 10 to 15 cm of the Vancouver Island margin sediments (i.e., <2 µg/g). An obvious authigenic accumulation (up to 5.8 µg/g) is only observed below a depth of 20 cm in 09mc. There is also a suggestion of U enrichment in Cores 02mc and 05bc, but because U has a much higher lithogenic background relative to the concentration of dissolved U in seawater the authigenic signal is more difficult to detect (Chapter 5). Site 09 is overlain by the most severely oxygen-depleted water, which should lead to more intense reducing conditions than at the other sites, all other factors being equal. In turn, this should lead to greater authigenic enrichment of redox-sensitive metals like Re and U, which is exactly what is observed.

4.4.5. Cadmium

Cadmium may be enriched by a few µg/g in suboxic sediments (Rosenthal et al., 1995b; van Geen et al., 1995; McCorkle and Klinkhammer, 1991) and is often highly enriched (>8 µg/g) in anoxic sediments (Pedersen et al., 1989; van Geen et al., 1995; Morford et al., 2001; Ivanochko, 2001). The most probable mechanism for such enrichment is the formation of CdS (Rosenthal et al., 1995a). Thus, although Cd is not directly affected by redox conditions, its enrichment does require the presence of at least trace amounts of dissolved sulphide (Pedersen et al., 1989; Rosenthal et al., 1995b; van Geen et al., 1995), which is related to the sedimentary redox state. Cadmium is supplied to reducing sediments by diffusion from the overlying water column and in sinking organic detritus. The organically-bound Cd is released into the porewater as organic matter degrades (McCorkle and Klinkhammer, 1991; Rosenthal et al., 1995b) and will be incorporated into the solid phase if dissolved sulphide is present. Unlike many other trace metals, the Cd concentration

in the upper water column can fluctuate rapidly when upwelling of nutrient-rich (i.e., Cd-rich) waters changes (van Geen and Husby, 1996; Sanudo-Wilhelmy and Flegal, 1996; Segovia-Zavala et al., 1998). It is therefore possible that sedimentary Cd concentrations could be coupled to changes in upwelling via the incorporation of Cd into organic matter and its subsequently exported to the sediment. Upwelling would also increase bottom water Cd concentrations and thus the diffusive flux into the sediments would also increase.

The concentration of Cd is low ($\leq$ 0.3 µg/g) in the weakly suboxic, near-surface sediments off Vancouver Island. This result is consistent with porewater data that indicate no discernible sulphate reduction in these sediments, with the possible exception of Core 01mc (A. Mucci, unpubl. data). However, there is a slight Cd enrichment in the lower portion of Cores 09mc, 02mc and 05bc which suggests that minor sulphate reduction may be occurring at depth. The enrichment is greatest in Core 09mc (up to 1 µg/g) which is consistent with Re and U data that imply stronger reducing conditions at this OMZ site.

4.4.6. Molybdenum

In oxic sediments Mo concentrations can be high (>60 µg/g) as a result of Mo adsorption onto Mn oxyhydroxides (Bertine and Turekian, 1973; Calvert and Price, 1977; Shimmield and Price, 1986), but under suboxic conditions oxyhydroxides dissolve and adsorbed Mo is released into the porewater. As a result, suboxic sediments contain only lithogenic concentrations of Mo (~0.6 µg/g for terrigenous sediments derived from Vancouver Island; Morford et al., 2001). In contrast, anoxic sediments contain as much as 130 µg/g Mo (Bertine and Turekian, 1973; Koide et al., 1986; Francois,1988; Emerson and Huested, 1991; Crusius et al., 1996; Adelson et al., 2001; Zheng et al., 2000a). Molybdenum enrichment is typically associated with the precipitation of Fe-sulphides (Bertine, 1972; Huerta-Diaz and Morse, 1992), but at low dissolved sulphide concentrations (<100 µM; Zheng et al., 2000b), it is not related to Mo reduction and precipitation of MoS_2. Rather,

molybdate diffuses into the sediment from the overlying water column and is converted to thiomolybdate (Bertine, 1972; Helz et al., 1996) which is rapidly adsorbed by Fe-bearing particles such as Fe-sulphides (Helz et al., 1996). The conversion of molybdate (MoO_4^{-2}) to thiomolybdate (MoS_4^{-2}) appears to occur at a threshold H_2S concentration of ~11 μM (Erickson and Helz, 2000), although Mo accumulation has been documented at sulphide concentrations as low as 0.1 μM (Zheng et al., 2000b).

The low Mo concentrations (<1.4 μg/g) observed in all box- and multicores suggest that, in those sediments sampled, fully anoxic conditions never develop (i.e., active sulphate reduction is limited) and the formation of Fe-sulphides is negligible. This interpretation is consistent with the lack of a large Cd enrichment and with porewater data that show little, if any, depletion of porewater sulphate (A. Mucci, unpubl. data). The only possible exception is Core 01mc where porewater data indicate the occurrence of minor sulphate reduction (A. Mucci, unpubl. data). This is also the core with the highest Mo content. The fact that anoxic conditions are not developed within the upper 50 cm, even in sediments underlying the OMZ, is unexpected given the relatively high organic carbon content of the deposits and low bottom water oxygen concentration, both of which should favour the early (i.e., shallow) onset of sulphate reduction. The dominance of suboxic, rather than anoxic, conditions in these sediments presumably reflects the moderately low rates of hemipelagic sedimentation and the relatively deep bioturbation as indicated by ^{210}Pb data.

4.4.7. Barium

Barium is found in a number of mineral phases within sediments. Lithogenic barium occurs primarily within aluminosilicates and in particular potassium feldspar where Ba substitutes for K. Barium also occurs as discrete barite particles that form within decaying organic material (Dehairs et al., 1980; Bishop, 1988; Ganeshram et al., 2003). This biogenic Ba is commonly enriched in sediments that underlie highly productive surface waters

(Dehairs et al., 1980; Dehairs et al., 1992), where the supply of organic particles is high (Dymond and Collier, 1996).

In general, sedimentary Ba concentrations and Ba/Al ratios increase with increasing water depth off Vancouver Island (Fig. 4.5c). A similar Ba-depth relationship has been observed in sediments off the coasts of Chile (Klump et al., 2000), Peru (von Breymann et al., 1992), Namibia (Calvert and Price, 1983) and California (McManus et al., 1999), and in the Arabian Sea (McManus et al., 1998; Schenau et al., 2001). Three possible explanations have been put forth to explain increasing Ba content with increasing water depth: i) better preservation, ii) decreasing dilution and/or sediment focusing, and iii) an increase in the amount of biogenic barite delivered to the sediment. Preservation of barite may be influenced by a number of factors. Sulphate reduction in anoxic sediments leads to undersaturation and dissolution of barite (von Breymann et al., 1992; Falkner et al., 1993; McManus et al., 1994), but this cannot explain the pattern of barite accumulation in Holocene sediments off Vancouver Island because there is no evidence that significant sulphate reduction is occurring in the upper 50 cm of these deposits. Dymond et al. (1992) suggested that barite preservation increases with increasing sedimentation rate because barite is more rapidly isolated from undersaturated bottom waters. Off Vancouver Island however, the core with the highest sedimentation rate (i.e., 01mc, 40 cm/kyr) has the lowest Ba/Al ratios while cores with relatively low sedimentation rates (i.e., 09mc and 05bc, 5 cm/kyr) exhibit much higher Ba/Al ratios. Thus, sedimentation rate does not appear to control barite preservation in the study area.

If the increase in Ba with depth is caused by decreasing dilution or sediment focusing we would also expect other elements to be similarly affected. The concentration of Zr and the Zr/Al ratio both decrease with increasing water depth suggesting sediments become finer-grained offshore, and there is an inverse correlation between Zr and total Ba concentrations (Fig. 4.8). Given this result it is tempting to attribute the changes in Ba concentration solely to changes in sediment grain size; however, this would be wrong. The concentration of
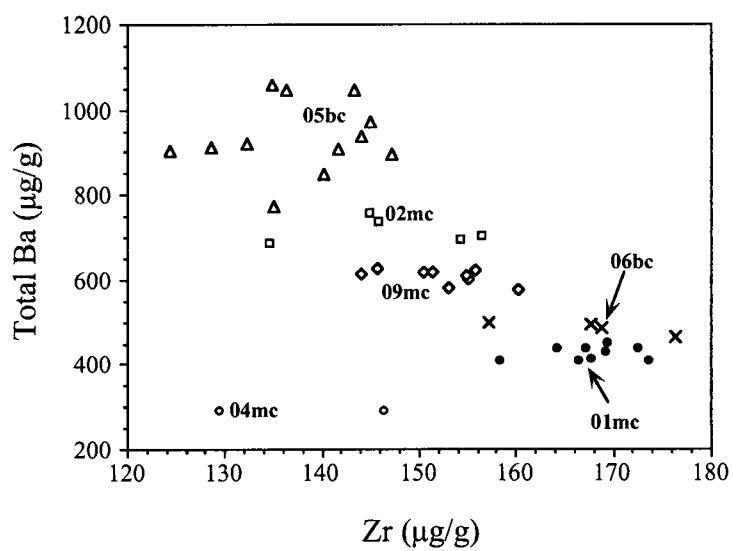
Fig. 4.8. Concentration of Zr versus the concentration of total Ba in near-surface sediments from the Vancouver Island margin.

lithogenic Ba (Ba_{lith}) was measured in a number of samples from which the biogenic fraction (Ba_{bio}) had been chemically extracted. The Ba_{bio} concentration was then estimated by difference ($Ba_{bio} = Ba_{tot} - Ba_{lith}$). The results show that the concentration of Ba_{bio} increases with water depth from ~96 ppm in 09mc up to 655 ppm in 05bc, while the Ba_{lith}/Al ratio remains relatively constant (0.0026 to 0.0038; Table 4.2). A large proportion of biogenic barite is formed in the upper water column where labile organic matter rapidly decays (Chan et al., 1977; Dehairs et al., 1980; Bishop, 1988; Dehairs et al., 1990). However, sediment trap data suggest that some biogenic barite also forms deeper in the water column as organic material settles (Dymond and Collier, 1996; Klump et al., 2000). Thus, we attribute the observed increase in Ba_{bio} (and Ba/Al ratios) with water depth to the continual formation of barite as organic material settles through the water column.

4.4.8. Silver

The concentration of Ag in oxic, marine sediments is low (70 to 100 ng/g; Bowen, 1966), and largely reflects the lattice-held fraction (i.e., lithogenic Ag). In comparison, Ag content in natural anoxic, marine sediments can be quite high (> 400 ng/g; Koide et al., 1986). This authigenic accumulation does not involve a change in the redox state of the metal. Rather, Ag readily precipitates as Ag_2S in the presence of trace amounts of dissolved sulphide because Ag_2S is highly insoluble (pK = 36; Dyrssen and Kremling, 1990). In this respect the sedimentary geochemistry of Ag is similar to that of Cd.

Dissolved Ag in seawater exhibits a "nutrient-type" depth profile (Martin et al., 1983; Flegal et al., 1995; Zhang et al., 2001) which is most similar to Si suggesting it is taken up by marine organisms and incorporated into their "hard parts" (Flegal et al., 1995; Zhang et al., 2001). Laboratory culture experiments show that Ag is actively incorporated into diatom frustules (Fisher and Wente, 1993; Lee and Fisher, 1994) and it is probable that some Ag is thus supplied to the sediments with the diatom flux (Friedl et al., 1997).

Cores 01mc, 04mc and 06bc contain background (i.e., lithogenic) concentrations of Ag ($\leq$ 100 ng/g) while cores 09mc, 02mc and 05bc are enriched in Ag (220 to 360 ng/g). The enrichments are not the result of in situ diagenesis under anoxic conditions. Iodine, Mn, Re and Mo data indicate that the upper 10 to 15 cm in these cores is only weakly suboxic, not reducing enough for Re and U precipitation, and certainly not anoxic. Furthermore, there is no correlation between Ag content and either opal or organic carbon contents (Figs. 4.9a and b, respectively) implying that the sedimentary Ag concentration is not directly related to these biogenic fluxes. Grain-size does seem to have some influence, as shown by the negative correlation between Ag concentrations and Zr/Al ratios (Fig. 4.9c). However, this would imply that the lithogenic fraction of the fine-grained sediments contains almost 600 ng/g of Ag which is 6x higher than the concentration typically observed (i.e., $\sim$ 100 ng/g; Bowen, 1966), so this correlation is probably deceptive. A more probable explanation for the very high Ag concentrations and the increase in Ag content with water depth is suggested by the very strong positive correlation between sedimentary Ag and biogenic Ba (r^2 = 0.89; Fig. 4.9d).

To our knowledge, this is the first report of a strong correlation between Ag and Ba concentrations in marine sediments and it is geochemically puzzling. The positive association suggests that Ag and Ba may be transported to the sediment in a similar manner. Barium enrichment of sinking organic detritus results from the formation of barite during settling. Recognizing that both dissolved Ba and Ag have similar overall distributions in the marine water column, the close correspondence between the two elements reported here implies that Ag is also scavenged from the water column by settling organic particles. Ag enrichment in these particles cannot be related to the substitution of Ag for Ba in barite since their ionic radii are dissimilar (1.29 and 1.49 Å, respectively) as is their valence. Nor can the correlation be the result of the precipitation of Ag sulphate, which is highly soluble. The leading candidate for Ag sequestration by sinking particles is the precipitation of a sulphide phase (e.g., Ag_2S), but this presents a paradox. The formation of barite and Ag_2S should be
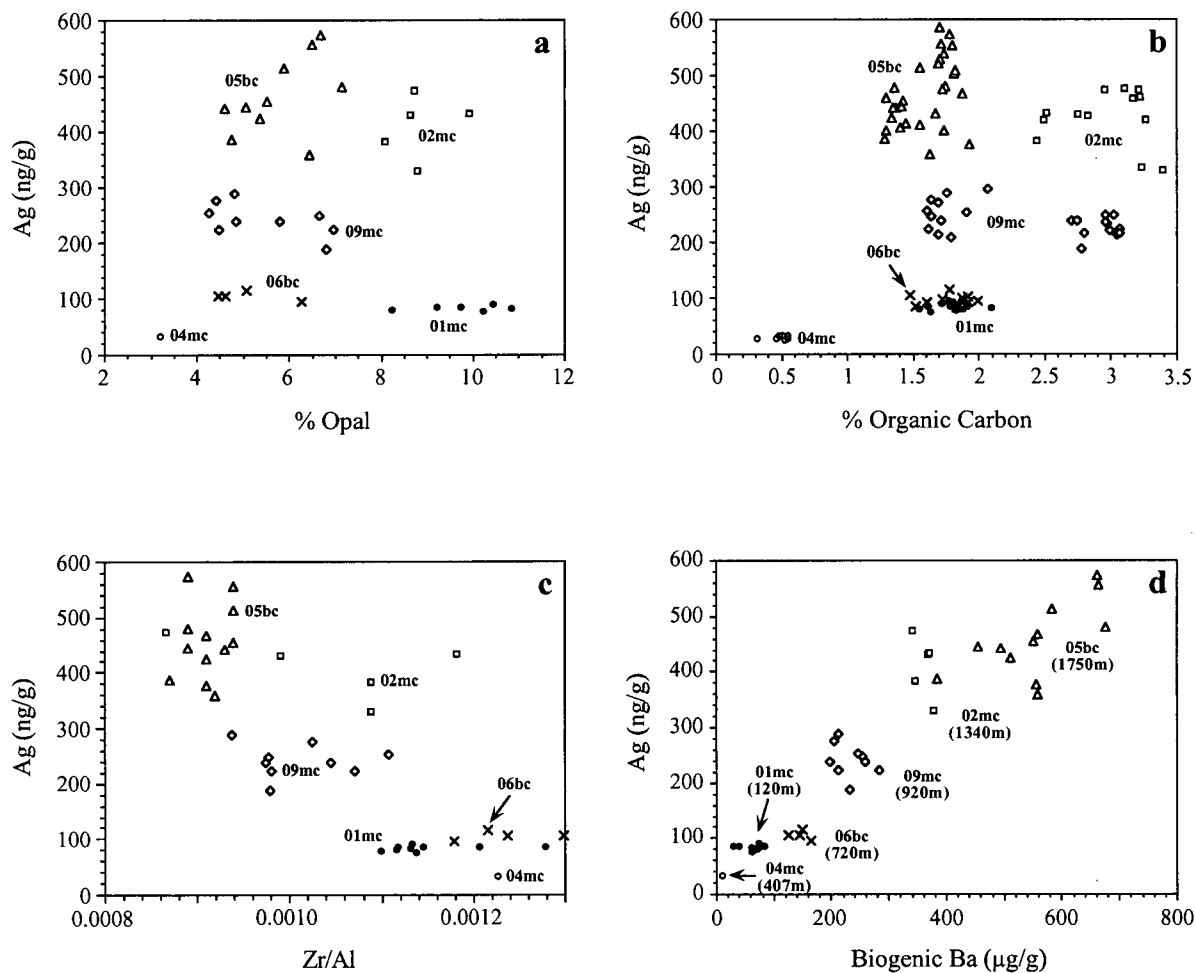
Fig. 4.9. Plots of Ag concentrations versus a) % opal, b) % organic carbon, c) Zr/Al ratios, and d) biogenic Ba content, in near-surface sediment cores. Note that there is a positive correlation between Ag and biogenic barium. A linear regression of these data yield the equation y = -22.22 + 1.1622x (r^2 = 0.89).

140

mutually exclusive since barite forms under oxic conditions and dissolves under anoxic conditions, while the precipitation of Ag_2S requires anoxia. We therefore tentatively hypothesize that within settling organic particles both oxic and anoxic microenvironments exist. Within the interior of sinking particles the degradation of organic matter could lead to the development of an anoxic microenvironment where sulphate reduction occurs and Ag_2S precipitates. Ag would be supplied from the water column and by opal dissolution. Surrounding the "anoxic core" the particle would remain oxic due to contact with the surrounding oxygenated seawater, and in this outer zone barite formation would occur. Although we have no direct evidence in support of this model, the higher concentration of Ag in sediments from deeper locations does imply that there is continual addition of Ag to particles as they settle. Confirmation or refutation of this hypothesis will require further work.

4.5 Summary

Despite the development of suboxic conditions within millimetres of the sediment-water interface there is little enrichment of redox-sensitive trace elements in the upper 10 to 15 cm of continental margin sediments off Vancouver Island. These results are consistent with minor element data that indicate near-surface sediments are poised within the suboxic zone. Below the depth of oxygen penetration (~10 to 15 cm) sediments do become sufficiently reducing to allow Re and U enrichment. This enrichment is greatest in Core 09mc, the only core collected from the OMZ, and reflects a lower sedimentation rate (5 cm/kyr) and low bottom water oxygen concentration at this location. There is no evidence that these sediments become fully anoxic (i.e., no Mo enrichment) despite productive surface waters and relatively low bottom water oxygen concentrations in the region. Suboxic conditions appear to be maintained because slow sedimentation and extensive bioturbation

allow a small, but continual, influx of oxygen and other oxidants from the overlying water column.

Silver concentrations in these continental margin deposits correlate closely with Ba/Al ratios and water depth. This is the first report of such an association and it presents a geochemical puzzle. The data imply that sedimentary Ag content is in large part controlled by the settling flux of particulate Ag and not exclusively by redox conditions within the sediment. We hypothesize that Ag, like Ba, may accumulate within organic particles as they settle through the water column. Thus, at a given location where water depth has been relatively invariant, sedimentary Ag concentrations may provide another palaeo-productivity proxy. However, at least two major questions need to be answered before such this occurs. First, the hypothesis that Ag precipitates as Ag_2S within anoxic microenvironments in setting organic particles must be explored, and second, the conditions under which this "biogenic" Ag is preserved need to be clarified.

4.6 References

Adelson, J.M., Helz, G.R., Miller, C.V., 2001. Reconstructing the rise of recent coastal anoxia; molybdenum in Chesapeake Bay sediments. Geochimica et Cosmochimica Acta 65, 237-252.

Anabar, A.D., Creaser, R.A., Papanastassiou, D.A., Wasserburg, G.J., 1992. Rhenium in seawater: Confirmation of generally conservative behavior. Geochimica et Cosmochimica Acta 56, 4099-4103.

Antoine, D., Andre, J.M., Morel, A., 1996. Oceanic primary production. 2. Estimation at global scale from satellite (coastal zone colour scanner) chlorophyll. Global Biogeochemical Cycles 10, 57-69.

Bertine, K.K., 1972. The deposition of molybdenum in anoxic waters. Marine Chemistry 1, 43-53.

Bertine, K.K., Turekian, K.K., 1973. Molybdenum in marine deposits. Geochimica et Cosmochimica Acta 37, 1415-1434.

Bishop, J.K.B., 1988. The barite-opal-organic carbon association in oceanic particulate matter. Nature 332, 341-343.

Bornhold, B.D., Yorath, C.J.,1984. Surficial geology of the continental shelf, northwestern Vancouver Island. Marine Geology 57, 89-112.

Bornhold, B.D., Barrie, J.V., 1991. Surficial sediments on the Western Canadian Continental Shelf. Continental Shelf Research 11, 685-699.

Bowen, H.J.M., 1966. Trace Metals in Biogeochemistry. Academic Press, New York.

Boyko, T.F., Baturin, G.N., Miller, A.D., 1986. Rhenium in recent ocean sediments. Geochemistry International 23, 38-47.

Calvert, S.E., 1976. The mineralogy and geochemistry of near-shore sediments. In: J.P. Riley, J.P., Chester, R. (Eds.), Chemical Oceanography, Vol. 6. Academic Press, London, 187-280pp.

Calvert, S.E., 1990. Geochemistry and origin of the Holocene sapropel in the Black Sea. In: Ittekkot, V., Kempe, S., Michaelis, W., Spitzy, A. (Eds.), Facets of Modern Biogeochemistry. Springer-Verlag, Berlin, 326-352pp.

Calvert, S.E., Price, N.B., 1977. Geochemical variations in ferromanganese nodules and associated sediments from the Pacific Ocean. Marine Chemistry 5, 43-74.

Calvert, S.E., Price, N.B., 1983. Geochemistry of Namibian shelf sediments. In: Suess, A., Thiede E. (Eds.), Coastal Upwelling. J. Plenum Publishing Corporation, 337-375pp.

Carpenter, R., Bennett, J.T., Peterson, M.L., 1981. [210]Pb activities in and fluxes to sediments of the Washington continental slope and shelf. Geochimica et Cosmochimica Acta 45, 1155-1172.

Chan, L.H., Drummond, D., Edmond, J.M., Grant, B., 1977. On the barium data from the Atlantic GEOSECS expedition. Deep Sea Research 24, 613-649.

Cochran, J.K., Carey, A.E., Sholkovitz, E.R., Surprenant, L.D., 1986. The geochemistry of uranium and thorium in coastal marine sediments and sediment pore water. Geochimica et Cosmochimica Acta 50, 663-680.

Colodner, D., Sachs, J., Ravizza, G., Turekian, K., Edmond, J., Boyle, E., 1993. The geochemical cycle of rhenium: A reconnaissance. Earth and Planetary Science Letters 117, 205-221.

Crusius, J., Calvert, S., Pedersen, T., Sage, D., 1996. Rhenium and molybdenum enrichments in sediments as indicators of oxic, suboxic and sulfidic conditions of deposition. Earth and Planetary Science Letters 145, 65-78.

Crusius, J., Pedersen, T.F., Calvert, S.E., Cowie, G.L., Oba, T., 1999. A 36kyr geochemical record from the Sea of Japan of organic matter flux variations and changes in intermediate water oxygen concentrations. Paleoceanography 14, 248-259.

Dean, W.E., Gardner, J.V., Piper, D.Z., 1997. Inorganic geochemical indicators of glacial-interglacial changes in productivity and anoxia on the California continental margin. Geochimica et Cosmochimica Acta 61, 4507-4518.

Dean, W.E., Piper, D.Z., Peterson, LC., 1999. Molybdenum acccumulation in Cariaco basin sediments over the past 24 k.y.: A record of water-column anoxia and climate. Geology 27, 507-210.

Dehairs, F., Chesselet, R., Jedwab, J., 1980. Discrete suspended particles of barite and the barium cycle in the open ocean. Earth and Planetary Science Letters 49, 528-550.

Dehairs, F., Goeyens, L., Stroobants, N., Bernard, P., Goyet, C., Poisson, A., Chesselet, R., 1990. On suspended barite and the oxygen minimum in the Southern Ocean. Global Biogeochemical Cycles 4, 85-102.

Dehairs, F., Baeyens, W., Goeyens, L., 1992. Accumulation of suspended barite at mesopelagic depths and export production in the Southern Ocean. Science 258, 1332-1335.

Dryssen, D. Kremling, K., 1990. Increasing hydrogen sulfide concentration and trace metal behaviour in the anoxic Baltic waters. Marine Chemistry 30, 193-204.

Dymond, J., Collier, R., 1996. Particulate barium fluxes and their relationships to biological productivity. Deep-Sea Research 43, 1283-1308.

Dymond, J., Suess, E., Lyle, M., 1992. Barium in deep-sea sediments: A geochemical proxy for paleoproductivity. Paleoceanography 7, 163-181.

Eakins, J.D., Morrison, R.T., 1978. A new procedure for the determination of lead-210 in lake and marine sediments. International Journal of Applied Radiation and Isotopes 29, 531-536.

Emerson, S.R., Huested, S.S., 1991. Ocean anoxia and the concentration of molybdenum and vanadium in seawater. Marine Chemistry 34, 177-196.

144

Erickson, B.E., Helz, G.R., 2000. Molybdenum(VI) speciation in sulfidic waters: Stability and lability of thiomolybdates. Geochimica et Cosmochimica Acta 64, 1149-1158.

Falkner, K.K., Klinkhammer, G.P., Bowers, T.S., Todd, J.F., Lewis, B.L., Landing, W.M., Edmond, J.M., 1993. The behavior of barium in anoxic marine waters. Geochimica et Cosmochimica Acta 57, 537-554.

Farrel, J.W., Pedersen, T.F., Calvert, S.E., Nielsen, B., 1995. Glacial-interglacial changes in nutrient utilization in the equatorial Pacific Ocean. Nature 377, 514-517.

Fisher, N.S., Wente, M., 1993. The release of trace elements by dying marine phytoplankton. Deep-Sea Research 40, 671-694.

Flegal, A.R., Sanudo-Wilhelmy, S.A., Scelfo, G.M., 1995. Silver in the eastern Atlantic Ocean. Marine Chemistry 49, 315-320.

Francois, R., 1987. The influence of humic substances on the geochemistry of iodine in nearshore and hemipelagic marine sediments. Geochimica et Cosmochimica Acta 51, 2417-2427.

Francois, R., 1988. A study on the regulation of the concentrations of some trace metals (Rb, Sr, Zn, Pb, Cu, V, Cr, Ni, Mn and Mo) in Saanich Inlet sediments, British Columbia, Canada. Marine Geology 83, 285-308.

Friedl, G., Pedersen, T.F., 1997. Relative enrichment of silver in marine sediments as a reflection of high paleoproductivity. Abstract, American Geophysical Union Fall Meeting, San Francisco.

Ganeshram, R.S., 1996. On the glacial-interglacial variability of upwelling, carbon burial and denitrification on the northwestern Mexican continental margin. Ph.D. dissertation thesis, University of British Columbia.

Ganeshram, R.S., Francois, R., Commeau, J., Brown-Leger, S.L.. 2003. An experimental investigation of barite formation in seawater. Geochimica et Cosmochimica Acta 67; 2599-2605.

Gobeil, C., Sundby, B., Macdonald, R.W., Smith, J.N., 2001. Recent change in organic carbon flux to Arctic Ocean deep basins: Evidence from acid volatile sulfide, manganese and rhenium discord in sediments. Geophysical Research Letters 28 , 1743-1746.

Helz, G.R., Miller, C.V., Charnock, J.M., Mosselmans, J.F.W., Pattrick, R.A.D., Garner, C.D., Vaughan, D.J., 1996. Mechanism of molybdenum removal from the sea and its concentration in black shales: EXAFS evidence. Geochimica et Cosmochimica Acta 60, 3631-3642.

Hickey, B.M., 1998. Coastal oceanography of Western North America from the tip of Baja California to Vancouver Island. In: Robinson, A.R., Brink, K.H. (Eds.), The Sea, Vol. 11, pp. 345-393.

Huerta-Diaz, M.A., Morse, J.W., 1992. Pyritization of trace metals in anoxic sediments. Geochimica et Cosmochimica Acta 56, 2681-2702.

Ivanochko, T.S., 2001. Productivity influences on oxygenation of the Santa Barbara Basin, California during the Late Quaternary. M.Sc. Thesis, The University of British Columbia, 133pp.

Klinkhammer, G.P., Palmer, M.R., 1991. Uranium in the oceans: Where it goes and why. Geochimica et Cosmochimica Acta 55, 1799-1806.

Klump, J., Hebbeln, D., Wefer, G., 2000. The impact of sediment provenance on barium-based productivity estimates. Marine Geology 169, 259-271.

Koide, M., Hodge, V.F., Yang, J.S., Stallard, M., Goldberg, E.G., Calhoun, J., Bertine, K.K., 1986. Some comparative marine chemistries of rhenium, gold, silver and molybdenum. Applied Geochemistry 1, 705-714.

Langmuir, D., 1978. Uranium solution-mineral equilibria at low temperatures with applications to sedimentary ore deposits. Geochimica et Cosmochimica Acta 42, 547-569.

Lee, B., Fisher, N., 1994. Effects of sinking and zooplankton grazing on the release of elements from planktonic debris. Marine Ecology Progress Series 110, 271-281.

Legeleux, F., Reyss, J.-L., Bonte, P., Organo, C., 1994. Concomitant enrichments of uranium, molybdenum and arsenic in suboxic continental margin sediments. Oceanologica Acta 17, 417-430.

Li, Y.-H., Gregory, S., 1974. Diffusion of ions in sea water and deep-sea sediments. Geochimica et Cosmochimica Acta 38, 703-714.

Mackas, D.L., Denman, K.L., Bennett, A.F., 1987. Least squares multiple tracer analysis of water mass coomposition. Journal of Geophysical Research 31, 2907-2918.

Malcolm, S.J., Price, N.B., 1984. The behaviour of iodine and bromine in estuarine surface sediments. Marine Chemisty 15, 263-271.

Manheim, F.T., 1970. The diffusion of ions in unconsolidated sediments. Earth and Planetary Science Letters 9, 307-309.

Martin, J.H., Knauer, G.A., Gordon, R.M., 1983. Silver distributions and fluxes in north-east Pacific waters. Nature 305, 306-309.

Martinez, P., Bertrand, P., Calvert, S.E., Pedersen, T.F., Shimmield, G.B., Lallier-Verges, E., Fontugne, M.R., 2000. Spatial variations in nutrient utilization, production and diagenesis in the sediments of a coastal upwelling regime (NW Africa): Implications for the paleoceanographic record. Journal of Marine Research 58, 809-835.

McCorkle, D.C., Klinkhammer, G.P., 1991. Porewater cadmium geochemistry and the porewater cadmium:δ^{13}C relationship. Geochimica et Cosmochimica Acta 55, 161-168.

McManus, J., Berelson, W.M., Klinkhammer, G.P., Kilgore, T.E., Hammond, D.E., 1994. Remobilization of barium in continental margin sediments. Geochimica et Cosmochimica Acta 58, 4899-4907.

McManus, J., Berelson, W.M., Klinkhammer, G.P., Johnson, K.S., Coale, K.H., Anderson, R.F., Kumar, N., Burdige, D.J., Hammond, D.E., Brumsack, H.J., McCorkle, D.C., Rushdi,

A., 1998. Geochemistry of barium in marine sediments: Implications for its use as a paleoproxy. Geochimica et Cosmochimica Acta 62, 3453-3473.

McManus, J., Berelson, W.M., Hammond, D.E., Klinkhammer, G.P., 1999. Barium cycling in the North Pacific: Implications for the utility of Ba as a paleoproductivity and paleoalkalinity proxy. Paleoceanography 14, 53-61

Morford, J.L., Emerson, S., 1999. The geochemistry of redox sensitive trace metals in sediments. Geochimica et Cosmochimica Acta 63, 1735-1750.

Morford, J.L., Russell, A.D., Emerson, S., 2001. Trace metal evidence for changes in the redox environment associated with the transition from terrigenous clay to diatomaceous sediment, Saanich Inlet, B.C.. Marine Geology 174, 355-369.

Mortlock, R.A., Froelich, P.N., 1989. A simple method for the rapid determination of biogenic opal in pelagic marine sediments. Deep Sea Research 36, 1415-1426.

Montoya, J.P., 1994. Nitrogen-isotope fractionation in the modern ocean: Implications for the sedimentary record. In: Zahn, R., Pedersen, T.F., Kaminski, M.A., Labeyrie, L. (Eds.), Carbon Cycling in the Glacial Ocean: Constraints on the Ocean's Role in Global Change, NATO ASI Series, Vol. 117, Springer-Verlag, Berlin, 259-279pp.

Nameroff, T.J., Balistrieri, L.S., Murray, J.W., 2002. Suboxic trace metal geochemistry in the eastern tropical North Pacific. Geochimica et Cosmochimica Acta 66, 1139-1158.

Nath, B.N., Bau, M., Rao, B.R., Rao, C.M., 1997. Trace and rare earth elemental variation in Arabian Sea sediments through a transect across the oxygen minimum zone. Geochimica et Cosmochimica Acta 61, 2375-2388.

Pailler, D., Bard, E., Rostek, F., Zheng, Y., Mortlock, R., van Geen, A., 2002. Burial of redox-sensitive metals and organic matter in the equatorial Indian Ocean linked to precession. Geochimica et Cosmochimica Acta 66, 849-865.

Pedersen, T.F., Waters, R.D., MacDonald, R.W., 1989. On the natural enrichment of cadmium and molybdenum in the sediments of Ucluelet Inlet, British Columbia. The Science of the Total Environment 79, 125-139.

Piper, D.Z., Isaacs, C.M., 1995. Minor elements in Quaternary sediment from the Sea of Japan: A record of surface-water productivity and interemediate-water redox conditions. Geological Society of America Bulletin 107, 54-67.

Price, N.B., Calvert, S.E., 1973. The geochemistry of iodine in oxidized and reduced recent marine sediments. Geochimica et Cosmochimica Acta 37, 2149-2158.

Price, N.B., Calvert, S.E., 1977. The contrasting geochemical behaviours of iodine and bromine in recent sediments from the Namibian shelf. Geochimica et Cosmochimica Acta 41, 1769-1775.

Ravizza, G., Turekian, K.K., Hay, B.J., 1991. The geochemistry of rhenium and osmium in recent sediments from the Black Sea. Geochimica et Cosmochimica Acta 55, 3741-3752.

Rosenthal, Y., Boyle, E.A., Labeyrie, L., Oppo, D.,1995a. Glacial enrichments of authigenic Cd and U in subantarctic sediments: A climatic control on the elements oceanic budget? Paleoceanography 10, 395-413.

147

Rosenthal, Y., Lam, P., Boyle, E.A., Thomson, J., 1995b. Authigenic cadmium enrichments in suboxic sediments: Precipitation and postdepositional mobility. Earth and Planetary Science Letters 132, 99-111.

Sanudo-Wilhelmy, S.A., Flegal, A.R., 1996. Trace metal concentrations in the surf zone and coastal waters off Baja California, Mexico. Environmental Science and Technology 30, 1575-1580.

Schenau, S.J., Prins, M.A., De Lange, G.J., Monnin, C., 2001. Barium accumulation in the Arabian Sea: Controls on barite preservation in marine sediments. Geochimica et Cosmochimica Acta 65, 1545-1556.

Segovia-Zavala, J.A., Delgadillo-Hinojosa, F., Alvarez-Borrego, S., 1998. Cadmium in the coastal upwelling area adjacent to the California-Mexico Border. Estuarine, Coastal and Shelf Science 46, 475-481.

Shimmield, G.B., Price, N.B., 1986. The behaviour of molybdenum and manganese during early sediment diagenesis - offshore Baja California, Mexico. Marine Chemistry 19, 261-280.

Stuiver, M., Reimer, P.J., Bard, E., Beck, J.W., Burr, G.S., Hughen, K.A., Kromer, B., McCormac, G., Van Der Plicht, J., Spurk, M., 1998. INTCAL98 radiocarbon age calibration, 24,000-0 cal BP. Radiocarbon 40, 1041-1083.

Taylor, R.S., McLennan, S.M., 1985. The Continental Crust: Its Composition and Evolution. Blackwell Scientific, Boston, 312pp.

Thomson, J., Wallace, H.E., Colley, S., Toole, J., 1990. Authigenic uranium in Atlantic sediments of the last glacial stage - a diagenetic phenomenon. Earth and Planetary Science Letters 98, 222-232.

Thomson, J., Higgs, N.C., Croudace, I.W., Colley, S., Hydes, D.J., 1993. Redox zonation of elements at an oxic-post-oxic boundary in deep-sea sediments. Geochimica et Cosmochimica Acta 57, 579-595.

Thomson, R.E., 1981. Oceanography of the British Columbia Coast. Canadian Special Publication of Fisheries and Aquatic Sciences 56, 291p.

Turekian, K.K., Wedepohl, K.H., 1961. Distribution of the elements in some major units of the earth's crust. Geological Society of America Bulletin 72, 175-192.

van Geen, A., McCorkle, D.C., Klinkhammer, G.P., 1995. Sensitivity of the phosphate-cadmium-carbon isotope relation in the ocean to cadmium removal by suboxic sediments. Paleoceanography 10, 159-169.

van Geen, A., Husby, D.M., 1996. Cadmium in the California Current system: Tracer of past and present upwelling. Journal of Geophysical Research 101, 3489-3507.

von Breymann, M.T., Emeis, K.-C., Suess, E., 1992. Water depth and diagenetic constraints on the use of barium as a palaeoproductivity indicator. In: Summerhayes, C.P., Prell, W.L., Emeis, K.C. (Eds.), Upwelling Systems: Evolution Since the Early Miocene. Geological Society Special Publication 64, 273-284pp.

Wu, J., Calvert, S.E., Wong, C.S., 1999. Carbon and nitrogen isotope ratios in sedimenting particulate organic matter at an upwelling site off Vancouver Island. Estuarine, Coastal and Shelf Science 48, 193-203.

Yang, Y.-L., Elderfield, H., Pedersen, T.F., Ivanovich, M., 1995. Geochemical record of the Panama Basin during the last glacial maximum carbon event shows that the glacial ocean was not suboxic. Geology 23, 1115-1118.

Yarincik, K.M., Murray, R.W., Lyons, T.W., Peterson, L.C., Haug, G.H., 2000. Oxygenation history of bottom waters in the Cariaco Basin, Venezuela, over the past 578,000 years: Results from redox-sensitive metals (Mo, V, Mn, and Fe). Paleoceanography 15, 593-604.

Yorath, C.J., Nasmith, H.W., 1995. The Geology of Southern Vancouver Island. Orca Book Publishers, Victoria, Canada, 172pp.

Zhang, Y., Amakawa, H., Nozaki, Y., 2001. Oceanic profiles of dissolved silver: Precise measurements in the basins of western North Pacific, Sea of Okhotsk, and the Japan Sea. Marine Chemistry 75, 151-163.

Zheng, Y., Anderson, R.F., van Geen, A., Kuwabara, J., 2000b. Authigenic molybdenum formation in marine sediments: A link to pore water sulfide in the Santa Barbara Basin. Geochimica et Cosmochimica Acta 64, 4165-4178.

Zheng, Y., van Geen, A., Anderson, R.F., 2000a. Intensification of the northeast Pacific oxygen minimum zone during the Bolling-Allerod warm period. Paleoceanography 15, 528-536.

Zheng, Y., Anderson, R.F., van Geen, A., Fleisher, M.Q., 2002. Remobilization of authigenic uranium in marine sediments by bioturbation. Geochimica et Cosmochimica Acta 66, 1759-1772.

5. Geochemical Response to Pulsed Sedimentation on the Western Canadian Continental Margin: Implications for the Use of Mo as a Palaeo-oxygenation Proxy

5.1 Introduction

It has become common practice to use the concentrations of certain metals (e.g., Mo and Re) as palaeo-proxies for sedimentary redox conditions. From such data temporal changes in organic carbon flux to the sediment and bottom water oxygen concentrations, both of which play a large role in sedimentary redox conditions, are inferred (e.g., Dean et al., 1997 and 1999; Zheng et al., 2000; Adelson et al., 2001). However, other factors such as sedimentation rate, sediment composition, metal source and post-depositional remobilization can also influence metal accumulation.

Reducing sediments are typically characterized by high concentrations of authigenic Re, U, Mo, Cd and Ag (e.g., Koide et al., 1986; Francois, 1988; Calvert, 1990; Calvert and Pedersen, 1993; Crusius et al., 1996; Morford et al., 2001; Nameroff, 2002). However, the redox conditions under which these metals accumulate and the manner in which they are fixed within the sediment differ. Rhenium and U typically are enriched in suboxic sediments (up to 150 ng/g and >5 µg/g, respectively) as a direct result of reduction and precipitation (Crusius et al., 1996). In contrast, Ag and Cd each have a single redox state but form insoluble sulphides when trace amounts of H_2S are available (Koide et al., 1986; Rosenthal et al., 1995). This can lead to minor Ag and Cd accumulation in suboxic sediments and large accumulations in anoxic sediments (often >400 ng/g Ag and >8 µg/g Cd). Recent experimental results suggest that Mo enrichment is due to the formation of thiomolybdate that is rapidly adsorbed by Fe-bearing particles such as Fe-sulphides (Helz et al., 1996). Thiomolybdate formation requires a threshold H_2S concentration of ~11 µM (Erickson and Helz, 2000) and thus Mo enrichment, often in excess of 10 µg/g, is restricted to anoxic sediments in which sulphate reduction has occurred.

In this paper we examine the distribution of redox-sensitive trace metals in Piston Core JT96-02, collected from a water depth of 1340 m off the west coast of Vancouver Island, Canada (49°12.8'N, 127°18.6'W; Fig. 5.1). The upper 16 cm of the core is composed of an olive green mud typical of Holocene deposits on the mid to lower continental slope in this area. This mud is underlain by 18 cm of greenish gray clay and a 56 cm thick zone of interbedded clays and sands with erosional contacts and loading features typical of turbidite deposits. The remainder of the core (90 to 211 cm) is a gray clay that upon opening of the core contained numerous thin (1 to 2 cm) black layers spaced ~5 to 10 cm apart and characterized by sharp upper surfaces and gradational lower boundaries. These black layers faded within hours, indicating that they were composed of FeS that was rapidly oxidized on exposure to air. Two AMS radiocarbon dates of a mixed assemblage of planktonic foraminifera (*N. pachyderma* and *G. bulloides*) were obtained for the gray clay (13,280 ± 60 and 14,240 ± 60 ^{14}C yrs from 102 and 202 cm, respectively). At this time the Cordilleran ice sheet, which had reached it maximum extent in southern British Columbia between 15,000 and 14,000 ^{14}C yrs, was rapidly retreating (Clague and James, 2002). The continental shelf west of Vancouver Island was deglaciated by ~ 13,000 ^{14}C yrs (Blaise et al., 1990; Josenhans et al., 1995).

The objectives of this study are: i) to explore the character of deglacial sedimentation on the Vancouver Island Margin; ii) to determine why the sulphide-rich layers formed; and iii) to understand better the controls on the accumulation of Mo and other redox-sensitive metals in continental margin sediments. To this end, a 16 cm interval containing three sulphide layers was sampled every 3 mm for high resolution geochemical analysis. Total carbon (C_{tot}), nitrogen (N_{tot}) and sulphur (S_{tot}) were measured by high temperature combustion using a Carlo Erba NA-1500 CNS elemental analyzer. The relative standard deviation (RSD, 1σ) is 3 %, 5 % and 6 % for C, N and S, respectively and the accuracy is within 7 % of the recommended values for all three elements. Carbonate carbon (C_{carb}) was determined by coulometry (RSD = 1 %). Percent organic carbon (C_{org}) was calculated by
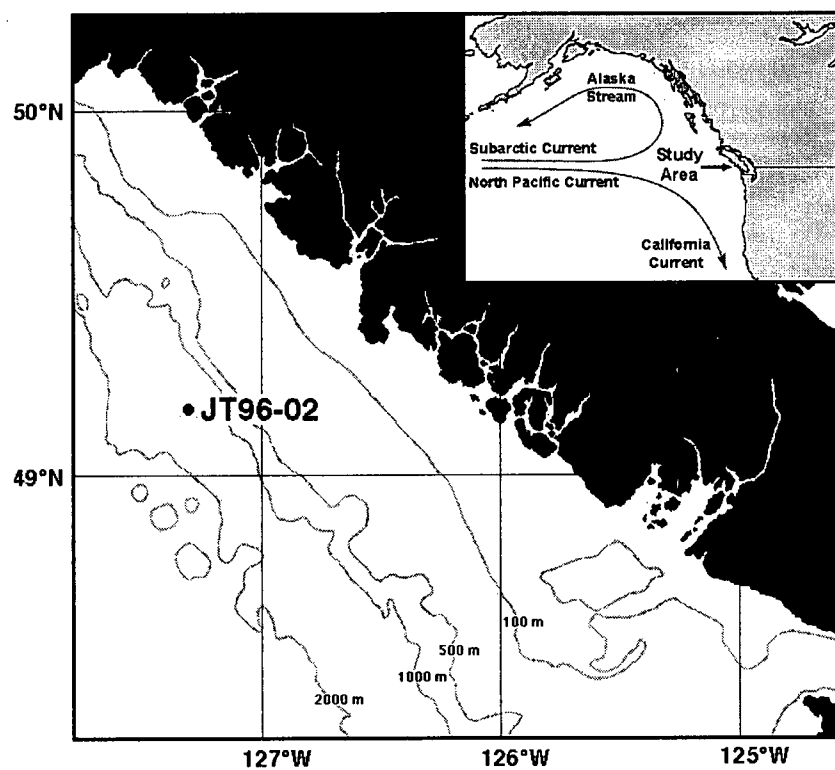
Fig. 5.1. The study area is located off the west coast of Vancouver Island, British Columbia, Canada (Inset). Piston Core JT96-02 was collected from the continental slope at a water depth of 1340 m.

difference ($C_{org} = C_{tot} - C_{carb}$) and has a RSD of ~4 %. The isotopic composition of organic matter ($\delta^{13}C_{org}$ and $\delta^{15}N$) was determined by continuous-flow mass spectrometry. Samples for $\delta^{13}C_{org}$ analysis were first decarbonated with 10% HCl and dried at 50°C overnight. Samples for $\delta^{15}N$ analysis were not pretreated. The reproducibility for isotopic data is ±0.1 ‰ for carbon and ±0.2 ‰ for nitrogen. Major and minor element concentrations were determined by X-ray fluorescence and have relative standard deviations of 5 % and 15 %, respectively. Following the standard practice these data are presented as element/Al ratios rather than concentrations, thus minimizing variability due to changes in dilution by non-lithogenic components such as organic matter and biogenic carbonate. The concentrations of Mo, Re, Ag, Cd and U were measured by isotope-dilution, inductively-coupled plasma mass spectrometry following the method described in Ivanochko (2001). The RSD is generally better than 10 % for all trace metals and the accuracy, measured for the National Research Council of Canada sediment standard MESS-1, is 8 % or better for Re, Mo and U, and ~14 % for Cd. The accuracy for Ag could not be evaluated as there is no accepted Ag value for MESS-1 at present.

5.2 Geochemical variations

The sulphide layers contain higher total sulphur (S_{tot}) and higher organic carbon (C_{org}) than intervening sediments. The concentration of S_{tot} within the sulphide layers ranges from 0.11 to 0.59 wt.% (avg. 0.25 wt.%) while the intervening sediment contains < 0.1 wt.% (Fig. 5.2a). The C_{org} content of the sulphide layers averages 0.49 wt.%, almost double the concentration in the clay (Fig. 5.2a). There is also a positive correlation between S_{tot} and C_{org} ($r^2 = 0.64$). The carbonate content is slightly higher within the sulphide layers (3.97 versus 3.26 wt.%) and progressively decreases upward before rising sharply at the base of the next sulphide layer (Fig. 5.2b). The $\delta^{13}C_{org}$ values are up to 1.7 ‰ higher within the sulphide layers (-23.4 vs -25.1 ‰; Fig. 5.2c) as are $\delta^{15}N$ values (+5.8 vs +4.3 ‰; Fig. 5.2c). The

combination of higher $\delta^{13}C_{org}$ and higher $\delta^{15}N$ values suggests the presence of slightly more marine organic matter within the sulphide-rich layers.

The ratios of Si/Al, Zr/Al and Ti/Al are highest immediately overlying each sulphide layer and then decrease upwards (Fig. 5.3). The lowest ratios are observed within and just below the sulphide layers (Fig. 5.3). Relatively high Si/Al, Zr/Al and Ti/Al ratios suggest higher concentrations of quartz, zircon and titanium-bearing minerals which typically occur in coarser-grained sediments (Calvert, 1976). These data therefore indicate that an abrupt increase in grain-size occurs immediately above each sulphide layer and the deposits then fine upward, characteristics that suggest the presence of thin turbidites overlying the sulphide layers.

Trace metal data, both as concentrations and metal/Al ratios, are plotted in Figure 5.4. Sulphide layers are significantly enriched in Mo (>2 µg/g) in comparison to the intervening sediments which contain only lithogenic amounts (Fig. 5.4a), and there is a strong positive correlation between Mo and S_{tot} concentrations ($r^2 = 0.77$; Fig. 5.5). Rhenium, and to a lesser extent Ag, are also enriched within the sulphide layers (Figs. 5.4b and c), but there is no correlation with S_{tot} content ($r^2 = 0.26$ and 0.41, Re and Ag respectively). Cadmium and U are present in lithogenic concentrations only, and there are no consistent downcore variations (Figs. 5.4d and e).

5.3 Origin of the sulphide layers

The occurrence of sharp peaks in metal concentrations, such as those for Mo in Core JT96-02pc, are often interpreted as evidence of metal remobilization due to the influx of oxygen (i.e., burndown) and subsequent reprecipitation in underlying reduced sediments (Colley et al., 1984; Colodner et al., 1992; Thomson et al., 1993; Rosenthal et al., 1995; Thomson et al., 1995; Crusius and Thomson, 2000a and b). These studies have shown that, given time, certain solid-phase metals can be remobilized when exposed to oxidants (i.e.,

5.2a)   **5.2b)**   **5.2c)**

Total Sulphur (wt. %)   Carbonate (wt. %) $\delta^{13}C_{org}$ (‰ vs VPDB)
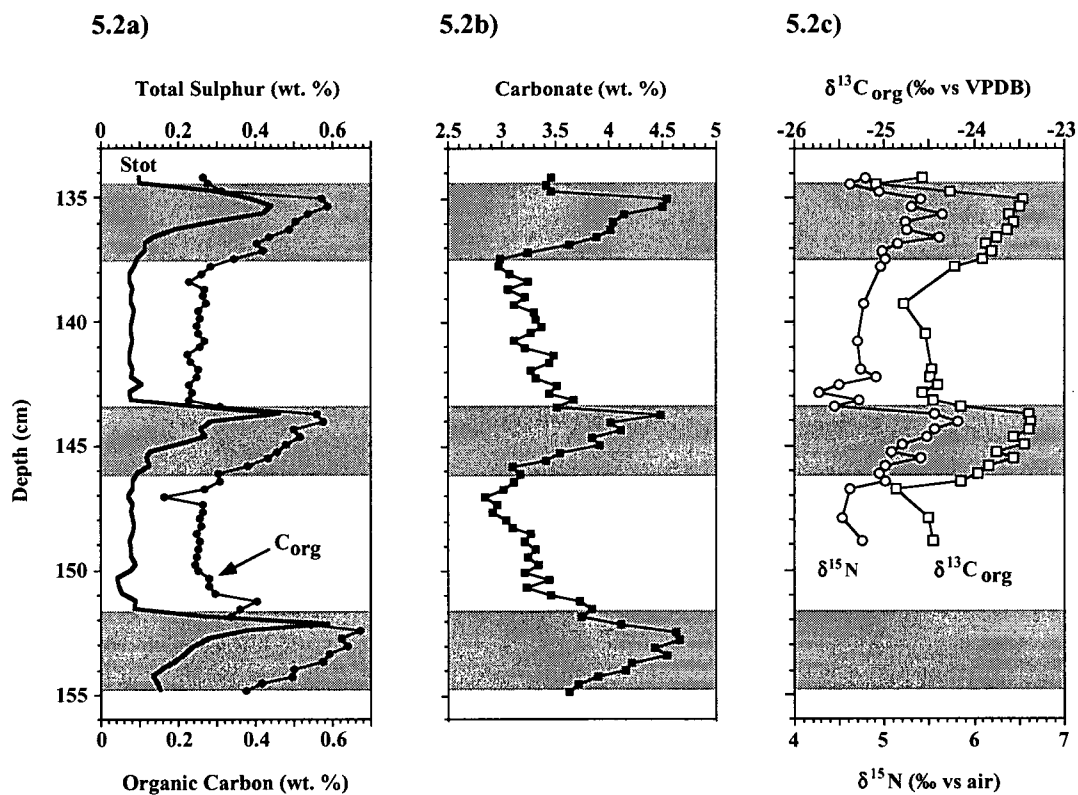
Fig. 5.2. Downcore profiles of a) total sulphur (S_{tot}) and organic carbon (C_{org}) contents, b) carbonate content, and c) $\delta^{13}C_{org}$ and $\delta^{15}N$ values. Shaded zones indicate the location of sulphide layers. The errors (as RSD) are 6 %, 4 % and 1 % for S_{tot}, C_{org} and carbonate respectively. The C- and N- isotopic data have errors of ±0.1 ‰ and ±0.2 ‰ respectively.

5.3a)

5.3b)
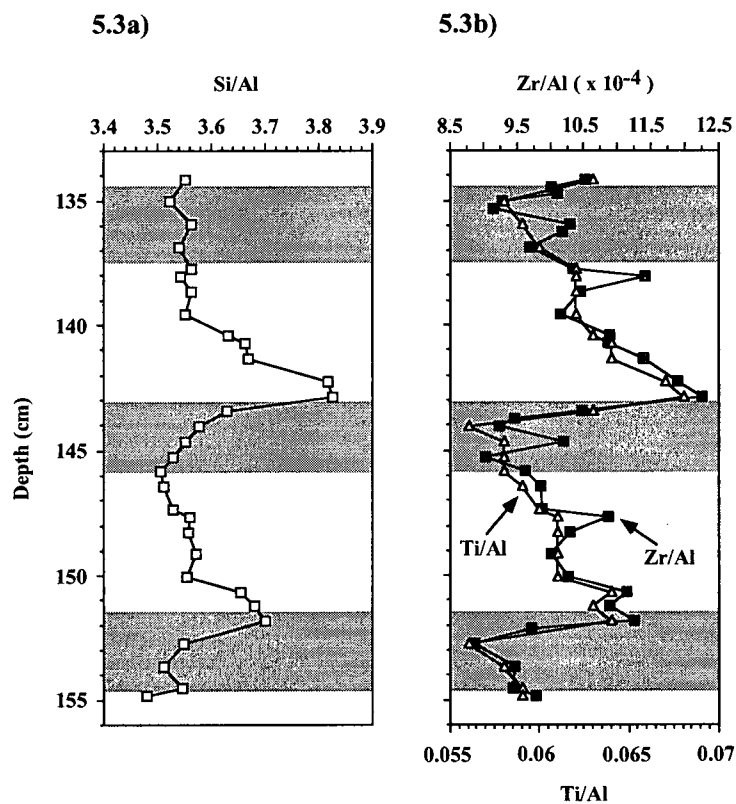
Fig. 5.3. Downcore profiles of the a) Si/Al ratio (RSD = 6 %) and b) Zr/Al and Ti/Al ratios (RSD = 17 % for both ratios). Shaded areas indicate the location of sulphide layers.

156

Fig. 5.4. a to e) Downcore profiles of trace metal concentrations (symbols) and metal/Al ratios (thick black lines). Shaded areas indicate the location of sulphide layers. Background (i.e., lithogenic) concentrations of the various metals are marked by the dashed lines (see Table 5.1 for references). f) Downcore profile of the sedimentary Re/Mo ratio. The dashed line represents both the Re/Mo ratio of seawater and the estimated lithogenic Re/Mo ratio. The precision (as RSD) for all trace metal data is 10 % or better (i.e., at most 2x the symbol size). The detection limits are as follows: 0.5 ppm for Mo, <1 ppb for Re, 57 ppb for Ag, 0.1 ppm for Cd and 0.04 ppm for U.

5.4a)

Molybdenum
(μg/g; open circles)

Mo/Al (x10^{-4})

5.4b)

Rhenium
(ng/g; open squares)

Re/Al (x10^{-7})

5.4c)

Silver
(ng/g; open diamonds)

Ag/Al (x10^{-7})

5.4d)

Cadmium
(μg/g; open triangles)

Cd/Al (x10^{-4})

5.4e)

Uranium
(μg/g; crosses)

U/Al (x10^{-4})

5.4f)

Re/Mo (ng/μg)
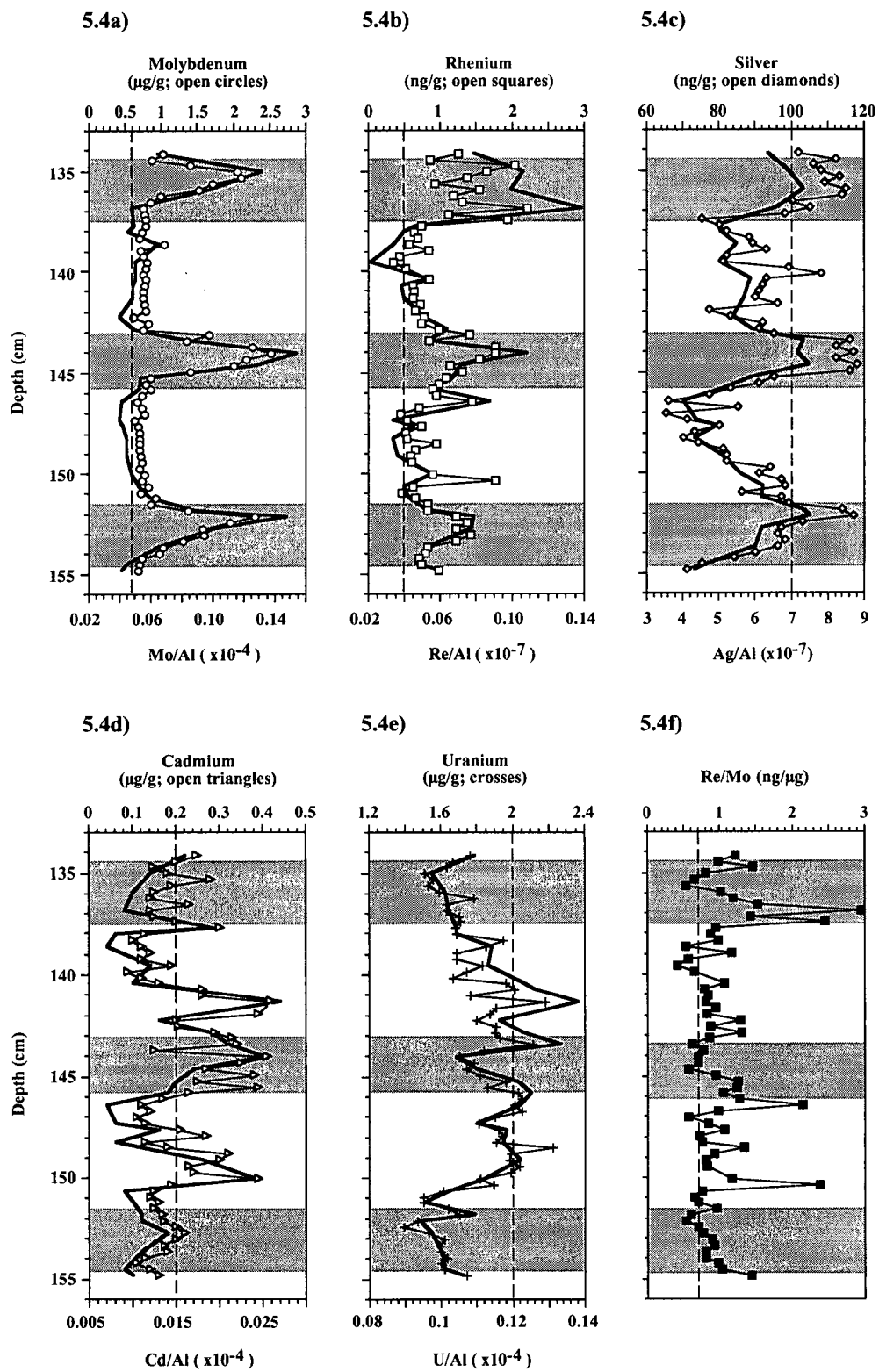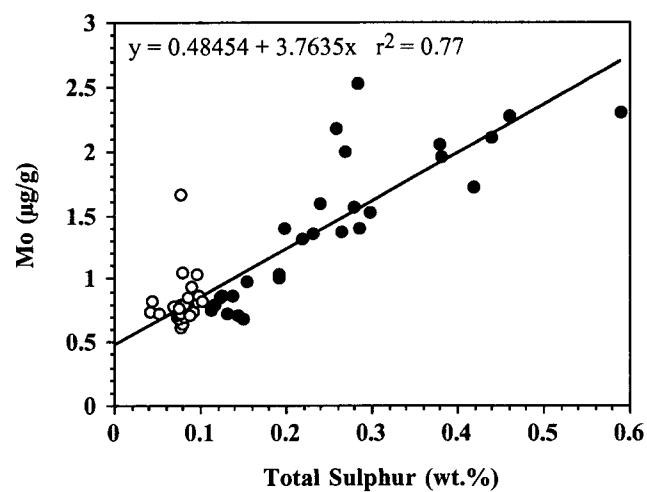
Fig. 5.5. Plot of Mo concentration versus total sulphur content
in the sulphide layers (solid circles) and the intervening sediments
(open circles). The regression equation shown was determined
using data from both the sulphide layers and the intervening sediment.

oxygen and nitrate). Subsequent diffusion and "recapture" by adsorption and/or reprecipitation in underlying reduced sediments can create sharp peaks at, or just below, the deepened redox boundary, although for some metals the zone of enrichment may extend for decimetres below the redox boundary because the trapping mechanism is relatively slow (e.g., Re and U; Colodner et al., 1992; Thomson et al., 1993; Crusius and Thomson, 2000a).

Post-depositional burndown can be rejected as a controlling influence on the trace metal distributions observed in Core JT96-02 for four major reasons. First, the average sedimentation rate in this section of the core is ~60 cm/kyr. Such rapid deposition would work to inhibit oxygen penetration into the sediments. Furthermore, the presence of multiple organic-rich layers, each of which would have had a significant associated oxidant demand, would have limited O_2 diffusion below any given layer. Second, the compositional characteristics (i.e., organic carbon and trace metal contents) of each sulphide layer are remarkably similar, yet it is highly unlikely that the degree of burndown would have been so consistent. Third, there is excellent correspondence between the major element compositional variations, inferred to reflect textural changes, and the distribution of trace metals. Burndown, if it had occurred, would have affected the latter without influencing the former, thus destroying or at least muting any relationship. Finally, all of the redox-sensitive trace metals should display similar trends (i.e., depletion within the clay and enrichment within the sulphide layers) if the result of burndown, but they do not. In fact, the highest concentrations of Cd and U occur within the clay and not in the sulphide layers. These four reasons strongly imply that the observed trace metal enrichments represent an early diagenetic signature and are not the result of subsequent oxidative burndown.

The sulphide layers in Core JT96-02pc are geochemically similar to the Mediterranean sapropels described in Calvert and Fontugne (2001), although by definition these layers are not sapropels as they do not contain >2 wt.% organic carbon. Both sapropels and sulphide layers are finer-grained and organic-rich relative to intervening sediments, and both exhibit trace metal enrichments. In the case of the sapropels increased productivity in

surface waters resulted in higher organic matter flux to the sediment and degradation of this material led to anoxic conditions and thus trace metal enrichment (Calvert and Fontugne, 2001). The sulphide layers described here are characterized by higher organic carbon and carbonate contents which could be interpreted as representing episodic increases in the settling flux of biogenic detritus, set against a backdrop of glacial rock-flour deposition. However, evidence provided by the Si/Al, Zr/Al and Ti/Al ratios (Fig. 5.3) argues against this hypothesis. These data strongly imply that hemipelagic sedimentation represented by the sulphide-rich layers was episodically interrupted by turbidite deposition, most probably related to rapid deglaciation of the nearby continental shelf. This "pulsed turbidite" model provides an explanation for the S and Mo enrichments observed in the organic-rich layers. Geologically instantaneous emplacement of the turbidites would have rapidly attenuated oxygen influx, thus inducing anoxic conditions in the organic-rich sediments that immediately underlie each turbidite. The resulting sulphate reduction and precipitation of FeS would then have provided the conditions necessary for Mo accumulation. Pulsed, rapid sedimentation can adequately explain the observed Mo enrichment in these sediments. It is not necessary to invoke oxygen depletion of the bottom-water as having influenced the Mo content. This observation potentially complicates the use of sedimentary Mo concentrations as a proxy for bottom-water anoxia in environments where large changes in sedimentation rate occur.

5.4 Trace metal geochemistry

While the rapid emplacement of turbidites on top of relatively organic-rich, hemipelagic deposits can explain the formation of the sulphide layers, it cannot explain why some redox-sensitive metals are enriched while others are apparently not. The precipitation of FeS clearly indicates that anoxic conditions developed. Under such conditions the accumulation of authigenic Mo, Re, U, Cd and Ag is to be expected, but only Mo and Re,

and to a lesser extent Ag, are significantly enriched in the sulphide layers. An explanation for the apparent contrasts among the redox-sensitive metals lies in how efficiently the metals are fixed under reducing conditions, as well as in the relative contributions of authigenic and lithogenic sources.

The enrichment of Mo in anoxic sediments is directly linked to sulphate reduction and the formation Fe-sulphides. At an H_2S concentration of ~11 µM the principal dissolved Mo species switches from MoO_4^{2-} to MoS_4^{2-}. Thiomolybdate is highly particle reactive and readily adsorbes on to Fe-bearing particles such as Fe-sulphides (Helz et al., 1996; Erickson and Helz, 2000). The link between S and Mo in the sulphide layers is clearly indicated by their very strong positive correlation ($r^2 = 0.77$; Fig. 5.5). The high Mo concentrations seen in the sulphide layers of Core JT96-02 is therefore explained by the downward diffusion of Mo from the overlying seawater, through the newly emplaced turbidite, to the underlying zone of sulphate reduction where it accumulated.

In contrast to Mo, Re reduction and precipitation, possibly as ReO_2 or a Re-organic complex, commences when suboxic conditions are attained and continues during sulphate reduction (Crusius et al., 1996; Crusius and Thomson, 2000a). There is evidence to suggest that the precipitation of Re is kinetically slow (Crusius and Thomson, 2000a) and that it may be hindered by the presence of dissolved sulphide (Colodner et al., 1992). This could account for the numerous examples of preferential enrichment of Mo relative to Re in anoxic marine sediments (e.g., Crusius et al., 1996; Crusius et al., 1999; Crusius and Thomson, 2000a). However, within the sulphide layers of Core JT96-02 no such preferential enrichment is observed. The primary source for both authigenic Re and Mo in sediments is seawater and if these metals accumulate quantitatively, that is if their concentrations in the porewater are zero or nearly so at a common precipitation point, then the sedimentary Re/Mo ratio should be very similar to that in seawater (~0.7 ng/µg). Higher ratios would indicate that suboxic conditions prevailed under which Re but not Mo would accumulate, while lower ratios would result from preferential Mo accumulation under oxic or anoxic conditions

(Crusius et al., 1996). In Core JT96-02 Re/Mo ratios range from 0.4 to 3.0 ng/µg and average ~1 ng/µg in both the sulphide layers and intervening clay (Fig. 5.4f). In general these values suggest that: i) anoxic conditions developed rapidly within the organic-rich layers, before substantial Re enrichment could occur under suboxic conditions; and ii) suboxic conditions either did not develop, or did not persist, within the turbidites for long enough to allow preferential enrichment of Re. Furthermore, the similarity to the seawater Re/Mo ratio indicates that removal of Mo and Re from seawater into the sulphide layers was quantitative. The higher Re/Mo ratios near the base of each sulphide layer suggest that suboxic conditions prevailed. This is consistent with the low sulphur content, indicating that minimal sulphate reduction occurred, most probably due to the lower concentration of organic carbon.

The precipitation of Cd and Ag in anoxic sediments does not involve a change in redox state. However, these metals are indirectly redox-sensitive because they precipitate as discrete sulphide minerals in the presence of trace amounts of dissolved sulphide (Koide et al., 1986; Rosenthal et al., 1995). Despite this, there is little if any observable Cd enrichment within the sulphide layers, and only a very slight Ag enrichment. The contrast between the distributions of this pair of metals and that of Mo reflects the relative importance of seawater and lithogenic metal sources. The contrast can be visualized by comparing the mean concentration of the metals in seawater to the content typical of lithogenic detritus (Table 5.1). The resulting unitless ratio emphasizes that Mo, unlike either Ag or Cd, is highly enriched in seawater relative to lithogenic materials. Since seawater is the primary source for the authigenic accumulation of metals, it follows that where geochemical conditions are appropriate (i.e., where sufficient H_2S occurs in porewaters), Mo enrichment should be relatively more obvious than that of Ag and Cd. A similar reasoning applies to U. Like Re, U is reduced and will precipitate in suboxic and anoxic sediments (Klinkhammer and Palmer, 1991). However, the high lithogenic background concentration in JT96-02, and

Table 5.1. Seawater and lithogenic concentrations of the redox-sensitive trace metals.

Metal	Seawater concentration [1] (SW, μg/g)	Lithogenic concentration (L, μg/g)	SW : L ratio
Mo	10.266 (Collier, 1985)	0.6 (McKay, unpubl. data) [2]	17.1
Re	0.008 (Anbar et al., 1992)	0.0005 (Koide et al., 1986)	16.0
Ag	0.003 (Zhang et al., 2001)	0.1 (Bowen, 1966)	< 0.1
Cd	0.112 (Bruland et al., 1994)	0.2 (McKay, unpubl. data) [2]	0.6
U	3.240 (Chen et al., 1986)	2 [3]	1.6

[1] Seawater data for the non-conservative elements Ag and Cd are for ~1000 m water depth.

[2] Data are for surface sediments at Site JT96-02 (see Chapter 4). Values are similar to those proposed for terrigenous sediments derived from Vancouver Island (Morford et al., 2001).

[3] Lithogenic values for U vary greatly depending on the sediment composition and grain-size. Morford et al. (2001) suggest a lithogenic value of 1 μg/g which is lower than the average shale value of ~4 μg/g (Turekian and Wedepohl, 1961). We assume an intermediate value of 2 μg/g which is similar to the average value in the gray clay.

corresponding low seawater to lithogenic ratio (Table 5.1), means that the authigenic U signal that must be present in these deposits is obscured.

Finally, one other factor could influence the accumulation of certain trace metals in continental margin settings such as that described here. While Mo, Re and U have essentially conservative (i.e., invariant) concentrations in the open-ocean water column, both Ag and Cd distributions are strongly influenced by biological cycling as both elements are taken up by phytoplankton in surface waters. Dissolved Ag distributions tend to follow Si, implying that the element is incorporated into the "hard parts" and regenerated in relatively deep waters (Flegal et al., 1995; Zhang et al., 2001), while Cd is known to be incorporated into the "soft parts" and is regenerated at shallower depths (Boyle, 1988). Thus, the concentrations of Ag and Cd in the bottom water, and hence the seawater to lithogenic ratio, will vary with water depth. Furthermore, the biogenic flux of Cd and Ag to the sediment must be considered as contributions from this source could also obscure the authigenic signal.

5.5 Summary

The relatively low organic carbon and carbonate contents, as well as lower $\delta^{13}C_{org}$ and $\delta^{15}N$ values that characterize the gray clay imply a more terrigenous provenance. The fining upward trend exhibited by each clay layer suggests that they are turbidites. Based on its texture and radiocarbon age, as well what is known about the deglacial history of western Canada, this material is most probably rock-flour generated as Cordilleran ice retreated from the nearby continental shelf. In contrast, the relatively organic-rich sediments that immediately underlie each turbidite layer have a more marine character as indicated by higher $\delta^{13}C_{org}$ and $\delta^{15}N$ values and most probably represent the background hemipelagic sedimentation.

The formation of sulphide-rich layers in Core JT96-02pc was the result of pulsed turbidite deposition that slowed the influx of oxygen into the underlying organic-rich sediments and thus allowed porewater anoxia to develop. This led to sulphate reduction and Fe-sulphide precipitation and in turn Mo enrichment. Concentration profiles for Re and Ag generally parallel that of Mo; however, Cd and U profiles do not. Contrasts among the profiles can be attributed to differences in the relative contributions of dissolved metals from the overlying bottom water (i.e., the authigenic flux) and background concentrations associated with the lithogenic flux. Where the seawater to lithogenic concentration ratio is relatively high (e.g., Mo and Re) the authigenic component can be readily identified, but where the ratio is low (e.g., Cd and U) the authigenic component may be obscured. In the latter instance observable enrichments would require time to develop. It follows that sediments characterized by a relatively high Mo content, but low concentrations of other redox-sensitive trace metals, and a Re/Mo ratio similar to that of seawater, must have experienced rapid onset of anoxic conditions and relatively rapid burial below the depth of active metal influx.

The episodic deposition of turbidites set against a backdrop of hemipelagic sedimentation created the necessary conditions for the development of Mo concentration spikes. The enrichments thus occurred largely independently of changes in bottom water oxygen content and organic carbon flux to the sediment. This observation potentially complicates the use of sedimentary Mo concentration as a proxy for bottom-water anoxia in environments that are characterized by abrupt changes in sedimentation rate. It also emphasizes the importance of understanding the sedimentalogy if trace metal data are to be utilized as paleo-proxies.

5.6 References

Adelson, J.M. Helz, G.R., Miller, C.V., 2001. Reconstructing the rise of recent coastal anoxia; molybdenum in Chesapeake Bay sediments. Geochimica et Cosmochimica Acta 65, 237-252.

Anabar, A.D., Creaser, R.A., Papanastassiou, D.A., Wasserburg, G.J., 1992. Rhenium in seawater: Confirmation of generally conservative behavior. Geochimica et Cosmochimica Acta 56, 4099-4103.

Blaise, B., Clague, J.J., Mathewes, R.W., 1990. Time of maximum Late Wisconsin glaciation, west coast of Canada. Quaternary Research 34, 282-295.

Boyle, E.A., 1988. Cadmium: Chemical tracer of deepwater paleoceanography. Paleoceanography 4, 471-489.

Bowen, H.J.M., 1966. Trace Metals in Biogeochemistry, Academic Press, New York.

Bruland, K.W., Orians, K.J., Cowen, J.P., 1994. Reactive trace metals in the stratified central North Pacific. Geochimica et Cosmochimica Acta 58, 3171-3182.

Calvert, S.E., 1976. The mineralogy and geochemistry of near-shore sediments. In: J.P. Riley, J.P., Chester, R. (Eds.), Chemical Oceanography, Vol. 6. Academic Press, London, 187-280pp.

Calvert, S.E., 1990. Geochemistry and origin of the Holocene sapropel in the Black Sea. In: V. Ittekkot, V., Kempe, S., Michaelis, W., Spitzy, A. (Eds.), Facets of Modern Biogeochemistry. Springer-Verlag, Berlin, 326-352pp..

Calvert, S.E., Fontugne, M.R., 2001. On the late Pleistocene-Holocene sapropel record of climatic and oceanographic variability in the eastern Mediterranean. Paleoceanography 16, 78-94.

Calvert, S.E., Pedersen, T.F., 1993. Geochemistry of Recent oxic and anoxic marine sediments: Implications for the geological record. Marine Geology 113, 67-88.

Chen, J.H., Edwards, R.L., Wasserburg, G.J., 1986. ^{238}U, ^{234}U and ^{232}Th in seawater. Earth and Planetary Science Letters 80, 241-251.

Clague, J.J., James, T.S., 2002. History and isostatic effects of the last ice sheet in southern British Columbia. Quaternary Science Reviews 21, 71-87.

Colley, S., Thomson, J., Wilson, T.R.S., Higgs, N.C., 1984. Post-depositional migration of elements during diagenesis in brown clay and turbidite sequences in the North East Atlantic. Geochimica et Cosmochimica Acta 48, 1223-1235.

Collier, R.W., 1985, Molybdenum in the Northeast Pacific Ocean. Limnology and Oceanography 30, 1351-1354.

Colodner, D.C., Boyle, E.A., Edmond, J.M., Thomson, J., 1992. Post-depositional mobility of platinum, iridium and rhenium in marine sediments. Nature 358, 402-404.

Crusius, J., Thomson, J., 2000a. Comparative behaviour of authigenic Re, U, and Mo during reoxidation and subsequent long-term burial in marine sediments. Geochimica et Cosmochimica Acta 64, 2233-2242.

Crusius, J., Thomson, J., 2000b. Behaviour of Re and Ag on oxidation of S1, the most recent Mediterranean sapropel. AGU Fall Meeting, F614 (OS52B-10).

Crusius, J., Calvert, S., Pedersen, T., Sage, D., 1996. Rhenium and molybdenum enrichments in sediments as indicators of oxic, suboxic and sulfidic conditions of deposition. Earth and Planetary Science Letters 145, 65-78.

Crusius, J., Pedersen, T.F., Calvert, S.E., Cowie, G.L., Oba, T., 1999. A 36 kyr geochemical record from the Sea of Japan of organic matter flux variations and changes in intermediate water oyxgen concentrations. Paleoceaography 14, 248-259.

Dean, W.E., Gardner, J.V., Piper, D.Z., 1997. Inorganic geochemical indicators of glacial-interglacial changes in productivity and anoxic on the California continental margin. Geochimica et Cosmochimica Acta 61, 4507-4518.

Dean, W.E., Piper, D.Z., Peterson, L.C., 1999. Molybdenum accumulation in Cariaco basin sediment over the past 24 k.y.: A record of water-column anoxia and climate. Geology 27, 507-510.

Erickson, B.E., Helz, G.R., 2000. Molybdenum(VI) speciation in sulfidic waters: Stability and lability of thiomolybdates. Geochimica et Cosmochimica Acta 64, 1149-1158.

Flegal, A.R., Sanudo-Wilhelmy, S.A., Scelfo, G.M., 1995. Silver in the eastern Atlantic Ocean. Marine Chemistry 49, 315-320.

Francois, R., 1988. A study on the regulation of the concentrations of some trace metals (Rb, Sr, Zn, Pb, Cu, V, Cr, Ni, Mn and Mo) in Saanich Inlet sediments, British Columbia, Canada. Marine Geology 83, 285-308.

Helz, G.R., Miller, C.V., Charnock, J.M., Mosselmans, J.F.W., Pattrick, R.A.D., Garner, C.D., Vaughaan, D.J., 1996. Mechanism of molybdenum removal from the sea and its concentration in black shales: EXAFS evidence. Geochimica et Cosmochimica Acta 60, 3631-3642.

Ivanochko, T.S., 2001. Productivity influences on oxygenation of the Santa Barbara Basin, California during the Late Quaternary. M.Sc. Thesis, The University of British Columbia, 133pp.

Josenhans, H.W., Fedje, D.W., Conway, K.W., Barrie, J.V., 1995. Post glacial sea levels on the Western Canadian continental shelf: Evidence for rapid change, extensive subaerial exposure, and early human habitation. Marine Geology 125, 73-94.

Klinkhammer, G.P., Palmer, M.R., 1991. Uranium in the oceans: Where it goes and why. Geochimica et Cosmochimica Acta 55, 1799-1806.

Koide, M., Hodge, V.F., Yang, J.S., Stallard, M., Goldberg, E.G., Calhoun, J., Bertine, K.K., 1986. Some comparative marine chemistries of rhenium, gold, silver and molybdenum. Applied Geochemistry 1, 705-714.

Morford, J.L., Russell, AD., Emerson, S., 2001. Trace metal evidence for changes in the redox environment associated with the transition from terrigenous clay to diatomaceous sediment, Saanich Inlet, BC. Marine Geology 174, 355-369.

Nameroff, T.J., Balistrieri, L.S., Murray, J.W., 2002. Suboxic trace metal geochemistry in the eastern tropical North Pacific. Geochimica et Cosmochimica Acta 66, 1139-1158.

Rosenthal, Y., Lam, P., Boyle, E.A., Thomson, J., 1995. Authigenic cadmium enrichments in suboxic sediments: Precipitation and postdepositional mobility. Earth and Planetary Science Letters 132, 99-111.

Thomson, J., Higgs, N.C., Croudace, I.W., Colley, S., Hydes, D.J., 1993. Redox zonation of elements at an oxic/post-oxic boundary in deep-sea sediments. Geochimica et Cosmochimica Acta 57, 579-595.

Thomson, J., Higgs, N.C., Wilson, T.R.S., Croudace, I.W., De Lange, G.J., van Santvoort, P.J.M., 1995. Redistribution and geochemical behaviour of redox-sensitive elements around S1, the most recent eastern Mediterranean sapropel. Geochimica et Cosmochimica Acta 59, 3487-3501.

Turekian, K.K., Wedepohl, K.H., 1961. Distribution of the elements in some major units of the earth's crust. Geological Society of America Bulletin 72, 175-192.

Zhang, Y., Amakawa, H., Nozaki, Y., 2001. Oceanic profiles of dissolved silver: Precise measurements in the basins of western North Pacific, Sea of Okhotsk and the Japan Sea. Marine Chemistry 75, 151-163.

Zheng, Y., Anderson, R.F., van Geen, A., Kuwabara, J., 2000. Authigenic molybdenum formation in marine sediments: A link to pore water sulfide in the Santa Barbara Basin. Geochimica et Cosmochimica Acta 64, 4165-4178.

6. Summary

6.1 Sedimentation on the Vancouver Island Margin

The last deglacial was a period of dramatic change off Vancouver Island. Glaciers, which at their maximum extent 15 to 14 ^{14}C kyr ago had extended on to the shelf, began rapidly to retreated (Barrie and Conway, 1999; Clague and James, 2002). At this time linear sedimentation rates on the mid-slope (920 m) increased from 47 cm/kyr to over 150 cm/kyr and remained high until ~12.5 ^{14}C kyr when deglaciation of the shelf was essentially complete (Barrie and Conway, 1999) and the primary source of detritus (i.e., glacial outwash) was gone. Isostatic rebound caused a brief period of relative sea level fall during the deglaciation but then the sea began to rise rapidly reaching, and in many areas exceeding, modern sea level at ~10 ^{14}C kyr. Flooding of the shelf and the resultant trapping of sediments within fjords caused a substantial decrease in sedimentation rates on the mid- and lower slope (to 5 to 20 cm/kyr). Holocene sedimentation rates on the shelf and upper slope are even lower (<2 cm/kyr) as a result of high wave and current energies (Bornhold and Yorath, 1984; Bornhold and Barrie, 1991). The exception is Station 01 (120 m water depth) which is located within a depression and may be a site of sediment focusing.

6.2 The sea-surface temperature record

Alkenone palaeothermometry has yielded evidence of large and rapid shifts in sea-surface temperature (SST) during the deglacial (1°C in 40 to 80 years; Kienast and McKay, 2001). Based on radiocarbon dating and striking similarities to the $\delta^{18}O$ temperature record of the GISP-2 ice core these SST fluctuations off Vancouver Island were essentially synchronous with changes in atmospheric temperature over Greenland (Kienast and McKay, 2001). Similar millennial-scale climate oscillations have been recognized in a number of palaeo-records from

the Northeast Pacific (e.g., Thunell and Mortyn, 1995; Hendy and Kennett, 1999; Mix et al., 1999) and Western North America (e.g. Benson et al., 1997; Grigg and Whitlock, 2002). One of the most widely recognized events, the "early Holocene" thermal maximum, is clearly evident in Core JT96-09 between 11 and 10 calendar kyr B.P. as it is in many other palaeo-records from the region (e.g., Sabin and Pisias, 1996; Doose et al., 1997; Pellatt and Mathewes, 1997; Heusser et al., 1998). The palaeotemperature profile from Core JT96-09 (Kienast and McKay, 2001) clearly defines warm and cold events that are inferred to represent the Bølling and Allerød warm periods (~14.3 to 13.5 kyr B.P. and 13.5 to 12.7 kyr B.P., respectively) and Younger Dryas (~12.7 to 11.0 kyr B.P.) cold event. This observation has allowed the palaeoceanographic data presented in this thesis to be placed in a more global context.

6.3 The marine productivity record

One of the primary objectives of this thesis was to determine how marine primary production along the continental margin of the northeastern Pacific has varied on glacial-interglacial and shorter timescales. The organic carbon content and/or mass accumulation rate are commonly used as proxies for palaeoproductivity but in continental margin sediments a significant fraction of the total organic matter may be of terrestrial origin. Radiocarbon dating of bulk organic carbon, isotopic analysis ($\delta^{13}C$ and $\delta^{15}N$) and organic geochemistry were thus used to quantify the abundance of terrestrial organic matter in Core JT96-09. This information was used to partition the total sedimentary organic carbon content into marine and terrestrial fractions, which permitted the marine organic carbon flux to the sediment to be computed.

As much as 70 % of the organic carbon found in late glacial and early deglacial (i.e., Bølling) sediments is terrestrial in origin. Prior to 14.3 calendar kyr B.P. marine organic carbon accumulation was generally low, a reflection of low primary production and resulting low export production, because glacial-mode atmospheric circulation (i.e., northerly winds driven by the Aleutian Low) did not favour coastal upwelling. In this respect the northern

California Current System (CCS) was similar to the central CCS, where a marked decrease in productivity was documented during the last glacial (Dymond et al., 1992; Lyle et al., 1992; Ortiz et al., 1997; Dean and Gardner, 1998; Mix et al., 1999; Kienast et al., 2002). At the start of the deglaciation (i.e., the Bølling) the accumulation of marine organic matter began to increase. However, this material was diluted by abundant terrestrial organic detritus generated as glaciers retreated from the continental shelf. At the start of the Allerød (~13.5 calendar kyr B.P.) terrestrial input dropped abruptly and marine organic matter accumulation increased 6-fold relative to glacial values. Other palaeoproductivity proxies (i.e., % biogenic Ba, % opal and alkenone abundances) also indicate that export production was high throughout this period. Increased marine productivity during the deglacial is also documented in palaeo-records from the central and southern CCS (Lyle et al., 1992; Gardner et al., 1997; Dean and Gardner, 1998; Mix et al., 1999; Kienast et al., 2002), as well as the Gulf of Alaska (de Vernal and Pedersen, 1997) and western Pacific (Keigwin et al., 1992). Given that this marine productivity pulse was a wide spread phenomenon it is possible that it had an impact on atmospheric CO_2 concentrations. However, since increased productivity was probably the direct result of the initiation and/or intensification of upwelling, any sequestration of atmospheric CO_2 via the "biological pump" may have been countered by the release of CO_2 as upwelled water warmed. A more detailed investigation of $\delta^{13}C_{org}$ records from throughout the region may help to clarify how CO_2 fluxes changed. There was a brief return to glacial-like conditions (i.e., relatively low productivity) during the Younger Dryas and a corresponding decrease in marine organic matter accumulation. In the Holocene, the accumulation of marine organic matter was, and still is, lower than during the Allerød. This is largely the result of low organic matter preservation due to low sedimentation rates (i.e., long oxygen exposure times) and intense biological recycling. Since primary production off Vancouver Island is controlled by upwelling the data collectively suggest that in the last 16 kyr upwelling was most intense during the Allerød, an interpretation that is supported by a slight decrease in the benthic-planktonic age difference.

6.4 Redox-sensitive trace metals and their palaeo-applications

Temporal changes in organic carbon flux to the sediment had a direct impact on sedimentary redox conditions and may also have influenced OMZ intensity. Such changes can be inferred from redox-sensitive trace metal data. At present sediments on the Vancouver Island Margin become suboxic within millimetres of the sediment-water interface but there is no evidence that fully anoxic conditions develop within the upper 50 cm (i.e., no Mo enrichment). This observation was unexpected given the highly productive surface waters and relatively low bottom water oxygen concentrations in the region. Suboxic conditions are maintained because low sedimentation rates and extensive bioturbation support a small, but continual, influx of oxygen and other oxidants from the overlying water column. Low sedimentation also favours substantial accumulation of Re decimetres below the sediment-water interface. Unfortunately, such diagenetic enrichment has overprinted the early to mid-Holocene palaeo-record. Where sedimentation rates are relatively high, as they are at station 01 (~ 40 cm/kyr) for example, trace metal concentrations are more likely to reflect the early diagenetic conditions that are in turn influenced by the depositional environment. It is thus assumed in this thesis that trace metal data in rapidly deposited glacial and deglacial sediments can be used as palaeo-environmental proxies. There is however one caveat. Sedimentation must be steady. In Core JT96-02 deglacial sedimentation was characterized by the episodic emplacement of centimetre-scale turbidites. Pulsed sedimentation led to the development of anoxic conditions by substantially reducing the rate of oxygen influx into relatively organic-rich sediments. The resulting Re and Mo enrichments occurred without any decrease in bottom water oxygen concentration and/or increase in organic carbon flux to the sediment, two factors that commonly lead to trace metal enrichment. In Core JT96-09 there is no evidence of abrupt changes in sedimentation during the deglacial with the exception of one turbidite deposited at ~13.5 calendar kyr. B.P. (i.e., the start of the Allerød).

The enrichment of redox sensitive trace metals during the Allerød, in particular the high Mo concentrations, indicate that anoxic conditions existed in near-surface sediments at this time. Benthic foraminifera species data (i.e., the dominance of *Bolivina* spp.) corroborate the trace metal results. Regardless of the exact cause (i.e., increased carbon flux and/or decreased ventilation) the development of anoxic conditions must have been associated with intensification of the oxygen minimum zone (OMZ).

6.5 Fluctuation in OMZ intensity

Trace metal and benthic foraminifera species data suggest that the OMZ off Vancouver Island was more intense (i.e., more oxygen-depleted) between 13.5 to 12.7 calendar kyr B.P. (i.e., the Allerød) and possibly again between 11 and 8 kyr B.P. Radiocarbon dating of benthic-planktonic foraminiferal pairs indicate that by ~16 kyr B.P. ventilation of the intermediate water mass (920 m water depth) off Vancouver Island was similar to that at present (~ 900 years). There is no evidence indicating that ventilation decreased during the Allerød (i.e., benthic-planktonic age differences did not increase) but there is substantial evidence for an increased biogenic flux to the sediment. Increased export production, most probably the direct result of increased primary production in surface waters, was the principal cause of OMZ intensification off Vancouver Island.

The OMZ along the entire margin of the northeastern Pacific from Mexico to Vancouver Island intensified during the deglacial; however, off Vancouver Island intensification appears to lag ~1500 years behind that off California. If OMZ intensification was controlled primarily by changes in ventilation of NPIW the entire northeastern margin of the Pacific should have responded at approximately the same time. The observed lag suggests that other factors, possibly regional changes in productivity and/or the transportation of oxygen-depleted water from south by the California Undercurrent, controls OMZ intensity.

6.6 Biogenic Ag?

Intriguing results were obtained from the measurement of sedimentary Ag concentrations in near-surface sediments. Unlike the other redox-sensitive trace metals, for example Cd that has a similar geochemical behaviour, the primary control on Ag concentrations is not sedimentary redox conditions. Rather, it seems that Ag accumulates in, and is transferred to the sediment by, settling organic particles in much the same way that Ba is, as argued in Chapter 4. The measurement of sedimentary Ag concentrations may thus provide another palaeo-productivity proxy. The potential of such a proxy is clearly seen when one looks at the Holocene record of Core JT96-09. Silver concentrations are consistently high throughout the Holocene while the other redox-sensitive trace metals, for example Re, are not (Fig. 6.1). As a preliminary inference, high Ag concentrations may reflect the relatively high primary productivity that has existed throughout the Holocene but which is not preserved in the sediments due to the intense degradation of organic matter in these slowly accumulating deposits.

A number of major questions remain to be answered if Ag is to be used as a palaeoproductivity proxy. First, the hypothesis that Ag precipitates as Ag_2S within anoxic microenvironments in setting organic particles must be tested. Second, the conditions under which this "biogenic" Ag is preserved need to be clarified. The work presented in this thesis has shown that sediments need only be weakly suboxic to preserve the signal, but the question remains about its preservation in oxic sediments. Third, the relative importance of the "direct biogenic" flux (i.e., Ag directly incorporated by organisms) relative to the "indirect biogenic" flux (i.e., Ag which accumulates as organic particles settle through the water column) must be evaluated.

6.7 Future work

Metal Concentrations
(Ag - ng/g; Re - ng/g x 10)
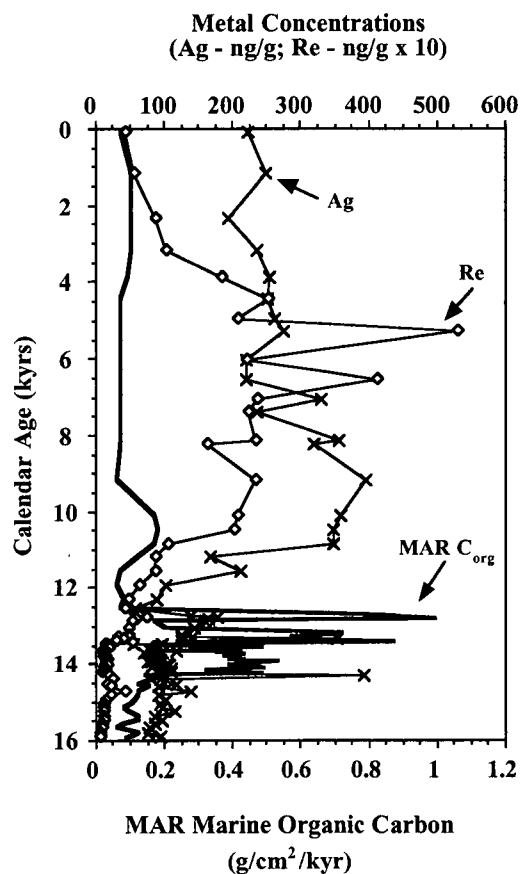
Fig. 6.1. A comparison of Re and Ag concentrations over the last 16 kyr B.P. in Core JT96-09. Note that in the weakly suboxic Late Holocene sediments the concentration of Re is low yet the Ag concentration is relatively suggesting that something other than redox is influencing Ag accumulation.

This thesis offers the first comprehensive palaeoceanographic investigation of the northeastern Pacific Ocean off the west coast of Vancouver Island. It provides a record for the past 16 kyr and in particular a very detailed record for the last deglaciation. Results indicate that in many respects the northern CCS behaved in a similar manner as the central and southern CCS. For example, both primary productivity and the accumulation of marine organic matter were substantially reduced in most regions during the deglacial and enhanced during the deglacial. However, the relatively short record present here must be extended back through Oxygen Isotope Stages 3 and 4 and if possible into OIS 5. Of particular interest is whether or not the Dansgaard-Oeschger events that are recognized in southern records (e.g., Santa Barbara Basin - Behl and Kennett, 1996; Hendy and Kennett, 1999) are evident in the sedimentary record off Vancouver Island.

6.7 References

Barrie, J. V., Conway, K.W., 1999. Late Quaternary glaciation and postglacial stratigraphy of the Northern Pacific Margin of Canada. Quaternary Research 51, p. 113-123.

Behl, R.J., Kennett, J.P., 1996. Brief interstadial events in the Santa Barbara basin, NE Pacific, during the past 60 kyr. Nature 379, 243-246.

Benson, L., Burdett, J., Lund, S., Kashgarian, M., Mensing, S., 1997. Nearly synchronous climate change in the Northern Hemisphere during the last deglacial termination. Nature 388, 263-265.

Bornhold, B.D., Barrie, J.V., 1991. Surficial sediments on the western Canadian continental shelf. Continental Shelf Research 11, 685-699.

Bornhold, B.D., Yorath, C.J., 1984. Surficial geology of the continental shelf, northwestern Vancouver Island. Marine Geology 57, 89-112.

Clague, J.J., James, T.S., 2002. History and isostatic effects of the last ice sheet in southern British Columbia. Quaternary Science Reviews 21, 71-87.

de Vernal, A., Pedersen T.F., 1997. Micropaleontology and palynology of core PAR87A-10: A 23,000 year record of paleoenvironmental changes in the Gulf of Alaska, northeast North Pacific. Paleoceanography 12, 821-830.

Dean, W.E., Gardner, J.V., 1998. Pleistocene to Holocene contrasts in organic matter production and preservation on the California continental margin. GSA Bulletin 110, 888-899.

Dymond, J., Suess, E., Lyle, M., 1992. Barium in deep-sea sediment: A geochemical proxy for paleoproductivity. Paleoceanography 7, 163-181.

Gardner, J.V., Dean, W.E., Dartnell, P., 1997. Biogenic sedimentation beneath the California Current system for the past 30 kyr and its paleoceanographic significance. Paleoceanography 12, 207-225.

Grigg, L.D., Whitlock, C., 2002. Patterns and causes of millennial-scale climate change in the Pacific Northwest during Marine Isotope Stages 2 and 3. Quaternary Science Reviews 21, 2067-2083.

Hendy, I., Kennett, J.P., 1999. Latest Quatnary North Pacific surface-water responses imply atmosphere-driven climate instability. Geology 27, 291-294.

Keigwin, L.D., Jones, G.D., Froelich, P.N., 1992. A 15,000 year paleoenvironmental record from Meiji Seamount, far northwestern Pacific. Earth and Planetary Science Letters 111, 425-440.

Kienast, S.S., McKay, J.L., 2001. Sea surface temperatures in the subarctic Northeast Pacific reflect millennial-scale climate oscillations during the last 16 kyrs. Geophysical Research Letters 28, 1563-1566.

Kienast, S.S., Calvert, S.E., Collier, R.W., Pedersen, T.F., 2002. Nitrogen isotope and productivity variations along the North East Pacific margin over the last 120 kyr: Surface and subsurface palaeoceanography. Paleoceanography 17, doi: 10.1029/2001PA000650.

Lyle, M., Zahn, R., Prahl, F., Dymond, J., Colier, R., Pisias, N., Suess, E., 1992. Paleoproductivity and carbon burial across the California Current: The mulitracers transect, 42°N. Paleoceanography 7, 251-272.

Mix, A.C., Lund, D.C., Pisias, N.G., Bodén, P., Bornmalm, L., Lyle, M., Pike, J., 1999. Rapid climate oscillations in the northeast Pacific during the last deglaciation reflect northern and southern hemisphere sources in Mechanisms of Global Climate Change at Millennian Time Scales, Geophysical Monograph 112 edited by P.U. Clark, R.S. Webb and L.D. Keigwin. American Geophysical Union, pp. 127-148.

Ortiz, J., Mix, A., Hostetler, S., Kashgarian, M., 1997. The California Current of the last glacial maximum: Reconstruction at 42°N based on multiple proxies. Paleoceanography 12, 191-205.

Thunell, R.C., Mortyn, P.G., 1995. Glacial climate instability in the Northeast Pacific Ocean. Nature 376, 504-506.

179

Appendix I. Methods

a) Total carbon, total nitrogen and total sulphur were measured by high temperature combustion using a Carlo Erba NA1500 elemental analyzer. Two marine sediment standards from the National Research Council of Canada (NRC standards PACS-1 and MESS-1) were analyzed with each batch of samples and yielded relative standard deviations (RSD, 1σ) of 3 %, 5 % and 6 % for C, N and S, respectively. The accuracy was within 7 % of the recommended values for all three elements.

b) Percent carbonate carbon (i.e., inorganic carbon) was measured using a Coulometrics 5010 coulometer. Approximately 50 mg of sample was reacted with 10% HCl. The CO_2 gas produced was bubbled into a dark blue solution of ethanolamine causing the pH to decrease and the blue colour to fade. The transmittance of the solution was continually measured and when it began to increase OH^- ions were generated electrically. The amount of CO_2 produced, and thus amount of $CaCO_2$ in the sample, was directly proportional to the current required to return the ethanol amine solution to its original colour. Results for a calcium carbonate standard run multiple times with each batch of samples yielded an RSD of ~1 % (i.e., 11.93 ± 0.13, n=141).

c) The amount of organic carbon in samples was calculated by difference (organic carbon = total carbon – inorganic carbon) and the aggregate RSD for these data is ~4 %.

d) Biogenic silica (i.e., opal) content was determined by alkaline dissolution following the procedure of Mortlock and Froelich (1989). The concentration of Si was measured by spectrophotometry and then converted to weight % opal by multiplying by 2.4 (this assumes

10% water in opal; Mortlock and Froelich, 1989). The RSD (1σ) for two in-house standards (SNB and JV5) and repeat samples was ≤4 %.

e) Organic geochemical analysis to determine the concentrations of C_{37} alkenones and C_{29} n-alkanes was carried out using the solvent extraction method of Villanueva et al. (1997). The organic fraction was extracted from 3 to 10 mg of freeze-dried sediment using dichloromethane (CH_2Cl) followed by saponification with a mixture of 6 % KOH in methanol. The organic fraction was then extracted with n-hexane and run through a silica column. The fraction containing the n-alkanes and C_{37} alkenones was eluted from the column with a mixture of dichloromethane and n-hexane. Analyses were made by manual-injection on an HP 5880 gas chromatograph. The n-alkanes and C_{37} alkenones were identified using an internal standard (i.e., mixture of C_{19}, C_{36} and C_{40}), and the identification of C_{37} alkenones was confirmed by GC-MS. The concentrations of C_{29} n-alkanes and C_{37} alkenones were calculated by assuming that their concentrations were proportional to the chromatogram peak area and that the response factor was the same as for the internal standards. Only the di- and tri-unsaturated C_{37} alkenones were quantified, as the amount of tetra-unsaturated C_{37} alkenone was generally below the detection limit of 10 ng.

f) The carbon- and nitrogen-isotopic composition of organic matter were obtained by continuous-flow mass spectrometry using a Fisons NA1500 elemental analyzer attached to a VG Prism mass spectrometer. Samples for carbon isotopic analysis of organic matter ($\delta^{13}C_{org}$) were pretreated with 10 % HCl to remove carbonate material and then dried at 50°C overnight. These samples were not washed with distilled water prior to drying. Nitrogen isotope results ($\delta^{15}N$) were obtained for untreated bulk sediment samples. Data are reported in the standard δ-notation relative to Vienna Peedee belemnite (VPDB) for carbon and atmospheric N_2 for nitrogen. The isotopic results for an in-house sediment standard are ±0.1

‰ for carbon and ±0.2 ‰ for nitrogen. Repeat analyses of samples are generally better than this.

g) Prior to isotopic analysis benthic and planktonic foraminifera were sonicated in methanol and roasted under vacuum for 30 minutes at 430°C. The samples were then reacted in a common orthophosphoric acid bath at 90°C and analyzed using a VG Prism mass spectrometer in dual inlet mode. Data are reported in the standard δ-notation relative to VPDB. The reproducibility of three in-house standards (Mexical, UQ6 and a foraminiferal standard), that were calibrated using the international standard NBS-19, was ±0.15 ‰ for $\delta^{18}O$ and ±0.07 for $\delta^{13}C$.

h) Major and minor element concentrations were measured by X-ray fluorescence (XRF) on a Philips PW2400 wavelength-dispersive sequential automatic spectrometer according to the method of Calvert (1990). Samples for major element analysis were combined with Spectroflux 105 in a 9:1 ratio and melted at 1100°C. To correct for the loss of volatiles during melting Spectroflux 100 was added to bring the samples back to their original weight. The samples were then re-melted and cast into glass disks. Minor elements were measured on pressed pellets backed with borax. The precision of the XRF method is estimated to be 5 % and 15 % for major and minor elements, respectively. Unless otherwise stated, all major and minor element data were corrected for the presence of sea salt in the dried sediment. The salt content was determined by measuring the chlorinity by titration with $AgNO_3$. A salinity of 35 ‰ was assumed.

i) The concentration of biogenic barium was calculated using the equation of Dymond et al. (1992):

Bio-barium = Total Ba - (Al x Ba/Al$_{lith}$)

A Ba/Al lithogenic ratio (Ba/Al$_{lith}$) of 0.0027 was estimated from the exponential regression of the Ba/Al ratios of surface sediments versus water depth following the method of Klump et al. (2000). This method assumes that the fraction of biogenic Ba increases seaward and that close to land (i.e., ~0 m water depth) all of the Ba is terrigenous in origin. The Ba/Al$_{lith}$ estimated using the regression method was confirmed by chemically extracting the bio-barium using a 2M solution of NH_4Cl (Schenau et al., 2001) and then measuring the barium content of the residue (i.e., the lithogenic Ba).

j) Trace metal concentrations (i.e., Re, Ag, Cd, Mo and U) were measured by isotope-dilution inductively-coupled plasma mass spectrometery. Sample preparation involved adding known amounts of isotopically-enriched spike solutions to ~20 mg of powdered sediment. Samples were then microwave digested in a mixture of concentrated HNO_3, HCl and HF. The digests were evaporated on a hotplate overnight and then re-digested in 5N HCl. Aliquots were taken for Mo and U analysis and the remaining sample was run through an anion exchange column (Dowex 1-X8 resin) to remove Zr and Nb that form compounds (i.e., ZrO, ZrOH, NbO) which interfere with the analysis of Ag, and Mo that forms MoO^- which interferes with Cd analysis. To check precision a University of British Columbia sediment standard (SNB) was analyzed with each batch of samples. The resulting RSD (1σ) for Re, U, Mo, Cd and Ag analyses were 11 %, 9 %, 7 %, 10 % and 8 %, respectively. Accuracy, which was assessed by measuring the concentrations of these metals in the NRC sediment standard MESS-1, was 8 % or better for Re, Mo and U, and ~14 % for Cd. The detection limits, calculated as 3x the relative standard deviation of the blank, were estimated to be <1 ppb for Re, 0.04 ppm for U, 0.5 ppm for Mo, 0.1 ppm for Cd and 57 ppb for Ag (data provided by K. Gordon).

References

Calvert, S.E., 1990. Geochemistry and origin of the Holocene sapropel in the Black Sea. In: Ittekkot, V., Kemp, S., Michaelis, W., Spitzy, A. (Eds.), Facets of Modern Biogeochemistry. Springer-Verlag, Berlin, 326-352pp.

Dymond, J., Suess, E., Lyle, M., 1992. Barium in deep-sea sediments: A geochemical proxy of paleoproductivity. Paleoceanography 7, 163-181.

Klump, J., Hebbeln, D., Wefer, G., 2000. The impact of sediment provenance on barium-based productivity estimates. Marine Geology 169, 259-271.

Mortlock, R.A., Froelich, P.N., 1989. A simple method for the rapid determination of biogenic opal in pelagic marine sediments. Deep Sea Research 36, 1415-1426.

Schenau, S.J., Prins, M.A., De Lange, G.J., Monnin, C., 2001. Barium accumulation in the Arabian Sea: Controls on barite preservation in marine sediemnts. Geochimica et Cosmochimica Acta 65, 1545-1556.

Villanueva, J., Pelejero, C., Grimalt, J.O., 1997. Clean-up procedures for the unbiased estimation of C37 alkenone sea surface temperatures and terrigenous n-alkane inputs in paleoceanography. Journal of Chromatography 757, 145-151.

Table A1. List of the cores collected, their geographic locations and water depths, as well as the various types of data provided in the appendices.

Station[1]	Location	Water Depth (m)	Sediment Core Type[2]	Stratigraphic Description	CTD data	Dissolved O$_2$ data	Magnetic Susceptibility	^{14}C data	^{210}Pb data	d^{13}C and d^{18}O for foraminifera	Geochemical Data
JT96-01	48° 45.945' N 125° 29.566' W	120	mc	Appendix 2	Appendix 3	Appendix 4	none	Appendix 6	Appendix 7	none	Appendix 9
JT96-04	49° 00.705' N 126° 49.818' W	407	mc	Appendix 2	Appendix 3	Appendix 4	none	none	none	none	Appendix 11
JT96-06	48° 58.727' N 126° 52.678' W	721	bc, mc, pc	Appendix 2 (bc only)	Appendix 3	Appendix 4	Appendix 5	none	none	Appendix 8	Appendix 13
JT96-09	48° 54.76' N 126° 53.44' W	920	mc, pc	Appendix 2	Appendix 3	Appendix 4	Appendix 5	Appendix 6	Appendix 7	Appendix 8	Appendix 14
JT96-02	49° 12.805' N 127° 18.567' W	1340	mc, pc	Appendix 2	Appendix 3	Appendix 4	Appendix 5	Appendix 6	Appendix 7	Appendix 8	Appendix 10
JT96-05	49° 07.910' N 127° 33.115' W	1750	bc, pc, tc	Appendix 2 (bc only)	none	Appendix 4	Appendix 5	Appendix 6	none	none	Appendix 12
Tul96-03	49° 03.33' N 126° 58.20' W	650	tc, pc	none	none	none	none	none	none	Appendix 8	Appendix 15
Tul96-05	49° 00.01' N 127° 03.27' W	1390	tc, pc	none	none	none	none	Appendix 6	none	Appendix 8	Appendix 16

[1] Data from the following cores were used in this thesis:

JT96-09pc (Chapters 2 and 3)

JT96-01mc, JT96-04mc, JT96-06bc, JT96-09mc, JT96-02mc and JT96-05bc (Chapter 4)

JT96-02pc (Chapter 5)

[2] mc - multicore, bc - box core, pc - piston core and tc - trigger core.

Table A2. Core Descriptions.

Core [1]	Latitude	Longitude	Water Depth (m)	Bottom Water O₂ (ml/l)	Depth in Core (cm) [2]	Core Description
JT96-01mc	48° 45.95' N	125° 29.57' W	120	2.4	0 - 38	olive green mud (38 cm)
JT96-04mc	49° 00.71' N	126° 49.82' W	407	1.0	0 - 9 9 -19	olive green muddy sand (9 cm) gray clay (10 cm)
JT96-06bc	48° 58.73' N	126° 52.68' W	720	0.4	0 - 18 18 - 35	olive green sandy mud (18 cm) gray clay (17 cm)
JT96-09mc	48° 54.76' N	126° 53.44' W	920	0.3	0 - 40	olive green mud (40 cm)
JT96-09pc	"	"	"	"	0 - 0.2 0.2 - 51 51 - 136 136 -152 152 - 320 320 - 360 360 - 374	brownish "fluff" layer (0.2 cm) olive green mud (50.8 cm) gray green clay (85 cm) sandy mud (16 cm) gray clay (168 cm) gray clay interbedded with mm-scale sandy layers (40 cm) gray clay (14 cm)
JT96-02mc	49° 12.81' N	127° 18.57' W	1340	0.4 [3]	0 - 18	olive green mud (18 cm)

JT96-02pc	"	"	"	"	0 - 16
					16 - 34
					34 - 90
					
					90 - 211
						olive green mud (16 cm)
						greenish gray clay (18 cm)
						interbedded sand and clay
						    with erosional base (56 cm)
						gray clay with abundant
						    sulphide-rich layers (121 cm)

JT96-05bc	49° 07.91' N	127° 33.12' W	1750	1.2	0 - 1 1 -48	brownish "fluff" layer (1 cm) olive green mud (47 cm)

[1] mc = multicores; bc = boxcores; pc = piston cores.

[2] uncorrected core depth.

[3] dissolved O₂ concentration was measured at 1240 m.

186

Table A3. CTD Data for Stations JT96-01, 2, 4, 6 and 9.

CTD Data for Station JT96-01

Depth (m)	Temperature (°C)	Salinity (psu)	Sigma-t
0.0	14.21	31.18	23.19
1.8	14.27	31.19	23.19
2.0	14.27	31.20	23.20
3.2	14.27	31.20	23.20
4.0	14.26	31.19	23.19
5.0	14.26	31.21	23.20
6.0	14.30	31.20	23.19
7.6	14.01	31.14	23.21
8.0	14.11	31.03	23.10
9.4	12.87	30.58	23.00
10.0	11.31	31.00	23.61
11.8	10.94	31.05	23.71
12.0	11.05	31.07	23.71
13.8	11.07	31.26	23.85
14.0	11.07	31.27	23.86
15.0	10.56	31.34	24.01
16.2	10.18	31.44	24.15
17.0	10.11	31.41	24.13
18.6	10.04	31.43	24.16
19.0	10.02	31.43	24.16
20.0	9.97	31.47	24.20
21.0	9.93	31.53	24.26
22.0	9.85	31.63	24.35
23.2	9.85	31.62	24.34
25.0	9.80	31.65	24.37
26.0	9.78	31.65	24.38
27.0	9.75	31.67	24.39
28.2	9.66	31.73	24.46
29.0	9.63	31.76	24.48
30.0	9.58	31.79	24.52
31.8	9.55	31.82	24.54
32.0	9.53	31.82	24.55
33.0	9.50	31.83	24.56
34.0	9.49	31.83	24.56
35.2	9.45	31.85	24.58
37.4	9.38	31.92	24.65
38.2	9.36	31.93	24.66
39.0	9.12	32.16	24.88
40.0	9.04	32.18	24.91
41.8	8.95	32.25	24.97
42.0	8.96	32.26	24.98
43.0	8.95	32.30	25.01
44.0	8.99	32.34	25.04
45.0	8.90	32.39	25.09
46.6	8.84	32.43	25.13
47.0	8.83	32.44	25.14
48.0	8.83	32.43	25.14
49.0	8.80	32.46	25.16
50.4	8.74	32.49	25.20
55.4	8.36	32.63	25.36
60.0	8.19	32.78	25.50
65.0	8.12	32.85	25.56
70.0	8.07	32.90	25.61
75.0	8.06	32.91	25.63
81.0	7.99	32.97	25.69
86.0	7.97	32.99	25.70
91.0	7.94	33.02	25.73
96.4	7.87	33.08	25.79
101.0	7.83	33.11	25.82
106.0	7.82	33.12	25.82
112.0	7.82	33.08	25.79

CTD Data for Station JT96-02

Depth (m)	Temperature (°C)	Salinity (psu)	Sigma-t	Depth (m)	Temperature (°C)	Salinity (psu)	Sigma-t	Depth (m)	Temperature (°C)	Salinity (psu)	Sigma-t
0.0	13.54	31.63	23.68	218.6	7.82	32.00	24.94	608.0	4.12	34.20	27.14
1.0	13.54	31.63	23.68	223.0	7.82	31.95	24.90	613.0	4.10	34.20	27.14
2.0	13.54	31.63	23.68	228.0	7.82	31.87	24.85	618.0	4.09	34.20	27.14
3.0	13.54	31.63	23.68	234.0	7.82	31.82	24.80	624.2	4.05	34.20	27.14
5.2	13.54	31.63	23.68	239.0	7.82	31.81	24.80	629.0	4.03	34.20	27.14
6.0	13.54	31.63	23.68	245.2	7.82	31.78	24.77	636.0	3.97	34.20	27.15
8.0	13.55	31.63	23.68	250.0	7.82	31.73	24.73	641.0	3.98	34.20	27.16
9.0	13.52	31.63	23.68	257.4	7.82	31.70	24.71	648.4	3.99	34.21	27.16
10.8	13.50	31.63	23.69	262.0	7.82	31.68	24.70	653.0	3.98	34.22	27.17
11.0	13.51	31.63	23.68	268.6	7.82	31.58	24.61	659.2	3.99	34.22	27.17
12.0	13.50	31.63	23.68	273.2	7.82	31.55	24.59	664.0	3.99	34.22	27.17
13.0	13.49	31.63	23.69	278.0	7.82	31.52	24.57	671.4	4.03	34.24	27.18
14.0	13.45	31.64	23.70	283.0	7.82	31.50	24.55	676.0	4.03	34.24	27.18
15.0	13.39	31.63	23.71	288.6	7.82	31.50	24.55	681.0	4.03	34.24	27.18
17.2	12.16	31.75	24.04	293.0	5.16	34.04	26.89	686.2	4.03	34.25	27.19
20.0	11.33	31.74	24.18	298.0	5.15	34.04	26.90	691.4	4.02	34.25	27.19
21.0	11.21	31.76	24.22	304.2	5.10	34.04	26.90	696.0	4.02	34.25	27.19
22.0	11.05	31.78	24.26	309.0	5.06	34.03	26.90	702.8	3.97	34.26	27.20
23.0	10.96	31.78	24.28	314.0	5.05	34.04	26.91	707.0	3.95	34.26	27.20
24.0	10.81	31.90	24.40	319.0	5.03	34.05	26.92	712.0	3.94	34.26	27.20
25.0	10.48	31.88	24.44	324.2	5.02	34.04	26.91	719.0	3.90	34.27	27.21
26.2	10.19	31.90	24.50	329.0	4.98	34.04	26.92	724.0	3.89	34.27	27.21
27.0	10.18	31.90	24.50	334.6	4.94	34.05	26.93	729.0	3.88	34.27	27.22
28.0	10.17	31.90	24.50	339.0	4.92	34.06	26.94	734.8	3.88	34.27	27.22
29.0	10.16	31.93	24.53	344.0	4.92	34.06	26.94	739.0	3.87	34.28	27.22
30.0	10.17	31.91	24.51	350.4	4.89	34.06	26.94	744.0	3.84	34.28	27.23
31.0	10.19	31.92	24.52	355.0	4.85	34.06	26.95	750.2	3.83	34.28	27.23
34.4	10.38	32.04	24.58	360.0	4.84	34.07	26.95	755.0	3.81	34.28	27.23
35.0	10.40	32.05	24.59	365.8	4.82	34.07	26.96	760.0	3.81	34.29	27.24
36.6	10.42	32.07	24.60	370.0	4.82	34.07	26.96	765.0	3.82	34.30	27.25
37.0	10.43	32.07	24.60	375.0	4.82	34.07	26.96	770.6	3.81	34.30	27.25
39.2	10.47	32.10	24.61	382.0	4.80	34.07	26.96	775.0	3.81	34.30	27.25
40.0	10.47	32.12	24.62	387.0	4.79	34.06	26.96	780.0	3.78	34.31	27.26
41.0	10.46	32.12	24.63	394.0	4.76	34.07	26.97	786.4	3.75	34.30	27.25
42.0	10.52	32.19	24.67	399.0	4.71	34.07	26.97	791.0	3.68	34.30	27.26
43.0	10.64	32.29	24.73	404.0	4.73	34.08	26.97	796.0	3.65	34.30	27.27
44.6	10.06	32.48	24.97	409.0	4.74	34.09	26.98	802.4	3.67	34.31	27.27
45.0	9.96	32.33	24.88	415.2	4.74	34.09	26.99	807.0	3.67	34.31	27.27
46.6	9.93	32.18	24.76	420.0	4.72	34.09	26.99	812.0	3.67	34.31	27.27
47.0	9.75	32.28	24.87	425.0	4.70	34.09	26.99	819.0	3.66	34.32	27.28
48.6	9.67	32.21	24.83	431.0	4.70	34.10	27.00	824.2	3.66	34.32	27.28
49.0	9.64	32.27	24.88	436.0	4.68	34.10	27.00	830.4	3.60	34.32	27.28
50.6	9.52	32.20	24.85	441.0	4.67	34.11	27.00	835.0	3.59	34.31	27.28
55.0	9.13	32.33	25.01	447.8	4.66	34.11	27.01	840.0	3.58	34.32	27.28
60.8	8.97	32.38	25.07	452.0	4.66	34.11	27.01	846.2	3.57	34.32	27.29
65.6	8.91	32.49	25.17	457.0	4.64	34.11	27.01	851.0	3.57	34.33	27.29
71.0	8.73	32.56	25.25	462.8	4.64	34.13	27.02	856.0	3.56	34.33	27.30
77.0	8.57	32.63	25.33	467.4	4.62	34.13	27.03	861.8	3.54	34.33	27.30
82.0	8.41	32.68	25.39	472.0	4.61	34.13	27.03	867.4	3.53	34.33	27.30
88.0	8.39	32.78	25.48	477.0	4.60	34.14	27.04	874.0	3.52	34.33	27.30
93.4	8.32	32.89	25.57	483.4	4.58	34.14	27.04	879.0	3.52	34.33	27.31
98.0	8.17	32.94	25.63	488.2	4.54	34.15	27.05	885.4	3.51	34.34	27.31
104.6	8.06	32.99	25.69	493.0	4.53	34.15	27.05	890.0	3.51	34.34	27.31
109.0	8.04	33.03	25.72	499.4	4.53	34.15	27.06	895.0	3.50	34.34	27.31
114.2	8.02	33.08	25.77	504.0	4.50	34.16	27.06	901.2	3.48	34.35	27.32
119.0	7.95	33.20	25.87	509.0	4.49	34.16	27.07	906.0	3.48	34.35	27.32
124.2	7.92	33.22	25.89	515.6	4.46	34.17	27.08	911.0	3.46	34.35	27.32
129.0	7.84	33.31	25.97	520.0	4.45	34.17	27.08	916.8	3.45	34.35	27.33
134.2	7.82	33.38	26.03	525.0	4.44	34.17	27.08	921.0	3.45	34.36	27.33
139.0	7.82	33.36	26.01	530.0	4.42	34.17	27.09	926.0	3.44	34.36	27.34
146.2	7.82	33.22	25.90	535.4	4.41	34.18	27.09	931.4	3.44	34.37	27.34
151.0	7.82	33.19	25.88	540.0	4.39	34.17	27.09	936.0	3.44	34.37	27.34
156.6	7.82	33.13	25.83	545.0	4.38	34.18	27.09	941.0	3.46	34.37	27.34
161.0	7.82	33.05	25.77	551.8	4.36	34.18	27.09	947.2	3.45	34.38	27.35
166.0	7.82	32.92	25.66	556.0	4.34	34.18	27.10	952.2	3.44	34.38	27.35
171.8	7.82	32.80	25.57	561.0	4.32	34.18	27.10	957.0	3.44	34.38	27.35
176.0	7.82	32.74	25.53	566.0	4.30	34.18	27.10	962.6	3.53	34.40	27.35
181.0	7.82	32.66	25.47	572.0	4.29	34.18	27.11	967.0	3.52	34.41	27.37
187.2	7.82	32.56	25.38	577.0	4.28	34.19	27.11	973.2	3.53	34.41	27.37
192.0	7.82	32.48	25.32	582.0	4.28	34.19	27.11	978.0	3.52	34.42	27.37
197.0	7.82	32.41	25.27	587.0	4.26	34.19	27.12	984.4	3.51	34.42	27.37
202.8	7.82	32.24	25.14	592.0	4.25	34.19	27.12	989.0	3.51	34.42	27.37
207.0	7.82	32.18	25.08	597.0	4.17	34.20	27.13	994.0	3.51	34.42	27.37
212.0	7.82	32.08	25.01	602.0	4.13	34.20	27.13	1000.8	3.50	34.42	27.37

Table A3. (continued)

CTD Data for Station JT96-04

Depth (m)	Temperature (°C)	Salinity (psu)	Sigma-t	Depth (m)	Temperature (°C)	Salinity (psu)	Sigma-t
0.0	14.68	31.30	23.19	185.6	6.74	33.89	26.58
1.6	14.69	31.29	23.18	190.0	6.68	33.91	26.60
2.0	14.69	31.29	23.18	195.0	6.60	33.93	26.63
3.0	14.69	31.29	23.18	200.4	6.53	33.94	26.65
4.6	14.69	31.28	23.18	206.0	6.40	33.95	26.68
5.0	14.67	31.28	23.18	211.0	6.29	33.96	26.70
7.2	13.67	31.65	23.66	216.4	6.19	33.97	26.72
8.0	13.56	31.65	23.69	221.0	6.11	33.97	26.73
9.0	13.41	31.65	23.72	227.2	6.06	33.98	26.74
10.0	13.21	31.62	23.74	232.0	6.00	33.98	26.75
11.8	12.96	31.63	23.79	237.8	5.92	33.99	26.76
12.2	12.93	31.64	23.80	242.0	5.89	33.98	26.76
13.0	12.42	31.68	23.94	247.0	5.82	33.98	26.77
14.0	11.73	31.73	24.10	252.2	5.79	33.98	26.77
15.0	11.56	31.75	24.15	257.0	5.70	33.98	26.79
16.8	11.05	31.82	24.29	263.2	5.65	33.98	26.79
17.0	10.98	31.82	24.30	268.2	5.60	33.98	26.80
18.0	10.79	31.86	24.36	274.2	5.52	33.98	26.81
19.0	10.59	31.87	24.41	279.0	5.50	33.98	26.81
20.0	10.45	31.92	24.48	284.2	5.43	34.00	26.83
21.0	10.25	31.97	24.54	291.2	5.41	34.00	26.83
22.0	10.11	32.01	24.60	297.2	5.36	34.00	26.84
23.0	10.07	32.12	24.69	302.0	5.34	34.00	26.84
24.2	9.87	32.10	24.71	307.4	5.34	34.00	26.85
25.0	9.72	32.12	24.75	312.0	5.34	34.01	26.85
26.4	9.47	32.12	24.79	318.0	5.34	34.01	26.85
27.0	9.55	32.13	24.79	323.0	5.33	34.01	26.85
28.8	9.38	32.18	24.85	328.6	5.34	34.01	26.85
29.0	9.39	32.19	24.86	333.0	5.34	34.01	26.85
30.0	9.37	32.24	24.90	339.0	5.35	34.01	26.85
31.0	9.31	32.24	24.91	344.0	5.32	34.02	26.86
32.2	9.45	32.29	24.92	349.0	5.27	34.03	26.88
33.0	9.59	32.33	24.93	354.8	5.25	34.03	26.88
34.0	9.52	32.33	24.95	359.0	5.24	34.03	26.88
35.0	9.63	32.41	24.99	365.0	5.22	34.03	26.88
36.0	9.45	32.43	25.04	370.0	5.19	34.04	26.89
37.0	9.34	32.45	25.07	375.4	5.15	34.04	26.90
38.0	9.29	32.46	25.08	380.2	5.11	34.05	26.91
39.0	9.25	32.46	25.09	386.2	5.08	34.06	26.92
40.0	9.22	32.47	25.11	391.0	5.04	34.06	26.92
41.0	9.17	32.48	25.12	396.2	5.02	34.06	26.93
42.0	9.14	32.48	25.13	401.0	4.99	34.06	26.93
43.6	9.09	32.49	25.14	406.0	4.96	34.07	26.94
44.0	9.00	32.50	25.16	411.0	4.93	34.08	26.95
45.0	8.94	32.51	25.18				
46.6	8.81	32.53	25.22				
47.0	8.80	32.54	25.22				
48.0	8.80	32.54	25.22				
49.8	8.77	32.56	25.24				
50.0	8.77	32.55	25.24				
55.0	8.48	32.63	25.35				
60.0	8.40	32.68	25.39				
67.8	8.18	32.83	25.55				
72.0	8.13	32.87	25.58				
77.0	7.89	32.92	25.66				
82.0	7.97	32.99	25.70				
87.0	7.92	33.03	25.74				
93.2	7.92	33.07	25.77				
98.0	7.80	33.25	25.93				
103.2	7.74	33.37	26.03				
109.4	7.74	33.43	26.08				
114.0	7.69	33.50	26.14				
119.0	7.69	33.54	26.17				
125.2	7.75	33.59	26.20				
130.0	7.80	33.64	26.23				
136.2	7.66	33.70	26.30				
141.0	7.52	33.72	26.33				
147.4	7.39	33.76	26.39				
152.0	7.24	33.78	26.43				
157.0	7.09	33.80	26.46				
163.6	6.95	33.84	26.51				
168.0	6.91	33.85	26.53				
174.4	6.86	33.86	26.54				
179.0	6.79	33.88	26.56				

Table A3. (continued)

CTD Data for Station JT96-06

Depth (m)	Temperature (°C)	Salinity (psu)	Sigma-t	Depth (m)	Temperature (°C)	Salinity (psu)	Sigma-t	Depth (m)	Temperature (°C)	Salinity (psu)	Sigma-t
0.0	13.12	31.78	23.88	229.6	6.06	33.98	26.74	623.0	4.43	34.22	27.12
1.0	13.12	31.73	23.84	234.0	6.03	33.99	26.75	629.0	4.42	34.23	27.13
3.2	13.11	31.79	23.89	240.0	5.97	33.99	26.76	634.0	4.41	34.23	27.13
4.0	13.10	31.80	23.89	245.0	5.84	33.99	26.77	639.0	4.41	34.23	27.13
6.4	13.12	31.79	23.88	250.0	5.82	33.99	26.78	644.2	4.40	34.24	27.14
7.0	13.12	31.78	23.88	256.0	5.80	34.00	26.78	649.0	4.38	34.24	27.14
8.0	13.12	31.79	23.88	261.0	5.72	34.00	26.80	654.0	4.38	34.24	27.14
10.2	13.12	31.79	23.88	266.0	5.64	34.00	26.81	659.0	4.37	34.24	27.14
11.0	13.12	31.79	23.89	271.6	5.62	34.00	26.81	664.2	4.35	34.25	27.15
13.6	13.03	31.79	23.90	276.0	5.60	34.00	26.82	669.0	4.32	34.25	27.16
14.0	13.03	31.79	23.90	281.0	5.59	34.00	26.82	674.0	4.31	34.25	27.16
15.0	12.98	31.81	23.93	286.0	5.53	34.01	26.82	679.4	4.28	34.26	27.17
16.6	12.86	31.79	23.93	292.6	5.45	34.01	26.84	684.0	4.28	34.26	27.17
17.0	12.85	31.79	23.94	297.0	5.43	34.01	26.84	689.0	4.26	34.27	27.18
18.0	12.37	31.82	24.05	302.0	5.42	34.01	26.84	694.0	4.25	34.27	27.18
19.0	12.14	31.80	24.08	307.0	5.39	34.01	26.85	699.0	4.23	34.28	27.19
20.6	11.48	31.86	24.25	312.0	5.38	34.02	26.85				
21.0	11.38	31.86	24.26	317.8	5.33	34.02	26.86				
22.0	11.37	31.85	24.26	322.2	5.32	34.02	26.86				
23.0	11.33	31.86	24.27	327.0	5.29	34.02	26.87				
25.2	11.02	31.88	24.35	332.0	5.26	34.03	26.88				
26.0	10.97	31.88	24.36	337.0	5.23	34.03	26.88				
27.0	10.83	31.92	24.41	343.4	5.22	34.03	26.88				
28.6	10.22	32.01	24.58	348.4	5.22	34.04	26.89				
29.0	10.20	32.01	24.59	353.0	5.18	34.05	26.90				
30.0	9.98	32.05	24.66	358.0	5.18	34.05	26.90				
31.0	9.95	32.06	24.66	364.2	5.13	34.06	26.91				
32.8	9.86	32.10	24.71	369.0	5.11	34.05	26.91				
33.0	9.85	32.11	24.72	374.0	5.08	34.06	26.92				
34.0	9.71	32.16	24.79	379.0	5.00	34.05	26.93				
36.6	9.61	32.21	24.83	384.0	4.99	34.06	26.93				
37.0	9.61	32.21	24.83	390.0	4.97	34.06	26.94				
38.0	9.60	32.21	24.84	395.0	4.92	34.07	26.95				
39.0	9.56	32.22	24.86	402.6	4.88	34.07	26.95				
40.4	9.50	32.24	24.88	407.0	4.84	34.07	26.96				
41.0	9.44	32.25	24.90	412.0	4.82	34.07	26.96				
42.0	9.38	32.28	24.93	418.2	4.82	34.09	26.97				
45.4	9.28	32.32	24.97	423.0	4.81	34.09	26.98				
48.2	9.17	32.37	25.03	428.0	4.79	34.09	26.98				
49.0	9.19	32.38	25.04	434.8	4.77	34.10	26.99				
50.0	9.14	32.40	25.06	439.0	4.76	34.10	26.99				
57.2	8.74	32.53	25.23	444.0	4.75	34.10	26.99				
62.0	8.56	32.60	25.30	450.2	4.73	34.10	26.99				
69.0	8.46	32.65	25.36	455.0	4.71	34.11	27.00				
74.0	8.30	32.75	25.46	460.0	4.67	34.11	27.00				
80.8	8.23	32.82	25.53	466.8	4.65	34.11	27.01				
85.0	8.11	32.94	25.64	471.0	4.64	34.11	27.01				
90.0	8.05	32.99	25.69	476.0	4.61	34.11	27.01				
97.8	7.85	33.18	25.87	482.6	4.56	34.12	27.03				
102.0	7.83	33.26	25.94	487.0	4.54	34.12	27.03				
107.4	7.80	33.36	26.02	492.0	4.53	34.13	27.03				
112.0	7.74	33.43	26.08	499.0	4.52	34.13	27.04				
117.0	7.68	33.49	26.13	504.0	4.51	34.14	27.05				
122.0	7.59	33.56	26.20	510.0	4.51	34.15	27.06				
127.0	7.51	33.61	26.25	515.0	4.53	34.15	27.06				
132.0	7.44	33.64	26.29	522.6	4.54	34.16	27.06				
137.0	7.39	33.71	26.35	527.0	4.56	34.16	27.06				
142.6	7.29	33.75	26.40	532.0	4.57	34.16	27.06				
147.0	7.24	33.77	26.42	537.6	4.58	34.17	27.06				
152.2	7.19	33.80	26.44	542.0	4.59	34.17	27.06				
157.4	6.97	33.85	26.52	547.0	4.59	34.17	27.06				
162.0	6.91	33.86	26.53	554.2	4.59	34.17	27.06				
168.2	6.87	33.87	26.54	559.0	4.58	34.17	27.07				
173.0	6.80	33.89	26.57	565.4	4.58	34.18	27.08				
178.4	6.78	33.89	26.58	570.0	4.56	34.19	27.08				
183.1	6.72	33.90	26.59	575.0	4.54	34.19	27.08				
188.0	6.62	33.93	26.62	580.0	4.55	34.19	27.09				
193.1	6.58	33.93	26.63	585.0	4.55	34.20	27.09				
198.0	6.53	33.93	26.64	590.0	4.54	34.20	27.09				
203.1	6.47	33.95	26.66	595.0	4.52	34.21	27.10				
209.8	6.37	33.97	26.69	602.0	4.50	34.21	27.11				
214.0	6.31	33.99	26.71	607.0	4.49	34.21	27.11				
219.0	6.20	33.98	26.72	613.8	4.48	34.22	27.11				
224.0	6.11	33.98	26.73	618.0	4.46	34.22	27.12				

190

CTD Data for Station JT96-09

Depth (m)	Temperature (°C)	Salinity (psu)	Sigma-t	Depth (m)	Temperature (°C)	Salinity (psu)	Sigma-t	Depth (m)	Temperature (°C)	Salinity (psu)	Sigma-t
0.0	14.59	31.52	23.38	208.0	6.66	33.94	26.63	599.0	4.34	34.17	27.09
1.0	14.59	31.52	23.38	213.0	6.59	33.94	26.64	604.8	4.32	34.17	27.09
3.0	14.60	31.52	23.38	218.2	6.53	33.94	26.65	609.0	4.32	34.17	27.09
4.0	14.59	31.53	23.38	223.0	6.50	33.94	26.65	615.8	4.32	34.17	27.10
6.2	14.59	31.52	23.38	228.4	6.45	33.95	26.66	620.2	4.31	34.17	27.10
7.0	14.58	31.54	23.40	233.0	6.43	33.94	26.66	625.0	4.29	34.18	27.10
8.0	14.52	31.57	23.43	238.8	6.38	33.95	26.68	630.6	4.29	34.18	27.10
9.4	14.32	31.58	23.48	243.0	6.31	33.95	26.69	635.0	4.26	34.19	27.11
10.0	14.32	31.58	23.48	250.4	6.21	33.95	26.70	641.8	4.23	34.19	27.12
12.8	14.29	31.58	23.48	255.0	6.17	33.95	26.70	646.0	4.22	34.19	27.12
13.0	14.27	31.59	23.50	260.4	6.11	33.95	26.71	651.0	4.21	34.19	27.12
15.4	14.18	31.62	23.54	265.0	6.06	33.96	26.72	657.6	4.21	34.20	27.13
16.0	14.19	31.63	23.54	271.2	5.98	33.97	26.74	662.0	4.19	34.20	27.13
17.0	14.11	31.69	23.61	276.0	5.93	33.97	26.75	667.0	4.18	34.21	27.14
18.8	13.95	31.75	23.68	282.2	5.91	33.96	26.75	672.8	4.17	34.21	27.14
19.0	13.97	31.72	23.66	287.0	5.91	33.96	26.75	677.0	4.15	34.22	27.15
20.0	13.91	31.75	23.69	292.6	5.87	33.97	26.75	683.2	4.14	34.22	27.15
21.8	13.77	31.92	23.86	297.0	5.82	33.97	26.76	688.0	4.14	34.23	27.16
22.0	13.73	31.95	23.89	303.0	5.78	33.98	26.77	695.0	4.14	34.23	27.16
23.0	13.04	32.12	24.16	308.0	5.76	33.98	26.78	700.2	4.10	34.24	27.17
24.0	12.78	32.19	24.26	313.0	5.75	33.99	26.79	707.2	4.10	34.25	27.18
25.0	12.44	32.54	24.60	319.0	5.68	33.99	26.79	712.0	4.09	34.25	27.18
26.0	12.34	32.41	24.51	324.0	5.65	34.00	26.80	717.0	4.09	34.26	27.19
27.0	12.23	32.33	24.47	329.0	5.62	33.99	26.81	723.0	4.08	34.26	27.19
28.8	11.71	32.43	24.65	335.0	5.59	34.00	26.81	728.0	4.06	34.27	27.20
29.0	11.72	32.44	24.65	340.0	5.56	34.00	26.82	733.0	4.06	34.27	27.20
30.0	11.64	32.50	24.71	345.0	5.54	34.01	26.83	738.6	4.05	34.28	27.21
31.0	11.51	32.46	24.71	351.8	5.50	34.01	26.83	743.0	4.05	34.28	27.21
32.2	11.29	32.56	24.83	356.0	5.48	34.01	26.83	748.2	4.03	34.29	27.22
33.0	11.19	32.69	24.95	361.0	5.45	34.02	26.85	754.2	4.03	34.29	27.22
34.0	11.12	32.46	24.78	366.0	5.44	34.02	26.85	759.0	4.02	34.30	27.22
36.2	11.00	32.53	24.85	372.0	5.42	34.02	26.85	764.2	4.00	34.30	27.23
37.0	10.94	32.51	24.85	377.0	5.40	34.03	26.86	770.2	3.99	34.30	27.23
39.6	10.81	32.47	24.84	382.0	5.35	34.03	26.87	775.0	3.96	34.31	27.24
40.0	10.80	32.47	24.84	387.8	5.30	34.04	26.88	780.2	3.95	34.32	27.25
41.0	10.84	32.47	24.83	392.0	5.29	34.03	26.87	786.6	3.94	34.32	27.25
42.8	10.63	32.47	24.87	397.0	5.25	34.04	26.88	791.0	3.94	34.32	27.25
43.0	10.61	32.47	24.88	402.0	5.20	34.04	26.89	796.2	3.93	34.32	27.26
44.0	10.55	32.47	24.88	408.0	5.15	34.04	26.90	801.8	3.92	34.33	27.26
45.0	10.49	32.47	24.90	413.0	5.12	34.05	26.91	806.0	3.90	34.33	27.27
46.0	10.41	32.48	24.92	418.0	5.11	34.04	26.90	811.0	3.90	34.34	27.27
47.0	10.34	32.47	24.92	424.6	5.10	34.04	26.91	816.0	3.90	34.34	27.27
48.0	10.27	32.47	24.93	429.0	5.10	34.05	26.91	822.2	3.89	34.34	27.27
49.8	10.07	32.59	25.06	434.0	5.05	34.05	26.92	827.0	3.89	34.34	27.27
50.0	10.03	32.50	24.99	439.0	5.04	34.06	26.92	832.0	3.89	34.34	27.27
55.0	9.73	32.50	25.04	445.2	5.02	34.06	26.93	841.0	3.89	34.34	27.28
60.6	9.40	32.49	25.09	450.0	5.00	34.06	26.93	846.0	3.88	34.34	27.28
65.0	9.27	32.51	25.13	456.4	4.96	34.07	26.95	852.6	3.88	34.34	27.28
72.0	9.04	32.55	25.19	461.0	4.93	34.09	26.96	857.0	3.89	34.34	27.28
77.0	8.72	32.65	25.32	466.0	4.88	34.08	26.96	862.0	3.88	34.35	27.28
82.8	8.37	32.74	25.45	472.4	4.85	34.09	26.97	867.6	3.85	34.35	27.29
87.0	8.17	32.82	25.54	477.0	4.82	34.10	26.98	872.2	3.83	34.36	27.29
92.0	8.28	32.89	25.57	484.2	4.80	34.10	26.98	877.0	3.80	34.36	27.30
97.4	8.08	33.11	25.78	489.0	4.75	34.10	26.99	885.4	3.78	34.37	27.31
102.0	7.88	33.28	25.94	495.0	4.70	34.10	26.99	890.2	3.76	34.37	27.31
108.0	7.92	33.36	26.00	500.0	4.68	34.10	27.00	895.0	3.73	34.38	27.32
113.0	7.89	33.44	26.06	505.6	4.68	34.10	27.00	900.0	3.72	34.38	27.32
119.4	7.83	33.55	26.16	510.0	4.68	34.10	27.00				
124.0	7.71	33.64	26.24	515.0	4.70	34.12	27.01				
129.6	7.67	33.68	26.29	521.2	4.66	34.12	27.02				
134.0	7.61	33.71	26.32	526.0	4.67	34.13	27.02				
140.8	7.51	33.78	26.39	531.6	4.66	34.13	27.03				
145.0	7.40	33.81	26.42	536.2	4.64	34.14	27.03				
150.0	7.36	33.81	26.43	541.0	4.62	34.14	27.03				
155.4	7.33	33.83	26.45	546.0	4.58	34.14	27.04				
160.0	7.28	33.84	26.46	551.2	4.57	34.15	27.05				
166.0	7.17	33.86	26.50	556.2	4.55	34.15	27.05				
171.0	7.12	33.87	26.51	562.2	4.50	34.15	27.06				
177.2	7.02	33.88	26.54	567.0	4.44	34.15	27.07				
182.0	6.96	33.90	26.56	572.2	4.44	34.15	27.06				
187.8	6.88	33.91	26.58	578.0	4.42	34.16	27.07				
192.0	6.83	33.92	26.59	583.0	4.40	34.16	27.07				
197.0	6.78	33.93	26.60	589.0	4.38	34.16	27.08				
203.8	6.71	33.93	26.62	594.0	4.37	34.16	27.08				

Table A4. Dissolved oxygen data for Stations JT96-01, 2, 4, 5, 6 and 9.

Station JT96-01

Depth (m)	Oxygen (ml/L)	Oxygen (μmol/L)
10	7.69	343.49
20	5.88	262.56
30	5.44	242.79
50	4.49	200.48
75	3.02	134.73
100	2.72	121.39
115	2.38	106.22

Station JT96-05

Depth (m)	Oxygen (ml/L)	Oxygen (μmol/L)
100	4.93	220.25
300	2.31	103.00
450	1.24	55.18
650	0.72	32.19
800	0.41	18.39
900	0.52	22.99
1000	0.45	20.23
1100	0.41	18.39
1250	0.42	18.85
1400	0.63	28.05
1720	1.19	53.34

Station JT96-02

Depth (m)	Oxygen (ml/L)	Oxygen (μmol/L)
25	5.92	264.40
50	6.06	270.38
75	5.56	248.30
100	5.01	223.47
200	2.18	97.48
400	0.95	42.30
600	0.52	22.99
800	0.36	16.09
1000	0.37	16.55
1200	0.37	16.55
1240	0.43	19.31

Station JT96-06

Depth (m)	Oxygen (ml/L)	Oxygen (μmol/L)
10	6.34	283.25
50	4.39	195.88
100	4.44	198.18
200	2.12	94.72
300	1.56	69.43
400	1.03	45.98
500	0.72	32.19
550	0.60	26.67
600	0.52	22.99
650	0.46	20.69
700	0.41	18.39

Station JT96-04

Depth (m)	Oxygen (ml/L)	Oxygen (μmol/L)
10	6.76	301.64
20	6.31	281.87
30	5.72	255.20
50	4.99	222.55
75	5.30	236.81
100	n.a.	n.a.
150	2.91	130.13
200	2.08	92.88
300	1.59	70.81
350	1.35	60.24
410	0.98	43.68

Station JT96-09

Depth (m)	Oxygen (ml/L)	Oxygen (μmol/L)
10	6.19	276.35
20	6.20	276.81
30	6.79	303.02
50	6.72	299.80
75	6.28	280.49
100	4.33	193.13
200	2.73	121.85
400	1.29	57.48
600	0.58	25.75
800	0.35	15.63
900	0.32	14.25

Table A5. Magnetic Susceptibility Data for Sediment Cores from Stations JT96-02, 5, 6 and 9.

Piston Core JT96-02		Piston Core JT95-05 (1)		Piston Core JT96-05 (2)		Piston Core JT96-05 (4)		Trigger Core JT96-05 (3)	
Depth (cm)	Mag. Susc.	Depth (cm)	Mag. Susc.	Depth (cm)	Mag. Susc.	Depth (cm)	Mag. Susc.	Depth (cm)	Mag. Susc.
5	0.93	5	0.75	5	1.89	5	1.69	5	0.99
10	1.22	10	0.92	10	2.07	10	2.44	10	1.10
15	1.63	15	0.90	15	2.35	15	3.48	15	1.16
20	2.16	20	0.90	20	2.74	20	3.48	20	1.27
25	2.27	25	0.92	25	3.18	25	3.30	25	1.34
30	2.24	30	0.88	30	3.54	30	3.47	30	1.47
35	2.47	35	0.86	35	4.01	35	3.91	35	1.58
40	3.13	40	0.89	40	3.53	40	5.69	40	1.59
45	3.83	45	1.11	45	3.29	45	4.99	45	1.62
50	3.71	50	1.04	50	3.83	50	2.56	50	1.81
55	4.05	55	1.10	55	4.16	55	2.01	55	1.92
60	4.43	60	1.16	60	4.09	60	1.93	60	2.06
65	4.42	65	1.16	65	5.23	65	1.17	65	2.26
70	5.16	70	1.21	70	4.90	70	0.86	70	2.33
75	5.37	75	1.37	75	4.97	75	0.91	75	2.38
80	5.48	80	1.47	80	5.12	80	0.74	80	2.57
85	4.35	85	1.46	85	4.95	85	0.58	85	2.49
90	2.62	90	1.31	90	4.77	90	0.53	90	2.68
95	2.22	95	1.48	95	4.89	95	0.59	95	2.68
100	2.26	100	1.75	100	5.57	100	0.70	100	2.44
105	2.40	105	1.89	105	5.45	105	0.47	105	1.84
110	2.17	110	1.95	110	4.64	110	0.47	110	1.27
115	2.27	115	2.02	115	4.13	115	0.72	115	1.22
120	2.25	120	2.10	120	3.94	120	0.97	120	1.28
125	2.37	125	2.68	125	4.26	125	1.07	125	1.30
130	2.34	130	3.10	130	4.36	130	1.07	130	1.30
135	2.25	135	3.49	135	4.38	135	0.72		
140	2.31	140	3.32	140	3.91	140	0.67		
145	2.32	145	4.24	145	3.66	145	0.76		
150	2.30	150	4.72			150	0.80		
155	2.25	155	2.78			155	0.68		
160	2.35					160	0.62		
165	2.40					165	0.58		
170	2.26					170	0.62		
175	2.12					175	0.73		
180	2.34					180	0.85		
185	2.23					185	0.72		
190	2.21					190	0.62		
195	2.45					195	0.67		
200	2.57					200	0.64		
205	2.32					205	0.30		

Table A5. (continued)

Piston Core JT96-06   Piston Core JT96-09

Depth (cm)	Mag. Susc.	Depth (cm)	Mag. Susc.
5	2.52	5	1.20
10	2.37	10	1.47
15	1.71	15	1.50
20	2.41	20	1.41
25	2.58	25	1.25
30	2.75	30	1.04
35	2.70	35	0.92
40	3.52	40	0.90
45	3.19	45	1.06
50	3.24	50	1.69
55	2.56	55	2.19
60	2.19	60	2.54
65	2.19	65	2.99
70	2.44	70	2.85
75	2.59	75	1.33
80	2.14	80	1.51
85	1.83	85	1.60
90	1.78	90	1.57
95	1.86	95	1.58
100	1.82	100	1.58
105	2.23	105	1.62
110	2.34	110	1.66
115	2.35	115	1.68
120	2.46	120	1.69
125	2.46	125	1.73
130	2.43	130	2.02
135	2.48	135	3.01
140	2.72	140	4.20
145	2.77	145	4.45
150	2.58	150	2.63
155	2.34	155	2.32
160	2.25	160	2.30
165	2.12	165	2.63
170	2.52	170	2.73
175	2.81	175	2.39
180	2.80	180	2.15
185	2.43	185	2.52
190	2.05	190	2.77
195	2.78	195	2.81
200	3.10	200	2.91
205	2.95	205	2.90
210	2.84	210	2.74
215	2.45	215	2.72
220	2.57	220	2.74
225	2.48	225	2.29
230	2.46	230	n.a.
235	2.60	235	2.77
240	2.86	240	2.68
245	2.81	245	2.51
250	2.57	250	2.74
255	2.62	255	2.62
260	2.90	260	2.66
265	2.68	265	2.60
270	2.94	270	3.09
275	2.92	275	2.70
280	3.10	280	2.53
285	3.43	285	2.63
290	3.30	290	2.63
295	4.31	295	2.61
300	5.22	300	2.54
305	4.48	305	2.77
310	3.00	310	2.93
		315	2.78
		320	2.61
		325	2.57
		330	2.91
		335	2.81
		340	2.75
		345	2.86
		350	2.89
		355	3.07
		360	2.65
		365	2.56
		370	2.40

194

Table A6. Radiocarbon Data for Planktonic and Benthic Foraminifera, and Bulk Organic Carbon.

Core / Sample	Depth (cm)	Corrected Depth (cm)	Calendar Age (kyr B.P.)	^{14}C Age Mixed Planktonics	^{14}C Age Benthic Foraminifera Uvigerina spp.	Bolivina argentea	^{14}C Age Organic Carbon	CAMS#[4]
JT96-01								
35-38 mc	36.5		0.92[1]				1780 ± 30	67353
JT96-02								
101-103 pc	102.0		14.09[2]	13280 ± 60				70907
201-203 pc	202.0		15.68[2]	14240 ± 60				70908
JT96-05								
46-48 bc	47.0		10.29[1]	9960 ± 50				60245
JT96-09								
38-40 mc	39.0	39.0			9830 ± 110		9920 ± 40	40427, 56704
20-21 pc	20.5	32.5			10050 ± 110			40426
35-36 pc	35.5	47.5	10.03[1]	9760 ± 70	10710 ± 60	10650 ± 90		60240, 60241, 62464
36-37 pc	36.5	48.5					11390 ± 80	78516
45-46 pc	45.5	57.5		9360 ± 240		10910 ± 70[3]		78456, 78457
65-66 pc	65.5	77.5	12.24[1]	11210 ± 120		12380 ± 280[3]		42160, 78458
66-67 pc	66.5	78.5					14790 ± 450	78517
75-76 pc	75.5	87.5	12.73[1]	11500 ± 110		12110 ± 80		60242, 62465
90-91 pc	90.5	102.5	12.84[1]	11600 ± 80		12700 ± 70[3]		60243, 78459
96-97 pc	96.5	108.5					15660 ± 70	62468
100-101 pc	100.5	112.5	13.17[2]	12460 ± 120		13170 ± 100		40428, 48152
130-131 pc	130.5	142.5	13.43[2]	12640 ± 90		13500 ± 80		62466, 62797
165-166 pc	165.5	161.5		10090 ± 50	13210 ± 150			60244, 62469
166-167 pc	166.5	162.5		9850 ± 70			24480 ± 120	62467, 62471
170-171 pc	170.5	166.5		13240 ± 200				62798
265-266 pc	265.5	261.5	14.14[2]	13410 ± 80	14290 ± 110			40430, 42161
266-267 pc	266.5	262.5					24500 ± 120	62469
290-291 pc	290.5	286.5	14.30[2]	13520 ± 70	14350 ± 120			40431, 42162
350-351 pc	350.5	346.5	15.57[2]	14140 ± 70	14830 ± 280			40432, 78460
351-352 pc	351.5	347.5					21440 ± 100	57327
370-371 pc	370.5	366.5					20320 ± 90	57104
Tul96-05								
31-32 pc	31.5	77.5					3760 ± 40	58708
199-200 pc	199.5	234.5	10.13[1]	9800 ± 90	11150 ± 70			58463, 58460
200-201 pc	200.5	235.5		11200 ± 340	11140 ± 60			57558, 57324
290-291 pc	290.5	306.5		28120 ± 390	28980 ± 290			58463, 58461
360-361 pc	360.5	371.5		32590 ± 1000	32900 ± 740			58465, 58462
480-481 pc	480.5	481.5		38400 ± 1200	38300 ± 2600			57325, 57326

[1] Calculated using Calib 4.3 (Stuiver et al., 1998) and a reservoir age of 800 yrs.
[2] Calculated using Calib 4.3 (Stuiver et al., 1998) and a reservoir age of 1100 yrs.

[3] For sample 45-46 the species was *Bolivina spicca* (not *Bolivina argentea*) and for samples 65-66 and 90-91 a mixture of Bolivina species were used.

[4] Lawrence Livermore laboratory reference number

Table A7. ^{210}Pb data for multicores (mc) JT96-01, 02 and 09

Multicore JT96-01

Sample	Depth (cm)	Total ^{210}Pb (dpm/g)	Excess ^{210}Pb (dpm/g)
0-1 mc	0.5	24.47	22.65
2-3 mc	2.5	20.27	18.45
4-5 mc	4.5	20.32	18.50
6-8 mc	7.0	21.20	19.37
10-12 mc	11.0	18.94	17.12
14-16 mc	15.0	18.28	16.46
18-20 mc	19.0	13.21	11.38
25-30 mc	27.5	4.00	2.17
35-38 mc	36.5	1.82	0.00

Multicore JT96-02

Sample	Depth (cm)	Total ^{210}Pb (dpm/g)	Excess ^{210}Pb (dpm/g)
0-1 mc	0.5	58.84	56.06
2-3 mc	2.5	27.50	24.71
4-5 mc	4.5	17.74	15.95
6-8 mc	7.0	9.19	6.41
10-12 mc	11.0	3.80	1.02
14-16 mc	15.0	2.22	-0.57
18-20 mc	19.0	2.79	0.00

Multicore JT96-09

Sample	Depth (cm)	Total ^{210}Pb (dpm/g)	Excess ^{210}Pb (dpm/g)
0-2 mc	1.0	23.64	22.04
2-3 mc	2.5	38.23	36.63
4-5 mc	4.5	17.50	15.90
6-8 mc	7.0	9.41	7.51
8-10 mc	9.0	12.16	10.56
14-16 mc	15.0	6.62	5.02
18-20 mc	19.0	1.93	0.34
24-26 mc	25.0	1.37	-0.22
28-30 mc	29.0	1.60	0.00
34-36 mc	35.0	1.54	-0.06
38-40 mc	39.0	1.77	0.17

Table A8. Stable Isotope Data for Foraminifera from Cores JT96-02pc, 06pc, 09mc and 09pc, and Tul96-05pc, 03tc and 03pc.

Data for Piston Core (pc) JT96-02.

Sample	Depth (cm)	Calendar Age (kyrs)	Uvigerina spp. δ¹³C	δ¹⁸O	Bolivina argentea δ¹³C	δ¹⁸O	Bolivina pacifica δ¹³C	δ¹⁸O	N. pachyderma δ¹³C	δ¹⁸O	G. bulloides δ¹³C	δ¹⁸O
1-3 pc	2.0											
11-13 pc	12.0											
21-23 pc	22.0											
31-33 pc	32.0											
41-43 pc	No sample											
51-53 pc	No sample											
61-63 pc	No sample											
71-73 pc	No sample											
81-83 pc	No sample											
91-93 pc	92.0											
101-103 pc	102.0											
111-113 pc	112.0											
121-123 pc	122.0											
131-133 pc	132.0											
141-143 pc	142.0											
151-153 pc	152.0		-1.13	4.40	-1.30	3.94						
161-163 pc	162.0		-1.21	4.42	-1.21	4.08						
171-173 pc	172.0		-1.10	4.43								
181-183 pc	182.0		-1.05	4.39	-1.55	3.81						
191-193 pc	192.0											
210-203 pc	212.0				-1.49	4.06						

Data for Piston Core (pc) JT96-06.

Sample	Depth (cm)	Calendar Age (kyrs)	Uvigerina spp. δ¹³C	δ¹⁸O	Bolivina argentea δ¹³C	δ¹⁸O	Bolivina pacifica δ¹³C	δ¹⁸O	N. pachyderma δ¹³C	δ¹⁸O	G. bulloides δ¹³C	δ¹⁸O
0-1 pc	0.5											
10-11 pc	11.5											
20-21 pc	21.5		-0.79	3.66								
30-31 pc	31.5				-0.99	3.55						
40-41 pc	41.5		-0.89	3.26	-1.12	3.55						
50-51 pc	51.5											
60-61 pc	61.5		-0.65	3.24	-1.14	3.29						
70-71 pc	71.5				-0.9	3.64						
80-81 pc	81.5				-0.78	3.75						
90-91 pc	91.5				-0.87	3.22						
100-101 pc	101.5		-0.75	3.97	-0.95	3.66						
110-111 pc	111.5		-0.82	3.39								
120-121 pc	121.5											
130-131 pc	131.5		-0.56	3.08	-0.55	3.71						
140-141 pc	141.5											
150-151 pc	151.5		-0.95	3.30								
160-161 pc	161.5		-1.14	3.24								
170-171 pc	171.5		-1.20	3.75								
180-181 pc	181.5		-0.95	3.44								
190-191 pc	191.5											
200-201 pc	201.5		-1.32	3.15								
210-211 pc	211.5		-1.35	3.70								
220-221 pc	221.5											
230-231 pc	231.5		-1.07	2.74								
240-241 pc	241.5											
250-251 pc	251.5		-0.47	2.79								
260-261 pc	261.5		-1.35	3.62								
270-271 pc	271.5		-0.94	3.88								
280-281 pc	281.5		-1.26	3.87								
290-291 pc	291.5		-1.27	3.87								
300-301 pc	301.5		-1.33	3.95								
310-311 pc	309.5		-1.24	3.99								

Table A8. (continued)

Data for Multicore (mc) and Piston Core (pc) JT96-09.

Sample	Depth * (cm, corr)	Calendar Age (kyrs)	Uvigerina spp.		Bolivina argentea		Bolivina pacifica		N. pachyderma		G. bulloides	
			δ^{13}C	δ^{18}O	δ^{13}C	δ^{18}O	δ^{13}C	δ^{18}O	δ^{13}C	δ^{18}O	δ^{13}C	δ^{18}O
24-26 mc	25.0	5.28	-1.23	3.02								
15-16 pc	27.5	5.81	-0.83	2.96								
30-32 mc	31.0	6.54	-0.94	2.96	-0.97	2.87						
20-21 pc	32.5	6.86	-0.59	3.02	-0.89	2.93						
34-36 mc	35.0	7.39	-0.75	3.00								
25-26 pc	37.5	7.92	-0.81	3.17	-1.27	2.89	-1.04	2.86				
38-40 mc	39.0	8.23	-0.66	3.16	-0.84	3.20						
30-31 pc	42.5	8.97	-0.70	3.21	-1.12	3.06						
35-36 pc	47.5	10.03	-0.85	3.16	-0.65	3.09						
40-41 pc	52.5	10.40			-0.90	3.21						
45-46 pc	57.5	10.76					-1.57	3.14	0.42	1.25		
50-51 pc	62.5	11.13	-1.15	3.64	-1.21	3.30			0.49	1.10		
55-56 pc	67.5	11.50	-1.37	3.49								
65-66 pc	77.5	12.24	-1.20	3.34								
75-76 pc	87.5	12.73	-0.88	3.61	-1.03	3.42			0.32	1.54	0.03	1.80
80-81 pc	92.5	12.77			-1.22	3.43	-2.31	3.53	-0.09	1.03		
85-86 pc	97.5	12.80			-1.06	3.54	-2.15	3.39				
90-91 pc	102.5	12.84			-1.42	3.55			-0.06	1.36		
95-96 pc	107.5	13.00					-2.56	3.84	0.09	1.23		
100-101 pc	112.5	13.17					-2.33	3.39	0.14	1.23		
105-106 pc	117.5	13.21					-2.36	3.85	0.05	1.32		
110-111 pc	122.5	13.26							0.06	1.07		
115-116 pc	127.5	13.30					-2.68	3.84	0.13	1.53	-0.26	1.50
120-121 pc	132.5	13.35			-1.16	3.61	-2.53	3.59				
125-126 pc	137.5	13.39			-1.18	3.75			0.01	1.21		
130-131 pc	142.5	13.43			-1.48	3.58			0.22	1.36		
135-136 pc	147.5	13.46			-1.03	3.69	-2.40	3.70			-0.27	2.12
150-151 pc	148.5	13.47			-1.12	3.92			-0.23	1.84		
155-156 pc	151.5	13.49			-1.08	3.94						
160-161 pc	156.5	13.52			-1.11	3.66			0.26	2.88		
165-166 pc	161.5	13.55	-1.03	4.00					0.08	2.42	-0.14	2.75
170-171 pc	166.5	13.58	-1.04	4.02					-0.45	0.71	-0.22	0.59
175-176 pc	171.5	13.61	-1.00	4.03							-0.14	2.68
185-186 pc	181.5	13.67	-1.08	4.26					0.50	2.57	0.28	1.64
190-191 pc	186.5	13.70	-1.35	4.01							-0.32	2.46
195-196 pc	191.5	13.72	-1.20	4.16								
200-201 pc	196.5	13.75	-1.39	3.94					-0.27	2.15	-0.44	2.66
210-211 pc	206.5	13.81	-1.21	3.98							-0.37	2.62
215-216 pc	211.5	13.84							-0.23	2.35		
220-221 pc	216.5	13.87	-1.28	4.17							-0.28	2.58
260-261 pc	256.5	14.11	-1.09	4.04	-1.21	3.99						
265-266 pc	261.5	14.14							-0.15	2.20		
275-276 pc	271.5	14.21	-1.09	4.09					-0.21	2.43	-0.42	2.70
280-281 pc	276.5	14.24	-1.01	4.15					0.01	2.48	-0.24	2.60
290-291 pc	286.5	14.30	-1.01	4.11					-0.37	2.34	-0.70	2.44
300-301 pc	296.5	14.52	-0.95	4.14					-0.30	2.88	-0.60	2.85
310-311 pc	306.5	14.73	-1.10	4.14	-1.17	4.17					-0.70	2.45
320-321 pc	316.5	14.94	-1.12	4.12					-0.24	2.57	-0.48	2.18
330-331 pc	326.5	15.15							-0.07	2.42	-0.58	2.49
340-341 pc	336.5	15.36	-1.10	4.14					-0.24	2.41	-0.48	2.55
350-351 pc	346.5	15.57	-1.36	4.08					-0.32	2.50	-0.57	2.67
360-361 pc	356.5	15.78	-1.24	4.10	-1.23	4.10			-0.13	2.48	-0.55	2.47
370-371 pc	366.5	15.99							-0.03	2.64	-0.86	2.54

* Corrected Depth

Data for Trigger Core (tc) and Piston Core (pc) Tul96-03.

Sample	Depth (cm)	Calendar Age (kyrs)	Uvigerina spp.		Bolivina argentea		Bolivina pacifica		N. pachyderma		G. bulloides	
			$\delta^{13}C$	$\delta^{18}O$	$\delta^{13}C$	$\delta^{18}O$	$\delta^{13}C$	$\delta^{18}O$	$\delta^{13}C$	$\delta^{18}O$	$\delta^{13}C$	$\delta^{18}O$
5-6 tc	5.5											
10-11 tc	10.5											
15-16 tc	15.5		-1.20	3.39								
20-21 tc	20.5		-1.21	4.00								
25-26 tc	25.5											
10-11 pc	10.5											
15-16 pc	15.5											
20-21 pc	No sample											
25-26 pc	25.5											
30-31 pc	30.5											
40-41 pc	40.5											
50-51 pc	No sample											
60-61 pc	No sample											
65-66 pc	65.5											
70-71 pc	70.5											
80-81 pc	80.5											
90-91 pc	90.5											
100-101 pc	100.5											
110-111 pc	110.5											
120-121 pc	120.5		-1.74	4.00								
130-131 pc	130.5											
140-141 pc	140.5											
150-151 pc	No sample											
160-161 pc	No sample											
165-166 pc	165.5											
170-171 pc	170.5		-1.37	3.92								
180-181 pc	180.5											
190-191 pc	190.5											
200-201 pc	200.5		-1.05	3.87								
210-211 pc	210.5											
220-221 pc	220.5											
230-231 pc	230.5		-1.08	4.04								
240-241 pc	240.5											
250-251 pc	250.5											
260-261 pc	No sample											
270-271 pc	270.5											
280-281 pc	280.5											
290-291 pc	290.5											
300-301 pc	300.5		-0.97	3.68								
310-311 pc	310.5											
320-321 pc	320.5											
330-331 pc	330.5											
340-341 pc	340.5		-0.84	3.77								
350-351 pc	350.5											
360-361 pc	360.5											
370-371 pc	370.5											
380-381 pc	380.5											
390-391 pc	390.5		-0.95	3.63								
400-401 pc	400.5											
410-411 pc	410.5											
420-421 pc	420.5											
430-431 pc	430.5		-0.84	3.94								

Table A8. (continued)

Data for Piston Core (pc) Tul96-05.

Sample	Depth * (cm, corr.)	Calendar Age (kyrs)	Uvigerina spp.		Bolivina argentea		Bolivina pacifica		N. pachyderma		G. bulloides	
			δ¹³C	δ¹⁸O	δ¹³C	δ¹⁸O	δ¹³C	δ¹⁸O	δ¹³C	δ¹⁸O	δ¹³C	δ¹⁸O
10-11 pc	56.5	2.35	-0.84	2.38								
20-21 pc	66.5	2.76	-1.29	3.09								
30-31 pc	76.5	3.18										
40-41 pc	86.5	3.62										
50-51 pc	No sample											
60-61 pc	65.5	4.01										
70-71 pc	105.5	4.45	-1.30	3.22	-0.95	3.20						
80-81 pc	115.5	4.89										
90-91 pc	125.5	5.33	-1.49	2.65	-0.98	3.03						
100-101 pc	135.5	5.77	-1.26	3.04								
110-111 pc	145.5	6.21	-1.27	2.90								
120-121 pc	155.5	6.65										
130-131 pc	165.5	7.09	-1.52	2.70	-0.99	3.00			0.60	0.82	0.33	0.75
140-141 pc	175.5	7.53	-1.18	2.26							0.26	1.05
150-151 pc	185.5	7.97	-1.45	2.81	-1.23	2.91						
160-161 pc	195.5	8.41	-1.39	2.51	-1.20	2.65						
170-171 pc	205.5	8.85			-1.01	3.02						
180-181 pc	215.5	9.29			-1.19	2.94						
190-191 pc	225.5	9.73	-1.45	3.32	-1.11	3.21			0.48	1.28		
200-201 pc	235.5	10.17	-1.49	3.52	-1.23	3.25			0.18	1.09	-0.06	1.05
210-211 pc	245.5	10.61	-1.26	3.58	-0.54	3.19			0.33	1.56		
220-221 pc	No sample											
230-231 pc	Turbidite		-1.24	3.86								
240-241 pc	256.5	27.89							0.01	2.92	-0.38	3.04
250-251 pc	266.5	28.70							0.15	2.89		
260-261 pc	276.5	29.50	-1.44	4.31					-0.01	2.86	-0.27	2.84
270-271 pc	286.5	30.30							0.29	3.37	-0.11	2.28
280-281 pc	296.5	31.11							0.19	2.64		
290-291 pc	306.5	31.91	-1.34	4.21					-0.07	2.42	-0.05	2.81
300-301 pc	316.5	32.71	-1.20	4.05					0.11	2.70		
310-311 pc	326.5	33.52							0.04	2.59		
320-321 pc	336.5	34.32	-1.42	4.08					0.09	2.58	-0.05	2.60
330-331 pc	No sample											
340-341 pc	351.5	35.53							-0.09	2.38		
350-351 pc	361.5	36.33	-1.36	3.94					0.07	2.71	-0.05	2.24
360-361 pc	371.5	37.13	-1.70	4.14					-0.36	2.00	-0.43	2.25
370-371 pc	381.5	37.75	-1.71	4.28					-0.38	1.86	-0.86	1.96
380-381 pc	391.5	38.37	-1.62	4.09					-0.46	2.55	-0.82	2.32
390-391 pc	401.5	38.98	-1.41	4.17					-0.21	2.74		
400-401 pc	411.5	39.60	-1.55	3.77					0.01	2.73		
410-411 pc	421.5	40.22	-1.40	4.32					-0.39	2.61		
420-421 pc	No sample											
430-431 pc	431.5	40.83	-1.54	4.21					-0.22	2.18		
440-441 pc	441.5	41.45	-1.64	4.09					0.34	2.05		
450-451 pc	451.5	42.07	-1.40	4.26					-0.32	2.75	-0.83	2.45
460-461 pc	461.5	42.68	-1.58	4.20					-0.10	2.66	-0.33	2.82
470-471 pc	471.5	43.30	-1.51	4.26					0.05	2.50	-0.20	2.05
480-481 pc	481.5	43.92	-1.52	4.20					-0.11	2.44	-0.38	2.10
490-491 pc	491.5	44.53	-1.45	4.16					0.04	2.65		
500-501 pc	501.5	45.15	-1.63	4.19					-0.33	2.57	-0.30	2.14

Table A9. Geochemical Data for Multicore JT96-01.

General Geochemical Data for Multicore (mc) JT96-01.

Sample	Depth (cm)	Calendar Age (kyrs)	Cl⁻ (wt. %)	$\delta^{15}N$ (‰ vs air)	$\delta^{13}C_{org}$ (‰ vs PDB)	N_{tot} (wt. %)	C_{tot} (wt. %)	S_{tot} (wt. %)	$CaCO_3$ (wt. %)	C_{org} (wt. %)	C_{org}/N	Opal (wt. %)	Ba_{bio} (µg/g)
0-1 mc	0.5	0.01	4.52	4.81	-21.81	0.24	2.18	0.31	0.72	2.09	8.6	10.9	61
1-2 mc	1.5	0.04	2.56			0.22	1.95	0.24	0.60	1.88	8.7		
2-3 mc	2.5	0.06	2.73			0.22	1.97	0.24	0.64	1.89	8.7		
3-4 mc	3.5	0.09	2.30			0.21	1.92	0.25	0.68	1.84	8.6		
4-5 mc	4.5	0.11	2.18			0.22	1.95	0.25	0.63	1.87	8.7		
5-6 mc	5.5	0.14	2.46	4.77	-22.15	0.21	1.98	0.26	0.63	1.91	9.0	9.2	80
6-8 mc	7.0	0.18	2.16			0.21	1.87	0.26	0.62	1.80	8.7		
8-10 mc	9.0	0.23	1.88			0.21	1.87	0.26	0.68	1.78	8.7		
10-12 mc	11.0	0.28	2.00	4.81	-22.25	0.21	1.93	0.28	0.75	1.84	8.9	9.7	85
12-14 mc	13.0	0.33	1.80			0.20	1.87	0.27	0.72	1.78	8.8		
14-16 mc	15.0	0.38	2.02	5.29	-22.30	0.20	1.92	0.30	0.71	1.83	9.0	10.2	65
16-18 mc	17.0	0.43	1.67			0.19	1.85	0.32	0.65	1.77	9.1		
18-20 mc	19.0	0.48	1.95	4.82	-22.33	0.20	1.87	0.33	0.66	1.79	9.2		40
20-25 mc	22.5	0.57	1.90	5.16	-22.31	0.19	1.80	0.41	0.68	1.72	9.2	10.4	73
25-30 mc	27.5	0.70	1.87	4.86	-22.25	0.17	1.71	0.49	0.82	1.61	9.3		29
30-35 mc	32.5	0.82	1.89	5.51	-22.06	0.17	1.64	0.54	0.80	1.55	9.2	8.2	72
35-38 mc	37.5	0.92	1.81	5.17	-22.07	0.16	1.73	0.57	0.82	1.63	10.0		61

Major Element Data for Multicore (mc) JT96-01.

Sample	Depth (cm)	Al_2O_3 (%)	Fe_2O_3 (%)	K_2O (%)	MgO (%)	P_2O_5 (%)	SiO_2 (%)	CaO (%)	MnO (%)	TiO_2 (%)	Na_2O (%)
0-1 mc	0.5	14.00	6.34	1.44	2.10	0.26	61.22	2.38	0.074	0.82	-0.28
1-2 mc	1.5										
2-3 mc	2.5										
3-4 mc	3.5										
4-5 mc	4.5										
5-6 mc	5.5	14.03	6.32	1.62	1.86	0.22	60.80	2.46	0.059	0.85	0.99
6-8 mc	7.0										
8-10 mc	9.0										
10-12 mc	11.0	13.02	6.28	1.64	1.84	0.20	57.51	2.42	0.074	0.83	1.15
12-14 mc	13.0										
14-16 mc	15.0	14.93	6.27	1.69	2.25	0.21	64.14	2.46	0.063	0.86	2.04
16-18 mc	17.0										
18-20 mc	19.0	15.00	6.43	1.74	2.24	0.20	64.03	2.43	0.061	0.87	2.11
20-25 mc	22.5	14.75	6.29	1.74	2.19	0.19	63.17	2.44	0.057	0.87	2.01
25-30 mc	27.5	15.16	6.33	1.74	2.43	0.19	64.07	2.62	0.065	0.87	2.44
30-35 mc	32.5	15.18	6.33	1.71	2.44	0.19	64.59	2.58	0.059	0.87	2.46
35-38 mc	37.5	15.16	6.35	1.71	2.47	0.19	64.94	2.63	0.064	0.88	2.56

Sample	Depth (cm)	V (µg/g)	Cr (µg/g)	Mn (µg/g)	Co (µg/g)	Ni (µg/g)	Cu (µg/g)	Zn (µg/g)	As (µg/g)	Rb (µg/g)	Sr (µg/g)	Y (µg/g)	Zr (µg/g)	Ba (µg/g)	Pb (µg/g)	Br (µg/g)
0-1 mc	0.5	142	87	532	7	40	30	96	8	76	231	17	158	411	20	145
1-2 mc	1.5															
2-3 mc	2.5															
3-4 mc	3.5															
4-5 mc	4.5															
5-6 mc	5.5	148	92	449	11	38	29	97	5	70	238	18	169	430	19	111
6-8 mc	7.0															
8-10 mc	9.0															
10-12 mc	11.0	152	96	454	11	37	29	97	8	68	235	19	166	410	17	104
12-14 mc	13.0															
14-16 mc	15.0	151	92	454	12	37	29	98	6	69	239	19	164	438	20	101
16-18 mc	17.0															
18-20 mc	19.0	146	86	418	12	38	30	102	7	67	234	19	168	415	19	99
20-25 mc	22.5	152	92	438	11	39	28	97	10	67	236	19	167	442	13	91
25-30 mc	27.5	147	94	430	12	39	28	94	11	69	246	20	174	408	14	71
30-35 mc	32.5	150	94	443	10	39	27	87	10	67	242	19	169	452	13	70
35-38 mc	37.5	152	94	442	13	38	27	88	8	65	248	19	172	440	12	66

Table A9. (continued)

Trace Metal Data for Multicore (mc) JT96-01.

Sample	Depth (cm)	Ag (ng/g)	Cd (µg/g)	Re (ng/g)	Mo (µg/g)	U (µg/g)
0-1 mc	0.5	84	0.15	2.13	0.62	1.12
1-2 mc	1.5	81	0.23	2.70	0.66	1.28
2-3 mc	2.5	94	0.20	2.91	0.72	1.26
3-4 mc	3.5	89	0.23	2.53	0.68	1.38
4-5 mc	4.5	97	0.23	3.50	0.74	1.58
5-6 mc	5.5	87	0.18	3.30	0.68	1.28
6-8 mc	7.0	94	0.25	2.34	0.81	1.32
8-10 mc	9.0	86	0.21	2.87	0.95	1.40
10-12 mc	11.0	85	0.23	3.40	1.02	1.44
12-14 mc	13.0	87	0.20	2.90	0.99	1.34
14-16 mc	15.0	79	0.23	3.87	1.22	1.31
16-18 mc	17.0	96	0.21	3.77	0.96	1.61
18-20 mc	19.0	86	0.20	3.29	0.95	1.49
20-25 mc	22.5	92	0.23	4.10	1.22	1.63
25-30 mc	27.5	85	0.20	5.32	1.30	1.84
30-35 mc	32.5	82	0.22	5.31	1.35	1.96
35-38 mc	37.5	75	0.25	5.91	1.42	2.12

Table A10. Geochemical Data for Multicore and Piston Core JT96-02.

General Geochemical Data for Multicore (mc) and Piston Core (pc) JT96-02.

Sample	Depth (m)	Calendar Age (kyrs)	Cl⁻ (wt. %)	$\delta^{15}N$ (‰ vs air)	$\delta^{13}C_{org}$ (‰ vs PDB)	N_{tot} (wt. %)	C_{tot} (wt. %)	S_{tot} (wt. %)	$CaCO_2$ (wt. %)	$\%C_{org}$ (wt. %)	C_{org}/N	Opal (wt. %)	Ba_{bio} ($\mu g/g$)
0-1 mc	0.5	0.02	5.02	6.60	-21.50	0.40	3.49	0.38	0.83	3.39	8.5	8.8	378
1-2 mc	1.5	0.06	4.24			0.39	3.33	0.35	0.83	3.23	8.4		
2-3 mc	2.5	0.10	3.67			0.39	3.34	0.27	0.63	3.26	8.4		
3-4 mc	3.5	0.14	3.23			0.39	3.29	0.27	0.54	3.23	8.3		
4-5 mc	4.5	0.19	3.57			0.39	3.22	0.27	0.40	3.17	8.2		
5-6 mc	5.5	0.23	3.38	6.24	-21.06	0.38	3.25	0.29	0.33	3.21	8.5	8.7	341
6-8 mc	7.0	0.29	2.67			0.37	3.14	0.25	0.33	3.10	8.5		
8-10 mc	9.0	0.37	2.39			0.35	2.99	0.25	0.31	2.95	8.4		
10-12 mc	11.0	0.45	2.35	6.84	-21.11	0.31	2.78	0.23	0.25	2.75	8.8	8.6	368
12-14 mc	13.0	0.53	2.55			0.33	2.86	0.25	0.32	2.82	8.6		
14-16 mc	15.0	0.62	2.57	6.73	-21.09	0.29	2.56	0.28	0.33	2.52	8.8	9.9	371
16-18 mc	17.0	0.70	2.09			0.29	2.53	0.28	0.37	2.49	8.7		
18-20 mc	19.0	0.78	2.36	6.69	-21.14	0.28	2.48	0.32	0.42	2.43	8.8	8.1	345

Sample	Depth (m)	Calendar Age (kyrs)	Cl⁻ (wt. %)	$\delta^{15}N$ (‰ vs air)	$\delta^{13}C_{org}$ (‰ vs PDB)	N_{tot} (wt. %)	C_{tot} (wt. %)	S_{tot} (wt. %)	$CaCO_2$ (wt. %)	$\%C_{org}$ (wt. %)	C_{org}/N	Opal (wt. %)	Ba_{bio} ($\mu g/g$)
5-6 pc	5.5		2.50	6.84	-21.04	0.32	2.83	0.25	0.25	2.80	8.81		
10-11 pc	10.5		2.17	6.62	-21.12	0.24	2.18	0.22	0.25	2.15	8.96		
15-16 pc	15.5		2.19	6.99	-22.05	0.16	1.59	0.32	0.89	1.48	9.33		
20-21 pc	20.5		1.70	6.83	-22.75	0.07	1.06	0.26	1.67	0.86	12.81		
25-26 pc	25.5		1.66	6.84	-22.74	0.09	1.08	0.24	1.92	0.85	9.57		
30-31 pc	30.5		1.64	6.40	-22.81	0.09	1.13	0.26	1.67	0.93	10.09		
35-36 pc	35.5		1.20	6.05	-22.55	0.08	0.94	0.18	1.67	0.74	9.62		
40-41 pc	40.5		1.07	6.68	-22.72	0.08	0.97	0.25	1.67	0.77	9.70		
45-46 pc	45.5		0.44		-23.96	0.01	0.24	0.08	0.80	0.15	10.43		
50-51 pc	50.5		0.71		-23.26	0.05	0.71	0.22	2.17	0.45	9.04		
55-56 pc	55.5		0.57		-23.47	0.03	0.55	0.14	2.15	0.30	10.96		
60-61 pc	60.5		0.48		-23.71	0.02	0.49	0.12	2.27	0.22	9.95		
65-66 pc	65.5		0.73		-23.22	0.04	0.61	0.22	1.74	0.40	10.10		
70-71 pc	70.5		0.48		-23.47	0.03	0.59	0.16	1.67	0.39	14.44		
75-76 pc	75.5		0.50		-23.46	0.03	0.52	0.16	2.22	0.25	9.77		
80-81 pc	80.5		0.47		-23.63	0.01	0.28	0.07	1.46	0.10	7.85		
85-86 pc	85.5		0.42		-23.91	0.01	0.26	0.08	1.42	0.09	7.33		
90-91 pc	90.5		0.96	5.08	-24.41	0.05	0.76	0.11	3.00	0.40	8.15		
95-96 pc	95.5		0.89		-24.65	0.05	0.82	0.16	3.33	0.42	8.53		
100-101 pc	100.5		0.97		-24.51	0.05	0.72	0.12	2.92	0.37	7.61		
105-106 pc	105.5		0.83		-24.63	0.04	0.72	0.09	3.33	0.32	7.85		
110-111 pc	110.5		1.01	5.31	-24.45	0.05	0.77	0.10	3.21	0.39	8.37		
115-116 pc	115.5		0.81		-24.41	0.05	0.84	0.23	3.33	0.44	9.39		
120-121 pc	120.5		0.90		-24.60	0.05	0.80	0.11	3.25	0.41	8.59		
125-126 pc	125.5		0.86		-24.78	0.05	0.77	0.08	3.33	0.37	7.60		
130-131 pc	130.5		0.98	4.75	-24.49	0.05	0.75	0.11	2.92	0.40	7.65		
135-136 pc	135.5		1.04		-23.73	0.08	1.21	0.36	4.20	0.71	8.90		
140-141 pc	140.5		0.99		-24.82	0.05	0.73	0.11	3.00	0.37	8.11		
145-146 pc	145.5		0.95		-23.88	0.07	0.98	0.12	3.33	0.58	8.46		
150-151 pc	150.5		0.79	5.17	-24.57	0.05	0.74	0.11	3.33	0.34	7.03		
155-156 pc	155.5		1.20		-24.23	0.06	0.82	0.11	3.33	0.42	7.05		
160-161 pc	160.5		1.16		-23.56	0.07	1.17	0.47	4.17	0.67	9.16		
165-166 pc	165.5		0.82		-24.28	0.04	0.76	0.12	3.33	0.36	8.07		
170-171 pc	170.5		0.99	5.45	-23.82	0.06	0.94	0.13	3.50	0.52	8.68		
175-176 pc	175.5		0.85		-24.53	0.05	0.76	0.10	3.33	0.36	7.52		
180-181 pc	180.5		0.71		-24.47	0.04	0.72	0.10	3.17	0.34	9.44		
185-186 pc	185.5		0.79		-24.55	0.04	0.70	0.09	3.29	0.31	8.13		
190-191 pc	190.5		0.91	5.50	-24.39	0.04	0.76	0.09	3.08	0.39	9.51		
195-196 pc	195.5		0.97		-23.34	0.10	1.48	0.43	4.17	0.98	9.96		
200-201 pc	200.5		0.88		-23.50	0.09	1.36	0.40	4.08	0.87	9.21		
205-206 pc	205.5		0.86		-24.25	0.05	0.89	0.13	3.33	0.49	9.39		

Table A10. (continued)

Major Element Data for Multicore (mc) and Piston Core (pc) JT96-02.

Sample	Depth (m)	Al_2O_3 (%)	Fe_2O_3 (%)	K_2O (%)	MgO (%)	P_2O_5 (%)	SiO_2 (%)	CaO (%)	MnO (%)	TiO_2 (%)	Na_2O (%)
0-1 mc	0.5	12.36	6.57	1.72	2.77	0.26	50.27	2.58	0.066	0.76	1.00
1-2 mc	1.5										
2-3 mc	2.5										
3-4 mc	3.5										
4-5 mc	4.5										
5-6 mc	5.5	16.71	7.99	2.18	3.05	0.23	63.94	2.52	0.064	0.94	4.18
6-8 mc	7.0										
8-10 mc	9.0										
10-12 mc	11.0	14.72	6.61	2.26	2.76	0.21	59.15	2.37	0.054	0.84	4.00
12-14 mc	13.0										
14-16 mc	15.0	13.05	6.48	2.07	2.74	0.19	53.46	2.29	0.063	0.84	1.48
16-18 mc	17.0										
18-20 mc	19.0	14.38	6.30	2.24	2.81	0.19	59.39	2.50	0.053	0.83	3.15

Sample	Depth (m)	Al_2O_3 (%)	Fe_2O_3 (%)	K_2O (%)	MgO (%)	P_2O_5 (%)	SiO_2 (%)	CaO (%)	MnO (%)	TiO_2 (%)	Na_2O (%)
5-6 pc	5.5	14.65	6.28	1.74	3.02	0.19	58.42	2.16	0.050	0.78	1.88
10-11 pc	10.5	11.89	6.84	2.03	2.83	0.18	52.46	2.45	0.052	0.78	0.55
15-16 pc	15.5	15.67	6.61	2.24	2.97	0.20	59.09	2.98	0.073	0.81	4.25
20-21 pc	20.5	15.56	6.62	2.17	3.06	0.20	59.49	3.83	0.083	0.79	3.74
25-26 pc	25.5	16.20	7.30	2.53	3.24	0.20	60.17	3.79	0.082	0.84	4.20
30-31 pc	30.5	16.55	6.94	2.51	3.04	0.20	62.55	3.92	0.082	0.82	5.08
35-36 pc	35.5	15.49	7.31	2.14	2.89	0.18	62.85	3.94	0.082	0.84	3.34
40-41 pc	40.5	15.52	5.84	1.93	2.81	0.18	61.63	3.69	0.071	0.76	3.99
45-46 pc	45.5										
50-51 pc	50.5										
55-56 pc	55.5										
60-61 pc	60.5										
65-66 pc	65.5										
70-71 pc	70.5										
75-76 pc	75.5										
80-81 pc	80.5										
85-86 pc	85.5										
90-91 pc	90.5	16.14	7.16	2.84	2.94	0.23	56.41	3.62	0.081	1.02	3.56
95-96 pc	95.5	16.26	7.46	2.88	2.98	0.25	58.07	4.00	0.091	1.08	3.41
100-101 pc	100.5	14.76	7.53	3.04	2.89	0.26	54.24	3.77	0.081	1.10	2.14
105-106 pc	105.5	15.03	7.08	2.89	2.84	0.26	56.59	4.08	0.091	1.09	3.28
110-111 pc	110.5	15.69	7.08	2.83	3.06	0.24	56.03	3.42	0.090	0.97	2.53
115-116 pc	115.5	14.98	7.04	3.22	2.78	0.24	56.07	4.02	0.091	0.99	4.47
120-121 pc	120.5	16.57	7.35	3.20	2.92	0.25	58.93	3.71	0.091	1.05	4.12
125-126 pc	125.5	13.75	7.16	2.84	2.81	0.24	51.85	3.80	0.091	1.03	1.48
130-131 pc	130.5	16.99	7.38	3.36	2.94	0.26	60.51	3.65	0.081	1.06	4.66
135-136 pc	135.5	16.38	7.33	2.33	3.51	0.22	57.08	4.39	0.100	0.92	3.19
140-141 pc	140.5	14.49	6.92	2.96	2.91	0.25	53.95	3.77	0.092	1.04	1.90
145-146 pc	145.5	16.36	7.34	2.99	3.06	0.23	58.26	3.93	0.081	0.99	4.39
150-151 pc	150.5	15.33	7.07	3.16	2.82	0.26	57.64	3.90	0.101	1.06	3.08
155-156 pc	155.5	16.33	7.19	3.07	2.98	0.26	57.26	3.52	0.082	0.99	3.53
160-161 pc	160.5	15.58	7.35	2.44	3.14	0.22	55.65	4.44	0.092	0.93	3.37
165-166 pc	165.5	16.85	6.93	2.85	3.15	0.24	59.77	3.63	0.100	0.98	3.36
170-171 pc	170.5	17.10	7.10	3.13	3.00	0.25	59.94	3.91	0.081	0.98	4.09
175-176 pc	175.5	16.38	6.80	3.05	2.90	0.24	57.45	3.39	0.091	0.98	3.73
180-181 pc	180.5	14.56	6.78	2.95	2.79	0.25	57.36	4.08	0.091	1.02	2.82
185-186 pc	185.5	14.16	7.23	3.25	2.75	0.25	54.65	3.79	0.091	1.02	2.65
190-191 pc	190.5	16.34	7.37	3.35	2.88	0.26	57.84	3.67	0.092	1.04	3.89
195-196 pc	195.5	15.50	7.84	2.60	3.13	0.22	56.62	5.04	0.102	0.90	4.08
200-201 pc	200.5	15.97	6.87	2.12	2.98	0.22	57.76	4.53	0.091	0.86	4.42
205-206 pc	205.5	17.60	7.50	2.82	3.25	0.26	60.45	4.02	0.110	1.06	3.41

Table A10. (continued)

Minor Element Data for Multicore (mc) and Piston Core (pc) JT96-02.

Sample	Depth (m)	V (µg/g)	Cr (µg/g)	Mn (µg/g)	Co (µg/g)	Ni (µg/g)	Cu (µg/g)	Zn (µg/g)	As (µg/g)	Rb (µg/g)	Sr (µg/g)	Y (µg/g)	Zr (µg/g)	Ba (µg/g)	Pb (µg/g)	Br (µg/g)	I (µg/g)
0-1 mc	0.5	141	113	521	20	58	46	126		99	227	16	134	687	24	135	968
1-2 mc	1.5																
2-3 mc	2.5																
3-4 mc	3.5																
4-5 mc	4.5																
5-6 mc	5.5	161	126	430	19	60	47	132		95	222	18	145	759	20	116	669
6-8 mc	7.0																
8-10 mc	9.0																
10-12 mc	11.0	167	130	446	20	59	44	129		86	228	19	146	736	18	99	472
12-14 mc	13.0																
14-16 mc	15.0	164	131	451	20	59	45	132		86	230	20	154	697	17	75	347
16-18 mc	17.0																
18-20 mc	19.0	159	125	455	19	56	42	125		83	237	20	156	705	18	81	357

Sample	Depth (m)	V (µg/g)	Cr (µg/g)	Mn (µg/g)	Co (µg/g)	Ni (µg/g)	Cu (µg/g)	Zn (µg/g)	As (µg/g)	Rb (µg/g)	Sr (µg/g)	Y (µg/g)	Zr (µg/g)	Ba (µg/g)	Pb (µg/g)	Br (µg/g)	I (µg/g)
5-6 pc	5.5	165	131	459	19	57	43	122		85	227	19	141	779	22	94	483
10-11 pc	10.5	170	143	499	20	53	39	118		79	244	20	158	737	22	61	309
15-16 pc	15.5	200	141	650	21	57	38	108		79	255	22	137	673	26	21	95
20-21 pc	20.5	196	129	711	21	50	34	97		74	294	22	143	625	25	-3	36
25-26 pc	25.5	204	126	727	22	51	37	101		80	286	23	131	637	23	-1	36
30-31 pc	30.5	198	131	740	21	50	35	100		79	298	22	137	659	22	-4	37
35-36 pc	35.5	185	128	663	20	45	30	93		70	303	23	156	613	21	7	65
40-41 pc	40.5	182	119	669	18	44	28	89		68	306	21	154	630	20	6	38
45-46 pc	45.5	125	86	498	16	30	13	51	2		343	17	128	510	16	17	14
50-51 pc	50.5	148	102	616	23	39	25	77	4		318	20	158	562	14	23	25
55-56 pc	55.5	142	107	598	22	35	19	67	2		325	21	184	528	14	18	13
60-61 pc	60.5	138	109	596	23	33	16	63	1		333	21	196	506	16	17	16
65-66 pc	65.5	147	110	629	19	40	22	75	5		332	20	166	559	15	23	25
70-71 pc	70.5	126	96	559	28	27	11	51	3		364	17	151	513	15	15	22
75-76 pc	75.5	145	108	650	23	36	19	68	8		346	21	196	532	13	17	16
80-81 pc	80.5	118	83	503	22	26	11	49	4		361	16	146	491	13	15	18
85-86 pc	85.5	118	92	558	24	29	12	51	4		357	17	158	533	12	14	21
90-91 pc	90.5	199	81	740	23	31	32	107		126	224	34	181	664	30	-4	8
95-96 pc	95.5	200	80	807	23	31	34	106		122	231	33	181	674	29	-4	15
100-101 pc	100.5	205	76	733	25	32	35	110		123	229	34	179	647	27	-3	18
105-106 pc	105.5	181	70	784	16	33	33	107	7	116	240	33	186	608	15	-5	16
110-111 pc	110.5	169	76	703	17	34	35	108	6	133	220	34	176	614	23	-7	9
115-116 pc	115.5	172	71	762	20	35	34	107	6	122	232	32	182	615	19	-5	16
120-121 pc	120.5	172	74	690	18	34	34	109	6	133	223	35	183	595	23	-5	3
125-126 pc	125.5	172	69	758	19	31	33	110	7	128	229	35	194	619	20	-8	5
130-131 pc	130.5	173	75	659	22	32	34	109	7	128	222	33	182	576	20	-6	14
135-136 pc	135.5	181	97	744	19	49	36	105	21	102	261	31	165	626	15	1	20
140-141 pc	140.5	174	72	755	20	32	36	107	5	126	225	34	188	624	23	-10	8
145-146 pc	145.5	174	90	698	14	43	36	105	5	115	239	32	169	611	22	-3	14
150-151 pc	150.5	171	73	757	16	34	33	103	4	123	224	34	187	604	25	-6	14
155-156 pc	155.5	166	75	672	17	35	35	108	4	132	216	35	177	613	28	-16	11
160-161 pc	160.5	178	91	764	22	46	39	104	13	106	257	30	170	587	17	-7	8
165-166 pc	165.5	175	72	741	18	31	37	106	4	124	222	34	182	635	22	-5	12
170-171 pc	170.5	169	87	702	14	43	36	106	11	126	232	33	177	624	14	-6	15
175-176 pc	175.5	163	74	728	16	35	34	105	5	132	215	34	180	628	21	-5	11
180-181 pc	180.5	166	74	742	17	33	34	100	7	115	240	33	203	590	15	-3	10
185-186 pc	185.5	168	75	737	19	33	35	105	4	125	226	35	191	594	24	-4	10
190-191 pc	190.5	172	72	723	20	33	35	105	7	129	217	36	182	591	19	-4	-3
195-196 pc	195.5	187	110	824	19	57	38	101	21	83	289	27	157	603	12	3	11
200-201 pc	200.5	179	113	810	18	52	37	100	8	78	286	25	145	582	14	2	10
205-206 pc	205.5	180	78	729	19	37	36	111	7	117	237	34	178	586	16	-3	8

Trace Metal Data for Multicore (mc) and Piston Core (pc) JT96-02.

Sample	Depth (m)	Ag (ng/g)	Cd (µg/g)	Re (ng/g)	Mo (µg/g)	U (µg/g)
0-1 mc	0.5	330	0.21	3.53	0.69	1.21
1-2 mc	1.5	335	0.20	3.92	0.65	1.27
2-3 mc	2.5	420	0.23	4.20	0.68	1.36
3-4 mc	3.5	462	0.30	4.02	0.73	1.54
4-5 mc	4.5	458	0.24	4.16	0.67	1.54
5-6 mc	5.5	475	0.37	4.57	0.68	1.62
6-8 mc	7.0	476	0.51	5.29	0.69	1.80
8-10 mc	9.0	473	0.47	8.54	0.67	1.74
10-12 mc	11.0	430	0.43	11.06	0.61	1.64
12-14 mc	13.0	428	0.59	15.12	0.90	1.79
14-16 mc	15.0	434	0.64	25.02	0.85	2.11
16-18 mc	17.0	422	0.61	30.18	0.82	2.83
18-20 mc	19.0	384	0.45	16.89	0.86	2.83

Table A10. (continued)

General geochemical data for the sulphide layers (in bold print) and intervening sediments, Piston Core JT96-02.

Sample	Depth (cm)	δ¹⁵N (permil vs air)	δ¹³C_org (permil vs VPDB)	Ntot [1] (wt.%)	Ctot [1] (wt.%)	Stot [1] (wt.%)	%Ccarb	%carb	%Corg (wt.%)	Corg/N
1	134.15	4.79	-24.57	0.033	0.679	0.096	0.415	3.46	0.264	7.95
2	134.45	4.61	-25.09	0.033	0.689	0.098	0.411	3.42	0.278	8.41
3	**134.75**	**4.94**	**-24.26**	**0.039**	**0.726**	**0.285**	**0.415**	**3.46**	**0.311**	**8.01**
4	**135.05**	**5.40**	**-23.46**	**0.063**	**1.117**	**0.379**	**0.546**	**4.55**	**0.571**	**9.02**
5	**135.35**	**5.30**	**-23.49**	**0.065**	**1.128**	**0.440**	**0.540**	**4.50**	**0.588**	**8.99**
6	**135.65**	**5.65**	**-23.61**	**0.059**	**1.035**	**0.418**	**0.498**	**4.15**	**0.537**	**9.06**
7	**135.95**	**5.24**	**-23.57**	**0.056**	**0.989**	**0.297**	**0.485**	**4.04**	**0.504**	**9.00**
8	**136.25**	**5.25**	**-23.64**	**0.056**	**0.970**	**0.191**	**0.483**	**4.02**	**0.487**	**8.72**
9	**136.55**	**5.62**	**-23.75**	**0.049**	**0.904**	**0.138**	**0.466**	**3.88**	**0.438**	**8.88**
10	**136.85**	**5.15**	**-23.87**	**0.047**	**0.841**	**0.112**	**0.436**	**3.63**	**0.405**	**8.63**
11	**137.15**	**4.98**	**-23.80**	**0.045**	**0.810**	**0.113**	**0.389**	**3.24**	**0.421**	**9.30**
12	137.45	5.02	-23.90	0.039	0.702	0.092	0.358	2.98	0.344	8.81
13	137.75	4.96	-24.22	0.033	0.642	0.086	0.356	2.97	0.286	8.72
14	138.05			0.031	0.629	0.073	0.368	3.07	0.261	8.36
15	138.35			0.030	0.617	0.072	0.390	3.25	0.227	7.51
16	138.65			0.030	0.637	0.080	0.367	3.06	0.270	8.87
17	138.95			0.031	0.651	0.076	0.386	3.22	0.265	8.46
18	139.25	4.77	-24.78	0.032	0.646	0.075	0.374	3.12	0.272	8.54
19	139.55			0.032	0.648	0.083	0.396	3.30	0.252	7.93
20	139.85			0.030	0.653	0.079	0.397	3.31	0.256	8.64
21	140.15			0.032	0.652	0.075	0.404	3.37	0.248	7.80
22	140.45		-24.54	0.030	0.645	0.078	0.393	3.27	0.252	8.49
23	140.75	4.71		0.029	0.644	0.079	0.374	3.12	0.270	9.23
24	141.05			0.030	0.643	0.077	0.385	3.21	0.258	8.69
25	141.35			0.029	0.645	0.074	0.419	3.49	0.226	7.77
26	141.65			0.030	0.646	0.074	0.413	3.44	0.233	7.74
27	141.95	4.73	-24.48	0.062	0.645	0.082	0.393	3.27	0.252	4.07
28	142.25	4.91	-24.49	0.028	0.646	0.078	0.399	3.32	0.247	8.82
29	142.55	4.50	-24.40	0.031	0.651	0.103	0.423	3.52	0.228	7.47
30	142.85	4.27	-24.58	0.028	0.651	0.074	0.414	3.45	0.237	8.49
31	143.15	4.72	-24.45	0.029	0.667	0.078	0.440	3.67	0.227	7.82
32	**143.45**	**4.45**	**-24.15**	**0.037**	**0.730**	**0.232**	**0.421**	**3.51**	**0.309**	**8.32**
33	**143.75**	**5.56**	**-23.39**	**0.063**	**1.098**	**0.460**	**0.538**	**4.48**	**0.560**	**8.84**
34	**144.05**	**5.81**	**-23.38**	**0.062**	**1.058**	**0.283**	**0.483**	**4.02**	**0.575**	**9.22**
35	**144.35**	**5.56**	**-23.40**	**0.058**	**0.996**	**0.258**	**0.495**	**4.12**	**0.501**	**8.66**
36	**144.65**	**5.48**	**-23.56**	**0.057**	**0.979**	**0.269**	**0.461**	**3.84**	**0.518**	**9.09**
37	**144.95**	**5.20**	**-23.44**	**0.053**	**0.951**	**0.199**	**0.471**	**3.92**	**0.480**	**9.06**
38	**145.25**	**5.08**	**-23.76**	**0.051**	**0.883**	**0.126**	**0.425**	**3.54**	**0.458**	**9.00**
39	**145.55**	**5.40**	**-23.57**	**0.047**	**0.842**	**0.116**	**0.411**	**3.42**	**0.431**	**9.12**
40	**145.85**	**5.02**	**-23.84**	**0.043**	**0.751**	**0.123**	**0.372**	**3.10**	**0.379**	**8.86**
41	146.15	4.94	-23.96	0.037	0.686	0.091	0.380	3.17	0.306	8.29
42	146.45	5.01	-24.14	0.037	0.682	0.079	0.374	3.12	0.308	8.40
43	146.75	4.61	-24.86	0.034	0.629	0.079	0.361	3.01	0.268	7.77
44	147.05			0.027	0.506	0.069	0.342	2.85	0.164	6.06
45	147.35			0.033	0.619	0.079	0.355	2.96	0.264	8.05
46	147.65			0.029	0.613	0.076	0.350	2.92	0.263	9.16
47	147.95	4.53	-24.51	0.031	0.623	0.080	0.365	3.04	0.258	8.37
48	148.25			0.031	0.631	0.083	0.372	3.10	0.259	8.32
49	148.55			0.032	0.640	0.081	0.392	3.27	0.248	7.77
50	148.85	4.76	-24.45	0.031	0.642	0.073	0.386	3.22	0.256	8.19
51	149.15			0.032	0.652	0.075	0.399	3.32	0.253	7.92
52	149.45			0.029	0.639	0.077	0.389	3.24	0.250	8.48
53	149.75			0.034	0.647	0.087	0.402	3.35	0.245	7.28
54	150.05			0.029	0.639	0.075	0.385	3.21	0.254	8.63
55	150.35			0.038	0.694	0.042	0.414	3.45	0.280	7.29
56	150.65	3.43		0.037	0.667	0.043	0.388	3.23	0.279	7.59
57	150.95			0.038	0.710	0.052	0.415	3.46	0.295	7.80
58	151.25			0.047	0.851	0.090	0.448	3.73	0.403	8.55
59	151.55			0.046	0.823	0.085	0.461	3.84	0.362	7.86
60	**151.85**			**0.042**	**0.787**	**0.264**	**0.449**	**3.74**	**0.338**	**8.07**
61	**152.15**			**0.060**	**1.039**	**0.589**	**0.494**	**4.12**	**0.545**	**9.02**
62	**152.45**			**0.075**	**1.227**	**0.381**	**0.556**	**4.63**	**0.671**	**8.98**
63	**152.75**			**0.071**	**1.185**	**0.280**	**0.559**	**4.66**	**0.626**	**8.82**
64	**152.05**			**0.067**	**1.171**	**0.239**	**0.532**	**4.43**	**0.639**	**9.48**
65	**153.35**			**0.065**	**1.139**	**0.218**	**0.546**	**4.55**	**0.593**	**9.13**
66	**153.65**			**0.061**	**1.082**	**0.191**	**0.507**	**4.22**	**0.575**	**9.39**
67	**153.95**			**0.056**	**1.001**	**0.155**	**0.499**	**4.16**	**0.502**	**8.98**
68	**154.25**			**0.055**	**0.965**	**0.131**	**0.468**	**3.90**	**0.497**	**8.97**
69	**154.55**			**0.048**	**0.861**	**0.143**	**0.446**	**3.72**	**0.415**	**8.66**
70	**154.85**			**0.044**	**0.812**	**0.151**	**0.436**	**3.63**	**0.376**	**8.56**

[1] Data have not been salt corrected.

Trace metal [1] and major element data[1] for the sulphide layers (in bold) and intervening sediments, Piston Core JT96-02.

Sample	Depth (cm)	Ag (ng/g)	Cd (µg/g)	Re (ng/g)	Mo (µg/g)	U (µg/g)	Al_2O_3 wt.%	Fe_2O_3 wt.%	K_2O wt.%	MgO wt.%	Na_2O wt.%	P_2O_5 wt.%	SiO_2 wt.%	CaO wt.%	Mn_3O_4 wt.%	TiO_2 wt.%
1	134.15	102	0.25	1.26	1.03	1.76	16.09	7.05	2.85	3.14	5.21	0.253	57.17	3.61	0.1	1.02
2	134.45	112	0.20	0.85	0.87	1.67	16.25	7.13	2.98	3.19	4.82	0.253	57.24	3.58	0.101	1.02
3	**134.75**	**106**	**0.15**	**2.04**	**1.40**	**1.63**	**16**	**7.39**	**2.96**	**3.18**	**5.12**	**0.245**	**56.54**	**3.65**	**0.1**	**1**
4	**135.05**	**108**	**0.18**	**1.65**	**2.05**	**1.51**	**15.63**	**7.53**	**2.32**	**3.37**	**5.17**	**0.222**	**55.06**	**4.57**	**0.1**	**0.9**
5	**135.35**	**113**	**0.28**	**1.38**	**2.11**	**1.56**	**15.53**	**7.5**	**2.37**	**3.4**	**5.39**	**0.22**	**55.49**	**4.57**	**0.097**	**0.89**
6	**135.65**	**109**	**0.19**	**0.93**	**1.71**	**1.53**										
7	**135.95**	**115**	**0.15**	**1.55**	**1.52**	**1.59**	**15.69**	**7.32**	**2.52**	**3.28**	**5.77**	**0.223**	**55.89**	**4.25**	**0.092**	**0.93**
8	**136.25**	**114**	**0.14**	**1.18**	**1.00**	**1.78**	**15.59**	**7.12**	**2.63**	**3.3**	**5.12**	**0.227**	**56.11**	**4.23**	**0.094**	**0.93**
9	**136.55**	**100**	**0.23**	**1.31**	**0.86**	**1.63**										
10	**136.85**	**105**	**0.14**	**2.21**	**0.75**	**1.63**	**16**	**7.18**	**2.57**	**3.28**	**5.11**	**0.232**	**56.65**	**3.81**	**0.089**	**0.96**
11	**137.15**	**98**	**0.15**	**1.11**	**0.78**	**1.7**										
12	137.45	75	0.20	1.94	0.79	1.71										
13	137.75	80	0.30	0.74	0.79	1.68	16.18	7.27	2.93	3.12	5.28	0.243	57.64	3.38	0.086	1.01
14	138.05	82	0.13	0.64	0.73	1.69	16.27	7.03	2.96	3.11	6.96	0.245	57.66	3.38	0.091	1.01
15	138.35	88	0.10	0.68	0.70	1.95										
16	138.65	89	0.12	0.56	1.05	1.85	16.28	7.1	2.96	3.11	5.81	0.249	58.01	3.44	0.092	1.01
17	138.95	93	0.14	0.84	0.72	1.69										
18	139.25	82	0.12	0.43	0.76	1.69										
19	139.55	81	0.19	0.34	0.81	1.83	16.22	7.09	2.96	3.13	6.16	0.249	57.59	3.48	0.095	1.01
20	139.85	99	0.09	0.51	0.79	1.74										
21	140.15	108	0.12		0.76	1.67										
22	140.45	93	0.16	0.84	0.79	1.96	15.92	7.14	2.79	3.12	4.73	0.245	57.8	3.58	0.096	1.01
23	140.75	92	0.26	0.61	0.77	2.01	15.91	7.09	2.85	3.07	4.85	0.25	58.3	3.66	0.098	1.02
24	141.05	91	0.26	0.63	0.75	1.76										
25	141.35	90	0.42	0.61	0.76	2.18	15.84	7.05	2.83	3.06	5.28	0.251	58.12	3.67	0.098	1.02
26	141.65	96		0.72	0.77	1.91										
27	141.95	77	0.39	0.65	0.79	1.87										
28	142.25	83	0.20	0.78	0.61	1.8	15.49	7.02	2.63	3.07	4.37	0.251	59.11	3.84	0.099	1.04
29	142.55	92	0.20	0.73	0.83	1.91										
30	142.85	91	0.29	0.98	0.75	1.9	15.45	6.96	2.64	3.07	6.96	0.249	59.09	3.92	0.1	1.05
31	143.15	95	0.33	1.41	1.66	1.93										
32	**143.45**	**116**	**0.34**	**0.84**	**1.35**	**2.11**	**15.82**	**7.33**	**2.65**	**3.16**	**4.86**	**0.237**	**57.39**	**3.78**	**0.099**	**1**
33	**143.75**	**112**	**0.15**	**1.76**	**2.27**	**1.84**	**15.6**	**7.63**	**2.29**	**3.4**	**5.8**	**0.218**	**55.34**	**4.47**	**0.099**	**0.89**
34	**144.05**	**117**	**0.41**	**1.76**	**2.52**	**1.7**	**16.34**	**7.69**	**2.49**	**3.49**	**5.65**	**0.225**	**58.46**	**4.52**	**0.098**	**0.92**
35	**144.35**	**112**	**0.35**	**1.55**	**2.18**	**1.78**										
36	**144.65**	**118**	**0.27**	**1.13**	**2.00**	**1.74**	**15.81**	**7.28**	**2.47**	**3.34**	**5.57**	**0.218**	**56.15**	**4.12**	**0.092**	**0.92**
37	**144.95**	**116**	**0.38**	**1.31**	**1.40**	**1.82**										
38	**145.25**	**95**	**0.25**	**1.08**	**0.86**	**1.96**	**16.15**	**7.07**	**2.6**	**3.34**	**5.52**	**0.224**	**57.01**	**3.86**	**0.091**	**0.94**
39	**145.55**	**91**	**0.39**	**0.97**	**0.79**	**1.86**										
40	**145.85**	**83**	**0.23**	**0.89**	**0.85**	**2.03**	**16.29**	**7.24**	**2.77**	**3.25**	**4.96**	**0.228**	**57.13**	**3.46**	**0.086**	**0.95**
41	146.15	77	0.17	0.94	0.74	2.05										
42	146.45	66	0.12	1.44	0.67	2.01	16.47	7.01	2.9	3.21	5.26	0.238	57.82	3.39	0.088	0.97
43	146.75	85	0.14	0.71	0.73	2.05										
44	147.05	65	0.11	0.44	0.78	1.9										
45	147.35	71	0.13	0.54	0.64	1.81	16.39	7.09	2.96	3.11	6.87	0.242	57.86	3.26	0.089	0.99
46	147.65	80	0.21	0.73	0.69	1.92	16.26	7.03	3.01	3.12	4.91	0.24	57.87	3.34	0.088	0.99
47	147.95	73	0.27	0.51	0.71	1.94										
48	148.25	70	0.13	0.53	0.71	1.91	16.28	6.98	2.97	3.12	5.63	0.243	57.93	3.41	0.092	1
49	148.55	74	0.18	0.94	0.70	2.22										
50	148.85	81	0.32	0.66	0.71	1.99										
51	149.15	82	0.30	0.58	0.72	1.98	16.22	7	2.93	3.13	4.94	0.245	57.92	3.48	0.095	0.99
52	149.45	82	0.23	0.60	0.73	2.04										
53	149.75	94	0.24		0.71	1.99										
54	150.05	91	0.39	0.89	0.77	1.82	16.28	7.01	2.91	3.09	4.98	0.241	57.87	3.47	0.098	1
55	150.35	97	0.19	1.76	0.74	1.89										
56	150.65	98	0.15	0.62	0.83	1.61	15.85	6.97	2.97	3.05	5.03	0.249	57.93	3.62	0.099	1.01
57	150.95	86	0.14	0.47	0.72	1.5										
58	151.25	97	0.16	0.66	0.93	1.5	15.76	7.04	2.62	3.19	5.15	0.239	58.02	4.14	0.096	0.99
59	151.55	99	0.15	0.82	0.85	1.64										
60	**151.85**	**114**	**0.17**	**0.82**	**1.37**	**1.7**	**15.66**	**7.26**	**2.62**	**3.15**	**4.85**	**0.242**	**57.96**	**3.91**	**0.099**	**1**
61	**152.15**	**117**	**0.17**	**1.21**	**2.30**	**1.47**	**15.61**	**7.89**	**2.51**	**3.25**	**5.68**	**0.224**	**55.63**	**4.16**	**0.101**	**0.92**
62	**152.45**	**103**	**0.20**	**1.37**	**1.95**	**1.39**										
63	**152.75**	**97**	**0.22**	**1.21**	**1.57**	**1.53**	**15.77**	**7.21**	**2.31**	**3.43**	**5.27**	**0.214**	**55.95**	**4.54**	**0.097**	**0.89**
64	**152.05**	**96**	**0.20**	**1.42**	**1.59**	**1.62**										
65	**153.35**	**98**	**0.17**	**1.21**	**1.31**	**1.59**										
66	**153.65**	**96**	**0.18**	**0.83**	**1.03**	**1.6**	**16.01**	**7.15**	**2.48**	**3.32**	**5.48**	**0.223**	**56.22**	**4.24**	**0.094**	**0.93**
67	**153.95**	**90**	**0.13**	**0.79**	**0.98**	**1.63**										
68	**154.25**	**84**	**0.11**	**0.71**	**0.73**	**1.6**										
69	**154.55**	**75**	**0.14**	**0.73**	**0.71**	**1.62**	**16.01**	**7.08**	**2.88**	**3.24**	**5.19**	**0.237**	**56.75**	**3.76**	**0.089**	**0.95**
70	**154.85**	**71**	**0.16**	**0.98**	**0.68**	**1.74**	**16.48**	**7.1**	**2.84**	**3.23**	**5.01**	**0.24**	**57.33**	**3.68**	**0.089**	**0.97**

[1] Data have not been salt corrected.

Minor element data [1] for the sulphide layers (in bold print) and intervening sediments, Piston Core JT96-02.

Sample	Depth (cm)	V (ppm)	Cr (ppm)	Mn (ppm)	Co (ppm)	Ni (ppm)	Cu (ppm)	Zn (ppm)	Rb (ppm)	Sr (ppm)	Y (ppm)	Zr (ppm)	Ba (ppm)	Pb (ppm)	Nb (ppm)
1	134.15	184.4	76.1	799.2	33.6	28.6	32.8	100.2	99.4	214	30.9	169.1	662.3	27.4	13.9
2	134.45	170.9	67.3	727.4	29.7	29	30.6	96.3	97.3	206.1	29.1	162.8	579.9	21.2	13.4
3	**134.75**	**180.6**	**75.9**	**767.2**	**34.6**	**31.6**	**30.2**	**102.4**	**97.7**	**209.7**	**27.2**	**161.4**	**668.1**	**27.1**	**13.2**
4	**135.05**	**205.9**	**113.7**	**870.2**	**41.8**	**51.5**	**39.8**	**105.5**	**78.2**	**260**	**26.9**	**145.1**	**784.6**	**37**	**13.3**
5	**135.35**	**190.5**	**104.8**	**758.5**	**37.6**	**46.6**	**32.9**	**92.6**	**71.2**	**249.2**	**25.1**	**142**	**654.3**	**39.3**	**13.7**
6	135.65														
7	135.95	191.8	98.3	754.3	35.6	43	36.3	102.2	86.9	254.6	27.4	161.4	688	47.9	12.9
8	136.25	195	101.9	763	34.4	40.3	33.7	102.2	87.6	251.5	27.9	158.4	701.5	40	13
9	136.55														
10	136.85	181.7	84	679	32	32.3	29.2	90.8	86.2	222.2	27.5	155.1	616.4	21.3	11
11	137.15														
12	137.45														
13	137.75	189.5	79.6	708.7	34.8	28.5	28.2	99	101.9	211.2	29.3	166.9	721.6	19.1	14.6
14	138.05	189.9	81.1	738.3	36.1	30.2	35.5	108.6	113.6	227.7	32.6	185.6	755.3	27.2	14.7
15	138.35														
16	138.65	181.2	71	712.7	32.9	27.2	29.9	94.7	101.4	209.3	28.4	170.1	646	21.6	13.7
17	138.95														
18	139.25														
19	139.55	177.6	71.3	717.9	33.3	26.3	28.8	91.4	99.4	203.9	28.4	164.4	640.9	26.3	14.2
20	139.85														
21	140.15														
22	140.45	190.3	84.8	799.8	36.7	29.6	33.8	98	101.3	220.7	31.9	173	726.7	21.3	17.4
23	140.75	175.8	64.8	716.7	30.6	26.8	33.6	91.6	98	217.1	30.6	172.7	618.3	20.4	13.1
24	141.05														
25	141.35	180.4	71.4	760	31.8	28.7	31.5	96.9	100.1	224.2	31.2	180.3	647.8	28.3	14.3
26	141.65														
27	141.95														
28	142.25	182.5	70.4	775.6	31.8	27.9	29.5	94.5	96	233.7	29.8	184.1	639.4	31.8	14.6
29	142.55														
30	142.85	187.9	71.7	784.1	32.5	28.6	30.7	94.6	93.6	235.5	29	189.1	628.9	19.1	15.3
31	143.15														
32	**143.45**	**174.9**	**70.4**	**731.6**	**31.6**	**31.6**	**31.5**	**88.7**	**91.5**	**216.3**	**27.7**	**165.7**	**594.1**	**22.5**	**13.5**
33	**143.75**	**218.6**	**125.7**	**897.1**	**46.6**	**49.2**	**35**	**99.7**	**76.8**	**258**	**27.6**	**147.8**	**865.8**	**44.1**	**11.6**
34	**144.05**	**181.8**	**101.3**	**733.6**	**34.4**	**44.6**	**34.4**	**93.1**	**76.8**	**252.3**	**25.4**	**150.9**	**637.6**	**21.3**	**12.5**
35	144.35														
36	**144.65**	**191.5**	**105.9**	**771.9**	**36.7**	**42.8**	**36.1**	**97.1**	**84.6**	**254.1**	**26.6**	**161.1**	**728**	**23.8**	**11.5**
37	144.95														
38	**145.25**	**182.2**	**89.4**	**698.3**	**33**	**34.5**	**28.6**	**85.1**	**83.3**	**220.6**	**25.8**	**145.8**	**639.6**	**23.9**	**12.4**
39	145.55														
40	**145.85**	**175.5**	**78.9**	**656.8**	**32.2**	**31.7**	**28.3**	**87.4**	**94**	**210**	**26.6**	**156.7**	**634.1**	**20.6**	**12.5**
41	146.15														
42	146.45	174.6	73.5	659.3	31	29.9	29.1	91.2	102.6	208.6	28.7	162.3	621.2	27.8	13
43	146.75														
44	147.05														
45	147.35	173.6	69.8	655.6	31.5	27.9	27.9	90.8	101.3	204.1	31.4	161.7	639	28.8	14.7
46	147.65	174.7	71.4	684.8	32.5	29	31.2	97.7	112.1	215.2	33.4	176.5	641.9	26.9	13.9
47	147.95														
48	148.25	176.9	71	708.4	32.7	26.3	27.7	93.2	104.3	206.6	27.3	167.5	633.8	24.4	13.8
49	148.55														
50	148.85														
51	149.15	167.7	69	698.4	30.8	26.1	26.2	85.7	95.5	200.7	29.2	162.5	611.2	18.5	12.6
52	149.45														
53	149.75														
54	150.05	169.7	69	733.3	31.4	26.5	28.3	91.2	101.4	205.4	30.8	166.9	624.5	29.1	14
55	150.35														
56	150.65	182.9	72.5	760.7	32.3	27.7	29	94.4	102.1	218.3	30.3	176.3	675.5	24.4	14.1
57	150.95														
58	151.25	185.7	82.6	767	33.9	32.5	32.3	89.4	88.5	235.8	28.1	171.3	661.9	23.1	13.8
59	151.55														
60	**151.85**	**186.2**	**82**	**777.5**	**35.5**	**31.8**	**31.6**	**94.5**	**90.4**	**229.1**	**28.9**	**176.1**	**659.6**	**25.8**	**13.7**
61	**152.15**	**187.8**	**97.1**	**804.9**	**41.9**	**41.5**	**33.3**	**95.5**	**85**	**235.4**	**26.7**	**151.5**	**728**	**21.8**	**11.3**
62	152.45														
63	**152.75**	**188.3**	**100.3**	**758.2**	**34.4**	**42.1**	**33.6**	**87.2**	**73.4**	**248.6**	**24.6**	**139.9**	**655.7**	**30.2**	**10.1**
64	152.05														
65	153.35														
66	**153.65**	**184.4**	**95.1**	**736.1**	**33.8**	**37.2**	**35.5**	**91.6**	**81.9**	**234**	**25.7**	**151.6**	**655.7**	**34.8**	**11.8**
67	153.95														
68	154.25														
69	154.55	174.8	81.6	683	32.4	31.5	27.9	89.6	90.6	213.7	26.9	150.9	637.8	30.2	12.9
70	154.85	179.2	80.7	696.4	33.4	31	29.4	93.2	97.9	214.8	27.5	161	655.2	18.5	13.4

[1] Data have not been salt corrected.

Table A11 Geochemical Data Multicore JT96-04.

General Geochemical Data for Multicore (mc) JT96-04.

Sample	Depth (m)	Calendar Age (kyrs)	Cl⁻ (wt. %)	δ¹⁵N (‰ vs air)	δ¹³C$_{org}$ (‰ vs PDB)	N$_{tot}$ (wt. %)	C$_{tot}$ (wt. %)	S$_{tot}$ (wt. %)	CaCO$_3$ (wt. %)	%C$_{org}$ (wt. %)	C$_{org}$/N	Opal (wt. %)	Ba$_{bio}$ (μg/g)
0-1 mc	0.5		0.69		-20.49	0.06	0.54	0.04	0.27	0.51	8.2	2.5	9
1-2 mc	1.5		0.64			0.06	0.53	0.03	0.17	0.51	8.4		
2-3 mc	2.5		0.62			0.07	0.54	0.04	0.20	0.52	7.6		
3-4 mc	3.5		0.58			0.06	0.49	0.03	0.22	0.46	7.6		
4-5 mc	4.5		0.72			0.06	0.51	0.03	0.17	0.49	7.9		
5-6 mc	5.5		0.66		-20.51	0.06	0.51	0.03	0.22	0.48	7.9	3.2	9
6-7 mc	6.5		0.57			0.07	0.57	0.05	0.19	0.55	8.2		
7-8 mc	7.5		0.53			0.07	0.55	0.03	0.22	0.53	7.7		
8-9 mc	8.5		0.62			0.07	0.59	0.04	0.32	0.55	8.0		
9-10 mc	9.5		0.66			0.07	0.59	0.07	0.28	0.56	8.5		
10-11 mc	10.5		0.74		-22.40	0.06	0.58	0.15	0.41	0.51	8.8	3.2	59
11-12 mc	11.5		0.82			0.04	0.60	0.35	1.23	0.45	10.2		
12-13 mc	12.5		0.74			0.05	0.55	0.28	0.42	0.50	9.5		
13-14 mc	13.5		0.80			0.06	0.61	0.25	0.52	0.54	9.3		
14-16 mc	15.0		0.79		-23.60	0.05	0.58	0.29	0.94	0.46	9.5	2.9	-
16-18 mc	17.0		0.68			0.06	0.57	0.13	0.40	0.52	8.9		

Major Element Data for Multicore (mc) JT96-04.

Sample	Depth (m)	Al$_2$O$_3$ (%)	Fe$_2$O$_3$ (%)	K$_2$O (%)	MgO (%)	P$_2$O$_5$ (%)	SiO$_2$ (%)	CaO (%)	MnO (%)	TiO$_2$ (%)	Na$_2$O (%)
0-1 mc	0.5	11.70	8.18	1.63	2.27	0.15	66.37	3.07	0.060	0.56	5.94
1-2 mc	1.5										
2-3 mc	2.5										
3-4 mc	3.5										
4-5 mc	4.5										
5-6 mc	5.5	11.93	8.11	1.67	2.31	0.14	67.22	3.14	0.061	0.58	7.54
6-7 mc	6.5										
7-8 mc	7.5										
8-9 mc	8.5										
9-10 mc	9.5										
10-11 mc	10.5	14.33	7.61	1.77	2.86	0.17	63.55	2.95	0.079	0.72	8.27
11-12 mc	11.5										
12-13 mc	12.5										
13-14 mc	13.5										
14-16 mc	15.0	15.87	6.84	1.74	3.10	0.19	61.13	3.21	0.091	0.79	7.96

Minor Element Data for Multicore (mc) JT96-04.

Sample	Depth (m)	V (μg/g)	Cr (μg/g)	Mn (μg/g)	Co (μg/g)	Ni (μg/g)	Cu (μg/g)	Zn (μg/g)	As (μg/g)	Rb (μg/g)	Sr (μg/g)	Y (μg/g)	Zr (μg/g)	Ba (μg/g)	Pb (μg/g)	Br (μg/g)
0-1 mc	0.5	110	151	404	29	25	16	64	3	54	307	15	129	291	16	55
1-2 mc	1.5															
2-3 mc	2.5															
3-4 mc	3.5															
4-5 mc	4.5															
5-6 mc	5.5	112	133	397	26	26	15	62	2	53	307	16	146	293	14	41
6-7 mc	6.5															
7-8 mc	7.5															
8-9 mc	8.5															
9-10 mc	9.5															
10-11 mc	10.5	164	122	550	27	38	27	83	3	60	283	20	144	397	17	36
11-12 mc	11.5															
12-13 mc	12.5															
13-14 mc	13.5															
14-16 mc	15.0	187	118	672	22	45	32	89		57	288	22	144	450	20	32
16-18 mc	17.0															

210

Trace Metal Data for Multicore (mc) JT96-04.

Sample	Depth (m)	Ag (ng/g)	Cd (µg/g)	Re (ng/g)	Mo (µg/g)	U (µg/g)
0-1 mc	0.5	n.a.	0.09	1.58	0.39	n.a.
1-2 mc	1.5	32	0.11	1.43	0.30	0.92
2-3 mc	2.5	n.a.	0.09	1.60	0.42	0.73
3-4 mc	3.5	27	0.08	1.37	0.35	0.71
4-5 mc	4.5	27	0.07	1.78	0.28	0.65
5-6 mc	5.5	32	0.10	1.66	0.34	0.92
6-7 mc	6.5	27	0.09	1.76	0.28	0.75
7-8 mc	7.5	26	0.10	2.72	0.31	0.88
8-9 mc	8.5	33	0.15	4.17	0.37	1.16
9-10 mc	9.5	47	0.25	4.59	0.40	1.14
10-11 mc	10.5	70	0.30	5.19	0.61	1.41
11-12 mc	11.5	79	0.17	1.91	0.80	1.87
12-13 mc	12.5	77	0.31	3.27	0.83	1.51
13-14 mc	13.5	76	0.24	3.55	0.85	1.36
14-16 mc	15.0	81	0.18	2.50	0.73	1.61
16-18 mc	17.0	62	0.25	5.06	0.47	1.04

Table A12. Geochemical Data for Box Core and Trigger Core JT96-05.

General Geochemical Data for Box Core (bc) and Trigger Core (tc) JT96-05.

Sample	Depth (m)	Calendar Age (kyrs)	Cl^- (wt. %)	$\delta^{15}N$ (‰ vs air)	$\delta^{13}C_{org}$ (‰ vs PDB)	N_{tot} (wt. %)	C_{tot} (wt. %)	S_{tot} (wt. %)	$CaCO_2$ (wt. %)	$\%C_{org}$ (wt. %)	C_{org}/N	Opal (wt. %)	Ba_{bio} (µg/g)
0-1 bc	0.5	0.109	2.48	6.29	-21.27	0.20	1.71	0.21	0.62	1.64	8.3	6.5	560
1-2 bc	1.5	0.328	1.94			0.24	2.00	0.19	0.57	1.94	8.2		556
2-3 bc	2.5	0.547	1.97			0.23	1.94	0.18	0.55	1.88	8.2		559
3-4 bc	3.5	0.766	1.78			0.21	1.79	0.16	0.46	1.74	8.2		
4-5 bc	4.5	0.985	1.75			0.20	1.70	0.16	0.28	1.67	8.3		
5-6 bc	5.5	1.204	1.84	6.55	-20.99	0.21	1.79	0.17	0.32	1.75	8.4	7.1	677
6-7 bc	6.5	1.423	1.80			0.22	1.85	0.16	0.29	1.82	8.3		
7-8 bc	7.5	1.642	1.69			0.22	1.84	0.16	0.29	1.81	8.3		
8-9 bc	8.5	1.861	1.78			0.22	1.86	0.18	0.27	1.83	8.3		
9-10 bc	9.5	2.080	1.76			0.21	1.78	0.16	0.35	1.73	8.4		
10-12 bc	11.0	2.408	1.77	6.72	-21.05	0.21	1.83	0.17	0.37	1.78	8.4	6.7	664
12-14 bc	13.0	2.846	1.59			0.21	1.78	0.15	0.27	1.75	8.4		
14-16 bc	15.0	3.284	1.60	6.48	-21.07	0.20	1.74	0.15	0.25	1.71	8.4	6.5	665
16-18 bc	17.0	3.722	1.41			0.20	1.73	0.13	0.22	1.70	8.6		
18-20 bc	19.0	4.160	1.36			0.20	1.74	0.14	0.29	1.71	8.5		
20-22 bc	21.0	4.598	1.32	6.86	-21.16	0.18	1.60	0.13	0.35	1.56	8.7	5.9	584
22-24 bc	23.0	5.036	1.37			0.20	1.73	0.14	0.31	1.70	8.5		
24-26 bc	25.0	5.473	1.27	6.81	-21.26	0.16	1.47	0.12	0.30	1.43	8.7	5.5	552
26-28 bc	27.0	5.911	1.24			0.18	1.60	0.12	0.31	1.56	8.7		
28-30 bc	29.0	6.349	1.15			0.15	1.35	0.10	0.43	1.30	8.8		
30-32 bc	31.0	6.787	1.18	6.95	-21.46	0.15	1.41	0.12	0.59	1.34	8.8	5.4	513
32-34 bc	33.0	7.225	1.21			0.15	1.46	0.12	0.77	1.37	8.9		
34-36 bc	35.0	7.663	1.28	7.23	-21.62	0.16	1.51	0.12	1.11	1.38	8.7	4.6	496
36-38 bc	37.0	8.101	1.26			0.16	1.61	0.12	1.32	1.45	8.9		
38-40 bc	39.0	8.539	1.23			0.15	1.64	0.12	2.42	1.35	8.9		
40-42 bc	41.0	8.976	1.29	7.94	-21.69	0.16	1.74	0.13	2.68	1.42	8.8	5.1	456
42-44 bc	43.0	9.414	1.28			0.16	1.76	0.13	2.95	1.40	8.9		
44-46 bc	45.0	9.852	1.18	7.75	-21.90	0.14	1.65	0.20	3.08	1.28	9.0	4.8	385
46-48 bc	47.0	10.290	1.12			0.14	1.61	0.24	2.56	1.30	9.6		

Sample	Depth (m)	Calendar Age (kyrs)	Cl^- (wt. %)	$\delta^{15}N$ (‰ vs air)	$\delta^{13}C_{org}$ (‰ vs PDB)	N_{tot} ** (wt. %)	C_{tot} ** (wt. %)	S_{tot} ** (wt. %)	$CaCO_2$ (wt. %)	$\%C_{org}$ (wt. %)	C_{org}/N	Opal (wt. %)	Ba_{bio} (µg/g)
11-12 tc	11.5					0.25	2.13	0.20	0.73				
21-22 tc	21.5					0.28	2.51	0.30	0.71				
31-32 tc	31.5					0.29	2.57	0.33	0.75				
41-42 tc	41.5					0.30	2.60	0.45	0.79				
51-52 tc	51.5					0.26	2.34	0.40	0.82				
61-62 tc	61.5					0.24	2.14	0.30	0.60				
71-72 tc	71.5					0.22	1.99	0.33	0.58				
81-82 tc	81.5					0.20	1.80	0.18	0.54				
91-92 tc	91.5					0.19	1.75	0.24	1.00				
101-102 tc	101.5					0.17	1.67	0.20	1.54				
111-112 tc	111.5					0.17	1.90	0.18	3.53				
121-122 tc	121.5					0.16	1.89	0.29	3.88				
131-132 tc	131.5					0.14	1.69	0.40	2.77				
141-142 tc	141.5					0.10	1.28	0.36	3.12				

** Data have not been salt corrected.

Table A12. (continued)

Major Element Data for Box Core (bc) JT96-05.

Sample	Depth (m)	Al$_2$O$_3$ (%)	Fe$_2$O$_3$ (%)	K$_2$O (%)	MgO (%)	P$_2$O$_3$ (%)	SiO$_2$ (%)	CaO (%)	MnO (%)	TiO$_2$ (%)	Na$_2$O (%)
0-1 bc	0.5	14.40	5.70	1.52	2.28	0.17	63.83	3.10	0.085	0.67	1.33
1-2 bc	1.5	14.18	5.61	1.51	2.66	0.18	61.64	2.89	0.070	0.70	5.92
2-3 bc	2.5	13.71	5.61	1.56	2.56	0.17	60.64	2.87	0.060	0.71	10.60
3-4 bc	3.5										
4-5 bc	4.5										
5-6 bc	5.5	15.21	6.24	1.73	2.86	0.18	64.14	2.74	0.068	0.73	2.56
6-7 bc	6.5										
7-8 bc	7.5										
8-9 bc	8.5										
9-10 bc	9.5										
10-12 bc	11.0	15.29	6.04	1.76	2.89	0.17	64.10	2.76	0.057	0.73	2.62
12-14 bc	13.0										
14-16 bc	15.0	15.21	6.21	1.84	2.65	0.16	62.94	2.65	0.065	0.74	2.28
16-18 bc	17.0										
18-20 bc	19.0										
20-22 bc	21.0	15.45	6.02	1.84	2.59	0.16	63.58	2.72	0.067	0.76	2.23
22-24 bc	23.0										
24-26 bc	25.0	15.34	5.97	1.87	2.67	0.16	63.27	2.75	0.070	0.76	2.49
26-28 bc	27.0										
28-30 bc	29.0										
30-32 bc	31.0	15.66	6.12	1.85	2.74	0.16	63.79	2.88	0.064	0.77	2.64
32-34 bc	33.0										
34-36 bc	35.0	15.87	6.40	1.90	2.99	0.17	63.15	3.23	0.072	0.79	2.76
36-38 bc	37.0										
38-40 bc	39.0										
40-42 bc	41.0	15.69	6.31	1.85	3.03	0.17	61.82	4.16	0.075	0.78	2.71
42-44 bc	43.0										
44-46 bc	45.0	15.53	6.37	1.84	3.16	0.17	61.33	4.46	0.082	0.77	2.94
46-48 bc	47.0										

Minor Element Data for Box Core (bc) JT96-05.

Sample	Depth (m)	V (µg/g)	Cr (µg/g)	Mn (µg/g)	Co (µg/g)	Ni (µg/g)	Cu (µg/g)	Zn (µg/g)	As (µg/g)	Rb (µg/g)	Sr (µg/g)	Y (µg/g)	Zr (µg/g)	Ba (µg/g)	Pb (µg/g)	Br (µg/g)	I (µg/g)
0-1 bc	0.5	134	108	723	13	48	35	100	3	68	286	16	132	920	14	126	538
1-2 bc	1.5	145	118	543	16	49	37	103	3	70	277	17	129	911	16	123	502
2-3 bc	2.5	147	116	473	16	50	38	101	2	70	278	17	124	902	19	116	469
3-4 bc	3.5																
4-5 bc	4.5																
5-6 bc	5.5	149	111	475	12	55	43	110	5	71	268	19	135	1057	7	122	438
6-7 bc	6.5																
7-8 bc	7.5																
8-9 bc	8.5																
9-10 bc	9.5																
10-12 bc	11.0	153	116	472	12	54	41	112	3	70	271	18	136	1046	13	119	380
12-14 bc	13.0																
14-16 bc	15.0	155	110	478	13	56	43	117	3	71	270	20	143	1045	11	104	304
16-18 bc	17.0																
18-20 bc	19.0																
20-22 bc	21.0	173	122	503	11	54	41	117	3	70	271	19	145	970	8	95	234
22-24 bc	23.0																
24-26 bc	25.0	164	115	503	12	56	41	115	2	70	272	21	144	935	13	90	
26-28 bc	27.0																
28-30 bc	29.0																
30-32 bc	31.0	166	117	525	13	55	41	111	4	70	276	20	142	904	7	82	174
32-34 bc	33.0																
34-36 bc	35.0	169	114	539	15	55	42	113	3	71	275	22	147	892	10	83	155
36-38 bc	37.0																
38-40 bc	39.0																
40-42 bc	41.0	163	112	552	13	54	41	110	5	69	295	21	140	848	9	82	134
42-44 bc	43.0																
44-46 bc	45.0	166	110	586	16	52	39	103	4	66	302	21	135	774	12	76	113
46-48 bc	47.0																

Table A12. (continued)

Trace Metal Data for Box Core (bc) JT96-05.

Sample	Depth (m)	Ag (ng/g)	Cd (µg/g)	Re (ng/g)	Mo (µg/g)	U (µg/g)
0-1 bc	0.5	357	0.14	1.41	0.52	1.01
1-2 bc	1.5	375	0.09	1.61	0.41	1.11
2-3 bc	2.5	466	0.12	1.54	0.40	0.98
3-4 bc	3.5	400	0.18	3.00	0.37	1.32
4-5 bc	4.5	431	0.13	2.47	0.36	1.07
5-6 bc	5.5	478	0.09	2.64	0.33	1.16
6-7 bc	6.5	501	0.10	3.14	0.38	1.07
7-8 bc	7.5	553	0.15	2.79	0.39	1.11
8-9 bc	8.5	506	0.16	3.29	0.33	1.13
9-10 bc	9.5	474	0.22	3.37	0.41	1.07
10-12 bc	11.0	573	0.26	3.97	0.45	1.54
12-14 bc	13.0	538	0.20	4.90	0.39	1.37
14-16 bc	15.0	555	0.22	9.56	0.43	1.71
16-18 bc	17.0	584	0.43	14.13	0.49	1.93
18-20 bc	19.0	527	0.34	34.81	0.61	2.62
20-22 bc	21.0	513	0.70	43.31	0.54	2.59
22-24 bc	23.0	519	0.57	17.85	0.63	2.46
24-26 bc	25.0	453	0.63	42.22	0.80	2.92
26-28 bc	27.0	410	0.56	27.46	0.77	2.88
28-30 bc	29.0	459	0.45	30.26	0.58	1.92
30-32 bc	31.0	423	0.67	32.41	0.59	2.79
32-34 bc	33.0	477	0.65	32.75	0.78	2.89
34-36 bc	35.0	441	0.50	30.95	0.78	2.70
36-38 bc	37.0	413	0.43	15.95	0.60	2.69
38-40 bc	39.0	442	0.44	26.59	0.70	2.61
40-42 bc	41.0	445	0.44	15.41	0.70	2.92
42-44 bc	43.0	405	0.44	11.70	0.88	3.13
44-46 bc	45.0	385	0.42	18.52	0.90	3.18
46-48 bc	47.0	402	0.48	25.77	1.15	2.92

Table A13. Geochemical Data for Multicore, Box Core and Piston Core JT96-06.

Basic Geochemical Data for Multicore (mc), Box Core (bc) and Piston Core (pc) JT96-06.

Sample	Depth (m)	Calendar Age (kyrs)	Cl⁻ (wt. %)	δ¹⁵N (‰ vs air)	δ¹³C_org (‰ vs PDB)	N_tot (wt. %)	C_tot (wt. %)	S_tot (wt. %)	CaCO₃ (wt. %)	%C_org (wt. %)	C_org/N	Opal (wt. %)	Ba_bio (µg/g)
0-2 mc	1.0		2.48	6.40	-21.20	0.24	2.09	0.17	1.04	1.97	8.4		
2-4 mc	3.0		2.27			0.22	1.94	0.16	0.49	1.88	8.5		
4-6 mc	5.0		2.21	6.24	-21.03	0.21	1.80	0.10	0.36	1.75	8.6		
6-8 mc	7.0		1.25			0.18	1.59	0.11	0.27	1.56	8.6		
8-10 mc	9.0		1.17			0.18	1.59	0.10	0.26	1.56	8.5		
10-12 mc	11.0		1.27	6.35	-21.14	0.18	1.63	0.11	0.34	1.59	8.6		
12-14 mc	13.0		1.22			0.17	1.52	0.09	0.27	1.48	8.7		
14-16 mc	15.0		1.43	6.47	-21.13	0.17	1.52	0.10	0.28	1.49	8.8		
16-18 mc	17.0		1.32	6.65	-21.16	0.15	1.40	0.11	0.35	1.36	8.8		

Sample	Depth (m)	Calendar Age (kyrs)	Cl⁻ (wt. %)	δ¹⁵N (‰ vs air)	δ¹³C_org (‰ vs PDB)	N_tot (wt. %)	C_tot (wt. %)	S_tot (wt. %)	CaCO₃ (wt. %)	%C_org (wt. %)	C_org/N	Opal (wt. %)	Ba_bio (µg/g)
0-0.5 bc	0.3		1.25	6.84	-21.17	0.24	2.15	0.19	1.22	2.00	8.3	6.3	164
0.5-1 bc	0.8		0.92			0.23	2.06	0.11	1.12	1.93	8.2		
1-2 bc	1.5		1.01			0.22	1.93	0.11	0.73	1.84	8.4		
2-3 bc	2.5		0.80			0.23	1.95	0.10	0.57	1.88	8.3		
3-4 bc	3.5		0.86			0.23	1.98	0.12	0.52	1.92	8.3		
4-5 bc	4.5		0.84	6.86	-20.99	0.21	1.84	0.09	0.51	1.78	8.4	5.1	150
5-7 bc	6.0		0.86			0.21	1.78	0.10	0.41	1.73	8.4		
7-9 bc	8.0		0.76			0.19	1.66	0.09	0.39	1.61	8.4		
9-11 bc	10.0		0.78	6.58	-21.16	0.17	1.53	0.08	0.40	1.48	8.5	4.6	125
11-13 bc	12.0		0.83			0.18	1.58	0.09	0.40	1.53	8.4		
13-15 bc	14.0		0.87	6.45	-20.94	0.17	1.53	0.09	0.39	1.48	8.5	4.5	146
17-19 bc	18.0		0.85			0.16	1.39	0.09	0.48	1.34	8.6		
21-23 bc	22.0		0.65	6.61	-23.71	0.07	0.84	0.34	1.70	0.64	9.5	4.3	205
25-27 bc	26.0		0.62	6.31	-23.33	0.05	0.91	0.27	3.01	0.55	10.6	3.9	192
29-31 bc	30.0		0.61	5.80	-23.50	0.06	0.86	0.25	2.69	0.54	9.8		
33-35 bc	34.0		0.79	5.94	-23.46	0.06	0.85	0.38	2.25	0.58	9.7	5.2	142

Sample	Depth (m)	Calendar Age (kyrs)	Cl⁻ (wt. %)	δ¹⁵N (‰ vs air)	δ¹³C_org (‰ vs PDB)	N_tot (wt. %)	C_tot (wt. %)	S_tot (wt. %)	CaCO₃ (wt. %)	%C_org (wt. %)	C_org/N	Opal (wt. %)	Ba_bio (µg/g)
1-2 pc	0.5		1.49		-21.04	0.19	1.66	0.11	0.31	1.62	8.6		
11-12 pc	11.5		1.33		-23.36	0.07	0.79	0.32	1.59	0.60	9.1		
21-22 pc	21.5		1.01		-23.17	0.06	0.91	0.34	3.13	0.53	8.6		
31-32 pc	31.5		1.12		-23.19	0.06	1.00	0.28	3.68	0.56	8.9		
41-42 pc	41.5		1.06		-23.41	0.06	0.98	0.26	3.40	0.57	9.3		
51-52 pc	51.5		0.97		-23.70	0.06	0.93	0.25	3.36	0.52	9.5		
61-62 pc	61.5		1.27		-23.27	0.07	0.95	0.37	2.54	0.64	9.3		
71-72 pc	71.5		1.14		-23.23	0.06	0.87	0.29	2.22	0.60	9.9		
81-82 pc	81.5		1.16		-24.33	0.06	0.77	0.31	1.56	0.58	9.9		
91-92 pc	91.5		1.16		-24.20	0.06	0.93	0.38	2.59	0.62	9.7		
101-102 pc	101.5		1.20		-24.16	0.06	0.91	0.45	2.52	0.61	9.5		
111-112 pc	111.5		1.21		-24.56	0.06	0.72	0.26	1.21	0.57	10.0		
121-122 pc	121.5		1.08		-24.58	0.05	0.69	0.29	1.27	0.54	10.2		
131-132 pc	131.5		1.13		-24.58	0.05	0.69	0.27	1.34	0.53	10.0		
141-142 pc	141.5		1.14		-24.53	0.06	0.69	0.35	1.32	0.53	9.6		
151-152 pc	151.5		1.15		-24.68	0.05	0.70	0.28	2.05	0.46	9.7		
161-162 pc	161.5		1.09		-24.46	0.05	0.73	0.29	1.68	0.53	9.7		
171-172 pc	171.5		1.04		-24.28	0.05	0.72	0.28	1.59	0.53	9.9		
181-182 pc	181.5		1.01		-24.63	0.05	0.67	0.28	1.24	0.52	10.3		
191-192 pc	191.5		1.07		-24.55	0.04	0.77	0.16	3.32	0.37	8.7		
201-202 pc	201.5		0.97		-25.02	0.05	0.65	0.31	1.27	0.50	10.3		
211-212 pc	211.5		1.03		-24.59	0.05	0.69	0.29	1.46	0.51	10.1		
221-222 pc	221.5		0.99		-24.63	0.05	0.66	0.31	1.30	0.50	9.8		
231-232 pc	231.5		1.02		-24.51	0.05	0.71	0.33	1.36	0.55	10.2		
241-241 pc	241.5		0.08		-24.52	0.05	0.66	0.34	1.34	0.50	10.1		
251-252 pc	251.5		1.01		-24.61	0.05	0.71	0.24	1.58	0.52	10.1		
261-262 pc	261.5		0.97		-24.65	0.06	0.69	0.28	1.26	0.54	9.8		
271-272 pc	271.5		0.74		-24.44	0.06	0.72	0.33	1.56	0.53	9.3		
281-282 pc	281.5		0.76		-24.35	0.05	0.78	0.30	2.25	0.51	9.5		
291-292 pc	291.5		0.99		-24.54	0.06	0.71	0.28	1.37	0.54	9.9		
301-302 pc	301.5		0.75		-23.69	0.04	0.89	0.11	4.07	0.40	9.1		
309-310 pc	309.5		0.78		-23.81	0.04	0.90	0.20	4.53	0.36	8.5		

Table A13. (continued)

Major Element Data for Multicore (mc), Box Core (bc) and Piston Core (pc) JT96-06.

Sample	Depth (m)	Al₂O₃ (%)	Fe₂O₃ (%)	K₂O (%)	MgO (%)	P₂O₅ (%)	SiO₂ (%)	CaO (%)	MnO (%)	TiO₂ (%)	Na₂O (%)
0-2 mc	1.0	13.87	7.01	1.53	2.55	0.20	63.00	3.14	0.069	0.72	1.53
2-4 mc	3.0										
4-6 mc	5.0	14.38	7.29	1.69	2.57	0.19	65.53	2.89	0.063	0.74	2.12
6-8 mc	7.0										
8-10 mc	9.0										
10-12 mc	11.0	14.19	7.43	1.78	2.65	0.17	64.60	2.80	0.064	0.74	2.65
12-14 mc	13.0										
14-16 mc	15.0	14.55	7.18	1.83	2.71	0.17	65.62	2.86	0.065	0.75	2.73
16-18 mc	17.0	13.23	6.87	1.78	2.62	0.17	62.38	2.86	0.063	0.73	4.21

Sample	Depth (m)	Al₂O₃ (%)	Fe₂O₃ (%)	K₂O (%)	MgO (%)	P₂O₅ (%)	SiO₂ (%)	CaO (%)	MnO (%)	TiO₂ (%)	Na₂O (%)
0-0.5 bc	0.3	13.33	6.69	1.51	2.46	0.21	61.92	3.22	0.065	0.72	7.25
0.5-1 bc	0.8										
1-2 bc	1.5										
2-3 bc	2.5										
3-4 bc	3.5										
4-5 bc	4.5	13.78	6.70	1.60	2.52	0.17	63.04	2.81	0.060	0.73	5.70
5-7 bc	6.0										
7-9 bc	8.0										
9-11 bc	10.0	13.57	7.16	1.61	2.56	0.19	63.58	2.76	0.063	0.72	5.58
11-13 bc	12.0										
13-15 bc	14.0	13.64	6.65	1.66	2.54	0.17	63.94	2.91	0.066	0.73	6.43
17-19 bc	18.0										
21-23 bc	22.0	16.67	6.65	2.09	3.39	0.19	60.17	3.20	0.091	0.80	5.10
25-27 bc	26.0	15.97	6.30	2.01	3.19	0.19	61.03	3.87	0.088	0.78	5.04
29-31 bc	30.0										
33-35 bc	34.0	16.55	6.94	1.95	3.47	0.19	59.01	3.73	0.101	0.81	5.07

Sample	Depth (m)	Al₂O₃ (%)	Fe₂O₃ (%)	K₂O (%)	MgO (%)	P₂O₅ (%)	SiO₂ (%)	CaO (%)	MnO (%)	TiO₂ (%)	Na₂O (%)
1-2 pc	0.5	13.07	7.22	1.70	2.61	0.17	61.64	2.69	0.061	0.72	4.82
11-12 pc	11.5	15.96	6.86	2.46	3.38	0.19	57.45	3.01	0.100	0.81	4.56
21-22 pc	21.5	15.37	6.59	2.15	3.23	0.19	58.99	3.95	0.093	0.79	3.05
31-32 pc	31.5	15.66	6.67	2.27	3.34	0.20	57.86	4.07	0.096	0.80	2.95
41-42 pc	41.5	15.53	6.49	2.19	3.22	0.19	59.32	3.92	0.103	0.79	2.90
51-52 pc	51.5	15.19	6.28	2.16	3.10	0.19	59.59	4.00	0.099	0.77	3.56
61-62 pc	61.5	15.84	6.78	2.03	3.37	0.18	58.15	3.62	0.101	0.79	3.31
71-72 pc	71.5	15.46	6.82	1.86	3.38	0.18	58.28	3.83	0.087	0.79	4.16
81-82 pc	81.5	16.25	7.19	1.87	3.49	0.18	57.60	2.94	0.094	0.81	4.55
91-92 pc	91.5	15.91	6.95	1.98	3.32	0.18	56.92	3.27	0.099	0.82	4.02
101-102 pc	101.5	16.01	6.92	1.94	3.37	0.18	56.78	3.19	0.090	0.81	4.59
111-112 pc	111.5	16.25	7.49	1.93	3.64	0.20	56.17	2.93	0.101	0.85	7.89
121-122 pc	121.5	15.91	7.49	1.96	3.48	0.20	56.09	3.02	0.108	0.86	3.57
131-132 pc	131.5	17.62	7.81	2.05	3.72	0.22	61.42	3.09	0.102	0.88	3.56
141-142 pc	141.5	16.07	7.45	1.88	3.42	0.20	57.56	3.15	0.107	0.85	5.08
151-152 pc	151.5	16.22	7.30	1.98	3.46	0.20	57.81	3.31	0.101	0.87	2.84
161-162 pc	161.5	16.10	7.43	1.89	3.49	0.20	57.65	3.33	0.104	0.85	2.91
171-172 pc	171.5	16.25	7.31	1.84	3.46	0.20	57.96	3.27	0.103	0.85	2.90
181-182 pc	181.5	16.14	7.39	1.84	3.43	0.20	57.79	3.09	0.097	0.84	2.93
191-192 pc	191.5	16.01	6.77	2.56	3.34	0.22	56.65	3.47	0.104	0.88	3.80
201-202 pc	201.5	16.02	7.50	1.75	3.49	0.20	57.50	3.18	0.105	0.87	3.68
211-212 pc	211.5	16.05	7.31	1.83	3.45	0.20	56.92	3.10	0.110	0.85	6.42
221-222 pc	221.5	16.05	7.45	1.84	3.45	0.20	57.15	3.06	0.102	0.85	3.60
231-232 pc	231.5	16.18	7.48	1.80	3.49	0.20	56.56	2.98	0.102	0.86	5.90
241-241 pc	241.5										
251-252 pc	251.5	16.54	7.55	2.13	3.59	0.21	56.50	2.99	0.104	0.87	4.02
261-262 pc	261.5	16.74	7.80	1.93	3.59	0.20	58.35	3.00	0.102	0.87	3.77
271-272 pc	271.5										
281-282 pc	281.5										
291-292 pc	291.5	16.18	7.60	2.01	3.52	0.19	56.25	3.01	0.104	0.85	3.17
301-302 pc	301.5	14.25	6.46	1.88	2.98	0.19	59.59	4.88	0.089	0.90	3.01
309-310 pc	309.5	14.70	6.57	2.16	2.92	0.21	58.82	4.76	0.090	0.93	4.58

217

Table A13. (continued)

Minor Element Data for Multicore (mc), Box Core (bc) and Piston Core (pc) JT96-06.

Sample	Depth (m)	V (µg/g)	Cr (µg/g)	Mn (µg/g)	Co (µg/g)	Ni (µg/g)	Cu (µg/g)	Zn (µg/g)	As (µg/g)	Rb (µg/g)	Sr (µg/g)	Y (µg/g)	Zr (µg/g)	Ba (µg/g)	Pb (µg/g)	Br (µg/g)	I (µg/g)
0-2 mc	1.0	140	127	496	11	48	31	95	3	73	283	16	156	534	17	170	635
2-4 mc	3.0																
4-6 mc	5.0	152	141	493	14	51	31	97	7	68	279	18	161	542	8	104	430
6-8 mc	7.0																
8-10 mc	9.0																
10-12 mc	11.0	148	131	499	10	52	32	97	4	70	279	19	166	552	10	108	326
12-14 mc	13.0																
14-16 mc	15.0	151	129	506	9	49	30	92	5	68	287	20	160	547	11	95	312
16-18 mc	17.0	155	142	529	12	47	28	91	6	66	292	18	170	553	4	86	265

Sample	Depth (m)	V (µg/g)	Cr (µg/g)	Mn (µg/g)	Co (µg/g)	Ni (µg/g)	Cu (µg/g)	Zn (µg/g)	As (µg/g)	Rb (µg/g)	Sr (µg/g)	Y (µg/g)	Zr (µg/g)	Ba (µg/g)	Pb (µg/g)	Br (µg/g)	I (µg/g)
0-0.5 bc	0.3	146	130	495	20	44	32	99	2	69	289	19	157	498	22	154	484
0.5-1 bc	0.8																
1-2 bc	1.5																
2-3 bc	2.5																
3-4 bc	3.5																
4-5 bc	4.5	155	145	473	20	45	30	96	2	68	278	19	168	495	19	115	313
5-7 bc	6.0																
7-9 bc	8.0																
9-11 bc	10.0	146	147	472	20	43	29	92	2	66	285	18	176	465	20	100	256
11-13 bc	12.0																
13-15 bc	14.0	155	147	496	20	44	29	92	2	65	287	18	169	487	18	91	215
17-19 bc	18.0																
21-23 bc	22.0	187	127	718	21	54	37	102	2	82	287	23	131	622	23	29	27
25-27 bc	26.0	173	123	710	20	51	34	96	5	77	305	24	135	591	23	23	20
29-31 bc	30.0																
33-35 bc	34.0	195	124	791	23	54	40	101	4	71	304	23	129	555	25	22	18

Sample	Depth (m)	V (µg/g)	Cr (µg/g)	Mn (µg/g)	Co (µg/g)	Ni (µg/g)	Cu (µg/g)	Zn (µg/g)	As (µg/g)	Rb (µg/g)	Sr (µg/g)	Y (µg/g)	Zr (µg/g)	Ba (µg/g)	Pb (µg/g)	Br (µg/g)	I (µg/g)
1-2 pc	0.5	146	132	485	13	47	30	94	4	69	276	19	154	519	13	107	388
11-12 pc	11.5	182	123	743	16	61	40	109	8	89	284	24	137	683	8	16	2
21-22 pc	21.5	170	118	748	20	51	33	98	5	76	307	23	143	616	15	13	-11
31-32 pc	31.5	181	122	807	15	55	36	101	9	82	304	24	137	679	6	13	-10
41-42 pc	41.5	169	116	774	13	56	35	98	6	80	309	24	143	649	14	12	13
51-52 pc	51.5	166	115	790	15	52	34	96	7	77	311	23	136	647	10	11	0
61-62 pc	61.5	181	115	762	18	56	39	102	6	72	286	24	129	586	12	16	-1
71-72 pc	71.5	184	131	805	17	60	37	98	7	66	298	22	132	586	11	14	-7
81-82 pc	81.5	195	123	781	16	59	37	99	7	64	257	23	127	537	10	9	-1
91-92 pc	91.5	195	112	730	15	51	37	96	7	69	252	24	135	537	13	10	-9
101-102 pc	101.5	190	113	714	16	53	38	97	6	70	247	23	133	546	14	11	-12
111-112 pc	111.5	210	115	827	18	56	44	102	4	63	253	23	126	517	14	8	-23
121-122 pc	121.5	202	108	801	21	50	43	100	9	63	261	24	129	505	7	6	-14
131-132 pc	131.5	201	108	783	18	49	43	102	5	67	260	24	131	513	15	8	-17
141-142 pc	141.5	201	114	818	17	53	41	98	6	60	271	24	129	550	10	3	-5
151-152 pc	151.5	197	102	810	21	46	41	101	7	75	257	25	135	536	15	1	-6
161-162 pc	161.5	195	102	793	17	49	41	101	7	75	260	26	136	534	13	2	-1
171-172 pc	171.5	197	109	800	20	51	40	97	8	62	272	24	131	506	11	4	-8
181-182 pc	181.5	203	114	826	17	50	42	98	7	60	273	24	131	524	12	2	-6
191-192 pc	191.5	197	111	809	16	52	40	97	9	58	271	24	127	506	8	1	-11
201-202 pc	201.5	211	118	865	17	52	45	98	8	58	262	23	127	532	9	1	-7
211-212 pc	211.5	199	106	820	16	51	42	103	10	64	264	25	127	531	7	2	-6
221-222 pc	221.5	200	113	830	17	52	40	99	9	59	274	24	129	521	10	3	-2
231-232 pc	231.5	209	118	859	15	52	45	102	8	62	263	24	126	545	13	2	-16
241-241 pc	241.5																
251-252 pc	251.5	205	109	840	22	51	42	104	7	71	251	25	131	527	14	2	-11
261-262 pc	261.5	203	112	836	20	51	42	99	11	59	257	24	125	497	7	3	-15
271-272 pc	271.5																
281-282 pc	281.5																
291-292 pc	291.5	207	113	846	18	53	44	101	9	62	262	25	128	504	9	0	-8
301-302 pc	301.5	184	105	738	15	44	29	85	6	68	307	26	186	576	10	6	-5
309-310 pc	309.5	181	91	708	16	41	34	92	4	85	284	27	178	598	15	5	2

Table A13. (continued)

Trace Metal Data for Multicore (mc), Box Core (bc) and Piston Core (pc) JT96-06.

Sample	Depth (m)	Ag (ng/g)	Cd (µg/g)	Re (ng/g)	Mo (µg/g)	U (µg/g)
0-2 mc	1.0	111	0.15	2.44	0.62	1.07
2-4 mc	3.0	114	0.25	2.93	0.65	1.34
4-6 mc	5.0	111	0.22	4.26	0.56	1.21
6-8 mc	7.0	111	0.19	5.00	0.60	1.37
8-10 mc	9.0	105	0.18	4.48	0.53	1.33
10-12 mc	11.0	111	0.19	4.87	0.51	1.34
12-14 mc	13.0	97	0.21	4.98	0.56	1.52
14-16 mc	15.0	106	0.23	5.21	0.55	1.26
16-18 mc	17.0	115	0.26	4.73	0.55	1.28

Sample	Depth (m)	Ag (ng/g)	Cd (µg/g)	Re (ng/g)	Mo (µg/g)	U (µg/g)
0-0.5 bc	0.3	97	0.16	3.63	0.57	1.49
0.5-1 bc	0.8	94	0.16	2.59	0.53	0.96
1-2 bc	1.5	84	0.21	3.12	0.54	1.26
2-3 bc	2.5	100	0.29	3.64	0.58	1.38
3-4 bc	3.5	103	0.31	3.86	0.66	1.40
4-5 bc	4.5	117	0.24	3.65	0.60	1.53
5-7 bc	6.0	98	0.24	3.91	0.52	1.45
7-9 bc	8.0	94	0.17	4.20	0.47	1.38
9-11 bc	10.0	106	0.16	3.69	0.48	1.56
11-13 bc	12.0	85	0.16	3.90	0.43	0.99
13-15 bc	14.0	106	0.20	5.12	0.62	1.64
17-19 bc	18.0	91	0.30	5.63	0.51	1.15
21-23 bc	22.0	106	0.42	9.10	0.82	2.17
25-27 bc	26.0	96	0.22	5.44	1.05	2.44
29-31 bc	30.0	106	0.26	3.50	1.35	2.17
33-35 bc	34.0	119	0.24	3.23	1.18	2.03

219

Table A14. Geochemical Data for Multicore and Piston Core JT96-09.

General Geochemical Data for Multicore (mc) and Piston Core (pc) JT96-09.

Sample	Depth (cm)	Depth * (cm, corr.)	Calendar Age (kyrs)	Cl⁻ (wt. %)	$\delta^{15}N$ (‰ vs air)	$\delta^{13}C_{org}$ (‰ vs PDB)	N_{tot} (wt. %)	C_{tot} (wt. %)	S_{tot} (wt. %)	$CaCO_3$ (wt. %)	$\%C_{org}$ (wt. %)	C_{org}/N	Opal (wt. %)	Ba_{bio} (μg/g)
0-1 mc	0.5	0.5	0.11	4.04	6.74	-21.28	0.35	3.20	0.35	1.05	3.07	8.7	7.0	256
1-2 mc	1.5	1.5	0.32	3.47			0.36	3.16	0.35	0.92	3.05	8.4		
2-3 mc	2.5	2.5	0.53	3.08			0.37	3.17	0.29	0.85	3.07	8.3		
3-4 mc	3.5	3.5	0.74	2.72			0.36	3.07	0.26	0.64	2.99	8.4		
4-5 mc	4.5	4.5	0.95	2.46			0.36	3.09	0.25	0.53	3.03	8.4		
5-6 mc	5.5	5.5	1.16	2.31	7.03	-21.19	0.35	3.03	0.23	0.58	2.96	8.5	6.7	226
6-8 mc	7.0	7.0	1.48	2.23			0.35	3.01	0.22	0.36	2.97	8.5		
8-10 mc	9.0	9.0	1.90	2.16			0.35	3.01	0.22	0.30	2.97	8.5		
10-12 mc	11.0	11.0	2.32	2.31	6.66	-21.19	0.31	2.80	0.25	0.18	2.78	8.9	6.8	202
12-14 mc	13.0	13.0	2.74	2.06			0.33	2.84	0.22	0.29	2.80	8.6		
14-16 mc	15.0	15.0	3.17	2.17	6.81	-21.17	0.31	2.75	0.21	0.32	2.71	8.7	5.8	230
16-18 mc	17.0	17.0	3.59	2.51			0.32	2.79	0.22	0.33	2.75	8.6		
18-20 mc	19.0	19.0	4.01	1.84			0.23	2.11	0.17	0.35	2.07	8.9		
20-22 mc	21.0	21.0	4.43	1.92	6.50	-21.39	0.20	1.96	0.18	0.41	1.91	9.4	4.3	219
22-24 mc	23.0	23.0	4.86	1.63			0.19	1.79	0.14	0.72	1.70	9.1		
24-26 mc	25.0	25.0	5.28	1.50	7.71	-21.67	0.18	1.79	0.15	1.16	1.65	9.3	4.4	174
26-28 mc	27.0	27.0	5.70	1.61			0.18	1.83	0.15	1.87	1.61	9.0		
28-30 mc	29.0	29.0	6.12	1.68			0.18	1.90	0.17	2.10	1.64	9.0		
30-32 mc	31.0	31.0	6.54	1.63	7.35	-21.64	0.18	1.91	0.19	2.33	1.63	9.2	4.5	181
32-34 mc	33.0	33.0	6.97	1.80			0.19	1.99	0.20	2.40	1.70	9.1		
34-36 mc	35.0	35.0	7.39	1.68	7.93	-21.63	0.18	2.01	0.21	2.37	1.72	9.4	4.9	166
36-38 mc	37.0	37.0	7.81	1.95			0.20	2.08	0.23	2.39	1.79	9.1		
38-40 mc	39.0	39.0	8.23	1.77	7.45	-21.85	0.19	2.07	0.27	2.62	1.76	9.2	4.8	181

Sample	Depth (cm)	Depth * (cm, corr.)	Calendar Age (kyrs)	Cl⁻ (wt. %)	$\delta^{15}N$ (‰ vs air)	$\delta^{13}C_{org}$ (‰ vs PDB)	N_{tot} (wt. %)	C_{tot} (wt. %)	S_{tot} (wt. %)	$CaCO_3$ (wt. %)	$\%C_{org}$ (wt. %)	C_{org}/N	Opal (wt. %)	Ba_{bio} (μg/g)
6-7 pc	6.5	18.5	3.91	2.44	7.33	-21.13	0.30	2.67	0.22	0.83	2.57	8.5	6.6	249
11-12 pc	11.5	23.5	4.96	1.93	6.95	-21.55	0.21	2.02	0.20	0.71	1.94	9.2	4.7	168
16-17 pc	16.5	28.5	6.02	2.01	8.17	-21.56	0.20	2.08	0.22	2.15	1.82	9.1	4.5	
21-22 pc	21.5	33.5	7.07	2.13	7.77	-21.92	0.21	2.29	0.32	2.34	2.01	9.4	5.7	208
26-27 pc	26.5	38.5	8.13	2.11	8.33	-21.75	0.22	2.26	0.39	1.83	2.04	9.2	4.7	
31-32 pc	31.5	43.5	9.18	2.01	8.38	-22.04	0.20	2.23	0.62	2.74	1.90	9.3	5.9	240
36-37 pc	36.5	48.5	10.10	2.01	8.61	-22.02	0.20	2.46	0.64	4.91	1.87	9.1	5.9	
41-42 pc	41.5	53.5	10.47	2.01	8.34	-21.96	0.20	2.55	0.42	5.45	1.90	9.6	6.8	231
46-47 pc	46.5	58.5	10.84	2.05	8.89	-21.99	0.19	2.41	0.99	4.43	1.87	9.7	7.1	
51-52 pc	51.5	63.5	11.21	1.73	7.10	-22.19	0.12	1.47	0.45	2.50	1.17	9.4	4.8	202
56-57 pc	56.5	68.5	11.57	1.44	6.86	-22.67	0.07	0.93	0.26	1.83	0.71	10.0	4.8	178
61-62 pc	61.5	73.5	11.94	1.03	6.23	-23.11	0.06	0.80	0.21	2.26	0.53	8.7	3.7	169
66-67 pc	66.5	78.5	12.29	1.06	5.89	-23.08	0.05	0.77	0.16	1.87	0.55	11.2	4.1	
71-72 pc	71.5	83.5	12.54	0.68	6.21	-23.53	0.04	0.73	0.19	2.77	0.39	10.8	4.3	179
76-77 pc	76.5	88.5	12.74	1.64	7.41	-22.54	0.09	1.20	0.40	2.92	0.85	9.8	4.7	276
81-82 pc	81.5	93.5	12.78	1.48	7.75	-22.75	0.10	1.38	0.34	3.96	0.90	9.3	5.2	285
86-87 pc	86.5	98.5	12.81	1.39	7.20	-22.42	0.09	1.21	0.34	2.67	0.89	9.6	6.1	281
91-92 pc	91.5	103.5	12.87	1.36	7.52	-22.91	0.09	1.30	0.37	3.97	0.82	9.1	4.8	265
96-97 pc	96.5	108.5	13.04	1.35	7.38	-22.44	0.09	1.28	0.40	3.72	0.84	9.8	5.7	265
101-102 pc	101.5	113.5	13.18	1.31	7.36	-22.75	0.10	1.34	0.36	4.04	0.85	8.9		294
106-107 pc	106.5	118.5	13.22	1.31	7.28	-22.69	0.08	1.24	0.31	3.39	0.83	9.9	5.3	237
111-112 pc	111.5	123.5	13.27	1.36	7.10	-23.16	0.08	1.18	0.29	3.47	0.76	9.1	4.6	280
116-117 pc	116.5	128.5	13.31	1.26	6.77	-22.87	0.08	1.15	0.32	3.39	0.74	9.7	5.8	231
121-122 pc	121.5	133.5	13.36	1.38	7.37	-23.01	0.09	1.16	0.38	2.82	0.82	9.0	5.3	250
126-127 pc	126.5	138.5	13.40	1.26	6.75	-23.01	0.08	1.10	0.40	2.99	0.74	9.5	4.7	252
131-132 pc	131.5	143.5	13.44	1.26	7.23	-23.26	0.09	1.12	0.43	2.96	0.77	9.0	5.6	168
136-137 pc	136.5	148.5	13.47	0.64	4.92	-23.75	0.02	0.45	0.30	1.89	0.22	9.1		155
141-142 pc	141.5	153.5	13.47	0.77	7.02	-23.39	0.04	0.76	0.32	2.62	0.45	10.2		180
146-147 pc	146.5	158.5	13.47	0.46	2.93	-23.32	0.01	0.17	0.07	0.87	0.07	6.8		128
151-152 pc	151.5	163.5	13.47	1.01	4.79	-24.24	0.05	0.77	0.33	1.72	0.56	11.0		119
156-157 pc	156.5	168.5	13.49	1.26	4.84	-24.22	0.05	0.74	0.31	1.87	0.52	10.1	4.0	109
161-162 pc	161.5	157.5	13.52	0.93	4.22	-25.20	0.04	0.73	0.16	3.42	0.32	8.3	4.2	204
166-167 pc	166.5	162.5	13.55	0.95	5.00	-24.26	0.05	0.78	0.27	2.36	0.50	9.7		109
171-172 pc	171.5	167.5	13.58	1.06	4.81	-24.64	0.05	0.71	0.29	1.66	0.51	9.7	3.6	76
176-177 pc	176.5	172.5	13.61	0.94	3.98	-24.62	0.05	0.67	0.33	1.54	0.49	10.2		73
181-182 pc	181.5	177.5	13.64	0.95	4.33	-25.05	0.04	0.75	0.14	4.01	0.27	6.9	4.6	226
186-187 pc	186.5	182.5	13.67	0.96	4.57	-24.51	0.05	0.70	0.32	1.77	0.48	10.5		95
191-192 pc	191.5	187.5	13.70	1.00	4.44	-24.86	0.05	0.65	0.38	1.52	0.46	9.7	3.4	69
196-197 pc	196.5	192.5	13.73	0.91	4.21	-24.79	0.05	0.67	0.36	1.27	0.51	11.0		63
201-202 pc	201.5	197.5	13.76	0.91	4.11	-24.68	0.05	0.67	0.34	1.36	0.51	9.8	3.5	65
206-207 pc	206.5	202.5	13.79	0.85	3.72	-24.52	0.04	0.64	0.35	2.02	0.40	10.2		115
211-212 pc	211.5	207.5	13.82	0.99	4.38	-24.69	0.05	0.68	0.37	1.50	0.50	9.5	3.6	37
216-217 pc	216.5	212.5	13.85	0.89	3.50	-24.71	0.05	0.66	0.40	1.21	0.51	10.9		41
221-222 pc	221.5	217.5	13.88	1.17	4.06	-24.81	0.06	0.71	0.36	1.31	0.55	9.9	3.7	33
226-227 pc	226.5	222.5	13.91	0.92	3.81	-24.60	0.05	0.66	0.35	1.27	0.50	10.7		43
231-232 pc	231.5	227.5	13.94	0.81	4.03	-24.68	0.05	0.63	0.37	1.38	0.46	9.5	3.4	42
236-237 pc	236.5	232.5	13.97	0.86	3.85	-24.47	0.05	0.73	0.35	1.32	0.57	11.1		69
241-242 pc	241.5	237.5	14.00	0.91	4.29	-24.62	0.05	0.68	0.35	1.20	0.53	10.1	3.4	34
246-247 pc	246.5	242.5	14.03	1.01	4.31	-24.42	0.05	0.74	0.23	2.07	0.49	10.2		110
251-252 pc	251.5	247.5	14.06	0.83	3.96	-24.59	0.05	0.59	0.38	1.31	0.44	9.7	3.3	11
256-257 pc	256.5	252.5	14.09	0.97	3.85	-24.49	0.05	0.69	0.28	1.42	0.52	10.4		68
261-262 pc	261.5	257.5	14.12	0.97	5.08	-24.49	0.05	0.75	0.24	1.68	0.55	10.3	3.6	68

(continued on next page)

General Geochemical Data for Multicore (mc) and Piston Core (pc) JT96-09 (continued).

Sample	Depth (cm)	Depth * (cm, corr.)	Calendar Age (kyrs)	Cl⁻ (wt. %)	δ^{15}N (‰ vs air)	$\delta^{13}C_{org}$ (‰ vs PDB)	N_{tot} (wt. %)	C_{tot} (wt. %)	S_{tot} (wt. %)	$CaCO_2$ (wt. %)	%C_{org} (wt. %)	C_{org}/N	Opal (wt. %)	Ba_{bio} (μg/g)
266-267 pc	266.5	262.5	14.15	1.01	4.72	-24.27	0.05	0.76	0.24	1.68	0.56	10.5		82
271-272 pc	271.5	267.5	14.18	0.82	4.91	-24.74	0.05	0.74	0.18	2.77	0.41	8.9	4.1	131
276-277 pc	276.5	272.5	14.21	0.94	4.50	-24.41	0.05	0.78	0.35	2.45	0.49	10.0		129
281-282 pc	281.5	277.5	14.25	1.02	4.85	-24.71	0.06	0.81	0.24	2.27	0.53	9.5	3.8	88
286-287 pc	286.5	282.5	14.28	0.95	5.03	-24.24	0.05	0.92	0.23	3.07	0.55	10.3		119
291-292 pc	291.5	287.5	14.33	0.92	5.44	-24.37	0.06	0.91	0.29	3.33	0.51	9.2	4.4	122
296-297 pc	296.5	292.5	14.43	0.91	5.14	-24.15	0.06	0.96	0.22	3.22	0.57	10.2		101
301-302 pc	301.5	297.5	14.54	0.98	4.93	-24.60	0.05	0.88	0.17	3.12	0.50	9.2	3.5	105
306-307 pc	306.5	302.5	14.60	0.89	4.91	-24.43	0.05	0.84	0.21	2.29	0.57	10.3		88
311-312 pc	311.5	307.5	14.75	0.87	5.58	-24.28	0.05	0.93	0.28	4.14	0.43	8.8	4.1	115
316-317 pc	316.5	312.5	14.85	0.81	5.38	-24.07	0.04	0.83	0.13	3.85	0.36	8.8		199
321-322 pc	321.5	317.5	14.96	0.90	5.31	-24.30	0.04	0.80	0.11	3.45	0.39	9.0	4.9	167
326-327 pc	326.5	322.5	15.06	0.92	5.16	-24.23	0.04	0.78	0.16	3.49	0.36	9.1		211
331-332 pc	331.5	327.5	15.17	0.74	4.45	-24.42	0.04	0.75	0.11	3.86	0.29	7.7	4.8	156
336-337 pc	336.5	332.5	15.27	0.81	5.08	-24.36	0.04	0.75	0.12	3.72	0.31	8.7		227
341-342 pc	341.5	337.5	15.38	0.86	5.59	-24.09	0.04	0.82	0.17	3.66	0.38	8.6	4.4	135
346-347 pc	346.5	342.5	15.48	0.79	5.07	-24.09	0.04	0.89	0.09	4.31	0.37	9.4		
351-352 pc	351.5	347.5	15.59	0.86	4.98	-24.41	0.04	0.74	0.12	3.75	0.29	7.7	4.6	173
356-357 pc	356.5	352.5	15.69	0.74	4.58	-24.64	0.03	0.65	0.12	3.37	0.24	8.7		197
361-362 pc	361.5	357.5	15.80	0.92	5.81	-24.10	0.05	0.80	0.10	3.28	0.40	8.7	4.7	201
366-367 pc	366.5	362.5	15.90	0.73	5.65	-24.22	0.04	0.74	0.10	3.52	0.32	9.0		204
371-372 pc	371.5	367.5	16.01	0.78	4.66	-24.52	0.03	0.67	0.14	3.39	0.27	7.7	4.7	151

* Corrected piston core depth (12 cm added to account for loss of surface sediments during piston coring
and a 16 cm turbidite was removed from the depth tally).

Major Element Data for Multicore (mc) and Piston Core (pc) JT96-09.

Sample	Depth * (cm, corr.)	Al_2O_3 (%)	Fe_2O_3 (%)	K_2O (%)	MgO (%)	P_2O_5 (%)	SiO_2 (%)	CaO (%)	MnO (%)	TiO_2 (%)	Na_2O (%)
0-1 mc	0.5	13.61	6.88	1.77	3.08	0.25	52.64	2.66	0.054	0.82	1.56
1-2 mc	1.5										
2-3 mc	2.5										
3-4 mc	3.5										
4-5 mc	4.5										
5-6 mc	5.5	14.74	6.84	1.53	3.02	0.22	56.54	2.32	0.058	0.82	6.68
6-8 mc	7.0										
8-10 mc	9.0										
10-12 mc	11.0	15.38	6.85	1.84	3.21	0.20	58.10	2.22	0.058	0.84	2.21
12-14 mc	13.0										
14-16 mc	15.0	14.92	6.60	1.63	3.06	0.20	57.55	2.29	0.062	0.84	7.53
16-18 mc	17.0										
18-20 mc	19.0										
20-22 mc	21.0	14.01	6.32	1.97	2.92	0.20	54.56	2.58	0.062	0.85	2.07
22-24 mc	23.0										
24-26 mc	25.0	15.64	6.44	1.86	3.09	0.19	58.87	2.95	0.066	0.85	5.57
26-28 mc	27.0										
28-30 mc	29.0										
30-32 mc	31.0	15.81	6.40	1.96	3.26	0.20	57.76	3.42	0.069	0.86	2.82
32-34 mc	33.0										
34-36 mc	35.0	15.72	6.54	1.81	3.16	0.19	57.63	3.56	0.071	0.87	6.14
36-38 mc	37.0										
38-40 mc	39.0	16.16	6.83	2.30	3.10	0.22	58.03	3.72	0.072	0.91	3.84

Sample	Depth * (cm, corr.)	Al_2O_3 (%)	Fe_2O_3 (%)	K_2O (%)	MgO (%)	P_2O_5 (%)	SiO_2 (%)	CaO (%)	MnO (%)	TiO_2 (%)	Na_2O (%)
6-7 pc	18.5	14.94	6.68	1.92	2.86	0.20	58.29	2.31	0.063	0.87	7.32
11-12 pc	23.5	15.10	6.23	1.82	3.13	0.18	56.78	2.42	0.058	0.81	2.48
16-17 pc	28.5										
21-22 pc	33.5	15.67	6.67	1.80	3.18	0.20	55.62	3.30	0.073	0.87	7.79
26-27 pc	38.5	15.90	6.79	2.09	3.35	0.20	56.26	3.12	0.070	0.86	5.40
31-32 pc	43.5	14.83	6.63	1.94	3.11	0.21	53.04	3.49	0.052	0.83	2.70
36-37 pc	48.5	15.18	6.67	2.01	3.24	0.19	54.57	4.96	0.069	0.80	5.38
41-42 pc	53.5	15.20	6.12	1.84	3.43	0.18	53.33	5.05	0.065	0.79	2.37
46-47 pc	58.5	14.87	7.02	1.91	3.32	0.18	54.58	4.85	0.078	0.78	5.51
51-52 pc	63.5	15.41	6.76	2.18	3.13	0.20	56.98	3.82	0.072	0.83	3.66
56-57 pc	68.5	15.64	6.48	2.11	3.38	0.19	60.43	3.61	0.088	0.78	6.78
61-62 pc	73.5	15.90	6.49	2.13	2.83	0.18	64.47	3.81	0.082	0.77	4.50
66-67 pc	78.5	14.51	5.50	1.99	2.88	0.17	63.98	3.78	0.079	0.71	5.42
71-72 pc	83.5	13.92	5.20	1.65	2.38	0.17	64.89	4.03	0.091	0.74	12.30
76-77 pc	88.5	16.39	6.76	2.41	3.55	0.19	57.88	3.77	0.093	0.78	6.88
81-82 pc	93.5	15.93	6.68	2.37	3.28	0.21	54.55	4.23	0.092	0.78	3.55
86-87 pc	98.5	16.27	6.79	2.45	3.60	0.19	57.05	3.64	0.093	0.79	5.25
91-92 pc	103.5	16.97	6.75	2.35	3.73	0.19	57.11	4.10	0.094	0.76	2.99
96-97 pc	108.5	16.23	7.07	2.28	3.62	0.20	56.50	4.28	0.099	0.78	6.21
101-102 pc	113.5	16.37	6.70	2.33	3.36	0.20	55.68	4.16	0.092	0.79	3.57
106-107 pc	118.5	16.30	6.84	2.34	3.59	0.19	56.94	4.08	0.096	0.79	5.63
111-112 pc	123.5	14.67	6.90	2.18	3.33	0.19	51.27	3.89	0.092	0.79	1.45
116-117 pc	128.5	16.48	6.96	2.36	3.61	0.20	57.16	4.02	0.100	0.79	5.29
121-122 pc	133.5	16.03	6.93	2.34	3.30	0.21	56.20	3.64	0.092	0.80	4.00
126-127 pc	138.5	16.42	7.10	2.31	3.61	0.19	57.76	3.69	0.101	0.79	4.43
131-132 pc	143.5	16.28	6.79	2.17	3.63	0.18	57.84	3.60	0.091	0.76	2.73
136-137 pc	148.5	14.19	5.28	1.47	2.28	0.16	66.23	4.08	0.091	0.71	10.07
141-142 pc	153.5	15.49	6.24	1.61	2.95	0.19	58.87	3.10	0.091	0.73	12.39
146-147 pc	158.5	13.26	4.12	1.19	1.86	0.13	71.17	3.95	0.071	0.61	6.77
151-152 pc	163.5	14.57	5.97	1.66	2.40	0.16	63.94	7.12	0.092	0.71	12.42
156-157 pc	152.5	17.03	7.13	2.10	3.61	0.21	59.32	3.29	0.098	0.85	5.07
161-162 pc	157.5	15.94	6.47	2.79	2.98	0.22	59.93	3.86	0.081	0.92	4.40
166-167 pc	162.5	16.57	7.08	2.04	3.50	0.21	58.78	3.64	0.100	0.86	5.24
171-172 pc	167.5	16.68	7.21	2.05	3.30	0.22	57.98	3.33	0.092	0.87	4.30
176-177 pc	172.5	16.61	7.20	1.89	3.58	0.21	57.78	3.29	0.103	0.84	5.15
181-182 pc	177.5	16.55	6.45	2.97	3.06	0.23	59.14	3.79	0.092	0.94	4.59
186-187 pc	182.5	16.74	7.28	2.03	3.58	0.21	58.81	3.30	0.100	0.85	5.09
191-192 pc	187.5	16.70	7.26	1.94	3.25	0.21	58.35	3.23	0.102	0.85	4.64
196-197 pc	192.5	16.68	7.39	1.93	3.63	0.22	58.41	3.13	0.106	0.84	5.33
201-202 pc	197.5	16.70	7.25	1.93	3.24	0.21	58.31	3.23	0.102	0.84	4.67
206-207 pc	202.5	16.53	6.90	2.13	3.34	0.20	59.95	3.44	0.100	0.84	5.86
211-212 pc	207.5	16.93	7.25	1.81	3.71	0.20	57.82	3.11	0.104	0.84	3.35
216-217 pc	212.5	16.86	7.35	1.91	3.59	0.21	59.05	3.10	0.101	0.85	5.65
221-222 pc	217.5	16.93	7.25	1.94	3.29	0.20	57.69	3.06	0.092	0.86	4.39
226-227 pc	222.5	16.92	7.45	1.88	3.65	0.22	58.65	3.13	0.107	0.84	6.31
231-232 pc	227.5	16.44	7.05	1.87	3.14	0.20	58.73	3.21	0.091	0.84	3.88
236-237 pc	232.5	16.82	7.42	1.98	3.67	0.20	58.00	3.10	0.105	0.84	5.71
241-242 pc	237.5	15.92	7.68	2.08	3.28	0.23	55.99	3.14	0.102	0.87	3.26
246-247 pc	242.5	16.85	7.35	2.45	3.56	0.21	57.70	3.20	0.104	0.88	5.18
251-252 pc	247.5	16.83	6.82	1.75	3.42	0.19	60.18	3.22	0.093	0.80	3.40
256-257 pc	252.5	16.89	7.55	2.02	3.71	0.20	58.20	3.05	0.105	0.84	5.23
261-262 pc	257.5	16.55	7.06	2.11	3.28	0.21	58.61	3.45	0.092	0.87	4.12

Table A14. (continued)

Major Element Data for Multicore (mc) and Piston Core (pc) JT96-09 (continued).

Sample	Depth * (cm, corr.)	Al$_2$O$_3$ (%)	Fe$_2$O$_3$ (%)	K$_2$O (%)	MgO (%)	P$_2$O$_5$ (%)	SiO$_2$ (%)	CaO (%)	MnO (%)	TiO$_2$ (%)	Na$_2$O (%)
266-267 pc	262.5	16.93	7.41	1.98	3.71	0.20	58.50	3.31	0.102	0.87	4.80
271-272 pc	267.5	16.34	6.90	2.58	3.12	0.22	60.25	3.88	0.091	0.92	4.54
276-277 pc	272.5	16.39	7.27	2.28	3.56	0.21	58.03	3.55	0.100	0.87	5.19
281-282 pc	277.5	16.21	7.34	2.20	3.28	0.25	57.03	3.60	0.102	0.90	3.63
286-287 pc	282.5	16.20	7.03	2.05	3.45	0.21	58.47	4.18	0.101	0.85	5.30
291-292 pc	287.5	16.27	7.00	2.44	3.13	0.22	58.01	3.95	0.081	0.88	4.54
296-297 pc	292.5	16.38	7.17	1.99	3.52	0.21	58.03	4.10	0.101	0.86	5.15
301-302 pc	297.5	16.37	7.11	2.23	3.21	0.21	57.58	3.80	0.092	0.88	4.56
306-307 pc	302.5	16.58	7.31	2.01	3.63	0.21	57.92	3.60	0.105	0.85	5.79
311-312 pc	307.5	15.12	6.85	2.23	2.88	0.22	56.84	4.58	0.081	0.98	4.36
316-317 pc	312.5	15.54	7.02	2.55	3.13	0.23	59.29	4.31	0.094	1.01	7.53
321-322 pc	317.5	15.85	6.99	2.65	2.95	0.24	57.85	4.10	0.081	1.03	3.94
326-327 pc	322.5	16.04	7.43	2.75	3.18	0.25	57.85	4.00	0.096	1.04	5.01
331-332 pc	327.5	15.05	6.98	2.40	2.80	0.25	58.30	4.39	0.091	1.09	4.38
336-337 pc	332.5	15.53	6.93	2.76	3.04	0.23	58.82	3.97	0.093	0.99	4.82
341-342 pc	337.5	16.25	7.12	2.55	3.24	0.23	59.55	4.13	0.082	0.99	3.29
346-347 pc	342.5	15.41	6.79	2.34	3.07	0.23	59.89	4.68	0.096	0.96	4.87
351-352 pc	347.5	15.32	6.96	2.50	2.94	0.25	57.15	4.08	0.091	1.07	3.46
356-357 pc	352.5	14.99	7.00	2.56	2.99	0.26	61.09	4.26	0.105	1.10	4.64
361-362 pc	357.5	14.07	7.19	2.44	2.91	0.24	52.65	3.90	0.081	1.00	1.99
366-367 pc	362.5	15.68	6.99	2.61	3.10	0.24	59.88	4.06	0.098	1.03	4.59
371-372 pc	367.5	14.84	6.88	2.41	2.83	0.24	57.32	3.94	0.091	1.00	3.15

* Corrected piston core depth (12 cm added to account for loss of surface sediments during piston coring and a 16 cm turbidite was removed from the depth tally).

Table A14. (continued)

Minor Element Data for Multicore (mc) and Piston Core (pc) JT96-09.

Sample	Depth * (cm, corr.)	V (µg/g)	Cr (µg/g)	Mn (µg/g)	Co (µg/g)	Ni (µg/g)	Cu (µg/g)	Zn (µg/g)	As (µg/g)	Rb (µg/g)	Sr (µg/g)	Y (µg/g)	Zr (µg/g)	Ba (µg/g)	Pb (µg/g)	Br (µg/g)	I (µg/g)
0-1 mc	0.5	151	131	492	13	65	47	130	5	102	235	19	146	624	21		925
1-2 mc	1.5																
2-3 mc	2.5																
3-4 mc	3.5																
4-5 mc	4.5																
5-6 mc	5.5	159	138	456	21	60	45	130	3	89	233	19	139	624	20	167	722
6-8 mc	7.0																
8-10 mc	9.0																
10-12 mc	11.0	155	145	492	15	63	44	131	2	94	231	21	151	617	15	166	612
12-14 mc	13.0																
14-16 mc	15.0	165	139	475	20	59	45	130	2	87	237	20	153	633	18	150	541
16-18 mc	17.0																
18-20 mc	19.0																
20-22 mc	21.0	173	141	542	13	63	42	126	3	87	250	21	155	598	14	111	247
22-24 mc	23.0																
24-26 mc	25.0	187	132	534	20	55	39	115	3	80	258	23	156	596	18	76	114
26-28 mc	27.0																
28-30 mc	29.0																
30-32 mc	31.0	178	133	570	11	62	40	119	5	87	268	24	155	608	14	81	125
32-34 mc	33.0																
34-36 mc	35.0	182	129	533	20	56	41	118	3	82	269	23	147	591	20	73	113
36-38 mc	37.0																
38-40 mc	39.0	180	134	574	17	62	43	123	5	92	266	23	151	618	19	91	111

Sample	Depth * (cm, corr.)	V (µg/g)	Cr (µg/g)	Mn (µg/g)	Co (µg/g)	Ni (µg/g)	Cu (µg/g)	Zn (µg/g)	As (µg/g)	Rb (µg/g)	Sr (µg/g)	Y (µg/g)	Zr (µg/g)	Ba (µg/g)	Pb (µg/g)	Br (µg/g)	I (µg/g)
6-7 pc	18.5	168	128	492	14	64	47	132	6	91	243	20	160	652	9	120	479
11-12 pc	23.5	168	134	527	15	62	41	126	4	88	249	23	160	576	13	57	191
16-17 pc	28.5																
21-22 pc	33.5	186	135	571	16	65	44	129	7	93	257	25	148	631	15	46	90
26-27 pc	38.5																
31-32 pc	43.5	176	128	568	15	66	43	121	9	91	261	22	138	640	12	47	79
36-37 pc	48.5																
41-42 pc	53.5	183	129	606	15	60	42	115	4	85	280	23	135	642	12	39	55
46-47 pc	58.5																
51-52 pc	63.5	194	131	644	22	52	37	106	2	80	280	23	136	618	19	16	77
56-57 pc	68.5	195	130	733	21	48	33	95		74	290	22	134	600	21		
61-62 pc	73.5	179	128	682	18	46	28	87	5	70	302	21	140	599	21	2	22
66-67 pc	78.5																
71-72 pc	83.5	158	126	654	17	40	20	73	4	58	319	22	212	555	20	19	14
76-77 pc	88.5	205	136	777	22	54	37	110		89	304	23	127	718	25		
81-82 pc	93.5	201	128	780	21	54	38	109	5	91	317	22	120	715	24	8	28
86-87 pc	98.5	203	132	774	21	54	37	109		90	291	23	120	720	24		
91-92 pc	103.5	200	129	794	22	54	37	107	5	90	305	23	118	724	28	10	15
96-97 pc	108.5	204	131	812	23	56	38	107		87	314	23	121	704	26		
101-102 pc	113.5	201	130	807	22	54	38	108	5	90	308	23	122	736	24	9	30
106-107 pc	118.5	201	130	800	22	54	37	105		86	302	22	121	677	25		
111-112 pc	123.5	204	132	826	23	54	38	106	5	85	298	23	121	676	23	4	22
116-117 pc	128.5	201	127	811	23	55	38	104		85	300	24	123	676	24		
121-122 pc	133.5	203	127	801	23	54	37	105	4	86	290	23	124	683	24	6	24
126-127 pc	138.5	202	131	815	23	56	39	107		89	292	24	125	696	29		
131-132 pc	143.5	169	113	724	20	56	37	105	6	91	286	23	128	608	18	8	22
136-137 pc	148.5	145	113	665	51	25	19	64			355	20	172	539	17		
141-142 pc	153.5	157	122	669	27	42	26	78			344	20	226	598	14		
146-147 pc	158.5	124	103	575	23	28	10	46			377	17	165	486	16		
151-152 pc	163.5	179	113	696	23	50	33	90			276	22	131	512	16		
156-157 pc	152.5	209	117	791	23	47	38	100		76	259	24	131	569	26		
161-162 pc	157.5	188	86	767	20	33	30	100	8	109	248	31	173	635	31	-6	0
166-167 pc	162.5	210	115	799	23	45	37	96		72	268	25	138	556	28		
171-172 pc	167.5	214	122	831	24	47	38	97	7	63	266	24	124	526	25	-7	13
176-177 pc	172.5	212	116	821	24	47	40	99		64	266	25	127	522	29		
181-182 pc	177.5	187	88	802	20	32	32	109	9	126	241	33	167	673	32	-7	2
186-187 pc	182.5	214	118	827	24	45	39	98		67	265	25	126	547	31		
191-192 pc	187.5	216	122	847	24	46	39	96	7	58	273	24	125	520	26	-6	0
196-197 pc	192.5	221	123	852	24	47	41	97		58	263	24	119	513	25		
201-202 pc	197.5	221	123	844	25	46	41	95	8	58	268	23	121	516	26	-4	11
206-207 pc	202.5	204	112	814	22	42	38	97		74	271	26	137	561	26		
211-212 pc	207.5	186	116	809	18	53	41	99	7	66	273	22	126	494	14	-4	20
216-217 pc	212.5	214	122	820	24	46	40	96		57	262	23	120	496	24		
221-222 pc	217.5	197	119	827	18	52	42	101	7	66	262	23	125	490	10	-11	4
226-227 pc	222.5	219	122	859	25	47	44	99		58	261	24	119	500	22		
231-232 pc	227.5	186	111	789	16	51	39	94	8	61	280	23	133	486	8	-6	5
236-237 pc	232.5	223	124	860	25	47	40	97		60	258	23	119	523	27		
241-242 pc	237.5	191	116	816	20	52	42	100	7	64	264	25	124	464	14	-4	7
246-247 pc	242.5	207	109	804	24	44	40	103		85	247	26	131	565	26		
251-252 pc	247.5	187	117	800	16	50	38	93	9	60	286	23	135	466	9	-5	18
256-257 pc	252.5	220	125	858	25	49	40	100		62	258	24	122	524	25		
261-262 pc	257.5	190	110	781	18	50	39	98	8	73	272	25	136	515	9	-5	7

(continued on next page)

Minor Element Data for Multicore (mc) and Piston Core (pc) JT96-09 (continued).

Sample	Depth * (cm, corr.)	V (µg/g)	Cr (µg/g)	Mn (µg/g)	Co (µg/g)	Ni (µg/g)	Cu (µg/g)	Zn (µg/g)	As (µg/g)	Rb (µg/g)	Sr (µg/g)	Y (µg/g)	Zr (µg/g)	Ba (µg/g)	Pb (µg/g)	Br (µg/g)	I (µg/g)
266-267 pc	262.5	219	118	840	24	49	39	99		65	259	24	127	539	23		
271-272 pc	267.5	184	100	795	19	41	35	101	7	96	260	28	156	572	16	-3	8
276-277 pc	272.5	210	109	816	24	44	38	101		82	254	27	142	572	27		
281-282 pc	277.5	194	112	810	16	52	41	101	7	78	268	26	139	525	14	-5	16
286-287 pc	282.5	211	120	825	23	47	36	95		66	279	25	138	556	28		
291-292 pc	287.5	184	107	781	16	49	37	100	4	91	264	27	150	561	24	-2	19
296-297 pc	292.5	211	120	824	23	48	37	96		68	275	25	133	544	24		
301-302 pc	297.5	186	105	784	17	49	36	100	4	87	258	26	144	547	16	-4	6
306-307 pc	302.5	215	118	848	24	49	39	97		65	261	25	128	536	24		
311-312 pc	307.5	174	85	688	19	41	35	98	7	91	277	28	172	523	16	-3	17
316-317 pc	312.5	204	88	726	22	33	31	96		98	249	31	185	618	29		
321-322 pc	317.5	178	84	701	17	37	36	105	8	115	248	33	184	595	19	-4	14
326-327 pc	322.5	206	86	758	25	34	35	106		111	240	33	178	644	33		
331-332 pc	327.5	184	77	799	20	35	33	100	10	100	264	33	203	562	13	-2	7
336-337 pc	332.5	194	81	745	22	31	32	99		111	237	32	187	646	32		
341-342 pc	337.5	173	80	696	17	39	35	100	10	110	249	31	186	573	16	-3	15
346-347 pc	342.5																
351-352 pc	347.5	178	77	719	18	34	35	103	6	114	244	34	202	587	18	-5	0
356-357 pc	352.5	203	73	803	22	28	29	96		99	246	33	209	602	28		
361-362 pc	357.5	176	82	702	19	35	36	102	5	112	243	32	185	581	18	-4	7
366-367 pc	362.5	199	84	764	23	33	33	99		106	242	32	190	628	33		
371-372 pc	367.5	171	77	750	17	34	34	98	10	107	248	33	195	551	15	-5	-4

* Corrected piston core depth (12 cm added to account for loss of surface sediments during piston coring and a 16 cm turbidite was removed from the depth tally).

Table A14. (continued)

Trace Metal Data for Multicore (mc) and Piston Core (pc) JT96-09.

Sample	Depth * (cm, corr.)	Ag (ng/g)	Cd (μg/g)	Re (ng/g)	Mo (μg/g)	U (μg/g)
0-1 mc	0.5	223	0.18	4.15	0.89	1.64
1-2 mc	1.5	213	0.19	4.08	0.64	1.20
2-3 mc	2.5	215	0.29	3.85	0.68	1.35
3-4 mc	3.5	219	0.30	5.44	0.64	1.40
4-5 mc	4.5	247	0.26	5.26	0.67	1.38
5-6 mc	5.5	248	0.26	5.64	0.60	1.40
6-8 mc	7.0	231	0.20	5.75	0.61	1.34
8-10 mc	9.0	235	0.31	7.15	0.66	1.56
10-12 mc	11.0	187	0.28	8.39	0.63	1.66
12-14 mc	13.0	215	0.25	8.18	0.65	1.59
14-16 mc	15.0	236	0.32	10.32	0.64	1.67
16-18 mc	17.0	236	0.54	11.90	0.69	1.87
18-20 mc	19.0	295	0.86	22.37	0.71	2.27
20-22 mc	21.0	251	0.66	25.07	0.61	2.39
22-24 mc	23.0	271	0.95	29.56	0.81	3.70
24-26 mc	25.0	275	1.03	52.92	0.80	4.31
26-28 mc	27.0	254	0.71	64.45	0.80	5.36
28-30 mc	29.0	245	0.56	50.30	0.97	5.75
30-32 mc	31.0	221	0.41	37.79	0.95	4.98
32-34 mc	33.0	212	0.47	22.36	0.97	4.89
34-36 mc	35.0	236	0.51	16.77	1.04	4.06
36-38 mc	37.0	207	0.68	15.45	0.94	4.22
38-40 mc	39.0	287	0.65	16.62	1.09	3.81

Sample	Depth * (cm, corr.)	Ag (ng/g)	Cd (μg/g)	Re (ng/g)	Mo (μg/g)	U (μg/g)
6-7 pc	18.5	255	0.41	18.42	1.41	2.70
11-12 pc	23.5	263	0.53	20.70	0.86	3.36
16-17 pc	28.5	220	0.73	22.13	1.13	4.75
21-22 pc	33.5	329	1.35	23.66	1.56	3.59
26-27 pc	38.5	356	1.30	23.46	3.11	4.48
31-32 pc	43.5	395	1.11	23.42	3.46	3.93
36-37 pc	48.5	358	0.67	20.78	2.61	5.04
41-42 pc	53.5	349	0.85	20.08	1.64	3.23
46-47 pc	58.5	349	na	10.44	3.71	2.90
51-52 pc	63.5	167	0.34	8.78	1.32	2.04
56-57 pc	68.5	212	0.21	8.63	0.88	1.84
61-62 pc	73.5	101	0.21	6.38	0.65	1.68
66-67 pc	78.5	90	0.20	4.79	0.73	1.86
71-72 pc	83.5	57	0.16	4.30	0.82	1.58
76-77 pc	88.5	138	na	6.34	3.33	2.52
81-82 pc	93.5	177	0.51	7.38	2.13	3.23
86-87 pc	98.5	164	0.50	5.69	na	2.00
91-92 pc	103.5	159	na	5.23	2.05	2.74
96-97 pc	108.5	145	0.42	4.70	1.84	2.14
101-102 pc	113.5	na	na	na	na	na
106-107 pc	118.5	127	0.46	4.66	1.88	2.63
111-112 pc	123.5	142	0.40	4.67	1.81	2.76
116-117 pc	128.5	127	0.39	3.20	1.25	1.83
121-122 pc	133.35	353	0.71	4.00	1.35	1.95
126-127 pc	138.5	125	0.47	3.02	1.42	2.23
131-132 pc	143.5	179	na	5.25	2.08	2.66
136-137 pc	148.5	54	0.18	1.43	0.97	1.24
141-142 pc	153.5	105	0.17	1.98	0.79	1.49
146-147 pc	158.5	na	0.07	na	0.33	na
151-152 pc	163.5	95	0.14	1.50	0.77	1.95
156-157 pc	152.5	98	0.19	1.44	0.79	1.74
161-162 pc	157.5	91	na	1.76	0.93	1.97
166-167 pc	162.5	92	0.15	1.40	0.76	1.42
171-172 pc	167.5	90	0.16	1.90	0.89	1.66
176-177 pc	172.5	80	0.13	1.19	0.79	1.47
181-182 pc	177.5	119	na	0.81	1.00	2.00
186-187 pc	182.5	87	0.13	1.31	0.85	1.26
191-192 pc	187.5	96	0.14	1.10	1.11	1.79
196-197 pc	192.5	71	0.11	1.15	0.67	1.12
201-202 pc	197.5	81	0.13	1.04	0.91	1.21
206-207 pc	202.5	87	0.15	1.09	0.69	1.30
211-212 pc	207.5	90	0.13	1.24	0.61	1.25
216-217 pc	212.5	85	0.12	1.40	0.75	1.23
221-222 pc	217.5	94	0.10	1.52	0.74	1.42
226-227 pc	222.5	82	0.13	1.34	0.96	1.22
231-232 pc	227.5	82	0.12	1.45	0.99	1.35
236-237 pc	232.5	77	0.12	1.26	0.69	1.25
241-242 pc	237.5	104	0.10	1.40	0.53	1.44
246-247 pc	242.5	107	0.13	1.32	0.80	1.54
251-252 pc	247.5	106	0.12	1.55	0.81	1.53
256-257 pc	252.5	81	0.10	1.13	0.64	1.19
261-262 pc	257.5	111	0.57	1.27	0.70	1.44

(continued on next page)

Trace Metal Data for Multicore (mc) and Piston Core (pc) JT96-09 (continued).

Sample	Depth * (cm, corr.)	Ag (ng/g)	Cd (µg/g)	Re (ng/g)	Mo (µg/g)	U (µg/g)
266-267 pc	262.5	99	0.18	1.21	1.01	1.53
271-272 pc	267.5	94	0.29	1.37	1.12	1.58
276-277 pc	272.5	90	0.15	0.84	0.85	1.44
281-282 pc	277.5	111	0.13	1.26	0.90	1.87
286-287 pc	282.5	98	0.14	1.69	0.69	1.62
291-292 pc	287.5	394	0.34	1.94	0.95	2.13
296-297 pc	292.5	94	0.20	2.39	0.76	1.88
301-302 pc	297.5	118	0.18	1.58	0.91	1.98
306-307 pc	302.5	92	0.16	2.06	0.72	1.81
311-312 pc	307.5	140	0.46	4.12	1.31	2.18
316-317 pc	312.5	91	0.20	2.17	0.68	2.03
321-322 pc	317.5	102	0.12	1.31	0.68	1.99
326-327 pc	322.5	94	0.16	1.04	0.87	1.97
331-332 pc	327.5	97	0.19	1.00	0.90	1.76
336-337 pc	332.5	115	0.19	1.07	0.79	2.12
341-342 pc	337.5	86	0.08	1.02	1.56	2.35
346-347 pc	342.5	97	0.12	1.14	0.81	1.69
351-352 pc	347.5	86	0.18	0.88	1.13	1.97
356-357 pc	352.5	79	0.13	0.72	0.67	1.64
361-362 pc	357.5	77	0.07	0.50	1.16	2.26
366-367 pc	362.5	94	0.14	0.60	0.80	2.14
371-372 pc	367.5	105	0.15	0.63	1.65	2.10

* Corrected piston core depth (12 cm added to account for loss of surface sediments during piston coring and a 16 cm turbidite was removed from the depth tally).

Table A15. Geochemical Data for Trigger Core and Piston Core Tul96-03.

General Geochemical Data for Trigger Core (tc) and Piston Core (pc) Tul96-03.

Sample	Depth (m)	Calendar Age (kyrs)	Cl⁻ (wt. %)	δ¹⁵N (‰ vs air)	δ¹³C$_{org}$ (‰ vs PDB)	N$_{tot}$ (wt. %)	C$_{tot}$ (wt. %)	S$_{tot}$ (wt. %)	CaCO$_2$ (wt. %)	%C$_{org}$ (wt. %)	C$_{org}$/N	Opal (wt. %)	Ba$_{bio}$ (μg/g)
6-7 tc	6.5		0.80			0.10	0.91	0.09	0.52	0.85	8.5		
11-12 tc	11.5		0.70			0.04	0.82	0.17	2.50	0.52	13.7		
16-17 tc	16.5		0.79			0.05	0.68	0.24	1.83	0.46	9.9		
21-22 tc	21.5		0.92			0.05	0.79	0.22	2.50	0.49	10.8		
26-27 tc	26.5		0.86			0.04	0.63	0.33	2.17	0.37	8.4		

Sample	Depth (m)	Calendar Age (kyrs)	Cl⁻ (wt. %)	δ¹⁵N (‰ vs air)	δ¹³C$_{org}$ (‰ vs PDB)	N$_{tot}$ (wt. %)	C$_{tot}$ (wt. %)	S$_{tot}$ (wt. %)	CaCO$_2$ (wt. %)	%C$_{org}$ (wt. %)	C$_{org}$/N	Opal (wt. %)	Ba$_{bio}$ (μg/g)
11-12 pc	11.5		1.19			0.05	0.73	0.38	2.29	0.45	9.0		
16-17 pc	16.5		1.30			0.05	0.71	0.25	2.50	0.41	8.5		
26-27 pc	26.5		1.27			0.05	0.72	0.24	1.67	0.52	10.7		
31-32 pc	31.5		1.06			0.04	0.65	0.51	1.67	0.45	10.4		
41-42 pc	41.5		1.07			0.04	0.58	0.39	1.67	0.38	10.5		
66-67 pc	66.5		1.05			0.05	0.68	0.23	1.83	0.46	9.7		
71-72 pc	71.5		1.01			0.05	0.67	0.24	1.67	0.47	10.4		
81-82 pc	81.5		1.01			0.05	0.66	0.41	1.67	0.46	9.8		
91-92 pc	91.5		1.03			0.05	0.68	0.38	1.67	0.48	10.2		
101-102 pc	101.5		0.93			0.05	0.74	0.37	1.67	0.54	10.8		
111-112 pc	111.5		1.09			0.05	0.82	0.84	2.62	0.51	9.6		
121-122 pc	121.5		0.97			0.05	0.95	0.60	3.33	0.55	10.9		
131-132 pc	131.5		1.02			0.05	0.97	0.69	4.17	0.47	9.5		
141-142 pc	141.5		0.97			0.04	0.84	0.60	4.17	0.34	7.9		
151-152 pc	No sample												
161-162 pc	No sample												
166-167 pc	166.5		0.83			0.05	0.98	0.86	4.17	0.48	9.1		
171-172 pc	171.5		0.93			0.05	1.02	0.51	4.50	0.48	9.8		
181-182 pc	181.5		0.83			0.05	1.65	0.55	10.28	0.41	8.1		
191-192 pc	191.5		0.96			0.05	0.97	0.28	4.66	0.41	8.8		
201-202 pc	201.5		0.92			0.06	1.00	0.21	4.17	0.50	8.6		
211-212 pc	211.5		0.87			0.05	0.76	0.12	3.25	0.37	8.1		
221-222 pc	221.5		0.93			0.05	0.78	0.11	3.33	0.38	8.1		
231-232 pc	231.5		0.88			0.05	1.16	0.08	6.39	0.39	8.2		
241-242 pc	241.5		0.91			0.05	0.79	0.13	3.33	0.39	8.1		
251-252 pc	251.5		1.09			0.05	0.69	0.15	2.17	0.43	8.8		
261-262 pc	No sample												
271-272 pc	271.5		0.87			0.05	0.67	0.51	2.50	0.37	7.3		
281-282 pc	281.5		0.82			0.04	0.72	0.14	2.67	0.40	9.4		
291-292 pc	291.5		0.84			0.06	0.78	0.28	2.50	0.48	8.3		
301-302 pc	301.5		0.88			0.06	0.78	0.27	2.58	0.47	8.2		
311-312 pc	311.5		0.85			0.05	0.78	0.17	2.46	0.49	8.9		
321-322 pc	321.5		0.81			0.05	0.76	0.16	2.50	0.46	9.4		
331-332 pc	331.5		0.87			0.06	0.75	0.32	2.50	0.45	8.0		
341-342 pc	341.5		0.83			0.05	0.76	0.29	2.33	0.48	9.1		
351-352 pc	351.5		0.81			0.06	0.77	0.72	2.50	0.47	8.5		
361-362 pc	361.5		0.81			0.06	0.75	0.29	2.58	0.44	8.1		
371-372 pc	371.5		0.80			0.05	0.76	0.28	2.50	0.46	8.3		
381-382 pc	381.5		0.83			0.06	0.76	0.29	2.42	0.47	8.4		
391-392 pc	391.5		0.83			0.05	0.78	0.25	2.50	0.48	8.9		
401-402 pc	401.5		0.88			0.05	0.88	0.08	1.75	0.67	13.7		
411-412 pc	411.5		0.85			0.05	0.62	0.11	2.50	0.32	6.5		
421-422 pc	421.5		0.79			0.04	0.53	0.08	1.67	0.33	7.6		
431-432 pc	431.5		0.80			0.04	0.54	0.12	1.67	0.34	8.6		

Table A15. (continued)

Minor Element Data for Trigger Core (tc) and Piston Core (pc) Tul96-03.

Sample	Depth (m)	V (µg/g)	Cr (µg/g)	Mn (µg/g)	Co (µg/g)	Ni (µg/g)	Cu (µg/g)	Zn (µg/g)	As (µg/g)	Rb (µg/g)	Sr (µg/g)	Y (µg/g)	Zr (µg/g)	Ba (µg/g)	Pb (µg/g)	Br (µg/g)	I (µg/g)
6-7 tc	6.5	143	137	520	11	39	25	78	5	55	308	21	189	464	6	65	162
11-12 tc	11.5	173	120	692	17	45	33	81	7	56	327	22	178	491	9	22	8
16-17 tc	16.5	187	115	836	17	53	48	104	8	67	283	25	133	521	14	18	-4
21-22 tc	21.5	178	121	730	19	49	40	95	6	64	298	23	152	508	16	19	5
26-27 tc	26.5	183	114	853	18	53	47	101	8	66	294	24	132	525	15	15	6

Sample	Depth (m)	V (µg/g)	Cr (µg/g)	Mn (µg/g)	Co (µg/g)	Ni (µg/g)	Cu (µg/g)	Zn (µg/g)	As (µg/g)	Rb (µg/g)	Sr (µg/g)	Y (µg/g)	Zr (µg/g)	Ba (µg/g)	Pb (µg/g)	Br (µg/g)	I (µg/g)
11-12 pc	11.5	191	115	785	21	49	45	106	8	70	272	26	140	546	14	6	12
16-17 pc	16.5	186	118	738	17	48	37	93	10	63	304	23	163	520	10	5	14
26-27 pc	26.5	189	114	759	16	50	44	100	6	69	279	24	143	500	12	13	13
31-32 pc	31.5	186	119	877	19	55	50	102	12	66	280	24	138	535	8	10	-12
41-42 pc	41.5	174	115	821	18	52	44	101	10	61	302	24	130	512	13	6	0
66-67 pc	66.5	192	120	889	17	56	48	101	5	63	287	25	127	531	15	9	2
71-72 pc	71.5	193	117	883	20	58	49	103	9	62	280	24	128	512	7	11	6
81-82 pc	81.5	197	116	901	19	55	49	101	6	61	277	24	126	509	14	10	-1
91-92 pc	91.5	190	115	859	20	53	49	101	8	59	276	24	123	500	9	11	-11
101-102 pc	101.5	194	115	859	18	56	48	103	8	61	279	23	127	498	11	9	2
111-112 pc	111.5	193	110	818	16	53	46	106	5	75	261	26	138	503	14	13	5
121-122 pc	121.5	196	115	832	20	50	41	99	7	72	291	26	147	529	12	15	5
131-132 pc	131.5	184	102	756	18	46	39	98	4	79	292	27	158	539	17	11	21
141-142 pc	141.5	171	86	624	16	36	39	100	4	110	245	33	178	582	19	11	7
151-152 pc	No sample																
161-162 pc	No sample																
166-167 pc	166.5	183	113	765	14	49	41	95	5	68	307	27	150	504	15	13	8
171-172 pc	171.5	182	110	757	16	47	41	96	7	79	301	27	157	560	13	14	11
181-182 pc	181.5	159	106	678	17	47	36	92	9	74	363	25	163	529	12	13	18
191-192 pc	191.5	178	116	796	20	55	43	107	4	85	315	26	140	623	15	11	10
201-202 pc	201.5	189	121	876	22	59	49	113	5	83	301	26	130	612	16	13	0
211-212 pc	211.5	180	120	870	20	65	46	109	8	72	315	24	133	586	15	15	1
221-222 pc	221.5	182	118	878	21	62	47	111	6	66	316	25	132	575	13	13	4
231-232 pc	231.5	170	109	825	20	55	46	102	8	65	366	24	135	574	8	15	4
241-242 pc	241.5	167	104	824	22	53	44	107	4	74	336	23	122	575	12	15	18
251-252 pc	251.5	185	109	916	23	56	49	119	8	78	323	24	117	632	13	12	12
261-262 pc	No sample																
271-272 pc	271.5	168	99	843	18	50	43	105	5	73	348	22	123	648	11	13	22
281-282 pc	281.5	165	95	823	19	45	40	98	6	68	373	22	128	591	11	13	5
291-292 pc	291.5	184	110	886	19	49	45	106	9	72	342	24	125	623	10	19	31
301-302 pc	301.5	184	110	879	21	51	44	107	10	73	345	24	123	599	7	17	27
311-312 pc	311.5	180	105	863	17	50	43	106	8	72	345	24	122	627	10	18	29
321-322 pc	321.5	181	107	870	19	49	46	107	8	73	348	23	123	613	10	17	12
331-332 pc	331.5	178	105	856	18	49	45	104	9	72	345	23	125	608	9	17	26
341-342 pc	341.5	184	107	881	20	49	45	107	6	72	346	23	124	619	17	17	16
351-352 pc	351.5	175	106	858	20	49	45	106	7	71	350	23	122	610	15	14	15
361-362 pc	361.5	176	104	853	17	49	45	106	9	71	348	24	121	617	11	17	12
371-372 pc	371.5	178	104	862	20	49	44	104	7	71	347	23	122	605	14	16	10
381-382 pc	381.5	185	104	882	20	49	46	107	9	73	350	22	123	632	9	16	18
391-392 pc	391.5	167	97	824	18	48	44	104	6	70	360	24	124	579	12	16	9
401-402 pc	401.5	188	103	926	18	50	50	110	7	75	348	23	117	642	8	15	19
411-412 pc	411.5	179	99	893	20	49	46	109	5	72	351	23	116	635	14	15	11
421-422 pc	421.5	178	96	912	20	48	48	107	5	71	362	24	118	635	13	14	17
431-432 pc	431.5	177	93	900	20	46	46	107	6	70	364	23	116	632	12	14	11

Table A16. Geochemical Data for Trigger Core and Piston Core Tul96-05.

General Geochemical Data for Trigger Core (tc) and Piston Core (pc) Tul96-05.

Sample	Depth (cm)	Depth * (cm, corr.)	Calendar Age (kyrs)	Cl⁻ (wt. %)	$\delta^{15}N$ (‰ vs air)	$\delta^{13}C_{org}$ (‰ vs PDB)	N_{tot} (wt. %)	C_{tot} (wt. %)	S_{tot} (wt. %)	$CaCO_2$ (wt. %)	%C_{org} (wt. %)	C_{org}/N	Opal (wt. %)	Ba_{bio} (µg/g)
11-12 tc	11.5			2.58			0.29	2.59	0.46	0.83	2.49	8.6		
21-22 tc	21.5			2.62			0.29	2.67	0.61	1.67	2.47	8.6		
31-32 tc	31.5			2.44			0.26	2.45	0.53	1.67	2.25	8.6		
41-42 tc	41.5			2.50			0.26	2.44	0.51	1.67	2.24	8.8		
51-52 tc	51.5			2.32			0.25	2.41	0.65	2.08	2.16	8.7		
61-62 tc	61.5			2.24			0.22	2.17	0.61	1.67	1.97	8.9		
71-72 tc	71.5			2.15			0.21	2.10	0.63	1.67	1.90	9.0		
81-82 tc	81.5			2.65			0.28	2.65	0.41	1.42	2.48	8.7		

Sample	Depth (cm)	Depth * (cm, corr.)	Calendar Age (kyrs)	Cl⁻ (wt. %)	$\delta^{15}N$ (‰ vs air)	$\delta^{13}C_{org}$ (‰ vs PDB)	N_{tot} (wt. %)	C_{tot} (wt. %)	S_{tot} (wt. %)	$CaCO_2$ (wt. %)	%C_{org} (wt. %)	C_{org}/N	Opal (wt. %)	Ba_{bio} (µg/g)
11-12 pc	11.5	57.5	2.39	2.73	6.52	na	0.31	2.87	0.38	1.00	2.75	8.7		
16-17 pc	16.5	62.5	2.60	2.42	7.36	-21.00	0.32	2.75	0.36	1.12	2.62	8.2		
21-22 pc	21.5	67.5	2.81	2.42	6.76	-21.10	0.29	2.70	0.40	0.83	2.60	8.9		
26-27 pc	26.5	72.5	3.01	2.47	7.18	-21.02	0.29	2.57	0.43	1.04	2.44	8.3		
31-32 pc	31.5	77.5	3.22	2.46	6.96	-21.18	0.29	2.70	0.39	1.08	2.57	8.8		
36-37 pc	36.5	82.5	3.44	2.14	7.14	-21.18	0.28	2.90	0.46	1.36	2.74	9.7		
41-42 pc	41.5	87.5	3.66	2.25	6.84	-21.37	0.28	2.69	0.55	1.71	2.49	9.0		
46-47 pc	No sample													
51-52 pc	No sample													
56-57 pc	56.5	91.5	3.84	1.96	6.87	-21.24	0.26	2.42	0.50	1.05	2.30	9.0		
61-62 pc	61.5	96.5	4.06	2.11	7.11	-21.30	0.26	2.48	0.55	0.92	2.37	9.0		
66-67 pc	66.5	101.5	4.28	1.98	6.98	-21.29	0.26	2.47	0.63	1.15	2.33	9.0		
71-72 pc	71.5	106.5	4.50	1.92	6.83	-21.32	0.26	2.46	0.57	1.61	2.26	8.6		
76-77 pc	76.5	111.5	4.72	1.73	6.86	-21.27	0.24	2.33	0.48	1.63	2.13	8.9		
81-82 pc	81.5	116.5	4.94	2.11	7.32	-21.45	0.24	2.41	0.61	1.67	2.21	9.2		
86-87 pc	86.5	121.5	5.16	1.76	7.25	-21.35	0.22	2.14	0.59	1.42	1.97	9.0		
91-92 pc	91.5	126.5	5.38	1.83	6.79	-21.59	0.22	2.21	0.55	1.57	2.02	9.2		
96-97 pc	96.5	131.5	5.60	1.64	7.05	-21.40	0.22	2.11	0.60	1.37	1.94	8.9		
101-102 pc	101.5	136.5	5.82	1.79	7.01	-21.64	0.21	2.06	0.60	1.08	1.93	9.1		
106-107 pc	106.5	141.5	6.04	1.67	7.17	-21.50	0.21	2.06	0.64	1.17	1.92	9.0		
111-112 pc	111.5	146.5	6.26	1.72	7.05	-21.69	0.21	2.05	0.47	1.33	1.89	9.2		
116-117 pc	116.5	151.5	6.48	1.71	7.07	-21.92	0.20	2.01	0.56	1.26	1.86	9.2		
121-122 pc	No sample													
126-127 pc	No sample													
131-132 pc	131.5	166.5	7.14	1.63	7.27	-21.73	0.20	2.00	0.57	1.67	1.80	9.2		
136-137 pc	136.5	171.5	7.36	1.32	7.11	-21.63	0.17	1.81	0.61	2.17	1.55	8.9		
141-142 pc	141.5	176.5	7.58	1.65	7.41	-21.82	0.19	2.05	0.48	2.33	1.77	9.1		
146-147 pc	146.5	181.5	7.80	1.60	6.66	-21.73	0.19	1.97	0.71	2.30	1.70	9.0		
151-152 pc	151.5	186.5	8.02	1.71	7.57	-21.88	0.20	2.15	0.58	2.39	1.86	9.1		
156-157 pc	156.5	191.5	8.24	1.65	7.44	-21.65	0.20	2.05	0.50	2.15	1.80	9.0		
161-162 pc	161.5	196.5	8.46	1.68	8.02	-21.85	0.20	2.11	0.55	2.17	1.85	9.2		
166-167 pc	166.5	201.5	8.68	1.73	7.71	-21.64	0.20	2.16	0.73	3.25	1.77	9.0		
171-172 pc	171.5	206.5	8.90	1.91	8.45	-21.71	0.22	2.32	0.55	2.95	1.97	9.1		
176-177 pc	176.5	211.5	9.12	1.68	7.76	-21.57	0.21	2.30	0.52	3.17	1.92	9.0		
181-182 pc	181.5	216.5	9.34	1.75	8.27	-21.79	0.22	2.43	0.63	3.39	2.02	9.2		
186-187 pc	186.5	221.5	9.56	1.64	8.26	-21.65	0.22	2.40	0.53	3.27	2.00	9.3		
191-192 pc	191.5	226.5	9.78	1.72	7.92	-21.88	0.22	2.50	0.49	3.33	2.10	9.3		
196-197 pc	196.5	231.5	10.00	1.64	8.03	-21.75	0.20	2.25	0.47	3.65	1.81	9.1		
201-202 pc	201.5	236.5	10.22	2.00	7.91	-21.95	0.22	2.46	0.57	4.04	1.98	9.1		
206-207 pc	206.5	241.5	10.44	1.42	6.73	-22.54	0.11	1.41	0.31	2.57	1.10	9.6		
211-212 pc	211.5	246.5	10.66	1.39	6.54	-22.89	0.10	1.20	0.38	1.87	0.97	9.7		
216-217 pc	216.5	251.5	10.88	1.29	6.47	-22.80	0.09	1.24	0.30	2.70	0.92	10.2		
221-222 pc	No sample													
226-227 pc	No sample													
231-232 pc	Turbidite			1.03	6.79	-22.72	0.08	1.04	0.24	2.43	0.74	9.6		
236-237 pc	Turbidite			0.78	6.18	-23.19	0.06	0.87	0.19	2.38	0.59	10.1		
241-242 pc	241.5	257.5	27.97	0.97	4.93	-23.79	0.04	0.50	0.16	0.90	0.39	10.2		
246-247 pc	346.5	362.5	28.38	0.94	4.87	-23.15	0.05	0.61	0.23	1.45	0.43	9.4		
251-252 pc	251.5	267.5	28.78	1.07	4.85	-23.01	0.05	0.69	0.14	1.83	0.47	9.4		
256-257 pc	256.5	272.5	29.18	1.04	5.30	-22.75	0.06	0.88	0.24	2.72	0.56	9.1		
261-262 pc	261.5	277.5	29.58	1.07	4.94	-22.44	0.08	1.25	0.19	3.50	0.83	10.8		
266-267 pc	266.5	282.5	29.98	1.05	5.01	-22.12	0.08	1.26	0.27	4.21	0.75	8.9		
271-272 pc	271.5	287.5	30.38	1.03	5.78	-22.32	0.08	1.18	0.45	4.17	0.68	8.7		
276-277 pc	276.5	292.5	30.79	0.96	4.11	-22.44	0.07	1.07	0.24	3.72	0.62	8.7		
281-282 pc	281.5	297.5	31.19	1.13	5.86	-22.30	0.09	1.32	0.31	4.31	0.80	9.1		
286-287 pc	286.5	302.5	31.59	1.07	5.87	-22.14	0.09	1.40	0.34	4.75	0.83	9.4		
291-292 pc	291.5	307.5	31.99	1.08	6.15	-22.15	0.11	1.67	0.24	5.00	1.07	9.5		
296-297 pc	296.5	312.5	32.39	1.02	5.83	-22.28	0.09	1.39	0.19	4.66	0.83	9.1		
301-302 pc	301.5	317.5	32.79	0.83	5.57	-22.17	0.09	1.36	0.50	4.33	0.84	9.3		
306-307 pc	306.5	322.5	33.20	1.04	5.98	-22.09	0.10	1.46	0.30	5.10	0.84	8.8		
311-312 pc	311.5	327.5	33.60	1.11	5.91	-22.14	0.11	1.69	0.38	5.79	1.00	8.9		
316-317 pc	316.5	332.5	34.00	1.13	6.35	-22.12	0.11	1.66	0.35	5.11	1.05	9.4		
321-322 pc	321.5	337.5	34.40	1.10	6.27	-22.43	0.10	1.50	0.41	4.26	0.99	9.8		
326-327 pc	No sample													
331-332 pc	No sample													
336-337 pc	336.5	347.5	35.20	1.14	6.67	-22.03	0.12	1.78	0.56	5.52	1.11	9.1		
341-342 pc	341.5	352.5	35.61	1.11	5.91	-22.33	0.10	1.56	0.74	5.20	0.94	8.9		

(continued on next page)

General Geochemical Data for Trigger Core (tc) and Piston Core (pc) Tul96-05

Sample	Depth (cm)	Depth * (cm, corr.)	Calendar Age (kyrs)	Cl⁻ (wt. %)	$\delta^{15}N$ (‰ vs air)	$\delta^{13}C_{org}$ (‰ vs PDB)	N_{tot} (wt. %)	C_{tot} (wt. %)	S_{tot} (wt. %)	$CaCO_2$ (wt. %)	$\%C_{org}$ (wt. %)	C_{org}/N	Opal (wt. %)	Ba_{bio} (μg/g)
346-347 pc	346.5	357.5	36.01	1.10	5.87	-22.18	0.10	1.60	0.43	5.61	0.93	9.2		
351-352 pc	351.5	362.5	36.41	1.06	5.94	-22.16	0.10	1.58	0.58	6.08	0.85	8.3		
356-357 pc	356.5	367.5	36.81	1.05	5.79	-22.15	0.11	1.72	0.72	6.48	0.95	9.0		
361-362 pc	361.5	372.5	37.19	1.11	6.81	-21.97	0.12	2.09	0.81	7.50	1.19	9.7		
366-367 pc	366.5	377.5	37.50	1.17	6.38	-21.94	0.13	2.00	0.72	6.95	1.17	9.3		
371-372 pc	371.5	382.5	37.81	1.20	6.94	-22.09	0.12	1.96	1.05	7.25	1.09	9.2		
376-377 pc	376.5	387.5	38.12	1.07	5.21	-22.43	0.08	1.36	0.61	5.39	0.71	8.8		
381-382 pc	381.5	392.5	38.43	0.98	6.08	-22.75	0.08	1.32	0.69	4.87	0.73	9.0		
386-387 pc	386.5	397.5	38.74	1.00	5.41	-22.56	0.08	1.27	0.55	4.70	0.71	9.1		
391-392 pc	391.5	402.5	39.04	0.91	5.79	-23.04	0.06	1.02	0.48	3.32	0.62	9.9		
396-397 pc	396.5	407.5	39.35	1.08	4.78	-22.65	0.11	1.85	0.56	3.86	1.39	12.2		
401-402 pc	401.5	412.5	39.66	0.96	5.29	-22.37	0.09	1.28	0.71	4.17	0.78	9.0		
406-407 pc	406.5	417.5	39.97	1.03	5.10	-22.16	0.10	1.51	0.44	5.15	0.89	9.0		
411-412 pc	411.5	422.5	40.28	1.05	5.78	-22.11	0.11	1.63	0.64	5.08	1.02	9.4		
416-417 pc	416.5	427.5	40.59											
421-422 pc	No sample													
426-427 pc	No sample													
431-432 pc	431.5	432.5	40.89	1.01	6.21	-22.02	0.12	1.82	0.59	5.83	1.12	9.5		
436-437 pc	436.5	437.5	41.20	0.81	5.94	-22.18	0.07	1.23	0.82	6.62	0.44	6.2		
441-442 pc	441.5	442.5	41.51	1.17	6.37	-22.11	0.13	1.82	0.46	4.74	1.25	9.5		
446-447 pc	446.5	447.5	41.82	1.12	5.82	-21.99	0.11	1.71	0.43	5.55	1.05	9.2		
451-452 pc	451.5	452.5	42.13	1.04	5.77	-22.20	0.12	1.81	0.46	6.16	1.07	9.2		
456-457 pc	456.5	457.5	42.44	1.01	5.84	-22.11	0.11	1.79	0.42	6.54	1.00	9.3		
461-462 pc	461.5	462.5	42.75	1.04	5.69	-22.09	0.12	1.82	0.63	6.25	1.07	9.2		
466-467 pc	466.5	467.5	43.05	1.03	6.17	-22.06	0.11	1.72	0.34	6.15	0.98	9.2		
471-472 pc	471.5	472.5	43.36	1.05	6.28	-21.95	0.13	1.99	0.52	5.83	1.29	9.6		
476-477 pc	476.5	477.5	43.67	1.04	6.84	-22.02	0.14	2.00	0.44	6.12	1.27	9.3		
481-482 pc	481.5	482.5	43.98	1.06	5.81	-22.08	0.11	1.88	0.43	6.75	1.07	9.3		
486-487 pc	486.5	487.5	44.29	1.01	6.20	-22.10	0.11	1.82	0.44	7.16	0.96	9.1		
491-492 pc	491.5	492.5	44.60	1.04	5.66	-22.28	0.12	1.93	0.75	7.44	1.04	8.9		
496-497 pc	496.5	497.5	44.90	1.03	6.23	-22.08	0.11	1.95	0.39	7.56	1.04	9.1		
501-502 pc	501.5	502.5	45.21	0.99	6.07	-21.97	0.12	2.05	0.60	7.75	1.12	9.3		
506-507 pc	506.5	507.5	45.52	0.96	6.59	-22.01	0.12	2.07	0.58	8.30	1.08	9.2		

* Corrected piston core depth.

Major Element Data for Trigger Core (tc) and Piston Core (pc) Tul96-05.

Sample	Depth * (cm, corr.)	Al₂O₃ (%)	Fe₂O₃ (%)	K₂O (%)	MgO (%)	P₂O₅ (%)	SiO₂ (%)	CaO (%)	MnO (%)	TiO₂ (%)	Na₂O (%)
11-12 tc		14.48	6.56	1.89	3.13	0.19	56.39	2.45	0.056	0.83	3.29
21-22 tc		14.67	6.65	1.91	3.15	0.18	55.86	2.77	0.063	0.83	4.11
31-32 tc		14.47	6.45	1.91	3.15	0.18	56.76	2.76	0.058	0.83	3.16
41-42 tc		14.64	6.39	1.91	3.14	0.18	57.20	2.84	0.062	0.83	2.28
51-52 tc		14.43	6.42	1.85	3.08	0.18	56.91	2.99	0.058	0.81	2.62
61-62 tc		14.75	6.49	1.90	3.11	0.19	58.07	2.96	0.072	0.84	2.97
71-72 tc		14.63	6.43	1.94	3.08	0.18	57.87	2.88	0.071	0.83	2.85
81-82 tc		14.36	6.33	1.78	3.05	0.19	56.80	2.67	0.065	0.83	3.41

Sample	Depth * (cm, corr.)	Al₂O₃ (%)	Fe₂O₃ (%)	K₂O (%)	MgO (%)	P₂O₅ (%)	SiO₂ (%)	CaO (%)	MnO (%)	TiO₂ (%)	Na₂O (%)
11-12 pc	57.5	14.07	6.47	1.85	3.03	0.19	55.95	2.43	0.067	0.82	3.04
16-17 pc	62.5	14.66	6.08	1.83	3.10	0.19	57.28	2.55	0.061	0.82	5.75
21-22 pc	67.5	14.14	6.45	1.84	3.04	0.18	55.05	2.35	0.062	0.82	5.49
26-27 pc	72.5										
31-32 pc	77.5	14.13	6.23	1.79	3.04	0.19	55.96	2.65	0.066	0.82	3.06
36-37 pc	82.5										
41-42 pc	87.5	14.24	6.58	1.84	3.09	0.19	54.90	2.81	0.059	0.82	2.98
46-47 pc											
51-52 pc											
56-57 pc	91.5										
61-62 pc	96.5	14.28	6.52	1.96	3.07	0.18	55.04	2.41	0.066	0.83	7.30
66-67 pc	101.5	14.91	6.55	2.01	3.18	0.18	57.19	2.57	0.062	0.83	5.02
71-72 pc	106.5	14.26	6.36	1.90	3.05	0.18	56.28	2.85	0.066	0.82	7.47
76-77 pc	111.5	15.02	6.13	1.96	3.06	0.18	58.25	2.94	0.062	0.82	5.29
81-82 pc	116.5	13.81	6.46	1.90	2.99	0.18	54.72	2.96	0.064	0.81	9.13
86-87 pc	121.5	14.96	6.35	2.06	3.09	0.18	58.23	2.81	0.063	0.82	5.26
91-92 pc	126.5	14.54	6.43	1.97	3.09	0.19	57.21	2.80	0.068	0.83	5.61
96-97 pc	131.5	15.02	6.42	2.10	3.14	0.18	58.46	2.84	0.065	0.82	8.36
101-102 pc	136.5	14.40	6.41	1.96	3.07	0.19	57.41	2.71	0.069	0.82	6.32
106-107 pc	141.5	15.18	6.52	2.10	3.17	0.18	58.23	2.56	0.064	0.83	5.35
111-112 pc	146.5	14.66	6.39	2.03	3.10	0.19	57.35	2.72	0.070	0.84	4.33
116-117 pc	151.5	15.20	6.33	2.07	3.13	0.19	58.48	2.74	0.066	0.83	5.63
121-122 pc											
126-127 pc											
131-132 pc	166.5	14.57	6.43	1.97	3.06	0.19	57.44	2.94	0.065	0.83	4.10
136-137 pc	171.5	14.89	6.20	1.97	2.98	0.18	58.85	3.33	0.069	0.81	6.49
141-142 pc	176.5	14.57	6.55	1.94	3.10	0.19	56.92	3.30	0.070	0.85	2.90
146-147 pc	181.5	14.84	6.68	2.00	3.12	0.19	57.78	3.42	0.067	0.81	5.03
151-152 pc	186.5	14.81	6.90	2.01	3.27	0.19	55.93	3.24	0.066	0.85	2.70
156-157 pc	191.5	15.54	6.71	2.06	3.31	0.19	57.63	3.15	0.067	0.86	5.30
161-162 pc	196.5	14.70	6.77	2.02	3.22	0.20	55.65	3.27	0.067	0.84	3.26
166-167 pc	201.5	15.84	7.38	2.19	3.38	0.20	60.17	4.24	0.072	0.88	5.17
171-172 pc	206.5	14.63	6.82	2.02	3.24	0.19	55.09	3.59	0.066	0.84	2.35
176-177 pc	211.5	15.36	6.70	2.03	3.30	0.19	55.97	3.83	0.067	0.85	5.36
181-182 pc	216.5	14.51	6.79	2.02	3.20	0.20	54.09	3.90	0.062	0.83	2.95
186-187 pc	221.5	15.39	6.67	2.02	3.27	0.20	55.98	3.98	0.068	0.85	6.11
191-192 pc	226.5	14.72	6.60	2.04	3.34	0.20	53.75	3.95	0.074	0.84	4.57
196-197 pc	231.5	15.20	6.62	2.10	3.33	0.19	55.62	4.12	0.072	0.82	5.77
201-202 pc	236.5	14.79	7.02	1.96	3.40	0.19	53.78	4.28	0.077	0.82	5.30
206-207 pc	241.5	16.36	6.98	2.18	3.62	0.19	57.39	3.81	0.087	0.81	5.50
211-212 pc	246.5	15.29	7.08	2.29	3.56	0.19	55.79	3.44	0.086	0.80	4.11
216-217 pc	251.5										
221-222 pc											
226-227 pc											
231-232 pc											
236-237 pc											
241-242 pc	257.5	16.20	6.78	2.03	3.35	0.19	59.15	4.34	0.115	0.79	4.21
246-247 pc	362.5	17.20	7.10	2.15	3.74	0.19	58.24	4.35	0.120	0.82	5.49
251-252 pc	267.5	16.47	7.04	2.16	3.56	0.19	57.12	4.52	0.108	0.81	4.33
256-257 pc	272.5	17.02	6.94	2.27	3.74	0.19	56.82	4.58	0.108	0.78	6.20
261-262 pc	277.5	16.61	7.41	2.49	3.57	0.18	56.95	5.16	0.113	0.82	3.24
266-267 pc	282.5	13.55	6.60	2.38	3.71	0.19	56.07	4.95	0.102	0.76	5.41
271-272 pc	287.5	15.38	7.08	2.16	3.40	0.17	53.60	5.07	0.105	0.76	4.14
276-277 pc	292.5	16.63	6.77	2.36	3.66	0.18	56.82	4.93	0.108	0.77	5.97
281-282 pc	297.5	16.02	6.83	2.39	3.60	0.17	54.38	4.75	0.103	0.79	2.82
286-287 pc	302.5	16.49	6.69	2.51	3.67	0.17	55.79	4.89	0.091	0.79	5.04
291-292 pc	307.5	15.64	6.48	2.33	3.55	0.17	54.53	4.84	0.079	0.79	2.26
296-297 pc	312.5	16.39	6.52	2.43	3.66	0.19	55.98	5.09	0.091	0.77	5.16
301-302 pc	317.5	15.65	6.86	2.34	3.46	0.17	53.57	4.81	0.088	0.76	3.80
306-307 pc	322.5	16.69	6.33	2.49	3.71	0.18	56.02	4.88	0.085	0.80	5.27
311-312 pc	327.5	15.71	6.41	2.41	3.53	0.17	54.11	5.05	0.087	0.80	2.87
316-317 pc	332.5	16.09	6.41	2.38	3.56	0.18	56.11	4.98	0.080	0.80	5.08
321-322 pc	337.5	15.58	6.61	2.38	3.56	0.17	54.90	4.55	0.085	0.79	2.68
326-327 pc											
331-332 pc											
336-337 pc	347.5	15.71	6.37	2.36	3.52	0.17	56.00	4.95	0.077	0.80	5.25
341-342 pc	352.5	15.74	6.95	2.36	3.64	0.16	53.66	4.92	0.089	0.78	3.80

Major Element Data for Trigger Core (tc) and Piston Core (pc) Tul96-05 (continued).

Sample	Depth * (cm, corr.)	Al_2O_3 (%)	Fe_2O_3 (%)	K_2O (%)	MgO (%)	P_2O_5 (%)	SiO_2 (%)	CaO (%)	MnO (%)	TiO_2 (%)	Na_2O (%)
346-347 pc	357.5	16.12	6.52	2.53	3.63	0.16	55.23	5.02	0.081	0.77	4.99
351-352 pc	362.5	15.44	6.71	2.41	3.55	0.17	54.56	5.11	0.084	0.79	4.04
356-357 pc	367.5	15.50	6.68	2.42	3.50	0.17	54.99	5.49	0.076	0.76	4.79
361-362 pc	372.5	14.65	6.49	2.22	3.44	0.17	53.23	6.19	0.074	0.77	3.92
366-367 pc	377.5	15.34	6.72	2.36	3.53	0.17	54.19	5.82	0.082	0.78	4.93
371-372 pc	382.5	14.91	7.21	2.18	3.58	0.17	52.73	6.01	0.084	0.77	3.33
376-377 pc	387.5	16.07	6.74	2.31	3.78	0.17	54.66	5.26	0.099	0.75	4.82
381-382 pc	392.5	15.68	6.97	2.30	3.77	0.18	54.88	4.98	0.104	0.79	4.59
386-387 pc	397.5	16.37	7.06	2.32	3.89	0.18	55.48	5.07	0.106	0.79	5.78
391-392 pc	402.5	15.65	6.93	2.08	3.76	0.17	57.06	4.81	0.115	0.83	3.29
396-397 pc	407.5	15.94	7.48	2.19	3.57	0.17	57.60	4.53	0.098	0.77	5.29
401-402 pc	412.5	15.76	7.11	2.26	3.64	0.17	55.23	4.67	0.099	0.78	3.03
406-407 pc	417.5	16.02	6.79	2.59	3.73	0.17	54.46	4.97	0.090	0.78	5.60
411-412 pc	422.5	15.78	6.90	2.45	3.67	0.17	53.96	4.79	0.085	0.80	2.60
416-417 pc	427.5										
421-422 pc											
426-427 pc											
431-432 pc	432.5	15.40	6.50	2.35	3.64	0.17	53.65	5.19	0.079	0.79	2.61
436-437 pc	437.5	15.48	6.29	2.54	3.60	0.17	54.00	5.42	0.072	0.77	5.22
441-442 pc	442.5	15.31	6.63	2.24	3.64	0.17	54.81	4.40	0.076	0.79	2.27
446-447 pc	447.5	16.35	6.57	2.44	3.79	0.17	55.31	4.92	0.080	0.78	6.47
451-452 pc	452.5	15.73	6.27	2.41	3.56	0.16	54.06	5.33	0.078	0.77	2.71
456-457 pc	457.5	16.12	6.15	2.63	3.62	0.17	54.96	5.35	0.075	0.78	5.20
461-462 pc	462.5	15.56	6.59	2.57	3.47	0.17	54.03	4.95	0.073	0.77	2.67
466-467 pc	467.5	16.16	6.22	2.49	3.58	0.17	56.03	5.06	0.072	0.78	5.01
471-472 pc	472.5	15.34	6.09	2.34	3.43	0.17	54.56	5.04	0.071	0.79	4.42
476-477 pc	477.5	15.86	6.20	2.45	3.50	0.17	55.86	5.02	0.073	0.78	4.77
481-482 pc	482.5	15.41	6.27	2.44	3.56	0.17	54.01	5.38	0.076	0.77	4.09
486-487 pc	487.5	15.74	6.01	2.47	3.48	0.17	55.47	5.62	0.070	0.76	4.91
491-492 pc	492.5	15.25	6.35	2.41	3.34	0.17	54.15	5.44	0.069	0.77	3.27
496-497 pc	497.5	15.35	5.87	2.57	3.32	0.16	55.45	5.57	0.062	0.76	4.73
501-502 pc	502.5	14.83	5.90	2.43	3.26	0.17	54.76	5.76	0.066	0.76	3.81
506-507 pc	507.5	14.92	5.95	2.45	3.22	0.17	55.95	6.09	0.063	0.74	4.69

* Corrected piston core depth.

233

Table A16. (continued)

Minor Element Data for Trigger Core (tc) and Piston Core (pc) Tul96-05.

Sample	Depth * (cm, corr.)	V (µg/g)	Cr (µg/g)	Mn (µg/g)	Co (µg/g)	Ni (µg/g)	Cu (µg/g)	Zn (µg/g)	As (µg/g)	Rb (µg/g)	Sr (µg/g)	Y (µg/g)	Zr (µg/g)	Ba (µg/g)	Pb (µg/g)	Br (µg/g)	I (µg/g)
11-12 tc																	
21-22 tc																	
31-32 tc																	
41-42 tc																	
51-52 tc																	
61-62 tc																	
71-72 tc																	
81-82 tc																	

Sample	Depth * (cm, corr.)	V (µg/g)	Cr (µg/g)	Mn (µg/g)	Co (µg/g)	Ni (µg/g)	Cu (µg/g)	Zn (µg/g)	As (µg/g)	Rb (µg/g)	Sr (µg/g)	Y (µg/g)	Zr (µg/g)	Ba (µg/g)	Pb (µg/g)	Br (µg/g)	I (µg/g)
11-12 pc	57.5	171	123	492	15	65	49	132	5	88	233	20	144	833	16	158	603
16-17 pc	62.5	167	130	478	19	61	48	131		90	240	20	139	778	24	164	456
21-22 pc	67.5	164	123	479	15	66	48	134	7	86	229	20	141	814	11	157	499
26-27 pc	72.5	166	132	481	20	62	47	131		87	238	20	139	778	23	142	388
31-32 pc	77.5	155	119	478	12	62	45	128	5	85	241	19	148	773	14	162	589
36-37 pc	82.5	167	130	479	20	62	46	130		88	238	21	139	756	24	136	313
41-42 pc	87.5	168	129	495	13	67	49	132	8	87	238	20	146	795	14	145	407
46-47 pc																	
51-52 pc																	
56-57 pc	91.5	173	129	487	19	59	45	128		85	237	21	141	709	21	124	241
61-62 pc	96.5	166	126	499	12	64	46	132	6	87	228	20	147	759	6	133	359
66-67 pc	101.5	170	137	501	20	60	47	130		88	232	20	140	733	21	125	250
71-72 pc	106.5	165	121	498	14	59	45	125	4	83	240	20	143	749	13	120	312
76-77 pc	111.5	173	131	511	19	58	43	124		85	248	21	142	714	21	113	198
81-82 pc	116.5	162	122	503	14	63	45	128	6	84	246	20	145	740	13	110	293
86-87 pc	121.5	175	134	535	20	57	45	124		85	245	21	143	729	21	104	194
91-92 pc	126.5	168	125	538	13	59	46	125	5	84	243	22	151	753	10	100	246
96-97 pc	131.5	175	128	532	20	55	43	121		84	245	22	145	698	24	101	174
101-102 pc	136.5	160	116	511	16	58	44	121	4	82	242	21	149	688	17	98	201
106-107 pc	141.5	177	127	523	20	59	45	124		86	239	22	144	699	21	103	162
111-112 pc	146.5	163	118	520	13	58	44	122	4	82	244	21	150	707	10	100	199
116-117 pc	151.5	171	127	533	20	56	43	121		84	248	22	147	679	23	97	146
121-122 pc																	
126-127 pc																	
131-132 pc	166.5	160	116	531	13	59	44	120	3	80	252	22	161	706	13	94	187
136-137 pc	171.5	165	124	526	19	53	40	112		79	268	23	157	664	21	90	137
141-142 pc	176.5	172	122	556	13	58	43	119	5	82	261	22	151	731	15	87	154
146-147 pc	181.5	171	126	536	21	58	43	126		81	269	22	147	667	23	89	129
151-152 pc	186.5	176	126	564	15	60	44	123	5	83	251	24	144	749	9	91	169
156-157 pc	191.5	179	131	551	21	56	45	123		86	254	23	142	689	22	92	136
161-162 pc	196.5	171	125	557	16	60	47	125	5	85	257	22	145	709	12	89	161
166-167 pc	201.5	172	128	547	21	58	44	119		83	277	22	137	667	20	88	123
171-172 pc	206.5	167	123	551	16	61	48	127	5	86	267	23	145	759	12	90	174
176-177 pc	211.5	180	132	549	21	58	47	128		86	276	23	142	706	19	96	136
181-182 pc	216.5	172	120	551	15	62	47	127	3	83	271	23	141	747	12	95	171
186-187 pc	221.5	175	129	551	21	58	45	124		84	277	23	137	700	21	97	130
191-192 pc	226.5	173	118	563	16	62	49	127	6	83	274	22	140	754	13	96	167
196-197 pc	231.5	178	128	580	21	59	46	123		82	280	23	138	696	21	89	116
201-202 pc	236.5	182	125	620	14	64	49	122	4	80	271	22	135	730	14	79	107
206-207 pc	241.5																
211-212 pc	246.5	188	119	721	16	59	41	111	6	82	278	22	131	622	15	33	38
216-217 pc	251.5																
221-222 pc																	
226-227 pc																	
231-232 pc																	
236-237 pc		170	119	668	19	45	30	89		70	315	22	150	588	21	27	31
241-242 pc	257.5	184	87	931	17	43	46	98	4	63	379	21	108	669	11	5	5
246-247 pc	362.5	194	92	931	24	43	47	106		69	365	22	105	649	20	26	27
251-252 pc	267.5	180	82	893	18	45	47	106	4	70	369	22	108	660	12	14	11
256-257 pc	272.5	190	91	871	33	43	45	109		78	355	22	108	677	20	32	33
261-262 pc	277.5	171	94	781	15	47	44	111	3	83	343	22	118	706	15	27	12
266-267 pc	282.5	181	102	813	21	45	44	112		85	352	22	118	705	20	41	49
271-272 pc	287.5	160	87	791	16	50	44	110	9	80	361	22	115	679	11	25	26
276-277 pc	292.5	183	94	841	22	42	44	108		82	358	22	111	697	22	34	39
281-282 pc	297.5	177	103	776	20	47	45	115	6	91	323	21	122	741	12	28	32
286-287 pc	302.5	181	111	717	21	48	43	112		92	318	22	122	691	20	42	47
291-292 pc	307.5	174	117	663	18	51	44	114	6	93	308	22	134	717	14	43	51
296-297 pc	312.5	186	114	764	21	47	45	112		87	333	22	123	685	22	43	52
301-302 pc	317.5	173	101	730	15	51	44	113	7	88	327	22	127	710	12	36	38
306-307 pc	322.5	186	121	687	20	50	44	114		95	311	23	129	700	20	43	47
311-312 pc	327.5	174	117	646	17	51	45	116	4	95	308	23	135	698	17	40	39
316-317 pc	332.5	174	123	633	20	53	42	112		91	307	22	137	668	24	49	52
321-322 pc	337.5	174	113	702	15	53	46	116	3	89	308	23	130	691	14	35	49
326-327 pc																	
331-332 pc																	
336-337 pc	347.5	176	130	631	20	55	43	113		92	302	23	138	679	26	55	61
341-342 pc	352.5	169	103	675	15	54	46	116	9	92	307	22	122	689	13	33	45

(continued on next page)

234

Minor Element Data for Trigger Core (tc) and Piston Core (pc) Tul96-05 (continued).

Sample	Depth * (cm, corr.)	V (µg/g)	Cr (µg/g)	Mn (µg/g)	Co (µg/g)	Ni (µg/g)	Cu (µg/g)	Zn (µg/g)	As (µg/g)	Rb (µg/g)	Sr (µg/g)	Y (µg/g)	Zr (µg/g)	Ba (µg/g)	Pb (µg/g)	Br (µg/g)	I (µg/g)
346-347 pc	357.5	179	123	675	20	50	43	112		95	307	22	124	700	22	44	45
351-352 pc	362.5	165	111	622	17	52	41	110	7	92	303	22	135	665	13	31	45
356-357 pc	367.5	175	121	625	21	51	38	109		92	312	22	133	670	23	43	47
361-362 pc	372.5	160	112	606	16	55	40	110	7	87	322	22	138	671	14	43	26
366-367 pc	377.5	180	128	661	21	53	44	115		91	320	22	132	709	20	55	57
371-372 pc	382.5	165	113	668	17	58	45	114	7	86	323	23	128	733	10	33	46
376-377 pc	387.5	187	110	817	22	48	45	113		87	341	22	119	692	22	35	32
381-382 pc	392.5	179	101	802	16	49	46	113	4	83	321	22	122	696	15	23	17
386-387 pc	397.5	193	115	834	23	48	47	113		86	323	22	116	700	21	36	36
391-392 pc	402.5	186	105	870	18	48	50	110	8	74	313	23	124	638	7	15	18
396-397 pc	407.5	182	115	795	23	47	44	113		81	328	22	125	659	22	25	29
401-402 pc	412.5	170	106	730	20	52	44	113	5	85	307	21	129	705	13	25	19
406-407 pc	417.5	192	126	742	22	52	46	115		95	309	23	124	771	22	41	35
411-412 pc	422.5	173	115	646	18	55	44	116	7	97	295	22	130	767	11	32	40
416-417 pc	427.5																
421-422 pc																	
426-427 pc																	
431-432 pc	432.5	172	126	646	16	57	45	116	9	96	305	24	132	854	17	35	26
436-437 pc	437.5	174	135	616	20	55	43	112		96	312	23	137	783	21	56	49
441-442 pc	442.5	166	129	597	13	58	42	112	5	93	283	22	138	803	13	46	57
446-447 pc	447.5	·179	130	630	21	54	44	113		97	299	22	129	794	19	48	58
451-452 pc	452.5	169	119	612	15	54	40	110	6	96	297	23	134	860	11	33	39
456-457 pc	457.5	184	132	637	19	54	40	110		97	302	24	134	871	18	43	41
461-462 pc	462.5	161	116	542	16	55	38	109	2	99	287	24	140	804	18	35	42
466-467 pc	467.5	174	135	591	19	50	39	108		97	298	23	140	803	19	43	58
471-472 pc	472.5	162	122	558	14	54	40	110	6	92	294	22	140	862	12	46	43
476-477 pc	477.5	174	135	578	19	52	41	111		94	294	23	142	805	19	55	58
481-482 pc	482.5	161	115	570	14	52	40	108	5	96	294	23	144	828	13	39	36
486-487 pc	487.5	169	125	572	19	50	39	104		96	303	24	145	806	19	46	46
491-492 pc	492.5	163	117	538	14	53	40	107	5	98	299	22	149	879	15	36	35
496-497 pc	497.5	169	130	535	18	48	38	102		99	305	23	150	851	19	49	54
501-502 pc	502.5	151	116	494	11	51	37	103	5	95	303	24	156	829	14	42	27
506-507 pc	507.5	157	132	504	17	47	36	100		95	311	24	155	801	18	51	53

* Corrected piston core depth.

Table A16. (continued)

Trace Metal Data for Trigger Core (tc) and Piston Core (pc) Tul96-05.

Sample	Depth * (cm, corr.)	Ag (ng/g)	Cd (µg/g)	Re (ng/g)	Mo (µg/g)	U (µg/g)
11-12 tc						
21-22 tc						
31-32 tc						
41-42 tc						
51-52 tc						
61-62 tc						
71-72 tc						
81-82 tc						

Sample	Depth * (cm, corr.)	Ag (ppb)	Cd (ppm)	Re (ppb)	Mo (ppm)	U (ppm)
11-12 pc	57.5	474	0.54	19.19	1.29	2.88
16-17 pc	62.5	397	0.48	13.90	0.87	2.28
21-22 pc	67.5	531	0.74	25.76	1.25	3.92
26-27 pc	72.5	490	0.43	31.45	0.91	2.71
31-32 pc	77.5	403	0.38	12.46	1.14	2.70
36-37 pc	82.5	336	0.36	9.31	1.18	3.01
41-42 pc	87.5	458	0.56	16.88	1.25	3.48
46-47 pc						
51-52 pc						
56-57 pc	91.5	512	0.52	17.85	1.40	3.22
61-62 pc	96.5	470	0.38	12.05	1.70	3.96
66-67 pc	101.5	489	0.34	14.99	2.12	3.42
71-72 pc	106.5	426	0.36	11.31	1.74	3.63
76-77 pc	111.5	472	0.54	16.84	1.86	3.74
81-82 pc	116.5	456	0.32	14.21	1.50	2.50
86-87 pc	121.5	514	0.42	14.08	1.99	2.85
91-92 pc	126.5	445	0.46	11.36	1.91	3.36
96-97 pc	131.5	474	0.49	11.79	2.12	2.94
101-102 pc	136.5	549	0.45	10.54	2.47	2.93
106-107 pc	141.5	469	0.42	9.26	2.36	2.73
111-112 pc	146.5	445	0.36	9.02	1.73	2.79
116-117 pc	151.5	403	0.31	10.94	1.77	2.78
121-122 pc						
126-127 pc						
131-132 pc	166.5	381	0.27	7.84	1.43	2.52
136-137 pc	171.5	394	0.30	9.61	1.73	2.59
141-142 pc	176.5	390	0.32	15.32	1.57	2.55
146-147 pc	181.5	354	0.20	8.91	1.83	2.39
151-152 pc	186.5	324	0.30	11.20	1.55	2.32
156-157 pc	191.5	359	0.34	7.04	1.39	2.28
161-162 pc	196.5	417	0.39	9.19	1.35	2.24
166-167 pc	201.5	426	0.28	8.03	2.18	3.01
171-172 pc	206.5	386	0.31	11.19	1.71	2.94
176-177 pc	211.5	384	0.58	8.96	1.67	2.87
181-182 pc	216.5	304	0.42	10.68	1.41	3.07
186-187 pc	221.5	305	0.40	13.52	1.58	3.74
191-192 pc	226.5	300	0.64	21.58	1.53	3.84
196-197 pc	231.5	290	0.38	18.85	1.32	3.04
201-202 pc	236.5	na	na	na	na	na
206-207 pc	241.5	245	0.44	15.35	1.35	3.54
211-212 pc	246.5	216	0.37	6.45	1.48	2.48
216-217 pc	251.5	162	0.37	12.79	1.24	2.21
221-222 pc						
226-227 pc						
231-232 pc		121	0.28	5.60	0.75	1.32
236-237 pc		120	0.32	4.89	0.76	1.50
241-242 pc	257.5	73	0.19	1.51	0.92	1.15
246-247 pc	362.5	75	0.12	1.27	0.85	1.30
251-252 pc	267.5	68	0.11	1.15	0.95	1.63
256-257 pc	272.5	72	0.19	2.51	0.86	1.45
261-262 pc	277.5	88	0.19	2.32	1.08	2.00
266-267 pc	282.5	124	0.20	6.48	1.48	1.74
271-272 pc	287.5	123	0.15	2.30	1.55	2.03
276-277 pc	292.5	90	0.19	4.30	1.25	1.57
281-282 pc	297.5	106	0.22	5.63	1.61	2.12
286-287 pc	302.5	108	0.24	6.30	1.34	2.08
291-292 pc	307.5	150	0.33	11.70	1.25	2.54
296-297 pc	312.5	117	0.28	7.16	1.26	2.45
301-302 pc	317.5	107	0.21	6.04	1.31	2.10
306-307 pc	322.5	100	0.28	12.56	1.21	2.32
311-312 pc	327.5	154	0.38	13.70	1.16	2.62
316-317 pc	332.5	173	0.21	6.62	1.24	2.20
321-322 pc	337.5	198	0.25	4.73	1.34	1.89
326-327 pc						
331-332 pc						
336-337 pc	347.5	253	0.31	7.88	1.40	2.40
341-342 pc	352.5	167	0.36	17.00	2.00	2.57

(continued on next page)

Table A16. (continued)

Trace Metal Data for Trigger Core (tc) and Piston Core (pc) Tu196-05 (continued

Sample	Depth * (cm, corr.)	Ag (ppb)	Cd (ppm)	Re (ppb)	Mo (ppm)	U (ppm)
346-347 pc	357.5	na	0.19	5.52	2.05	2.34
351-352 pc	362.5	120	0.22	4.44	1.39	2.19
356-357 pc	367.5	147	0.31	11.22	1.37	2.09
361-362 pc	372.5	249	0.29	12.15	2.18	2.62
366-367 pc	377.5	226	0.40	9.09	1.78	2.85
371-372 pc	382.5	296	0.35	8.67	1.89	2.96
376-377 pc	387.5	109	0.27	7.67	1.26	2.68
381-382 pc	392.5	126	0.30	7.74	1.54	2.36
386-387 pc	397.5	111	0.25	7.25	1.32	2.17
391-392 pc	402.5	87	0.24	4.61	1.04	1.49
396-397 pc	407.5	172	0.23	9.44	1.54	2.64
401-402 pc	412.5	95	0.18	6.65	1.98	2.00
406-407 pc	417.5	96	0.36	6.12	1.80	2.76
411-412 pc	422.5	141	0.37	8.54	1.80	2.60
416-417 pc	427.5	na	na	na	na	na
421-422 pc						
426-427 pc						
431-432 pc	432.5	256	0.32	11.00	1.80	3.05
436-437 pc	437.5	172	0.37	6.80	1.43	2.31
441-442 pc	442.5	232	0.15	8.10	1.31	2.20
446-447 pc	447.5	145	0.36	14.12	1.11	2.38
451-452 pc	452.5	145	0.33	10.50	1.60	3.14
456-457 pc	457.5	114	0.39	9.87	1.52	3.24
461-462 pc	462.5	138	0.28	9.90	1.27	2.46
466-467 pc	467.5	77	0.15	6.26	1.32	2.40
471-472 pc	472.5	215	0.44	13.87	1.45	2.85
476-477 pc	477.5	234	0.47	14.53	1.38	2.52
481-482 pc	482.5	148	0.36	14.16	1.11	2.82
486-487 pc	487.5	86	0.26	10.01	1.25	2.84
491-492 pc	492.5	138	0.37	14.80	1.38	2.97
496-497 pc	497.5	101	0.26	12.46	1.00	2.70
501-502 pc	502.5	208	0.55	18.44	1.20	2.67
506-507 pc	507.5	200	0.31	10.30	0.78	2.32

* Corrected piston core depth.